

**DEVELOPMENT OF MASS SPECTROMETRIC METHODS FOR FAST  
IDENTIFICATION OF DRUG METABOLITES AND FOR  
DETERMINATION OF THE CHEMICAL COMPOSITIONS OF  
CRUDE OILS OF DIFFERENT API GRAVITIES**

by

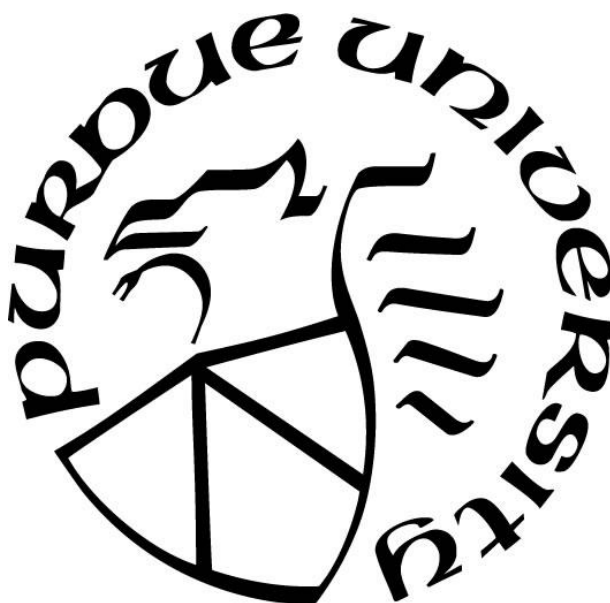
**Edouard Niyonsaba**

**A Dissertation**

*Submitted to the Faculty of Purdue University*

*In Partial Fulfillment of the Requirements for the degree of*

**Doctor of Philosophy**



Department of Chemistry

West Lafayette, Indiana

August 2019

**THE PURDUE UNIVERSITY GRADUATE SCHOOL**  
**STATEMENT OF COMMITTEE APPROVAL**

Dr. Hilikka I. Kenttämää, Chair

Department of Chemistry

Dr. Chittaranjan Das

Department of Chemistry

Dr. Cliff T. Johnston

Department of Agronomy

Dr. Andy W. Tao

Department of Chemistry

**Approved by:**

Dr. Dr. Christine A. Hrycyna

Head of the Graduate Program

*Mama,*

*Warakoze kwitanga kugira ngo abahungu bawe bose bazige.*

*Ubumenyi buri muri iki gitabo ndabugutuye.*

## ACKNOWLEDGMENTS

I would firstly like to acknowledge my advisor, Prof. Kenttämäa for accepting me in her research group. Joining her lab has been rewarding and I am extremely grateful for her constant guidance. She has provided me with opportunities to grow as a graduate student and to become an independent researcher. Her deduction towards training her students to become better researchers and better communicators has been extremely important for my success as a graduate student.

I would also like to thank many Kenttämäa group members whom I have enjoyed working with. Those include alumni: Dr. Chunfen Jin, Dr. Ravikiran Yerabolu, Dr. John Kong, Dr. Joann Max, Dr. McKay Easton, Dr. Yuan Jiang, Dr. Xueming Dong and Dr. Mark Romanczyk and current group members: Rashmi Kumar, Xin Ma, Jacob Milton, Yuyang Zhang, Duanchen Ding, Jeremy Manheim, Katherine Wehde, Lan Xu, Zaikuan Yu, Leah Easterling, Hao-Ran Lei, Jifa Zhang, Erlu Feng, Brent Modereger, Judy Kuan-Yu Liu, Wanru Li, Nancy Fu, Victoria Boulos, and Kawthar Alzarieni.

I would particularly like to thank Dr. Huaming Sheng, Dr. John Kong, and Dr. Zhoupeng Zhang from Merck & Co., Inc., and Dr. Cliff T. Johnston, Dr. Gozdem Kilaz, Dr. McKay Easton, Dr. Ravikiran Yerabolu, Dr. Yuan Jiang, Dr. Xueming Dong, Katherine Wehde, Zaikuan Yu, Erlu Feng, Judy Kuan-Yu Liu, and Kawthar Alzarieni from Purdue University whom I have collaborated with on different projects and have contributed greatly to my success.

I would like to thank the friends I have made while at Purdue University: Temitope Adeoye, Aristide Gumyusenge, Katherine Wehde, Jeremy Manheim, Ravikiran Yerabolu, Joann Max, Yuan Yu, Josh Yu, William Salloom, Mathew Campbell, Bryce Hamilton, Kedar Puvar and all my fellow Rwandan Presidential Scholars of class 2011. I would also like to thank the Coyle and



O'Quinn families who welcomed me in their homes during my first time in the United States. Thank you for making Arkansas my second home.

Finally, I would like to thank my family. My brothers: Peter, Paul, JMV, Deo, Vincent and Leodomird have shaped me to be the person I am today. I am forever grateful. My cousin Gilbert, thank you for motivating me to do science. My mother, I cannot thank you enough for your unconditional love and for how much you have sacrificed so all your sons can get education. Thank you, mother.

## TABLE OF CONTENTS

LIST OF TABLES .....	10
LIST OF FIGURES .....	12
LIST OF SCHEMES .....	17
ABSTRACT .....	18
CHAPTER 1. INTRODUCTION AND THESIS OVERVIEW .....	20
1.1 Introduction .....	20
1.2 Thesis Overview .....	21
1.3 References .....	23
CHAPTER 2. INSTRUMENTATION AND EXPERIMENTAL DETAILS OF LINEAR QUADRUPOLE ION TRAP MASS SPECTROMETER AND HIGH-RESOLUTION LINEAR QUADRUPOLE ION TRAP-ORBITRAP MASS SPECTROMETER.....	25
2.1 Introduction .....	25
2.2 Ion Generation .....	25
2.2.1 Electrospray Ionization .....	26
2.2.2 Atmospheric Pressure Chemical Ionization .....	27
2.3 Linear Quadrupole Ion Trap (LQIT) Mass Spectrometer .....	28
2.3.1 The API Region .....	29
2.3.2 The Ion Optics Region .....	30
2.3.3 The LQIT and Detector Region .....	31
2.3.3.1 Ion Radial Motion .....	32
2.3.3.2 Ion Axial Motion .....	34
2.3.3.3 Ion Ejection .....	35
2.3.3.4 Ion Detection with Electron Multipliers .....	36
2.4 Multi-Stage Tandem Mass Spectrometry (MS <sup>n</sup> ) .....	37
2.4.1 Ion Isolation .....	37
2.4.2 Collision-activated Dissociation (CAD) .....	38
2.4.3 Gas-phase Ion-molecule Reactions .....	40
2.4.3.1 Introduction of Neutral Reagents into the Ion Trap .....	40

2.4.3.2	Fundamental Aspects of Gas-phase Ion-molecule Reactions .....	41
2.5	Linear Quadrupole Ion Trap-Orbitrap (LQIT-orbitrap) Mass Spectrometer .....	42
2.5.1	Ion Injection into the Orbitrap .....	43
2.5.2	Ion Motion into the Orbitrap .....	44
2.5.3	Ion detection in the Orbitrap .....	45
2.5.4	Ion source CAD (ISCAD) .....	45
2.6	References .....	46
CHAPTER 3. DIFFERENTIATION OF DEPROTONATED ACYL, N- AND O-GLUCURONIDE DRUG METABOLITES BY USING TANDEM MASS SPECTROMETRY BASED ON GAS-PHASE ION-MOLECULE REACTIONS .....		50
3.1	Introduction .....	50
3.2	Experimental .....	51
3.2.1	Chemicals .....	51
3.2.2	Sample Preparation .....	52
3.2.3	High Performance Liquid Chromatography (HPLC) .....	52
3.2.4	Mass Spectrometry .....	53
3.2.5	Calculations .....	53
3.3	Results and Discussion .....	54
3.3.1	Gas-phase Ion-molecule Reactions of Deprotonated Acyl, <i>N</i> - and <i>O</i> -glucuronides with BF <sub>3</sub> Followed by CAD .....	54
3.3.2	HPLC/MS <sup>3</sup> of Acyl Glucuronides .....	65
3.3.3	Mechanism for the Formation of the Primary [M – H + BF <sub>3</sub> – 2 HF] <sup>–</sup> Diagnostic Product Ions .....	68
3.3.4	Mechanism for the Formation of the Secondary [M – H + 2 BF <sub>3</sub> – 3 HF] <sup>–</sup> Diagnostic Product Ions .....	71
3.3.5	Mechanism for the Loss of a Molecule with MW 88 Da Upon CAD of the [M – H + 2 BF <sub>3</sub> – 3 HF] <sup>–</sup> Product Ions .....	73
3.3.6	Application of this Methodology in Differentiating acyl, <i>N</i> -, and <i>O</i> -glucuronides in a Mixture .....	76
3.4	Conclusions .....	79
3.5	References .....	80

## CHAPTER 4. IDENTIFICATION OF PROTONATED PRIMARY CARBAMATES BY USING GAS-PHASE ION-MOLECULE REACTIONS FOLLOWED BY COLLISION-ACTIVATED DISSOCIATION IN TANDEM MASS SPECTROMETRY EXPERIMENTS ...84

4.1	Introduction .....	84
4.2	Experimental .....	86
4.2.1	Chemicals .....	86
4.2.2	Sample Preparation .....	86
4.2.3	Instrumentation .....	86
4.2.4	Computational Studies .....	87
4.3	Results and Discussion .....	88
4.3.1	Gas-phase Ion-molecule Reactions Between Protonated Carbamates and TMMS Followed by CAD .....	89
4.3.2	Gas-phase Ion-molecule Reactions Between Protonated Amides and TMMS Followed by CAD .....	96
4.4	Conclusions .....	100
4.5	References .....	101

## CHAPTER 5. DETERMINATION OF THE CHEMICAL COMPOSITIONS OF HEAVY, MEDIUM, AND LIGHT CRUDE OILS BY USING THE DISTILLATION, PRECIPITATION, FRACTIONATION MASS SPECTROMETRY (DPF MS) METHOD ..... 105

5.1	Introduction .....	105
5.2	Experimental .....	107
5.2.1	Materials .....	107
5.2.2	Samples .....	107
5.2.3	Fractionating the Crude Oils into Six Chemical Classes .....	108
5.2.4	Elemental Analysis .....	108
5.2.5	High-resolution Mass Spectrometry .....	109
5.3	Results and Discussion .....	111
5.3.1	Characterization of Crude Oils as a Whole .....	112
5.3.2	Characterization of the Compound Classes Derived from the Five Crude Oils .....	115
5.4	Conclusions .....	124
5.5	References .....	126

VITA .....	129
PUBLICATIONS.....	130

## LIST OF TABLES

Table 3.1	Product ions ( $m/z$ ) with their relative abundances (%) after 100 ms reaction of deprotonated acyl glucuronides with $\text{BF}_3$ and fragment ions ( $m/z$ ) with their relative abundances (%) formed upon CAD of the product ions $[\text{M} - \text{H} + 2 \text{BF}_3 - 3 \text{HF}]^-$ at a collision energy of 15 (arbitrary units) .....	57
Table 3.2	Product ions ( $m/z$ ) with their relative abundances (%) after 100 ms reaction of deprotonated <i>N</i> -glucuronides with $\text{BF}_3$ and fragment ions ( $m/z$ ) with their relative abundances (%) formed upon CAD of the product ions $[\text{M} - \text{H} + 2 \text{BF}_3 - 3 \text{HF}]^-$ at a collision energy of 15 (arbitrary units) .....	60
Table 3.3	Product ions ( $m/z$ ) and their relative abundance (%) observed after 100 ms reaction time between deprotonated <i>O</i> -glucuronides with $\text{BF}_3$ .....	62
Table 4.1	Product ions ( $m/z$ ) and their relative abundances in % observed after 300 ms reaction of protonated carbamates with TMMS and the fragment ions ( $m/z$ ) and their relative abundances in % formed upon CAD of the $[\text{M} + \text{H} + \text{TMMS} - \text{MeOH}]^+$ product ions. Also shown are the proton affinities (PAs) in kcal/mol for different atoms in two analytes. <sup>a</sup> .....	93
Table 4.2	Product ions (with their relative abundances) observed after 300 ms reaction of protonated amides and the fragment ions (with their relative abundances) formed upon CAD <sup>a</sup> of the product ions $[\text{M} + \text{H} + \text{TMMS} - \text{MeOH}]^+$ .....	98
Table 5.1	Optimized conditions for the analysis of volatile saturated hydrocarbons of the four crude oils by using GC×GC/(EI) TOF MS .....	111
Table 5.2	Gravimetric weight percents of different chemical classes obtained using the DPF method for five different crude oil samples. The crude oils are classified as heavy, medium, or light based on their API gravity (in parenthesis). .....	113
Table 5.3	Approximate weight percents of compounds with different elemental compositions (consolidated data) for each crude oil sample (API gravity shown in parenthesis). Elemental compositions are listed as $\text{C}_c\text{H}_h\text{N}_n\text{O}_o\text{S}_s$ , where <i>c</i> and <i>h</i> are any non-zero positive integer and <i>n</i> , <i>o</i> , and <i>s</i> are any positive integer between zero and five. ....	115
Table 5.4	The average nitrogen content in ppm determined via elemental analysis (for the five crude oils of different API gravity (shown in parenthesis). The total nitrogen content analysis was performed by Petr Vozka, Pavel Šimáček, and Josef Tomášek. ....	115

Table 5.5 Elemental compositions of the compounds in the volatile saturated hydrocarbon class derived from four different crude oils and the relative abundances of the ionized compounds measured by using GC×GC/(EI) TOF MS. The heaviest crude oil sample is not included as it contained no detectable volatile compounds. The data were collected by Katherine Wehde.....	120
Table 5.6 Elemental compositions of the compounds in the alkyl aromatic compound class derived from five different crude oils and the relative abundances of the ionized compounds measured by using (APCI) LQIT/orbitrap. ....	120
Table 5.7 Elemental compositions of the compounds in the heteroaromatic compound class derived from five different crude oils and the relative abundances of the ionized compounds measured by using (APCI) LQIT/orbitrap. ....	121
Table 5.8 Elemental compositions of the compounds in the polar compound class derived from five different crude oils and the relative abundances of the ionized compounds measured by using (APCI) LQIT/orbitrap. ....	121
Table 5.9 Elemental compositions of the compounds in the heavy saturated hydrocarbons class derived from five different crude oils and the relative abundances of the ionized compounds measured by using (APCI) LQIT/orbitrap. ....	122
Table 5.10 Elemental compositions of the compounds in the asphaltene compound class derived from five different crude oils and the relative abundances of the ionized compounds measured by using (APCI) LQIT/orbitrap. ....	122
Table 5.11 The change (%) in the $C_cH_hN/C_cH_h$ relative ion abundances for the heteroaromatic compound class derived from the five crude oils. The crude oils are classified as heavy, medium, or light based on their API gravity (shown in parenthesis). ....	123
Table 5.12 Average RDBE values for the compounds in each of the six compound classes derived from the five different crude oil samples. ....	124

## LIST OF FIGURES

Figure 2.1 Illustration of formation of gas-phase ions upon ESI (operated in positive ion mode), where S denotes solvent molecules. ....	26
Figure 2.2 The overall LQIT MS configuration along with typical operating pressures. ....	29
Figure 2.3 DC offset voltage gradient (V) applied to the elements of the API stack and ion optics to aid in transmission of positive ions in the z-direction. ....	31
Figure 2. 4 A schematic of the trapping regions of the LQIT mass analyzer. ....	32
Figure 2.5 The Mathieu stability diagram. Ions of different $m/z$ values whose $a$ and $q$ values locate them inside the diagram (shown as colored circles with larger circles being ions of larger $m/z$ ) have stable trajectories within the x- and y-directions of the LQIT. ....	34
Figure 2.6 A schematic of LQIT with typical DC voltages applied to the different sections of the quadrupole ion trap of LQIT. A lower potential is applied to the center section and a higher potential to the front and the back sections, resulting in a potential well that confines ions in the center section in the z-direction. The colored circles represent ions trapped in the potential energy well. ....	35
Figure 2.7 LQIT and its ion detection system, which consists of two conversion dynodes and two electron multipliers. Only one conversion dynode and one electron multiplier are shown in this figure. ....	37
Figure 2.8 Ion isolation process. a) All ions are confined in the ion trap. b) RF voltage amplitude (denoted as $V_{RF}$ ) is increased to place the ions of interest (green circle) to $q = 0.803$ to eject some ions with $m/z$ values lower than that of the ions of interest. c) The broad-band excitation waveform is applied to eject the remaining unwanted ions. d) Only the ions of interest remain in the ion trap. ....	38
Figure 2.9 Schematics of the CAD process. a) The RF voltage amplitude (denoted as $V_{RF}$ ) is decreased to lower the $q$ value of the ions of interest to 0.25. b) The dipolar resonance excitation (tickle voltage) is applied to the x-rods to increase the ions' kinetic energy, which is converted into internal energy when the ions collide with helium. When the internal is higher than the lowest barrier for fragmentation, the ions fragment. ....	39
Figure 2.10 A schematic of the reagent mixing manifold employed to introduce neutral reagents into the ion trap via the helium gas line. ....	41
Figure 2.11 The Brauman double-well potential energy surface model for gas-phase ion-molecule reactions. ....	42
Figure 2.12 Schematic of the LQIT-orbitrap along with the typical operating pressures. ....	43



Figure 2.13 DC offset voltage gradient (V) applied to the elements of the API stack and ion optics to aid in transmission of positive ions in the z-direction during normal mass spectrometric experiments and during ISCAD experiments.....46

Figure 3.1 (A) Mass spectra measured for after 200 ms reaction of a deprotonated *O*-, *N*-, and acyl glucuronide with BF<sub>3</sub>. Only the deprotonated *N*- and acyl glucuronides formed the diagnostic product ions:  $[M - H + BF_3 - 2 HF]^-$  and  $[M - H + 2 BF_3 - 3 HF]^-$ . (B) For the deprotonated *N*-glucuronide, CAD (collision energy 15 arbitrary units) of the  $[M - H + 2 BF_3 - 3 HF]^-$  ions yielded a major fragment ion corresponding to elimination of HF (MW 20 Da). (C) For the deprotonated acyl glucuronide, a diagnostic fragment ion was formed via the loss of a molecule with MW 88 Da. <sup>#</sup> Product ions that are due to hydrolysis of  $[M - H + BF_3 - HF]^-$  and  $[M - H + 2 BF_3 - 3 HF]^-$  product ions to form  $[M - H + BF_3 + H_2O - 2 HF]^-$  and  $[M - H + 2 BF_3 + H_2O - 4 HF]^-$  product ions, respectively, were also observed. <sup>\*</sup> Secondary product ions. ....56

Figure 3.2 Time-course HPLC chromatograms and mass spectra showing gas-phase ion molecule and CAD reactions for lumiracoxib acyl-β-D-glucuronide incubated in 0.1 % formic acid (by volume) in water (pH 2.7) and in phosphate buffer at pH 7.4. (A) After four hours, only one peak was observed in the HPLC chromatogram measured for lumiracoxib acyl-β-D-glucuronide dissolved in acidified water. (B) Multiple peaks due to isomerization via acyl migration were observed in the HPLC chromatogram for lumiracoxib acyl-β-D-glucuronides incubated in phosphate buffer. (C) The deprotonated unmigrated isomer did not form the diagnostic product ions in the mass spectrometer. (D) The migrated isomers formed the diagnostic product ions  $[M - H + BF_3 - 2 HF]^-$  (*m/z* 496) and  $[M - H + 2 BF_3 - 3 HF]^-$  (*m/z* 544) after 30 ms reaction. (E) The CAD (collision energy 15 arbitrary units) of the  $[M - H + 2 BF_3 - 3 HF]^-$  product ion (*m/z* 544) yielded a fragment ion (*m/z* 456) via loss of molecule with MW 88 Da.. ....67

Figure 3.3 Mass spectra measured after 100 ms reaction between deprotonated probenecid acyl β-D-glucuronide and BF<sub>3</sub> when the analyte was dissolved in water containing 0.1 % formic acid (v/v) (top) and when the analyte was dissolved in pure water (bottom). .68

Figure 3.4 (A) Proposed mechanism and potential energy surface calculated for the reaction between deprotonated glucuronic acid and BF<sub>3</sub>. Values shown are ΔG (black) and ΔH (blue) in kcal/mol calculated relative to the separated reactants. All calculations were performed at the M06-2X/6-311++G(d,p) level of theory. (B) The same mechanism for the formation of the primary diagnostic product ions,  $[M - H + BF_3 - 2 HF]^-$ , is proposed for the reaction between BF<sub>3</sub> and (B) a migrated deprotonated migrated (3-β-) acyl glucuronide and (C) *N*-glucuronide. The calculations were done by Dr. McKay W. Easton.....70

Figure 3.5 (A) Proposed mechanism for the formation of the secondary diagnostic product ions,  $[M - H + 2 BF_3 - 3 HF]^-$ , from deprotonated erythronic acid and  $BF_3$ . (B) Calculated potential energy surfaces for the formation of the secondary diagnostic product ions. Values shown are  $\Delta G$  (black) and  $\Delta H$  (blue) in kcal/mol calculated relative to the separated reactants. All calculations were performed at the M06-2X/6-311++G(d,p) level of theory. The same mechanism for the formation of the secondary diagnostic product ions is proposed for (C) deprotonated migrated 2- $\beta$ -acyl glucuronide and (D) deprotonated *N*-glucuronide with  $BF_3$ . The calculations were performed by Erlu Feng. ....72

Figure 3.6 (A) Calculated potential energy surfaces for the loss of 2-fluoro-1,3,2-dioxaborale. Values shown are  $\Delta G$  in kcal/mol calculated relative to the separated reactants. All calculations were performed at the M06-2X/6-311++G(d,p) level of theory. (B) Proposed mechanism for the loss of 2-fluoro-1,3,2-dioxaborale upon CAD of the  $[M - H + 2BF_3 - 3HF]^-$  product ion formed between 4- $\beta$ -O-acyl glucuronide and  $BF_3$ . The calculations were performed by Erlu Feng. ....73

Figure 3.7 Proposed mechanism for the loss of 2-fluoro-1,3,2-dioxaborale (MW 88 Da) upon CAD of the  $[M - H + 2 BF_3 - 3 HF]^-$  product ions formed between  $BF_3$  and deprotonated (A) 2- $\beta$ -acyl glucuronide, (B) 3- $\beta$ -acyl glucuronide and (C) 4- $\beta$ -acyl glucuronide. ....74

Figure 3.8 CAD mass spectrum ( $MS^3$ ) measured for the diagnostic secondary  $[M - H + 2 BF_3 - 3 HF]^-$  product ions ( $m/z$  458) formed upon reactions of  $^{13}C$ -labeled ibuprofen acyl  $\beta$ -D-glucuronide and  $BF_3$  and the relative abundances of the  $^{10}B$ -isotopes in the  $[M - H + 2 BF_3 - 3 HF]^-$  product ion (top right) and in the fragment ion formed from this product ion via the loss of a molecule with MW 88 Da (top left). These results demonstrate that upon elimination of this molecule, a boron atom was lost.....75

Figure 3.9 Proposed mechanism for the elimination of the HF molecule upon CAD of the  $[M - H + 2 BF_3 - 3 HF]^-$  diagnostic product ion formed between  $BF_3$  and deprotonated *N*-glucuronide or glucuronic acid and the elimination of 2-fluoro-1,3,2-dioxaborale upon CAD of the  $[M - H + 2 BF_3 - 3 HF]^-$  diagnostic product ion formed between  $BF_3$  and deprotonated, migrated acyl 2- $\beta$ -D-glucuronide. ....76

Figure 3.10 Deprotonated glucuronides used to demonstrate the utility of coupling HPLC with tandem mass spectrometry based on ion-molecule reactions followed by CAD. ....78

Figure 3.11 (A) HPLC chromatogram measured for a mixture of an *N*-, *O*-, and acyl glucuronide after 4 hours in phosphate buffer (pH 7.4). Mass spectra measured after 30 ms reaction with  $\text{BF}_3$  for (B) deprotonated PhIP-*N*- $\beta$ -D-glucuronide, (C) deprotonated unmigrated telmisartan acyl- $\beta$ -D-glucuronide, (D) deprotonated migrated telmisartan acyl- $\beta$ -D-glucuronide, and (E) ezetimibe *O*- $\beta$ -D-glucuronide. Both deprotonated PhIP-*N*- $\beta$ -D-glucuronide and deprotonated migrated telmisartan acyl- $\beta$ -D-glucuronide formed the diagnostic  $[\text{M} - \text{H} + 2 \text{BF}_3 - 3 \text{HF}]^-$  product ions while deprotonated ezetimibe *O*- $\beta$ -D-glucuronide did not. (F) The CAD (collision energy 15 arbitrary units) mass spectrum measured for the  $[\text{M} - \text{H} + 2 \text{BF}_3 - 3 \text{HF}]^-$  product ions of deprotonated PhIP-*N*- $\beta$ -D-glucuronide does not show fragment ions corresponding to the loss of 2-fluoro-1,3,2-dioxaborole. (G) The CAD mass spectrum measured for the  $[\text{M} - \text{H} + 2 \text{BF}_3 - 3 \text{HF}]^-$  product ions of deprotonated migrated telmisartan acyl- $\beta$ -D-glucuronide yielded fragment ions that are due to the loss of the 2-fluoro-1,3,2-dioxaborole (MW 88 Da).  
.....78

Figure 4.1  $\text{MS}^2$  spectra measured after CAD (collision energy 20 arbitrary units) of two protonated primary carbamates. (a) CAD of protonated methyl carbamate yields a fragment ion via ammonia loss ( $m/z$  59), a fragment ion via isocyanic acid loss ( $m/z$  33), and a fragment ion via carbon dioxide loss ( $m/z$  32). (b) CAD of protonated butyl carbamate only yields a fragment ion via a loss of but-1-ene ( $m/z$  62).  
.....89

Figure 4.2 (a)  $\text{MS}^2$  spectrum measured after 300 ms reaction between protonated ethyl carbamate ( $m/z$  90) and TMMS. The observed product ions are a stable adduct,  $[\text{M} + \text{H} + \text{TMMS}]^+$  ( $m/z$  226), an adduct that has lost methanol,  $[\text{M} + \text{H} + \text{TMMS} - \text{MeOH}]^+$  ( $m/z$  194), and protonated TMMS,  $[\text{TMMS} + \text{H}]^+$  ( $m/z$  137). (b)  $\text{MS}^3$  spectrum measured after CAD (collision energy 20 arbitrary units) of the  $[\text{M} + \text{H} + \text{TMMS} - \text{MeOH}]^+$  product ion ( $m/z$  194). The fragment ion with  $m/z$  151 was formed via the loss of isocyanic acid ( $\text{HN}=\text{C}=\text{O}$ ; MW 43 Da), which is diagnostic for protonated primary carbamates. The fragment ion of  $m/z$  162 corresponds to elimination of methanol.  
.....90

Figure 4.3 Potential energy surface calculated at the M06-2X/6-311++G-(d,p) level of theory for the formation of the ions  $[\text{M} + \text{H} + \text{TMMS}]^+$  and  $[\text{M} + \text{H} + \text{TMMS} - \text{MeOH}]^+$  upon reactions of protonated ethyl carbamate with TMMS. Also shown are the potential energy surfaces associated with the formation of fragment ions formed via a loss of isocyanic acid (**red**) and methanol (**blue**) upon CAD of the  $[\text{M} + \text{H} + \text{TMMS} - \text{MeOH}]^+$  product ion.  
.....95

Figure 4.4 2-Hydroxy-3-methoxypropyl carbamate and methocarbamol.  
.....96

Figure 4.5 Potential energy surface calculated at the M06-2X/6-311++G-(d,p) level of theory for two conformers of protonated 2-hydroxy-3-methoxypropyl carbamate.  
.....96

Figure 4.6 (a) MS<sup>2</sup> spectrum measured after 300 ms reaction of protonated propionamide ( $m/z$  74) with TMMS. The observed product ions are a stable adduct,  $[M + H + TMMS]^+$  ( $m/z$  210), and an adduct that has lost methanol,  $[M + H + TMMS - MeOH]^+$  ( $m/z$  178). (b) MS<sup>3</sup> spectrum measured after CAD (collision energy 20 arbitrary units) of the  $[M + H + TMMS - MeOH]^+$  product ion ( $m/z$  178). The major fragment ion observed ( $m/z$  146) corresponds to the loss of methanol. No fragment ion from the loss of isocyanic acid (MW 43 Da) was observed.....99

Figure 4.7 Proposed fragmentation pathway for CAD of the  $[M + H + TMMS - MeOH]^+$  product ion formed between TMMS and protonated allyl carbamate (top) and protonated acrylamide (bottom). CAD of the  $[M + H + TMMS - MeOH]^+$  product ion of protonated allyl carbamate yields a diagnostic fragment ion via the elimination of isocyanic acid ( $m/z$  163), a fragment ion via elimination of methanol ( $m/z$  174) and a fragment ion via elimination of both methanol and propa-1,2-diene ( $m/z$  134). This fragment ion ( $m/z$  134) reacts with water to form a water adduct ion ( $m/z$  152). CAD of  $[M + H + TMMS - MeOH]^+$  of protonated acrylamide only yields a fragment ion via elimination of methanol ( $m/z$  144). This fragment ion reacts with water to form a water adduct ion ( $m/z$  162). ..... 100

Figure 5.1 The approximate weight percent of compounds with the elemental composition C<sub>c</sub>H<sub>h</sub>N in the heteroaromatic compound class as a function of API gravity for five crude oils. .... 116

Figure 5.2 Approximate weight percentages of C<sub>c</sub>H<sub>h</sub>N compounds in five compound classes derived from each crude oil (API gravity given in parenthesis). Volatile saturated hydrocarbons are not included as they contained no nitrogen-containing compounds (Table 4). ..... 117

Figure 5.3 Relative abundances of ions with the elemental compositions C<sub>c</sub>H<sub>h</sub> and C<sub>c</sub>H<sub>h</sub>N in the mass spectra measured before and after ISCAD (marked as ISCAD above) for the heteroaromatic compound class for each crude oil sample (API gravity given in parenthesis). The percent change in the ratio of the C<sub>c</sub>H<sub>h</sub>N/C<sub>c</sub>H<sub>h</sub> ion abundances is also given above (obtained from Table 10). ..... 119

Figure 5.4 The RDBE values for compounds in the heteroaromatic compound class as a function of API gravity for five crude oils. .... 124

## LIST OF SCHEME

Scheme 2.1 Proposed mechanism for the generation of protonated analytes in positive ion mode APCI when using water as the solvent and APCI reagent and N <sub>2</sub> as the nebulizer gas. .....	28
---	----

## ABSTRACT

Author: Niyonsaba, Edouard PhD

Institution: Purdue University

Degree Received: August 2019

Title: Development of Mass Spectrometric Methods for Fast Identification of Drug Metabolites and for Determination of the Chemical Compositions of Crude Oils of Different API Gravities

Committee Chair: Hilkka I. Kenttämä

Mass spectrometry (MS) alone or coupled with high-performance liquid chromatography (HPLC) or gas chromatography (GC) is a versatile analytical tool that is routinely employed for identification of unknown compounds in complex mixtures. MS operates by separating ionized analytes based on their mass-to-charge ( $m/z$ ) ratios. If the analyte can be ionized without complete fragmentation, MS provides molecular weight information and, if performed at high resolution, elemental compositions for the ionized analytes. Tandem mass spectrometry ( $MS^n$ ,  $n \geq 2$  where each MS step corresponds to an ion isolation or separation event) also provides structural information of ionized analytes. With this approach, structural information of the ionized analytes is obtained by isolating the ionized analytes of interest and subjecting them to fragmentation experiments, such as collision-activated dissociation (CAD). The ions of interest can also be isolated and allowed to react with gaseous molecules to generate product ions (ion-molecule reactions).

The experiments described in this dissertation focused on the development of tandem mass spectrometry methods based on CAD and/or gas-phase ion-molecule reactions for the differentiation of acyl, *N*- and *O*-glucuronide drug metabolites and for identification of primary carbamates as potentially mutagenic impurities. Further, by using a previously published method titled Distillation, Precipitation, Fractionation Mass Spectrometry (DPF MS), the chemical

compositions of five crude oil samples, including heavy, medium, and light crude oils with different API gravities, were determined. Additionally, the gravimetric percentages of different compound classes found in these crude oils are reported as well as the correlations found between API gravities and the chemical compositions of crude oils.

## CHAPTER 1. INTRODUCTION AND THESIS OVERVIEW

### 1.1 Introduction

Following the invention of J.J. Thomson's first mass spectrometer (MS),<sup>1</sup> mass spectrometry has evolved into one of the most comprehensive and versatile tools for analysis for a wide range of complex mixtures. For instance, MS has been employed in the analysis of crude oils,<sup>2</sup> mixtures of proteins,<sup>3</sup> and fuels.<sup>4,5</sup> The simplest MS experiments involve three major events: generation of molecular and fragment ions from neutral analytes (this event is not necessary if the analyte is charged); separation of the ions based on their mass-to-charge ( $m/z$ ) ratios; and detection of the separated ions. The measured  $m/z$  values of the ions and their relative abundances are plotted to generate a mass spectrum. The  $m/z$  values of the ions are plotted on the x-axis and their relative abundances on the y-axis. With the emergence of high-resolution mass spectrometers, such as Fourier-transform ion cyclotron resonance mass spectrometers (FT-ICR),<sup>6</sup> and orbitraps,<sup>7</sup> the  $m/z$  values of the ions can be determined incredibly accurately, providing information about the elemental compositions of the ions.

The development of tandem mass spectrometry ( $MS^n$ ,  $n \geq 2$ ; where each MS step corresponds to an ion isolation or separation event) also provides structural information of ionized analytes.  $MS^n$  based on collision-activated dissociation (CAD) is the most commonly used  $MS^n$  approach. In this approach, ions of interest are isolated and subjected to energetic collisions with a gas (typically helium, argon or nitrogen), thereby causing fragmentation of the ions.<sup>8,9</sup> The measured fragment ions are then used to elucidate the structure of the unknown ions.<sup>10,11</sup>  $MS^n$  based on gas-phase ion-molecule reactions is another approach that is increasingly employed for the characterization of the structures of unknown ionized analytes.<sup>12</sup> This approach is based on isolating ions of interest and allowing them to react with a gaseous reagent. Based on the product ions formed, structural information can often be derived. For example, gas-phase ion-molecule reactions can be used to differentiate isomeric ionized glucuronides<sup>13</sup> and identify various



functional groups commonly found in drug metabolites, including sulfone,<sup>14</sup> sulfoxide,<sup>15</sup> *N*-oxide,<sup>16,17</sup> epoxide,<sup>18</sup> *N*-hydroxylamino,<sup>19</sup> and keto,<sup>20</sup> in protonated analytes.

## 1.2 Thesis Overview

The research discussed in this dissertation focuses on the development of tandem mass spectrometric methods for the rapid identification of glucuronide drug metabolites and carbamates and for the molecular-level characterization of crude oils of different densities and different origins. Chapter 2 discusses the principles and experimental details of the linear quadrupole ion trap (LQIT) mass spectrometers and the high-resolution linear quadrupole ion trap–orbitrap (LQIT-orbitrap) mass spectrometers employed in this research. The fundamental aspects of tandem mass spectrometry based on both CAD and gas-phase ion-molecule reactions are also discussed.

Chapter 3 discusses tandem mass spectrometric method development for the identification of the glucuronidation site in glucuronide drug metabolites. In this study, gas-phase ion-molecule reactions between deprotonated glucuronide metabolites and boron trifluoride (BF<sub>3</sub>) followed by CAD in the linear quadrupole ion trap (LQIT) enabled the differentiation of acyl, *N*- and *O*-glucuronides. These three metabolites are formed when glucuronic acid is conjugated to a drug or a drug metabolite via a carboxylic acid, hydroxy, or amino group, respectively.<sup>21</sup> Only deprotonated *N*-glucuronides and migrated acyl glucuronides were found to form diagnostic product ions: adducts with a BF<sub>3</sub> molecule that have lost two HF molecules,  $[M - H + BF_3 - 2 HF]^-$ , and adducts with two BF<sub>3</sub> molecules that have lost three HF molecules,  $[M - H + 2 BF_3 - 3 HF]^-$ . These product ions were not observed for deprotonated *O*-glucuronides. Upon CAD of the  $[M - H + 2 BF_3 - 3 HF]^-$  product ions, diagnostic fragment ions were formed via a loss of 2-fluoro-1,3,2-dioxaborole (MW 88 Da) only in the case of deprotonated migrated acyl glucuronides. Quantum chemical calculations at the M06-2X/6-311++G(d,p) level of theory were employed to rationalize the mechanisms for the reactions of interest.

Chapter 4 discusses the development of a tandem mass spectrometric approach based on gas-phase ion-molecule reactions and CAD for identifying primary carbamates compound class in protonated analytes using APCI. Primary carbamates are of interest because they are sometimes found as low-level impurities during drug manufacturing and as some of them are potentially mutagenic.<sup>22</sup> The neutral reagent employed was trimethoxymethylsilane (TMMS). Protonated primary carbamates were found to react with TMMS to form stable adduct ions,  $[M + H + TMMS]^+$ , and adduct ions that had lost methanol,  $[M + H + TMMS - CH_3OH]^+$ . Upon CAD, the  $[M + H + TMMS - MeOH]^+$  product ions generated diagnostic fragment ions via a loss of isocyanic acid. Quantum chemical calculations were employed to rationalize the possible mechanisms for the formation of the product ions and for the fragmentation of the  $[M + H^+ + TMMS - MeOH]^+$  product ion.

Chapter 5 discusses the molecular profiling of crude oils of different API (American Petroleum Institute) gravities by using a previously published method referred to as distillation, precipitation, fractionation mass spectrometry (DPF MS).<sup>23</sup> Crude oils are classified as heavy, medium or light based on their API gravity, which is a measure of the density of a crude oil relative to water. Although API gravity is a generally accepted tool for classifying crude oils, some crude oils with similar API gravities may have very different chemical compositions.<sup>24</sup> However, the chemical composition of the crude oil dictates how the crude oil is processed. Therefore a more accurate way of classifying crude oils needs to be developed. In this study, the chemical compositions of five heavy, medium, and light crude oils with different API gravities were determined by the DPF MS method. Two trends were identified for the five crude oils studied. As the API gravity decreases, the nitrogen content of the alkyl side chains of the compounds in the heteroaromatic compound class increases. This compound class contains most of the nitrogen-containing compounds in these crude oils. Further, as the API gravity decreases, the ring and double bond equivalence (RDBE; related to the level of unsaturation, nitrogen content, and/or number of rings) increases for the compounds in the heteroaromatic compound class for all the crude oils studied

## 1.3 References

- (1) Thomson, J. J. *Rays of Positive Electricity and Their Application to Chemical Analyses*; Longmans, Green and Company: London, 1921.
- (2) Niyonsaba, E.; Manheim, J. M.; Yerabolu, R.; Kenttämää, H. I. Recent Advances in Petroleum Analysis by Mass Spectrometry. *Anal. Chem.* **2018**, *91* (1), 156–177.
- (3) Yates, J. R.; Ruse, C. I.; Nakorchevsky, A. Proteomics by Mass Spectrometry: Approaches, Advances, and Applications. *Annu. Rev. Biomed. Eng.* **2009**, *11*, 49–79.
- (4) Hurt, M. R.; Borton, D. J.; Choi, H. J.; Kenttämää, H. I. Comparison of the Structures of Molecules in Coal and Petroleum Asphaltenes by Using Mass Spectrometry. *Energy Fuels* **2013**, *27* (7), 3653–3658.
- (5) Ibáñez, M.; Sancho, J. V.; Pozo, Ó. J.; Niessen, W.; Hernández, F. Use of Quadrupole Time-of-Flight Mass Spectrometry in the Elucidation of Unknown Compounds Present in Environmental Water. *Rapid Commun. Mass Spectrom.* **2005**, *19* (2), 169–178.
- (6) Comisarow, M. B.; Marshall, A. G. Fourier Transform Ion Cyclotron Resonance Spectroscopy. *Chem. Phys. Lett.* **1974**, *25* (2), 282–283.
- (7) Makarov, A. Electrostatic Axially Harmonic Orbital Trapping: A High-Performance Technique of Mass Analysis. *Anal. Chem.* **2000**, *72* (6), 1156–1162.
- (8) McLuckey, S. A. Principles of Collisional Activation in Analytical Mass Spectrometry. *J. Am. Soc. Mass Spectrom.* **1992**, *3* (6), 599–614.
- (9) Mayer, P. M.; Poon, C. The Mechanisms of Collisional Activation of Ions in Mass Spectrometry. *Mass Spectrom. Rev.* **2009**, *28* (4), 608–639.
- (10) Prakash, C.; Shaffer, C. L.; Nedderman, A. Analytical Strategies for Identifying Drug Metabolites. *Mass Spectrom. Rev.* **2007**, *26* (3), 340–369.
- (11) Lee, M. S.; Kerns, E. H. LC/MS Applications in Drug Development. *Mass Spectrom. Rev.* **1999**, *18* (3–4), 187–279.
- (12) Osburn, S.; Ryzhov, V. Ion–Molecule Reactions: Analytical and Structural Tool. *Anal. Chem.* **2013**, *85* (2), 769–778.
- (13) Kong, J. Y.; Yu, Z.; Easton, M. W.; Niyonsaba, E.; Ma, X.; Yerabolu, R.; Sheng, H.; Jarrell, T. M.; Zhang, Z.; Ghosh, A. K. Differentiating Isomeric Deprotonated Glucuronide Drug Metabolites via Ion/Molecule Reactions in Tandem Mass Spectrometry. *Anal. Chem.* **2018**, *90* (15), 9426–9433.
- (14) Tang, W.; Sheng, H.; Kong, J. Y.; Yerabolu, R.; Zhu, H.; Max, J.; Zhang, M.; Kenttämää, H. I. Gas-Phase Ion-Molecule Reactions for the Identification of the Sulfone Functionality in Protonated Analytes in a Linear Quadrupole Ion Trap Mass Spectrometer. *Rapid Commun. Mass Spectrom.* **2016**, *30* (12), 1435–1441.

- (15) Sheng, H.; Tang, W.; Yerabolu, R.; Max, J.; Kotha, R. R.; Riedeman, J. S.; Nash, J. J.; Zhang, M.; Kenttämä, H. I. Identification of N-Oxide and Sulfoxide Functionalities in Protonated Drug Metabolites by Using Ion-Molecule Reactions Followed by Collisionally Activated Dissociation in a Linear Quadrupole Ion Trap Mass Spectrometer. *J. Org. Chem.* **2016**, *81* (2), 575–586.
- (16) Duan, P.; Gillespie, T. A.; Winger, B. E.; Kenttämä, H. I. Identification of the Aromatic Tertiary N-Oxide Functionality in Protonated Analytes via Ion/Molecule Reactions in Mass Spectrometers. *J. Org. Chem.* **2008**, *73* (13), 4888–4894.
- (17) Duan, P.; Fu, M.; Gillespie, T. A.; Winger, B. E.; Kenttämä, H. I. Identification of Aliphatic and Aromatic Tertiary N-Oxide Functionalities in Protonated Analytes via Ion/Molecule and Dissociation Reactions in an FT-ICR Mass Spectrometer. *J. Org. Chem.* **2009**, *74* (3), 1114–1123.
- (18) Eismin, R. J.; Fu, M.; Yem, S.; Widjaja, F.; Kenttämä, H. I. Identification of Epoxide Functionalities in Protonated Monofunctional Analytes by Using Ion/Molecule Reactions and Collision-Activated Dissociation in Different Ion Trap Tandem Mass Spectrometers. *J. Am. Soc. Mass Spectrom.* **2012**, *23* (1), 12–22.
- (19) Sheng, H.; Tang, W.; Yerabolu, R.; Kong, J. Y.; Williams, P. E.; Zhang, M.; Kenttämä, H. I. Mass Spectrometric Identification of the N-monosubstituted N-hydroxylamino Functionality in Protonated Analytes via Ion/Molecule Reactions in Tandem Mass Spectrometry. *Rapid Commun. Mass Spectrom.* **2015**, *29* (8), 730–734.
- (20) Moraes, L.; Eberlin, M. N. Structurally Diagnostic Ion–Molecule Reactions: Acylium Ions with A-, B- and  $\Gamma$ -hydroxy Ketones. *J. Mass Spectrom.* **2002**, *37* (2), 162–168.
- (21) King, C.; Rios, G.; Green, M.; Tephly, T. UDP-Glucuronosyltransferases. *Curr. Drug Metab.* **2000**, *1* (2), 143–161.
- (22) Snodin, D. J. Genotoxic Impurities: From Structural Alerts to Qualification. *Org. Process Res. Dev.* **2010**, *14* (4), 960–976.
- (23) Yerabolu, R.; Kotha, R. R.; Niyonsaba, E.; Dong, X.; Manheim, J. M.; Kong, J.; Riedeman, J. S.; Romanczyk, M.; Johnston, C. T.; Kilaz, G.; Kenttämä, H. I. Molecular Profiling of Crude Oil by Using Distillation Precipitation Fractionation Mass Spectrometry (DPF-MS). *Fuel* **2018**, *234*, 492–501.
- (24) Hinkle, A.; Shin, E.; Liberatore, M.; Herring, A.; Batzle, M. Correlating the Chemical and Physical Properties of a Set of Heavy Oils from around the World. *Fuel* **2008**, *87* (13–14), 3065–3070.

## **CHAPTER 2. INSTRUMENTATION AND EXPERIMENTAL DETAILS OF LINEAR QUADRUPOLE ION TRAP MASS SPECTROMETER AND HIGH-RESOLUTION LINEAR QUADRUPOLE ION TRAP-ORBITRAP MASS SPECTROMETER**

### **2.1 Introduction**

A typical mass spectrometry (MS) experiment requires at least three steps: 1) evaporation and ionization of analyte(s); 2) separation of the gas-phase ions based on their mass-to-charge ratios ( $m/z$ ) and 3) the detection of ions and measurement of their abundances. In a mass spectrum,  $m/z$  values of the ions are shown on the x-axis and their relative abundance on the y-axis. Prior to detecting the ions, many MS experiments may be performed, including tandem mass spectrometry ( $MS^n$ ), to provide more details about the structures of unknown ions. Most tandem mass spectrometry experiments involve isolating the ion of interest and colliding it with a reagent gas (often nitrogen, helium or argon) to cause dissociation of that ion. This technique is called collision-activated dissociation (CAD). The ion of interest can also be isolated and allowed to react with a neutral molecule in an ion-molecule reaction. The experiments described in this dissertation were performed either using a linear quadrupole ion trap (LQIT) modified to allow introduction of neutral reagents into the ion trap or using a linear quadrupole ion trap coupled with an orbitrap detector (LQIT/Orbitrap). Details of each step involved in the MS experiments outlined above are discussed in the order in which they occur in an experiment, and this is followed by a discussion on collision-activated dissociation and gas-phase ion-molecule reactions.

### **2.2 Ion Generation**

Evaporation and ionization (either simultaneously or in separate steps) of the analytes constitute the first step in a mass spectrometry experiment. Previously, electron ionization<sup>1,2</sup> (EI) and chemical ionization<sup>3</sup> (CI) were the most commonly used ionization techniques. However, because these techniques only ionize gas-phase molecules, thermal heating had to be employed prior to EI or CI to evaporate analytes, limiting their use to thermally stable and volatile analytes.<sup>4</sup> Modern ionization methods have

overcome this limitation, including such methods as matrix-assisted laser desorption ionization (MALDI),<sup>5</sup> electrospray ionization (ESI),<sup>6</sup> atmospheric-pressure chemical ionization (APCI),<sup>7</sup> and atmospheric-pressure photoionization (APPI).<sup>8</sup> For this dissertation, ESI and APCI were used and are thus discussed in detail.

### 2.2.1 Electrospray Ionization

Electrospray ionization (ESI) is a soft ionization method that converts analytes in solution into gas-phase ions without significantly fragmenting them.<sup>9</sup> ESI is widely used in the mass spectrometry community due to its ability to ionize large, thermally labile, and non-volatile polar molecules.<sup>10,11</sup> The mechanism by which gas-phase ions are proposed to form from solution can be divided into three steps: 1) formation of charged droplets at the ESI capillary tip; 2) production of highly-charged nanodroplets; 3) formation of unsolvated gas-phase ions.<sup>12</sup> These three steps are illustrated in Figure 2.1 for the formation of positive ions.

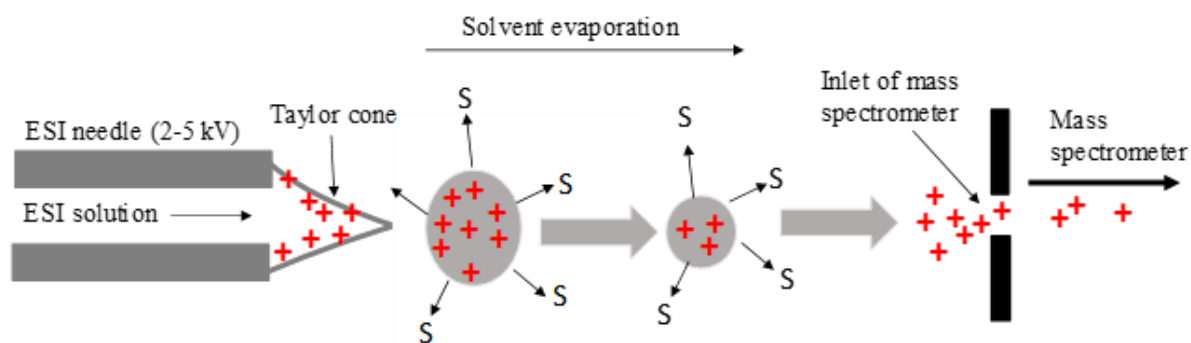


Figure 2.1 Illustration of formation of gas-phase ions upon ESI (operated in positive ion mode), where S denotes solvent molecules.

During an ESI MS experiment, the analyte is typically dissolved in water, methanol, acetonitrile or in a mixture of two of the three solvents. The analyte solution is pumped through an ESI capillary onto which a high voltage (2 – 5 kV) is applied.<sup>9</sup> The applied voltage creates an electric field at the tip of the capillary that charges the surface of the solution emerging from the capillary. The high voltage induces a

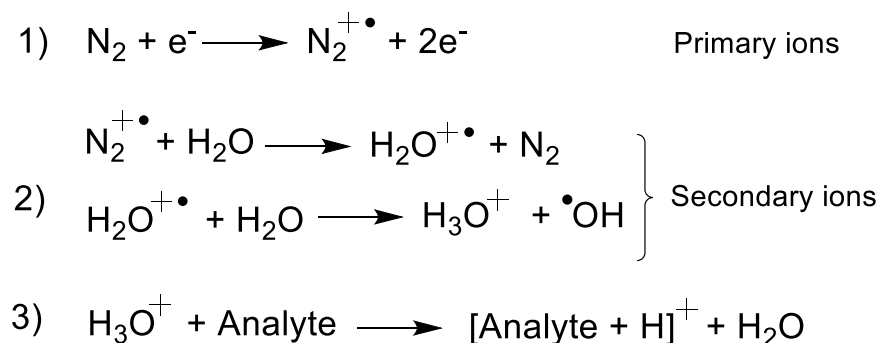
Taylor cone, which sprays a fine mist of micrometer-sized charged droplets.<sup>13,14</sup> The spraying process is assisted by a drying gas (nitrogen) which aids in both solvent nebulization and evaporation.<sup>15</sup> The droplets produced from the Taylor cone undergo solvent evaporation, causing an increase of charge density within the droplet until a critical limit, known as the Rayleigh limit, is reached.<sup>12,16</sup> At the Rayleigh limit, the droplets divide into smaller, highly charged progeny droplets via jet fission. The evaporation of the solvent and fission of the droplets is repeated many times, resulting in droplets with radii of a few nanometers.<sup>14</sup> It is believed that the gas-phase ions detected by MS are generated from these charged nanodroplets.<sup>14,17,18</sup>

The formation of gas-phase ions from charged nanodroplets is thought to occur via three different mechanisms: the charge residue model, the ion evaporation model, and the chain ejection model.<sup>14</sup> According to the charge residue model, each charged nanodroplet generated from the electrospray process contains just one analyte molecule.<sup>19</sup> As these charged nanodroplets evaporate to dryness, the charge is transferred from the droplet to the analyte, resulting in gas-phase ions.<sup>14,20</sup> This model is applied to large and multiply charged ions, including proteins.<sup>21</sup> In the ion evaporation model, the surface charge from a Rayleigh-charged nanodroplet is high enough to cause the emission of solvated ions, which evaporate into the gas phase.<sup>14</sup> This model is most applicable for small, singly charged ions.<sup>22</sup> Finally, the chain ejection model, which is mostly applied to unfolded proteins,<sup>23</sup> can be explained as follows: during an ESI experiment with unfolded proteins, the hydrophobic chains are exposed to the solvent, making unfolded proteins unfavorable in the charged droplet. The unfolded chains therefore migrate to the nanodroplet surface where they become charged and are ejected from the droplet.<sup>14,23</sup>

### 2.2.2 Atmospheric Pressure Chemical Ionization

Atmospheric pressure chemical ionization (APCI) is a relatively soft ionization method that ionizes analytes of low to medium polarities through a series of ion-molecule reactions at atmospheric pressure.<sup>7,24</sup> In a typical APCI MS experiment, the analyte (in a solution) is passed through a heated silica capillary where it is nebulized by a drying gas (typically nitrogen), creating a spray of droplets. The heat

transferred to these droplets vaporizes the solvent and the analyte, which are then carried by the nebulizer gas to a corona discharge needle where the ionization occurs.<sup>25</sup> A high voltage (2 – 5 kV) is applied to the corona discharge needle. It is hypothesized that the ionization of the analyte molecules occurs in three steps, which are shown in Scheme 2.1. In the first step, the corona discharge needle ionizes the nebulizer gas to form primary ions. Second, the primary ions then react with the gas-phase solvent molecules to produce solvent ions. In the final step, the solvent ions react with the analyte molecules to produce analyte ions. In this dissertation, 50:50 water:methanol and pure acetonitrile were used as the solvents in Chapters 3 and 4, respectively. Carbon disulfide, hexane, and 75:25 hexane:methanol were also used as the solvents and APCI reagents in Chapter 5.



Scheme 2.1 Proposed mechanism for the generation of protonated analytes in positive ion mode APCI when using water as the solvent and APCI reagent and N<sub>2</sub> as the nebulizer gas.

### 2.3 Linear Quadrupole Ion Trap (LQIT) Mass Spectrometer

A Thermo Linear Quadrupole Ion Trap (Thermo LTQ) coupled with an orbitrap detector (LQIT/orbitrap) and a modified Thermo LTQ equipped with an external reagent mixing manifold were used in this dissertation. Both instruments are discussed in this chapter. The LQIT MS can be divided into three differentially-pumped regions: the atmospheric-pressure ionization (API) region, the ion optics region, and the linear quadrupole ion trap and ion detection region. A schematic of the LQIT MS is shown in Figure 2.2.



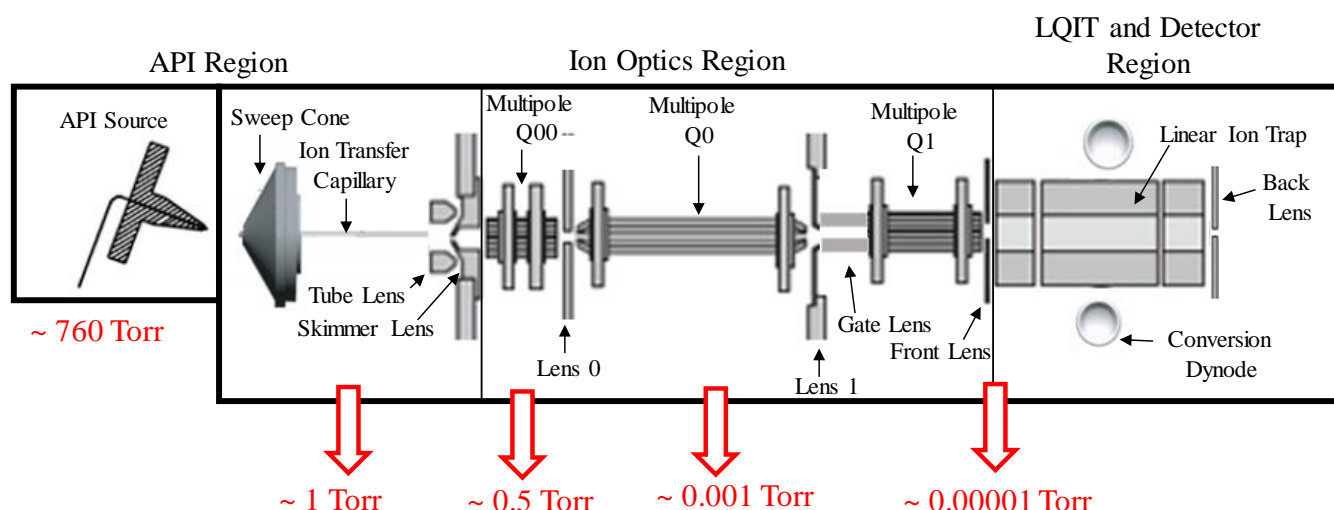


Figure 2.2 The overall LQIT MS configuration along with typical operating pressures.

### 2.3.1 The API Region

The API region consists of the ion source box, held at 760 Torr, and the API stack region, held at about one Torr. The low pressure in the API stack is achieved with two Edwards E2M30 mechanical pumps, each with an evacuation rate of 650 L/min.<sup>26</sup> The ion source box houses the ionization source (typically ESI, APCI or APPI), a corona discharge needle, and a sweep cone. The API stack region consists of an ion transfer capillary, a tube lens, and a skimmer lens.<sup>26</sup> When ions are generated in the ion source box region (as discussed in section 2.2), they are pulled into the API stack region through the ion transfer capillary. The pulling of the ion beam is due to a pressure gradient (760 Torr to one Torr) and a direct current (DC) voltage gradient (2 – 5 kV to 0 – 20 V) between the ion source and the API stack, respectively. The ion transfer capillary is kept at a temperature of 50-350 °C to aid in solvent evaporation, and a DC voltage is also applied to this capillary to cause ion transmission towards the tube lens. A DC voltage (10 – 130 V) is also applied to the tube lens to guide the ion beam to the off-centered orifice of the skimmer lens, preventing neutral molecules from continuing through.<sup>26</sup> When the mass spectrometer is operated in negative ion mode, a negative potential is applied to both the ion transfer capillary and the tube lens.

### 2.3.2 The Ion Optics Region

After the skimmer lens, the ions enter the optics region, which focuses them toward the linear quadrupole ion trap. The ion optics consist of three differentially pumped multipoles: two quadrupoles (Q00 and Q0) and an octupole (Q1), Figure 2.2.<sup>26</sup> The different pressures in these multipoles are achieved with a Leybold T220/150/15S triple-inlet turbomolecular pump. The Q00, Q0, and Q1 regions are pumped at rates of 1,500 L/min, 18,000 L/min, and 24,000 L/min, respectively, generating a vacuum of  $\sim 0.5$  Torr,  $\sim 0.001$  Torr, and 0.00001 Torr, respectively. Between each multipole, a lens acts as a vacuum baffle. All three of these multipoles function in a similar manner. For instance, when ions enter Q00 from the skimmer, a radio frequency (RF) voltage of the same amplitude and phase is applied to opposing rods of the quadrupole; however, this voltage is  $180^\circ$  out of phase on the adjacent rods, generating an electric field that causes the ions to have stable circular trajectories in the x- and y-directions (radial direction) while inside the quadrupole.<sup>26</sup> Further, a DC offset potential is applied to the quadrupole to drive the ions through the quadrupole in the z-direction along the length of the quadrupole. During ion transmission, the applied offset voltage is attractive (i.e. negative for positive ions and positive for negative ions). Typical values for the DC offset voltages applied to each element are shown in Figure 2.4 for positive ions.<sup>26</sup>

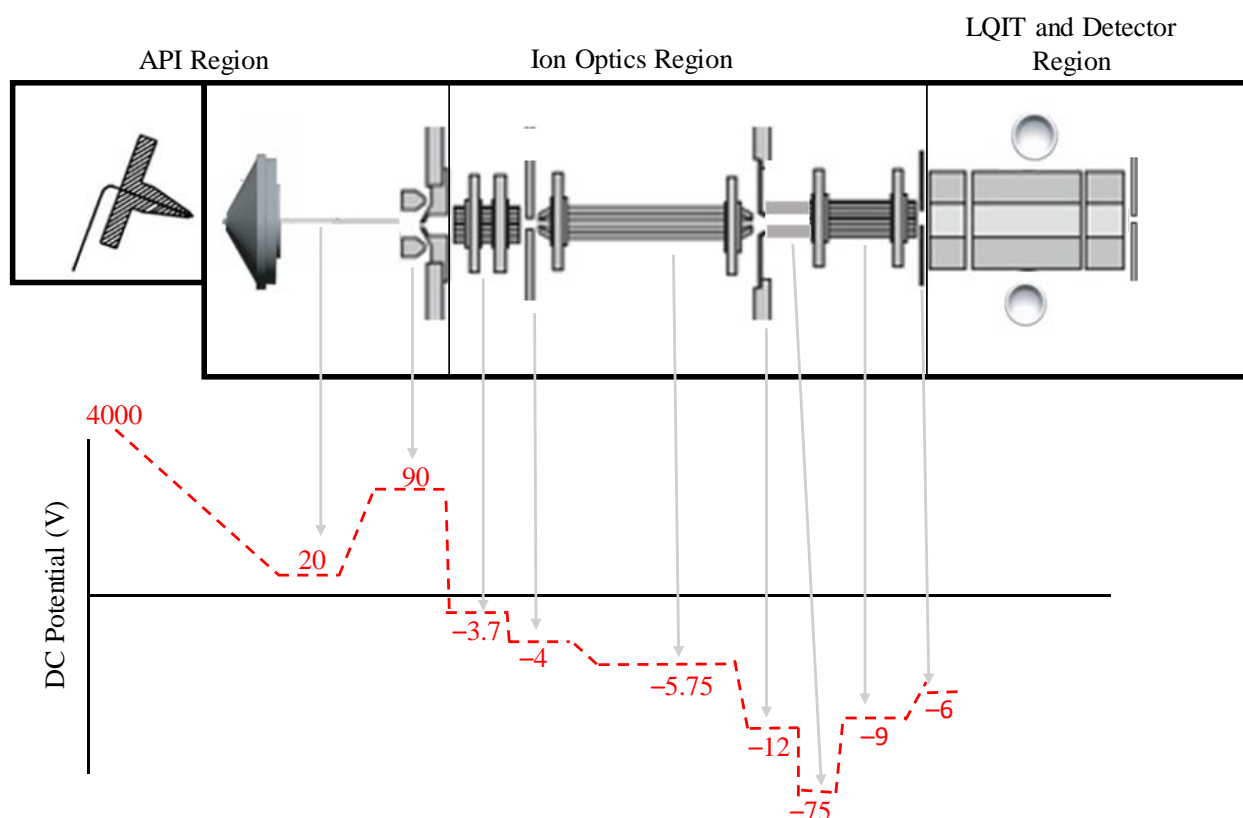


Figure 2.3 DC offset voltage gradient (V) applied to the elements of the API stack and ion optics to aid in transmission of positive ions in the z-direction.

### 2.3.3 The LQIT and Detector Region

The linear quadrupole ion trap consists of four parallel hyperbolic rods that are divided into three sections: front, center and back. In each section, the rods that are opposite each other are electrically connected.<sup>27,28</sup> The two center rods, referred to as exit rods, contain slits that allow the ejection of ions into the detector (Figure 2.4). The main functions of the ion trap are to store (trap) ions and eventually to perform mass analysis by ejecting them in a mass-selective manner into the detector. The ions are trapped in the radial direction by applying an RF voltage of the same amplitude and sign to a pair of rods that are opposite of each other and an RF voltage of the same amplitude but opposite sign to the other, adjacent pair of the rods. To trap the ions in the axial direction, DC voltages are applied to the rods. A supplemental

RF potential can also be applied to the exit rods to aid in ion excitation, isolation, and ejection.<sup>27</sup> The physics underlying the ion trapping, ejection, etc. are described next.

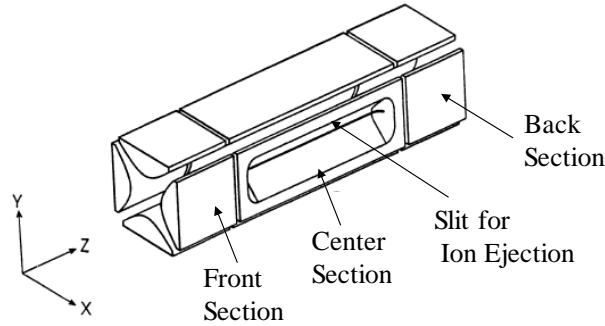


Figure 2. 4 A schematic of the trapping regions of the LQIT mass analyzer.

#### 2.3.3.1 Ion Radial Motion

A combination of RF and DC voltages applied to the four rods of the quadrupole ion trap results in a two-dimensional quadrupolar RF-field,  $\Phi_0$ , that confines the ions in the radial direction.<sup>27,28</sup> This field,  $\Phi_0$ , is described by Equation 2.1,

$$\pm\Phi_0 = \pm(U - V\cos\Omega t) \quad \text{Equation 2.1}$$

where  $U$  is the amplitude of the DC voltage and  $V$  is the amplitude of the RF voltage with an angular frequency  $\Omega$  applied continuously for time  $t$  to the x- and y-rods. Based on Equation 2.1, the electric potentials in the x- and y-directions,  $\Phi_{xy}$ , can be described by Equation 2.2,

$$\Phi_{xy} = \frac{\Phi_0(x^2 - y^2)}{r_0^2} = \frac{(U - V\cos\Omega t)(x^2 - y^2)}{r_0^2} \quad \text{Equation 2.2}$$

where  $r_0$  is the radius of the circle confined within the quadrupole rods. Additionally, the ions experience forces,  $F_x$  and  $F_y$ , in the x- and y-directions, respectively. The forces  $F_x$  and  $F_y$  are described by Equations 2.3 and 2.4, respectively,

$$F_x = m \frac{d^2x}{dt^2} = -ze \frac{d\Phi}{dx} \quad \text{Equation 2.3}$$

$$F_y = m \frac{d^2 y}{dt^2} = -ze \frac{d\Phi}{dy} \quad \text{Equation 2.4}$$

where  $m$  is the mass of the ion,  $z$  is the number of charges and  $e$  is the elementary charge ( $1.602 \times 10^{-19}$  Coulombs). Combining Equation 2.1 with Equations 2.3 and 2.4 gives rise to Equations 2.5 and 2.6 for ion motion in the x- and y-directions, respectively.

$$\frac{d^2 x}{dt^2} + \frac{2ze}{mr_0^2} (U - V \cos \Omega t) x = 0 \quad \text{Equation 2.5}$$

$$\frac{d^2 y}{dt^2} + \frac{2ze}{mr_0^2} (U - V \cos \Omega t) y = 0 \quad \text{Equation 2.6}$$

Equations 2.5 and 2.6 are similar to the Mathieu equation (Equation 2.7) that describes ion trajectory and the stability of the ion's trajectory in the ion trap,<sup>29,30</sup>

$$\frac{d^2 u}{d\xi^2} + (a_u - 2q_u \cos 2\xi) u = 0 \quad \text{Equation 2.7}$$

where  $\xi$ ,  $a_u$ , and  $q_u$  are variables that are expressed by the following equations,

$$\xi = \frac{\Omega t}{2} \quad \text{Equation 2.8}$$

$$a_u = a_x = -a_y = \frac{8zeU}{mr_0^2 \Omega^2} \quad \text{Equation 2.9}$$

$$q_u = q_x = -q_y = \frac{4zeV}{mr_0^2 \Omega^2} \quad \text{Equation 2.10}$$

wherein  $a_x$ ,  $q_x$ ,  $a_y$ , and  $q_y$  are parameters that describe ion motion in the x- and y-directions, respectively.

These parameters are the same as  $a_u$  and  $q_u$ , known as the Mathieu stability parameters. Solutions to the Mathieu equation are plotted on a diagram known as the Mathieu stability diagram with the values of  $q_u$

as the x-axis and the values of  $a_u$  as the y-axis. Because the motion of the ions in the x-direction and in the y-direction are independent of each other,<sup>27</sup> trapped ions are those with stable trajectories in both the x- and y-directions. Figure 2.5 shows a simplified Mathieu stability diagram illustrating regions in which ions have stable and unstable trajectories. According to Equations 2.9 and 2.10,  $a_u$  and  $q_u$  values are related to the ions'  $m/z$  values. As shown in Figure 2.5, ions with a  $a_u$  value of 0 and a  $q_u$  value between 0 and 0.908 are confined in the stable region of the Mathieu stability diagram; therefore they are trapped.

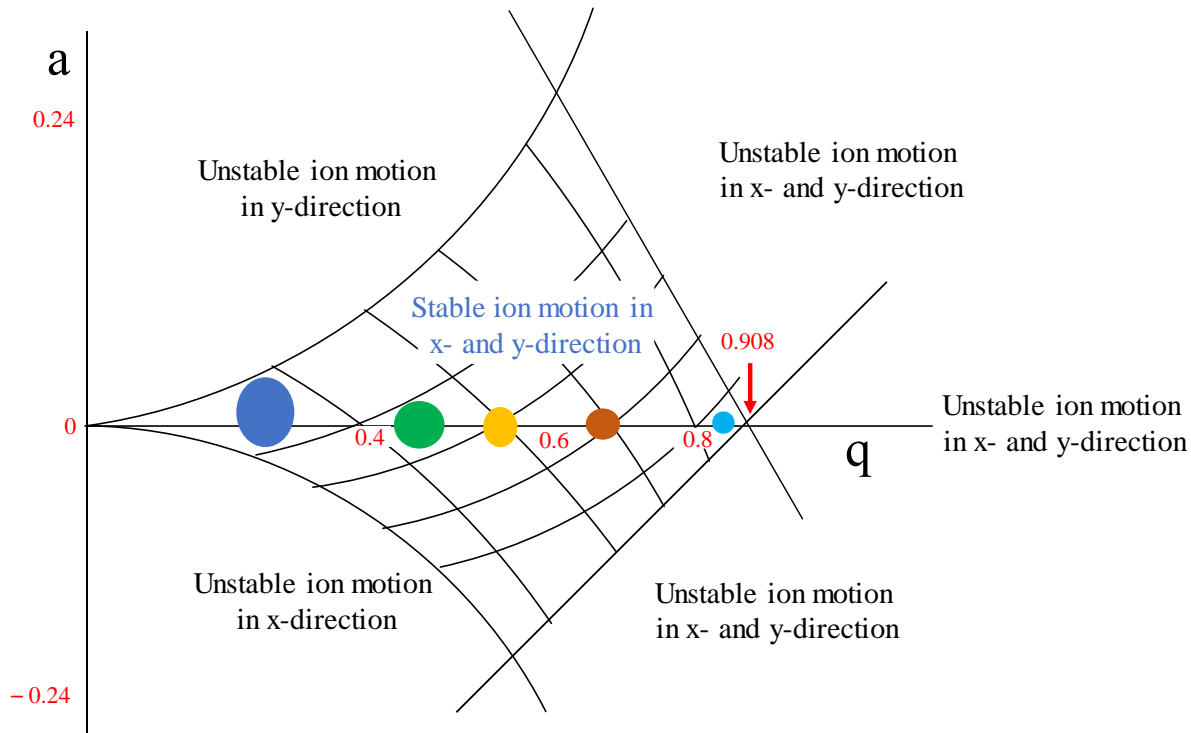


Figure 2.5 The Mathieu stability diagram. Ions of different  $m/z$  values whose  $a$  and  $q$  values locate them inside the diagram (shown as colored circles with larger circles being ions of larger  $m/z$ ) have stable trajectories within the x- and y-directions of the LQIT.

### 2.3.3.2 Ion Axial Motion

The LQIT uses three different DC voltages, each applied to a different section of the quadrupole ion trap (front, center, and back; Figure 2.4), that establish axial (z-direction) motion of the ions.<sup>27,28</sup> The DC voltage applied to the center section is lower than that applied to the front and back sections. This creates a potential well that restricts the ion motion in the z-direction into the center section (Figure 2.6). The typical DC voltages applied to the front, center, and back sections during ion trapping are  $-9$ ,  $-12$ ,

and  $-7$  V, respectively, for positive ions. For negative ions, only the polarity of the DC voltage is reversed. To enhance ion trapping efficiency, helium ( $\sim 10^{-3}$  Torr) is added to kinetically cool ions via multiple low-energy collisions, which confine them into the center of the ion trap as a tight packet.<sup>31</sup>

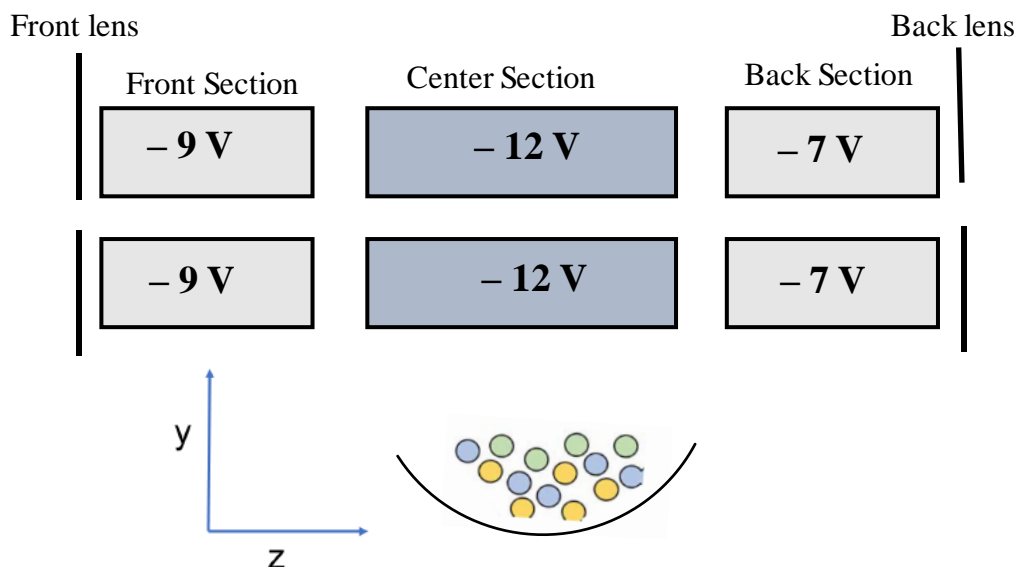


Figure 2.6 A schematic of LQIT with typical DC voltages applied to the different sections of the quadrupole ion trap of LQIT. A lower potential is applied to the center section and a higher potential to the front and the back sections, resulting in a potential well that confines ions in the center section in the  $z$ -direction. The colored circles represent ions trapped in the potential energy well.

### 2.3.3.3 Ion Ejection

Two methods are generally employed to eject ions from the ion trap for detection: axial instability scan and x-electrode bipolar resonance ejection.<sup>32</sup> In the axial instability scan, the  $q$  value of the ion is increased to 0.908 by increasing the RF amplitude. At  $q = 0.908$ , ions no longer have a stable motion in the  $x$ -direction. Consequently, they are ejected through the slits of the exit electrodes ( $x$ -electrodes). With this ejection method, however, some ions do not reach the detector, which compromises the sensitivity.<sup>32</sup> On the other hand, with x-electrode bipolar resonance ejection, the  $q$  value of the ions is increased to 0.88 by increasing the RF amplitude. In addition, a supplementary RF voltage is applied to the  $x$ -electrodes. At  $q = 0.88$ , the supplementary RF voltage is in resonance with the oscillation frequency of the ions,

which increases their kinetic energy and the oscillation amplitude to such an extent that most of the ions are ejected from the ion trap through the slits.<sup>32,33</sup>

#### 2.3.3.4 Ion Detection with Electron Multipliers

The LQIT is equipped with a two-component, off-axis ion detection system located on opposite sides of the linear quadrupole ion trap. Each ion detection system consists of a charged conversion dynode and a funnel-shaped electron multiplier. A +15 kV potential is applied to the conversion dynode for negative ions and a -15 kV potential for positive ions via a high voltage ring (Figure 2.7).<sup>26</sup> When ions are ejected from the ion trap for detection, they strike the surface of the charged conversion dynode, producing secondary particles.<sup>34</sup> The secondary particles include negative ions and electrons when positive ions strike the negatively charged conversion dynode and positive ions when negative ions strike the positively charged conversion dynode. These secondary particles are accelerated into the electron multiplier by a voltage gradient between the conversion dynode and the electron multiplier.<sup>34</sup> The electron multiplier consists of a cathode and an anode. When the secondary particles strike the walls of the electron multiplier cathode, they generate electrons. Due to the funnel-like shape of the cathode, the generated electrons collide with the surface of the cathode multiple times before they exit the cathode, thereby causing the emission of more electrons. This cascade of electrons eventually results in a measurable electric current at the anode, where the electrons are collected. The amplitude of the measured electric current for ejected ions is proportional to their abundance. The  $m/z$  values of the ions are obtained by scanning the RF voltage (Equation 2.10). Therefore, by relating the amplitude of the measured current and the timing of the ejection event during the RF voltage scan, a mass spectrum is obtained with the  $m/z$  values of the ions as the x-axis and the relative abundance of the ions as the y-axis.



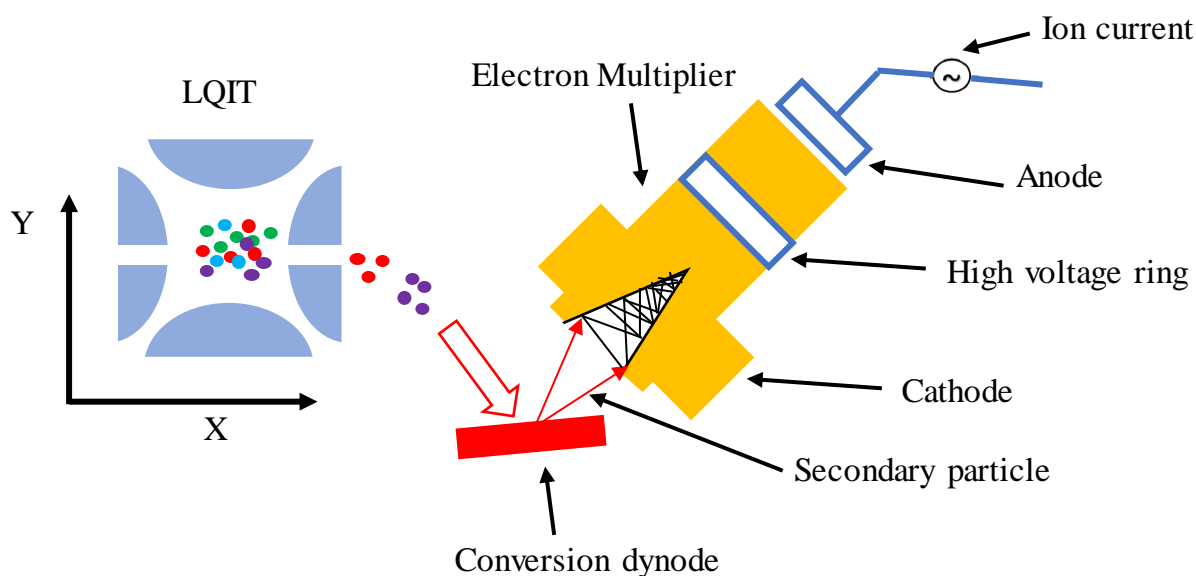


Figure 2.7 LQIT and its ion detection system, which consists of two conversion dynodes and two electron multipliers. Only one conversion dynode and one electron multiplier are shown in this figure.

## 2.4 Multi-Stage Tandem Mass Spectrometry ( $MS^n$ )

In multi-stage tandem mass spectrometry ( $MS^n$ ), multiple ion isolation/mass analysis events are performed.  $MS^n$  is particularly useful for identifying unknown compounds.<sup>33,35</sup> The simplest  $MS^n$  ( $MS^2$ ) experiments are performed by isolating the ions of interest, subjecting them to reactions, and detecting the product ions. The product ions can then be isolated and subjected to further reactions (in  $MS^3$  experiments). The reactions discussed in this chapter are collision-activated dissociation (CAD) reactions and gas-phase ion-molecule reactions.

### 2.4.1 Ion Isolation

Isolating the ions of interest occurs in two steps. First, the RF voltage applied to the x-rods of the linear quadrupole ion trap is increased, thus increasing the  $q$  value of the ions of interest until it reaches a value of 0.803.<sup>26</sup> At this point, the majority of ions with  $m/z$  values lower than that of the ions of the interest are ejected from the ion trap. Second, a broad-band excitation waveform is applied to the x-rods to eject unwanted ions.<sup>26</sup> This broad-band excitation waveform is an alternating current (AC) voltage that consists of a distribution of resonance frequencies (5 – 600 kHz) of all ions with the exception of the

frequency of the ions of interest.<sup>26</sup> Therefore, by applying the RF voltage followed by the broad-band excitation waveform to the x- rods, all unwanted ions are ejected from the ion trap (Figure 2.8).<sup>26</sup>

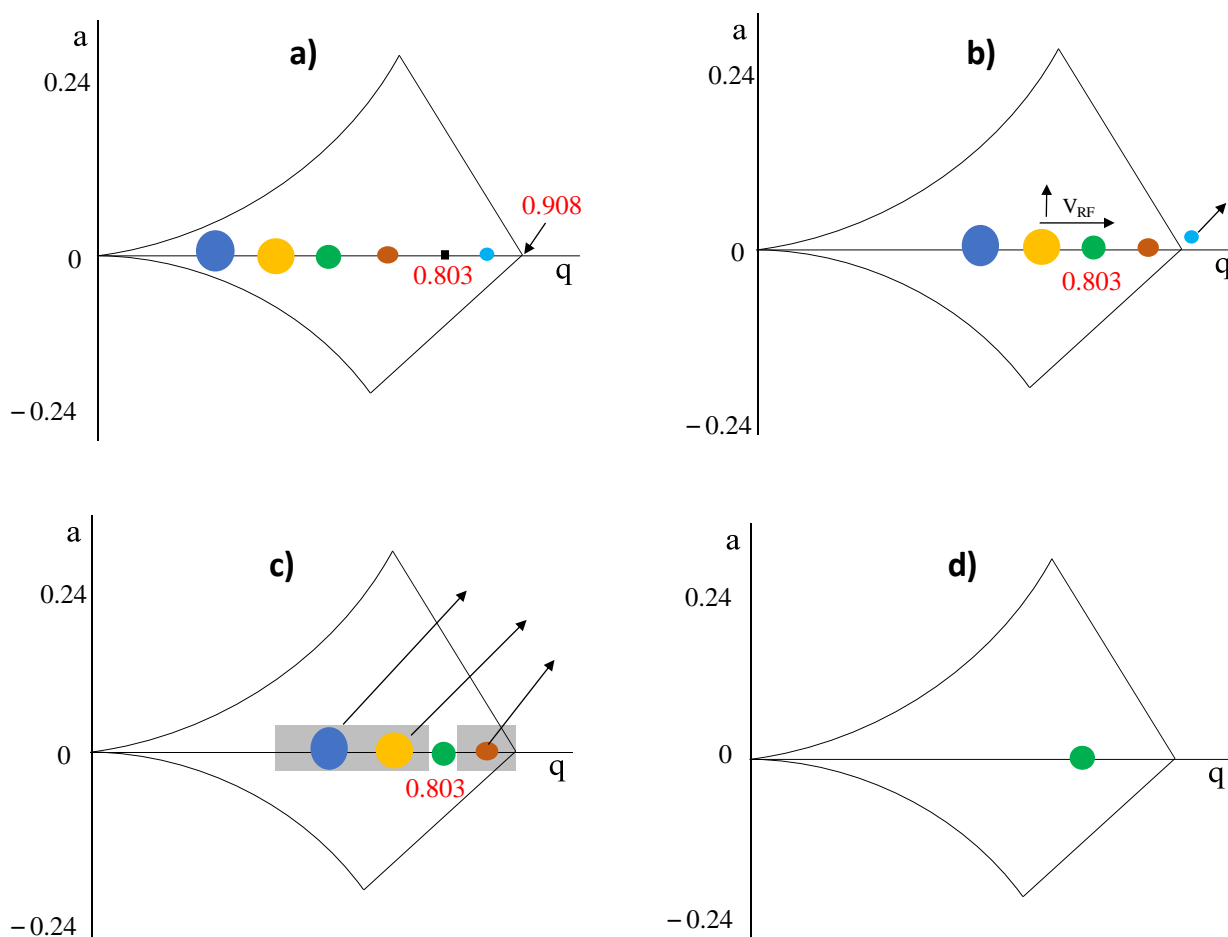


Figure 2.8 Ion isolation process. a) All ions are confined in the ion trap. b) RF voltage amplitude (denoted as  $V_{RF}$ ) is increased to place the ions of interest (green circle) to  $q = 0.803$  to eject some ions with  $m/z$  values lower than that of the ions of interest. c) The broad-band excitation waveform is applied to eject the remaining unwanted ions. d) Only the ions of interest remain in the ion trap.

#### 2.4.2 Collision-activated Dissociation (CAD)

CAD experiments in the LQIT first involve isolating the ions of interest (as discussed in section 2.4.1). The isolated ions are then accelerated and subjected to multiple low-energy collisions with the helium buffer gas present in the ion trap, thereby causing fragmentation of the ions.<sup>36,37</sup> The generated product ions are then mass analyzed. After the ions of interest have been isolated, the RF amplitude is decreased, thereby decreasing the  $q$  value of the ions of interest to  $q \sim 0.25$  (the reasoning behind choosing

this value will be discussed later). Next, the ions are accelerated by applying a supplementary RF voltage, referred to as a dipolar resonance excitation (tickle voltage), to the x-roads for a specified period of time (typically 30 ms). The dipolar resonance excitation increases the ions' kinetic energies without ejecting them from the ion trap. The accelerated ions collide with the helium buffer gas multiple times, which causes part of the ions' kinetic energy to be converted into their internal energy. This process continues until the ions have gained enough internal energy to overcome their fragmentation threshold. At this point, the ions fragment and the resulting fragment ions are mass analyzed.

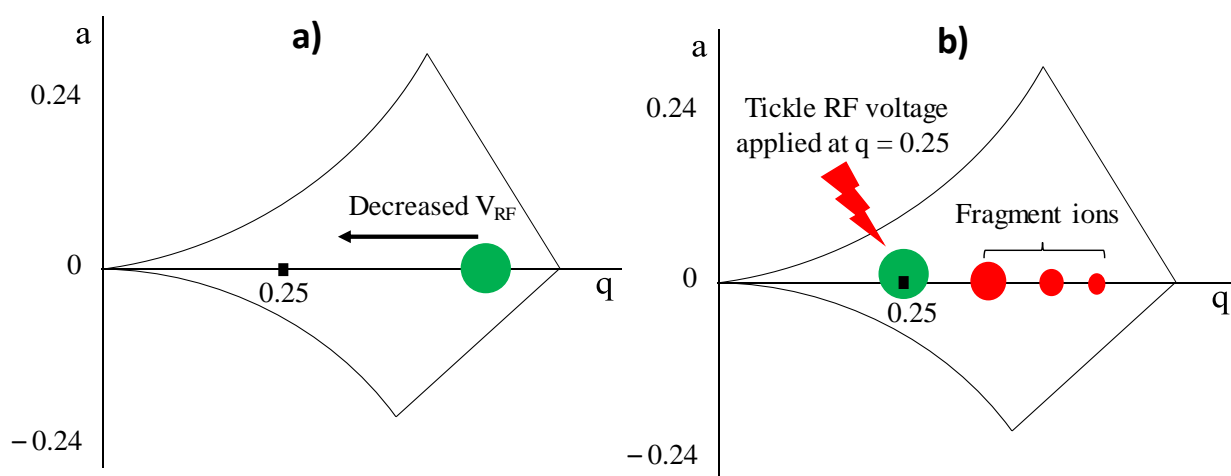


Figure 2.9 Schematics of the CAD process. a) The RF voltage amplitude (denoted as  $V_{RF}$ ) is decreased to lower the  $q$  value of the ions of interest to 0.25. b) The dipolar resonance excitation (tickle voltage) is applied to the x-roads to increase the ions' kinetic energy, which is converted into internal energy when the ions collide with helium. When the internal is higher than the lowest barrier for fragmentation, the ions fragment.

It should be noted that the  $q$  value chosen for CAD experiments is important because it determines the low mass cut-off of the fragment ions that have stable trajectories in the linear quadrupole ion trap. As discussed in section 2.3.3.1, ions with smaller  $m/z$  values have higher  $q$  values; therefore, depending on the  $q$  value of the fragmenting ions, very small fragment ions may or may not have stable trajectories. Ideally, the fragmenting ions should have low  $q$  values so that the smallest fragment ions have stable trajectories. However, at lower  $q$  values, the fragmenting ions have lower kinetic energies, which may not

be high enough to cause fragmentation. On the other hand, if the fragmenting ions have a higher  $q$  value, the smallest fragment ions may not be observed in the mass spectrum. For instance, for parent ions with  $q$  value of 0.25, the smallest fragment ions with stable trajectories have a  $m/z$  value that is  $1/4$  of the  $m/z$  value of the fragmenting ion.

### 2.4.3 Gas-phase Ion-molecule Reactions

The use of gas-phase ion-molecule reactions for determining the structures of unknown compounds is an alternative mass spectrometry method that addresses some of the limitations of CAD.<sup>38</sup> For instance, gas-phase ion-molecule reactions can often be used to differentiate isomeric ions without reference compounds<sup>39,40</sup> while CAD mass spectra of isomeric ions are sometimes identical or uninformative and usually require comparisons to authentic compounds.<sup>40</sup>

In gas-phase ion-molecule reaction experiments, ions are isolated in the linear quadrupole ion trap as discussed in section 2.4.1 and allowed to react with a neutral reagent for a user-defined period of time. The product ions are then mass analyzed. The product ions can also be isolated and subjected to CAD in MS<sup>3</sup> experiments, if further information is required. The ion-molecule reactions reported in this dissertation were performed by using a modified Thermo LQIT equipped with an external reagent mixing manifold that introduces neutral reagents into the ion trap, which will be discussed in the following section.

#### 2.4.3.1 Introduction of Neutral Reagents into the Ion Trap

The initial design for the external reagent mixing manifold was developed by Gronert et al.<sup>41,42</sup> The manifold setup used for the experiments discussed in this dissertation is shown in Figure 2.10. In a normal LQIT setup, helium is introduced into the ion trap via the helium line. However, with the manifold, a reagent is continuously introduced into the helium line prior to entering the ion trap via a syringe pump used at a flow rate of 3 – 10  $\mu\text{L/h}$ . The syringe port and surrounding areas are heated to 150 °C to ensure complete evaporation of the reagent. The amount of helium and reagent mixture entering the ion trap is

controlled through a leak valve to maintain a pressure close to the normal operating pressure of the instrument ( $(0.65 - 0.80) \times 10^{-5}$  Torr). A gas flow regulator is also used to allow part of the mixture to be directed to waste prior to passing through the leak valve. The reagent mixing manifold is also connected to a rough pump, which aids in removing neutral reagent that may still be present in the helium line after the experiments.

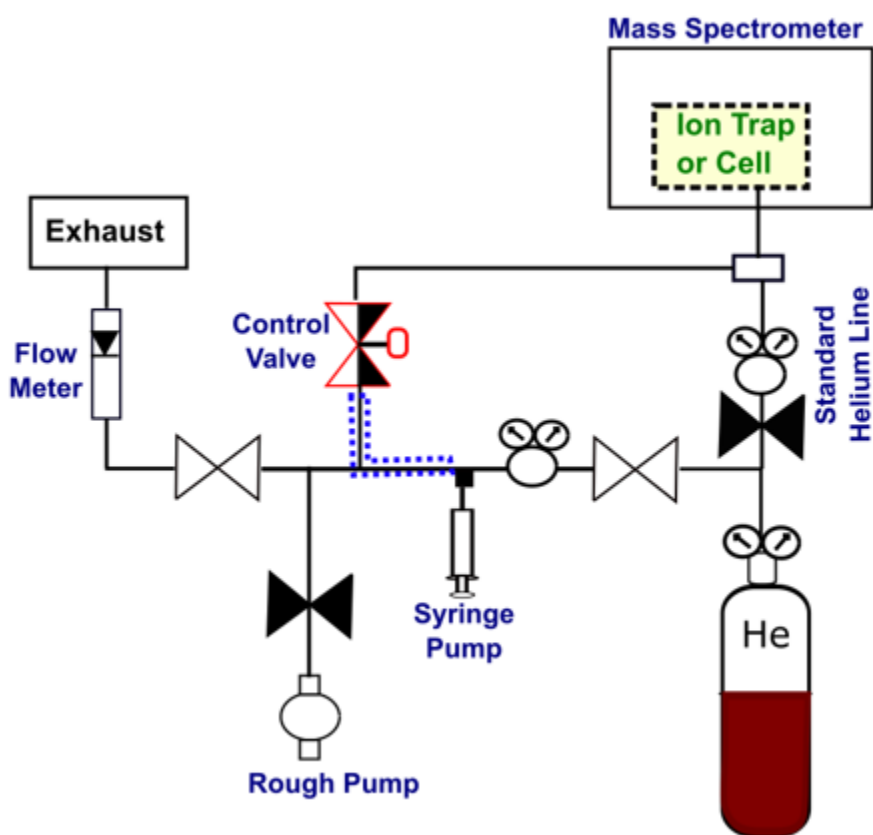


Figure 2.10 A schematic of the reagent mixing manifold employed to introduce neutral reagents into the ion trap via the helium gas line.

#### 2.4.3.2 Fundamental Aspects of Gas-phase Ion-molecule Reactions

The Brauman double-well potential energy surface provides a model to rationalize the energetics of gas-phase ion-molecule reactions.<sup>43,44</sup> An example of a potential energy surface generated according to this model is shown in Figure 2.11. According to this model, when an ion collides with a neutral molecule in the gas phase, they form a reactant complex. The potential energy of this reactant complex is lower than that of the separated reactants due to the solvation of the ion by the neutral molecule.<sup>43,44</sup> This

complex can dissociate back to the separated reactants or proceed to form the product complex, which then dissociates to form the separated products. In many cases, the reactant complex must overcome a reaction barrier (transition state) to form the product complex. The solvation energy may allow the reactant complex to overcome the reaction barrier. Hence, the height of the barrier dictates whether the reactant complex forms the products because the energy of a system in a vacuum is conserved. The reaction can only proceed to products when the magnitude of the barrier is less than the total energy of the system.<sup>43</sup> Additionally, the separated products must have equal or lower energy than the separated reactants (i.e., the reactions must be thermoneutral or exothermic). Furthermore, overcoming the transition state does not necessarily mean that the reaction will take place. This can be explained by entropy constraints.<sup>43</sup> For instance, if the reactant complex has a tight transition state to proceed to products, meaning that the reactant complex has fewer ways (low entropy) than the product complex, the reaction may not occur even if the reactant complex has enough energy to overcome the transition state.

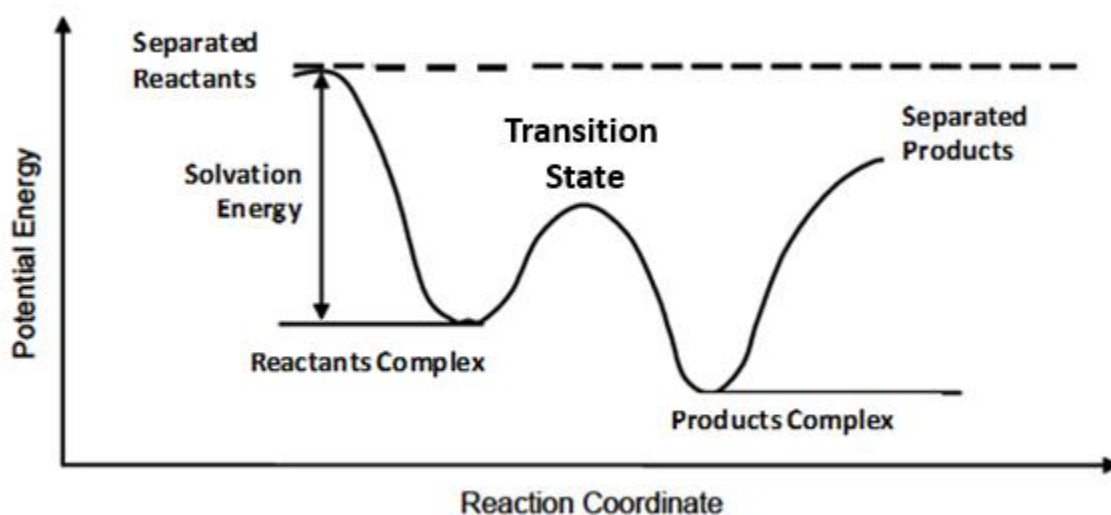


Figure 2.11 The Brauman double-well potential energy surface model for gas-phase ion-molecule reactions.

## 2.5 Linear Quadrupole Ion Trap-Orbitrap (LQIT-orbitrap) Mass Spectrometer

The LQIT-orbitrap mass spectrometer employed in the experiments discussed in this dissertation is a high-resolution Thermo LTQ/Orbitrap XL instrument. A schematic of this instrument is shown in

Figure 2.12. The LQIT-orbitrap can either detect ions in the LQIT (as described above) or in the orbitrap, which can perform high-resolution measurements. When the orbitrap is employed for detection, ions must first be injected into the C-trap that forms a tight ion packet and transfers it into the orbitrap.<sup>45</sup> The orbitrap measures the image current of the ions, which is converted into  $m/z$  values of the ions and their relative abundances, to produce a high-resolution mass spectrum.<sup>45</sup> Both the injection and the detection of the ions in the orbitrap are discussed below.

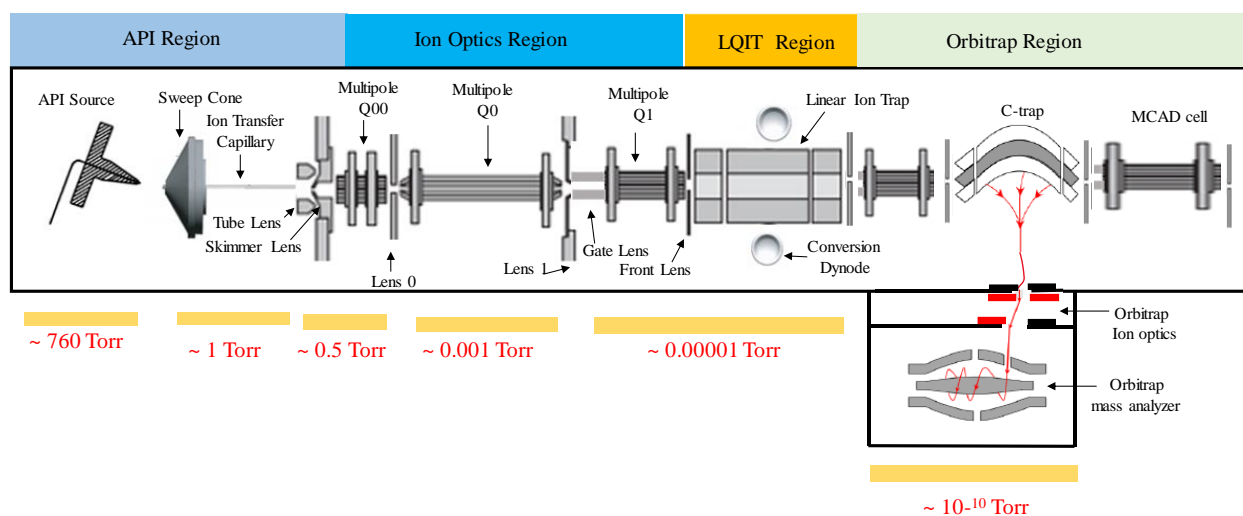


Figure 2.12 Schematic of the LQIT-orbitrap along with the typical operating pressures.

### 2.5.1 Ion Injection into the Orbitrap

In LQIT-orbitrap experiments, ions generated in the API source pass through the ion optics into the linear quadrupole ion trap, where they may be allowed to undergo reactions. Then they are transferred into the C-trap via a transfer octapole. The C-trap is filled with nitrogen gas, which kinetically cools the ions via collisions.<sup>45</sup> A high DC voltage is applied to the C-trap to collect the ions into the center for injection as a tight ion packet into the orbitrap. The ions are injected at high kinetic energy into the orbitrap off-center such that they start moving around (radially) and along (axially) the spindle electrode of the orbitrap. The axial ion motion has a frequency that is related to the  $m/z$  value of the ion.<sup>46</sup>

### 2.5.2 Ion Motion into the Orbitrap

The orbitrap is composed of two electrodes: an inner “spindle” electrode and an outer “barrel-like” electrode. A DC potential is applied between the two electrodes, resulting in a three-dimensional electrostatic field,  $U$ ,<sup>45,47</sup> described by Equation 2.11

$$U(r, z) = \frac{k}{2}(z^2 - r^2) + \frac{k}{2}(R_m)^2 \ln \left[ \frac{r}{R_m} \right] + C \quad \text{Equation 2.111}$$

where  $r$  and  $z$  are the angular and axial coordinates of the field, respectively,  $k$  is a constant related to the field curvature,  $R_m$  is the characteristic radius of ion motion, and  $C$  is a constant.

When ions enter the orbitrap’s electrostatic field, they experience three types of motion, each with a unique frequency: rotational motion around the inner electrode ( $\omega_\phi$ ), radial motion ( $\omega_r$ ) and oscillation motion along the axial direction ( $\omega_z$ ).<sup>45,47</sup> These motions can be expressed by the following equations for an ion of mass  $m$  and charge  $q$ .

$$\frac{\partial^2 r}{\partial t^2} - \left( \frac{\partial \phi}{\partial t} \right)^2 = - \frac{q}{m} \frac{k}{2} \left[ \frac{R_m^2}{r} - r \right] \quad \text{Equation 2.12}$$

$$\frac{d}{dt} \left( r^2 \frac{\partial \phi}{\partial t} \right) = 0 \quad \text{Equation 2.13}$$

$$\frac{\partial^2 z}{\partial t^2} = -kz \frac{q}{m} \quad \text{Equation 2.14}$$

Based on the above equations of ion motions  $\phi$ -,  $r$ -, and  $z$ -, only the frequency of the axial motion ( $z$ -direction) is independent of the position and energy of the ions. This frequency is therefore used to determine ion  $m/z$  values. The axial frequency is shown in Equation 2.15

$$\omega = \sqrt{\left( \frac{q}{m} \right) k} \quad \text{Equation 2.15}$$

where  $m$  and  $q$  are the mass and the charge and of the ion, respectively, and  $k$  is a constant that is related to the DC voltage applied between the inner and outer electrodes.



### 2.5.3 Ion detection in the Orbitrap

As discussed above, only the frequencies of the ions in the axial direction are used to determine the  $m/z$  values of the ions and their relative abundances. Detection is thus achieved by measuring the image current caused by the ions' axial motion. The measured image current is amplified and Fourier transformed to obtain the  $m/z$  values of the ions and the corresponding relative abundances.<sup>48</sup>

### 2.5.4 Ion source CAD (ISCAD)

In ion-source CAD (ISCAD), all ions formed in the ion source are subjected to collisions in the ion optics region.<sup>49</sup> The ISCAD experiments discussed in this dissertation were performed using the LQIT-orbitrap. During ISCAD experiments, ions are accelerated in the ion optics by increasing the DC voltage applied to the multipoles and gate lenses of the ion optics (Figure 2.13). The accelerated ions collide with atmospheric atoms and molecules in the ion optics, inducing fragmentation. The fragment ions are transferred into the mass analyzer for detection. It is worth noting here that ISCAD experiments do not require isolation of the ions.

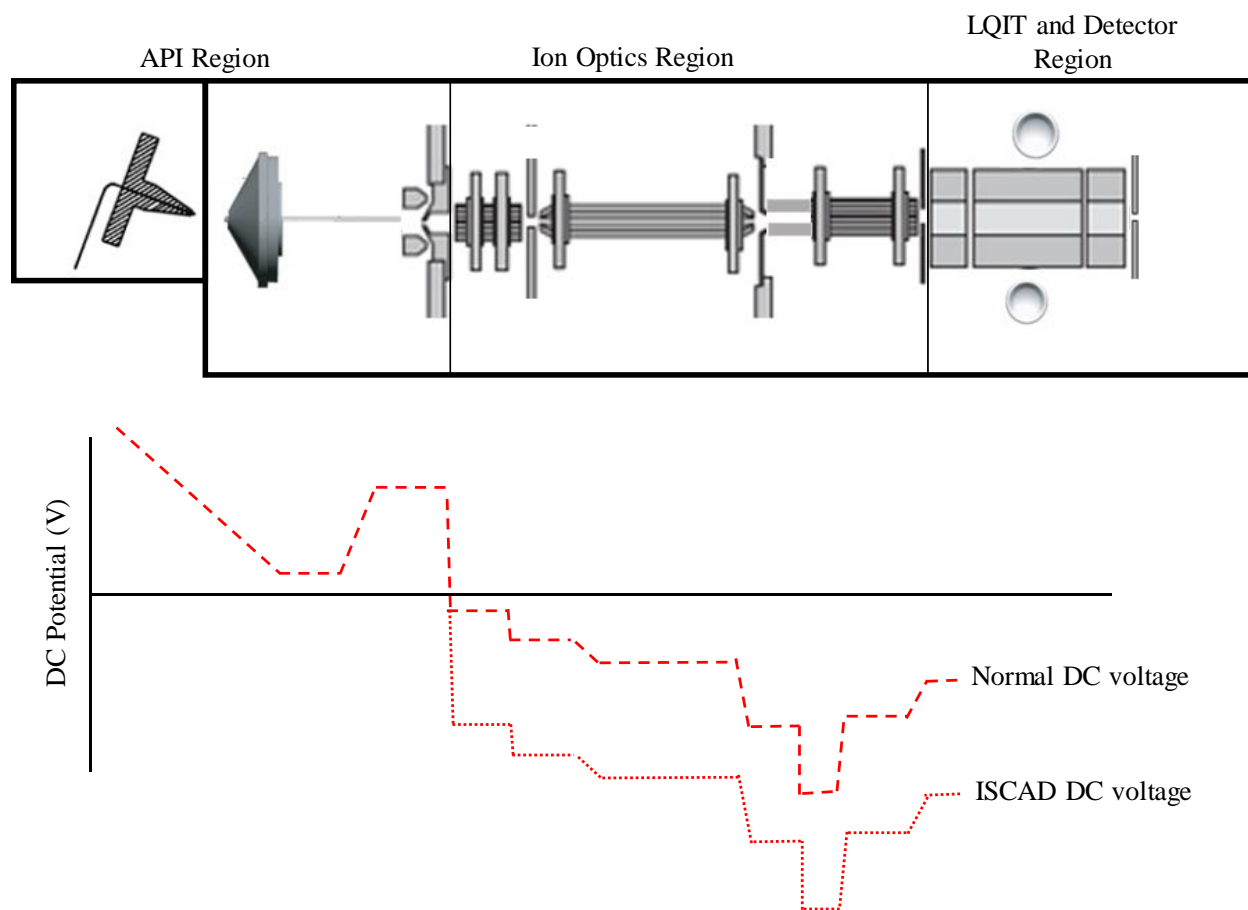


Figure 2.13 DC offset voltage gradient (V) applied to the elements of the API stack and ion optics to aid in transmission of positive ions in the z-direction during normal mass spectrometric experiments and during ISCAD experiments.

## 2.6 References

- (1) Dempster, A. J. Positive Ray Analysis of Lithium and Magnesium. *Phys. Rev.* **1921**, *18* (6), 415.
- (2) Nier, A. O. A Mass Spectrometer for Isotope and Gas Analysis. *Rev. Sci. Instrum.* **1947**, *18* (6), 398–411.
- (3) Munson, M. S.; Field, F.-H. Chemical Ionization Mass Spectrometry. I. General Introduction. *J. Am. Chem. Soc.* **1966**, *88* (12), 2621–2630.
- (4) Vestal, M. L. Methods of Ion Generation. *Chem. Rev.* **2001**, *101* (2), 361–375.
- (5) Karas, M.; Hillenkamp, F. Laser Desorption Ionization of Proteins with Molecular Masses Exceeding 10,000 Daltons. *Anal. Chem.* **1988**, *60* (20), 2299–2301.
- (6) Fenn, J. B.; Mann, M.; Meng, C. K.; Wong, S. F.; Whitehouse, C. M. Electrospray Ionization for Mass Spectrometry of Large Biomolecules. *Science* **1989**, *246* (4926), 64–71.

- (7) Carroll, D. I.; Dzidic, I.; Stillwell, R. N.; Haegele, K. D.; Horning, E. C. Atmospheric Pressure Ionization Mass Spectrometry. Corona Discharge Ion Source for Use in a Liquid Chromatograph-Mass Spectrometer-Computer Analytical System. *Anal. Chem.* **1975**, *47* (14), 2369–2373.
- (8) Robb, D. B.; Covey, T. R.; Bruins, A. P. Atmospheric Pressure Photoionization: An Ionization Method for Liquid Chromatography- Mass Spectrometry. *Anal. Chem.* **2000**, *72* (15), 3653–3659.
- (9) Cech, N. B.; Enke, C. G. Practical Implications of Some Recent Studies in Electrospray Ionization Fundamentals. *Mass Spectrom. Rev.* **2001**, *20* (6), 362–387.
- (10) Whitehouse, C. M.; Dreyer, R. N.; Yamashita, M.; Fenn, J. B. Electrospray Interface for Liquid Chromatographs and Mass Spectrometers. *Anal. Chem.* **1985**, *57* (3), 675–679.
- (11) Smith, R. D.; Loo, J. A.; Edmonds, C. G.; Barinaga, C. J.; Udseth, H. R. New Developments in Biochemical Mass Spectrometry: Electrospray Ionization. *Anal. Chem.* **1990**, *62* (9), 882–899.
- (12) Kebarle, P.; Verkerk, U. H. Electrospray: From Ions in Solution to Ions in the Gas Phase, What We Know Now. *Mass Spectrom. Rev.* **2009**, *28* (6), 898–917.
- (13) Wu, X.; Oleschuk, R. D.; Cann, N. M. Characterization of Microstructured Fibre Emitters: In Pursuit of Improved Nano Electrospray Ionization Performance. *Analyst* **2012**, *137* (18), 4150–4161.
- (14) Konermann, L.; Ahadi, E.; Rodriguez, A. D.; Vahidi, S. Unraveling the Mechanism of Electrospray Ionization. *Anal. Chem.* **2013**, *85* (1), 2–9.
- (15) Covey, T. R.; Thomson, B. A.; Schneider, B. B. Atmospheric Pressure Ion Sources. *Mass Spectrom. Rev.* **2009**, *28* (6), 870–897.
- (16) Crotti, S.; Seraglia, R.; Traldi, P. Some Thoughts on Electrospray Ionization Mechanisms. *Eur. J. Mass Spectrom.* **2011**, *17* (2), 85–99.
- (17) Fenn, J. B. Electrospray Wings for Molecular Elephants (Nobel Lecture). *Angew. Chem. Int. Ed.* **2003**, *42* (33), 3871–3894.
- (18) Nguyen, S.; Fenn, J. B. Gas-Phase Ions of Solute Species from Charged Droplets of Solutions. *Proc. Natl. Acad. Sci.* **2007**, *104* (4), 1111–1117.
- (19) Wilm, M. Principles of Electrospray Ionization. *Mol. Cell. Proteomics* **2011**, *10* (7), M111–009407.
- (20) Iavarone, A. T.; Williams, E. R. Mechanism of Charging and Supercharging Molecules in Electrospray Ionization. *J. Am. Chem. Soc.* **2003**, *125* (8), 2319–2327.
- (21) De La Mora, J. F. Electrospray Ionization of Large Multiply Charged Species Proceeds via Dole's Charged Residue Mechanism. *Anal. Chim. Acta* **2000**, *406* (1), 93–104.
- (22) Iribarne, J. V.; Thomson, B. A. On the Evaporation of Small Ions from Charged Droplets. *J. Chem. Phys.* **1976**, *64* (6), 2287–2294.

- (23) Konermann, L.; Rodriguez, A. D.; Liu, J. On the Formation of Highly Charged Gaseous Ions from Unfolded Proteins by Electrospray Ionization. *Anal. Chem.* **2012**, *84* (15), 6798–6804.
- (24) Sunner, J.; Nicol, G.; Kebarle, P. Factors Determining Relative Sensitivity of Analytes in Positive Mode Atmospheric Pressure Ionization Mass Spectrometry. *Anal. Chem.* **1988**, *60* (13), 1300–1307.
- (25) De Hoffmann, E.; Stroobant, V. *Mass Spectrometry: Principles and Applications*, 3rd ed.; West Sussex, 1997.
- (26) Schwartz, J. C.; Senko, M. W.; Syka, J. E. A Two-Dimensional Quadrupole Ion Trap Mass Spectrometer. *J. Am. Soc. Mass Spectrom.* **2002**, *13* (6), 659–669.
- (27) March, R. E. Ion Trap Mass Spectrometry. *Int. J. Mass Spectrom. Ion Process.* **1992**, *118*, 71–135.
- (28) March, R. E. An Introduction to Quadrupole Ion Trap Mass Spectrometry. *J. Mass Spectrom.* **1997**, *32* (4), 351–369.
- (29) Douglas, D. J. Linear Quadrupoles in Mass Spectrometry. *Mass Spectrom. Rev.* **2009**, *28* (6), 937–960.
- (30) Douglas, D. J.; Frank, A. J.; Mao, D. Linear Ion Traps in Mass Spectrometry. *Mass Spectrom. Rev.* **2005**, *24* (1), 1–29.
- (31) Stafford Jr, G. C.; Kelley, P. E.; Syka, J. E. P.; Reynolds, W. E.; Todd, J. F. J. Recent Improvements in and Analytical Applications of Advanced Ion Trap Technology. *Int. J. Mass Spectrom. Ion Process.* **1984**, *60* (1), 85–98.
- (32) Kaiser Jr, R. E.; Cooks, R. G.; Stafford Jr, G. C.; Syka, J. E.; Hemberger, P. H. Operation of a Quadrupole Ion Trap Mass Spectrometer to Achieve High Mass/Charge Ratios. *Int. J. Mass Spectrom. Ion Process.* **1991**, *106*, 79–115.
- (33) Busch, K. L.; Glish, G. L.; McLuckey, S. A. *Mass Spectrometry/Mass Spectrometry: Techniques and Applications of Tandem Mass Spectrometry*; VCH Publishers: New York, 1988.
- (34) Mellon, F. A. Mass Spectrometry| Principles and Instrumentation. In *Encyclopedia of Food Sciences and Nutrition (Second Edition)*; Caballero, B., Ed.; Academic Press: Oxford, 2003; pp 3739–3749.
- (35) de Hoffmann, E. Tandem Mass Spectrometry: A Primer. *J. Mass Spectrom.* **1996**, *31* (2), 129–137.
- (36) McLuckey, S. A. Principles of Collisional Activation in Analytical Mass Spectrometry. *J. Am. Soc. Mass Spectrom.* **1992**, *3* (6), 599–614.
- (37) Mayer, P. M.; Poon, C. The Mechanisms of Collisional Activation of Ions in Mass Spectrometry. *Mass Spectrom. Rev.* **2009**, *28* (4), 608–639.
- (38) Brodbelt, J. S. Analytical Applications of Ion-Molecule Reactions. *Mass Spectrom. Rev.* **1997**, *16* (2), 91–110.

- (39) Bjarnason, A.; Taylor, J. W.; Kinsinger, J. A.; Cody, R. B.; Weil, D. A. Isomer Discrimination of Disubstituted Benzene Derivatives through Gas-Phase Iron (I) Ion Reactions in a Fourier-Transform Mass Spectrometer. *Anal. Chem.* **1989**, *61* (17), 1889–1894.
- (40) Kong, J. Y.; Yu, Z.; Easton, M. W.; Niyonsaba, E.; Ma, X.; Yerabolu, R.; Sheng, H.; Jarrell, T. M.; Zhang, Z.; Ghosh, A. K. Differentiating Isomeric Deprotonated Glucuronide Drug Metabolites via Ion/Molecule Reactions in Tandem Mass Spectrometry. *Anal. Chem.* **2018**, *90* (15), 9426–9433.
- (41) Gronert, S. Estimation of Effective Ion Temperatures in a Quadrupole Ion Trap. *J. Am. Soc. Mass Spectrom.* **1998**, *9* (8), 845–848.
- (42) Gronert, S. Mass Spectrometric Studies of Organic Ion/Molecule Reactions. *Chem. Rev.* **2001**, *101* (2), 329–360.
- (43) Olmstead, W. N.; Brauman, J. I. Gas-Phase Nucleophilic Displacement Reactions. *J. Am. Chem. Soc.* **1977**, *99* (13), 4219–4228.
- (44) Pellerite, M. J.; Brauman, J. I. Intrinsic Barriers in Nucleophilic Displacements. *J. Am. Chem. Soc.* **1980**, *102* (19), 5993–5999.
- (45) Makarov, A.; Denisov, E.; Kholomeev, A.; Balschun, W.; Lange, O.; Strupat, K.; Horning, S. Performance Evaluation of a Hybrid Linear Ion Trap/Orbitrap Mass Spectrometer. *Anal. Chem.* **2006**, *78* (7), 2113–2120.
- (46) Perry, R. H.; Cooks, R. G.; Noll, R. J. Orbitrap Mass Spectrometry: Instrumentation, Ion Motion and Applications. *Mass Spectrom. Rev.* **2008**, *27* (6), 661–699.
- (47) Kingdon, K. H. A Method for the Neutralization of Electron Space Charge by Positive Ionization at Very Low Gas Pressures. *Phys. Rev.* **1923**, *21* (4), 408.
- (48) Badman, E. R.; Patterson, G. E.; Wells, J. M.; Santini, R. E.; Cooks, R. G. Differential Non-Destructive Image Current Detection in a Fourier Transform Quadrupole Ion Trap. *J. Mass Spectrom.* **1999**, *34* (8), 889–894.
- (49) Dong, X.; Zhang, Y.; Milton, J.; Yerabolu, R.; Easterling, L.; Kenttämä, H. I. Investigation of the Relative Abundances of Single-Core and Multicore Compounds in Asphaltenes by Using High-Resolution in-Source Collision-Activated Dissociation and Medium-Energy Collision-Activated Dissociation Mass Spectrometry with Statistical Considerations. *Fuel* **2019**, *246*, 126–132.

## CHAPTER 3. DIFFERENTIATION OF DEPROTONATED ACYL, N- AND O-GLUCURONIDE DRUG METABOLITES BY USING TANDEM MASS SPECTROMETRY BASED ON GAS-PHASE ION-MOLECULE REACTIONS

### 3.1 Introduction

During phase II drug metabolism, drugs often undergo glucuronidation, where glucuronic acid is conjugated with a carboxylic acid, hydroxyl, or amino group of a drug or drug metabolite to form an acyl, *O*-, or *N*-glucuronide metabolite, respectively.<sup>1,2</sup> This reaction, catalyzed by a superfamily of uridine 5'-diphospho-glucuronosyltransferase enzymes, expedites the secretion of drugs via urine or bile by increasing their water solubility.<sup>3-5</sup> While *N*- and *O*-glucuronides are generally safe, acyl glucuronides often form reactive and potentially toxic intermediate metabolites.<sup>6-9</sup> The toxicological effects of acyl glucuronides are associated with three processes, all of which may lead to toxicity. The most common process is the acyl migration via intramolecular rearrangement.<sup>10,11</sup> In this process, the acyl group begins at the 1-hydroxyl position of the glucuronic acid moiety (1- $\beta$ -acyl glucuronide) and migrates to the 2-, 3- or 4-hydroxyl group of the glucuronic acid to form 2-, 3-, or 4- $\beta$ - and  $\alpha$ -acyl glucuronides, respectively. This migration allows the glucuronic acid moiety to undergo ring-opening at the anomeric position, resulting in the formation of an aldehyde functionality.<sup>12</sup> The  $\beta$ -aldehyde can then covalently bind to nucleophilic macromolecules, potentially causing idiosyncratic drug toxicity (IDT).<sup>12-17</sup> The other two processes, spontaneous hydrolysis, which results in generation of the parent drug, and transacylation, wherein glucuronic acid is substituted by nucleophilic macromolecules, have also been reported to lead to IDT.<sup>12</sup> Because acyl glucuronides are potentially toxic, knowing the site of glucuronidation is vital for the drug development process because it could allow for earlier safety assessments of new drug candidates. Unfortunately, despite this great need, current analytical techniques cannot unambiguously differentiate *N*-, *O*-, and acyl glucuronides.

Liquid chromatography coupled with tandem mass spectrometry based on collision-activated dissociation (CAD) is the standard analytical method for detecting glucuronides.<sup>18</sup> The presence of glucuronides is based on the detection of aglycone ions, which are formed via elimination of

anhydroglucuronic acid (MW 176 Da) upon CAD of positively- or negatively-charged glucuronide ions.<sup>18</sup> This method, however, only detects the *presence* of glucuronide and cannot reliably differentiate between *O*-, *N*-, and acyl glucuronides. Chemical derivatization prior to tandem mass spectrometry has been used to differentiate between some glucuronide isomers, including estriol glucuronides,<sup>19</sup> carvedilol glucuronides,<sup>20</sup> morphine glucuronides,<sup>21</sup> and some acyl glucuronides;<sup>22</sup> However, this method is often impractical because it can be time-consuming and therefore ill suited for high-throughput analysis.  $\beta$ -Glucuronidase enzymes have also been employed to detect glucuronides by hydrolyzing glucuronides into their parent drugs;<sup>23</sup> however, it has been reported that the efficiency of hydrolysis depends on the nature of the glucuronide and the conditions used, and therefore, only glucuronides that are hydrolyzable in the conditions employed can be detected.<sup>24</sup>

Tandem mass spectrometry based on gas-phase ion-molecule reactions was recently utilized to differentiate deprotonated *N*- and *O*-glucuronides based on their differing reactions with trichlorosilane ( $\text{HSiCl}_3$ ).<sup>25</sup> This method, however, did not enable the differentiation of deprotonated *N*-glucuronides from acyl glucuronides. In this study, ion-molecule reactions are presented as a means for differentiating acyl, *N*-, and *O*-glucuronides using boron trifluoride ( $\text{BF}_3$ ) as the neutral reagent. Additionally, this approach can differentiate 1- $\beta$ -acyl glucuronides from isomeric acyl glucuronides formed following acyl migration.

## 3.2 Experimental

### 3.2.1 Chemicals

Boron trifluoride diethyl etherate (synthesis grade) was used to generate  $\text{BF}_3$  and was purchased from Sigma-Aldrich. All acyl glucuronide (Table 3.1), *N*-glucuronide (Table 3.2), and *O*-glucuronide (Table 3.3) drug metabolites were purchased from Toronto Research Chemical.  $^{18}\text{O}$ -Probenecid acyl  $\beta$ -D-glucuronide was prepared by dissolving probenecid acyl- $\beta$ -D-glucuronide in  $^{18}\text{O}$ -water containing 5 % (v/v) formic acid for a week as previously described.<sup>26</sup>  $^{13}\text{C}$ -Ibuprofen acyl  $\beta$ -D-glucuronide was synthesized following previously published method.<sup>27</sup> The synthesis was performed by Dr. Harry R.

Chobanian Dr. Nicholas R. Deprez from Merck & Co., Inc. LC/MS optima grade acetonitrile, water, and methanol were purchased from Fisher Scientific. Potassium phosphate buffer (100 mM, pH 7.4) was prepared by mixing 80.2 mL of 1.0 M potassium diphosphate ( $K_2HPO_4$ ) and 19.8 mL of 1.0 M potassium monophosphate ( $KH_2PO_4$ ). The mixture was adjusted to pH 7.4 by adding NaOH or HCl and diluted to 1 L with distilled water.

### 3.2.2 Sample Preparation

Acyl, *N*-, and *O*-glucuronide drug metabolites were prepared at 0.1 mM in 50:50 (v/v) methanol:water or in phosphate buffer (pH 7.4) at the same concentration. A mixture containing acyl, *N*- and *O*-glucuronides was prepared by incubating telmisartan acyl- $\beta$ -D-glucuronide, 2-amino-1-methyl-6-phenylimidazo[4,5-*b*]pyridine (abbreviated PhIP) *N*- $\beta$ -D-glucuronide, and ezetimibe *O*- $\beta$ -D-glucuronide in phosphate buffer at room temperature for 4 hours. The role of phosphate buffer is to expediate acyl migration.<sup>6-9</sup> Only acyl glucuronides known to undergo minor acyl migration (stable acyl glucuronides; telmisartan, repaglinide, and valproic acyl glucuronides) were dissolved in the phosphate buffer. The stability of these acyl glucuronides were based on their previously reported half-lives ( $t_{1/2}$ , a measure of the degradation rate (hydrolysis and acyl migration) of the 1- $\beta$ -acyl glucuronide isomer).<sup>28</sup>

### 3.2.3 High Performance Liquid Chromatography (HPLC)

HPLC was used to separate 1- $\beta$ -acyl glucuronides from their isomeric migrated acyl glucuronides. HPLC was also used to separate a mixture of *N*-, *O*- and acyl glucuronides incubated in phosphate buffer. All HPLC experiments were performed on a Thermo Surveyor Plus HPLC. Water (A) and acetonitrile (B) each containing 0.1 % (v/v) formic acid were used as the mobile phases at a flow rate of 500  $\mu$ L/min on an Agilent ZORBAX SB-C18 5 $\mu$ m, 4.6  $\times$  250 mm column. A nonlinear gradient was used as follows: 0.0 min, 20 % B; 2.0 min, 20 % B; 20.0 min, 80 % B; 23.0 min, 80 % B; 25.0 min, 20 % B; 20 % B; 30.0 min, 20 % B. Following HPLC separation, the analytes were ionized via electrospray ionization (ESI)



operated in negative ion mode and the ionized analytes were isolated in the ion trap and reacted with  $\text{BF}_3$  for 30 ms reaction time as discussed below.

### 3.2.4 Mass Spectrometry

All experiments were performed with a Thermo Scientific LQT MS equipped with ESI operated in negative ion mode. The operation of ESI LQIT and fundamental aspects of gas-phase ion-molecule reactions are discussed in detail in Chapter 2 of this dissertation. The analytes were either infused into the ESI source at a rate of 10  $\mu\text{L}/\text{min}$  by using a 500  $\mu\text{L}$  Hamilton syringe or eluted from HPLC at a flow rate of 500  $\mu\text{L}/\text{min}$ . An external reagent mixing manifold was used to introduce the neutral reagent (boron trifluoride diethyl etherate) into the helium buffer gas line via a syringe pump at a flow rate of 3  $\mu\text{L}/\text{h}$ , as described previously.<sup>29–31</sup> The syringe port and surrounding area were heated at approximately 110  $^{\circ}\text{C}$  to ensure complete evaporation of the boron trifluoride diethyl etherate. Because of the high temperature, boron trifluoride diethyl etherate dissociated to form  $\text{BF}_3$  and ethoxyethane. To determine whether  $\text{BF}_3$  was present in the ion trap, formic acid was introduced into the ion source, deprotonated (ion of  $m/z$  45), isolated (isolation width of 12  $m/z$  units) and allowed to react with  $\text{BF}_3$  for 100 ms. Trifluorohydroborate ions ( $\text{HBF}_3^-$ ,  $m/z$  69) were observed with a relative abundance of 30 % compared to that of the deprotonated formic acid ( $m/z$  45). After this, analytes were introduced into the ion source, deprotonated, isolated (isolation width of two  $m/z$  units) and allowed to react with  $\text{BF}_3$ . For CAD experiments, the product ions of interest were isolated and subjected to CAD in the ion trap. Typical reaction, isolation and CAD conditions were as follow: reaction time 100 ms, isolation width of two  $m/z$ -units, activation  $q$  value 0.25, and collision energy 15 (arbitrary units).

### 3.2.5 Calculations

All density functional theory calculations were performed at the M06-2X/6-311++G(d,p) level of theory by using the Gaussian16 program.<sup>32,33</sup> All transition state structures were determined to possess

one negative frequency, while minima possessed no negative frequencies. Intrinsic reaction coordinate (IRC) calculations were performed to confirm the transition state structures connected the correct reactant and product structures. The free energies used to construct the potential energy surfaces were calculated using ideal gas statistical mechanics. The calculations reported in Figure 3.4 were performed by Dr. McKay W. Easton and those reported in Figure 3.5 and 3.6 were performed by Erlu Feng.

### 3.3 Results and Discussion

The gas-phase reactivities of several deprotonated acyl, *N*- and *O*-glucuronides towards  $\text{BF}_3$  were studied in a LQIT mass spectrometer in an attempt to differentiate acyl, *N*- and *O*-glucuronide drug metabolites. Further, the fragmentation patterns of several product ions were studied to see whether these fragmentations could assist in differentiation. A total of 49 glucuronides were tested, including 21 acyl glucuronides, eight *N*-glucuronides, and 20 *O*-glucuronides. The gas-phase ion-molecule and CAD reactions of the above deprotonated glucuronides with  $\text{BF}_3$  are discussed first, followed by HPLC separation of selected glucuronides and computational results.

#### 3.3.1 Gas-phase Ion-molecule Reactions of Deprotonated Acyl, *N*- and *O*-glucuronides with $\text{BF}_3$ Followed by CAD

Several acyl, *N*-, and *O*-glucuronides were ionized via ESI in negative ion mode. The deprotonated analytes were isolated and allowed to react with  $\text{BF}_3$  for up to 100 ms. A set of example mass spectra measured for the reactions of a deprotonated *O*-, *N*- and acyl glucuronide are shown in Figure 3.1. Deprotonated carvedilol-*O*- $\beta$ -D-glucuronide ( $m/z$  581), deprotonated carvedilol-*N*- $\beta$ -D-glucuronide ( $m/z$  581), and clofibric acyl- $\beta$ -D-glucuronide ( $m/z$  389) were used as the examples. All three deprotonated analytes reacted with  $\text{BF}_3$  to form two primary product ions: adduct ions,  $[\text{M} - \text{H} + \text{BF}_3]^-$ , and adduct ions that had lost one HF molecule,  $[\text{M} - \text{H} + \text{BF}_3 - \text{HF}]^-$ . Additional secondary product ions were also observed, as well as product ions formed from hydrolysis. Primary product ions are here defined as product ions that are formed upon reactions between the deprotonated analytes and one  $\text{BF}_3$  molecule.

These primary product ions can react further with another  $\text{BF}_3$  molecule to form secondary product ions. Hydrolysis product ions refer to product ions formed when one  $\text{HF}$  molecule is replaced by a water molecule for  $[\text{M} - \text{H} + \text{BF}_3]^-$  and  $[\text{M} - \text{H} + \text{BF}_3 - \text{HF}]^-$  ions. In addition to the above product ions, deprotonated acyl and *N*-glucuronides formed primary adduct ions that had lost two  $\text{HF}$  molecules,  $[\text{M} - \text{H} + \text{BF}_3 - 2 \text{HF}]^-$ , and secondary adduct ions with two  $\text{BF}_3$  molecules that had lost three  $\text{HF}$  molecules,  $[\text{M} - \text{H} + 2 \text{BF}_3 - 3 \text{HF}]^-$ . The  $[\text{M} - \text{H} + \text{BF}_3 - 2 \text{HF}]^-$  and  $[\text{M} - \text{H} + 2 \text{BF}_3 - 3 \text{HF}]^-$  product ions were not observed for deprotonated *O*-glucuronides. This means that the formation of these ions can be used to differentiate acyl and *N*-glucuronides from *O*-glucuronides; therefore, these ions are hereafter referred to as diagnostic product ions.

To differentiate deprotonated *N*-glucuronides from acyl glucuronides, the  $[\text{M} - \text{H} + 2 \text{BF}_3 - 3 \text{HF}]^-$  product ions were isolated and subjected to CAD. For acyl glucuronides only, fragment ions were observed via a loss of a molecule with MW 88 Da (Figure 3.1). This molecule is proposed to be 2-fluoro-1,3,2-dioxaborole and the mechanism of its formation is discussed in section 3.3.5. All deprotonated acyl glucuronides (Table 3.1) and deprotonated *N*-glucuronides (Table 3.2) formed the  $[\text{M} - \text{H} + \text{BF}_3]^-$  and  $[\text{M} - \text{H} + \text{BF}_3 - \text{HF}]^-$  product ions as well as diagnostic product ions:  $[\text{M} - \text{H} + \text{BF}_3 - 2 \text{HF}]^-$  and  $[\text{M} - \text{H} + 2 \text{BF}_3 - 3 \text{HF}]^-$ . Among all 49 glucuronides studied, no false positives nor negatives were observed.

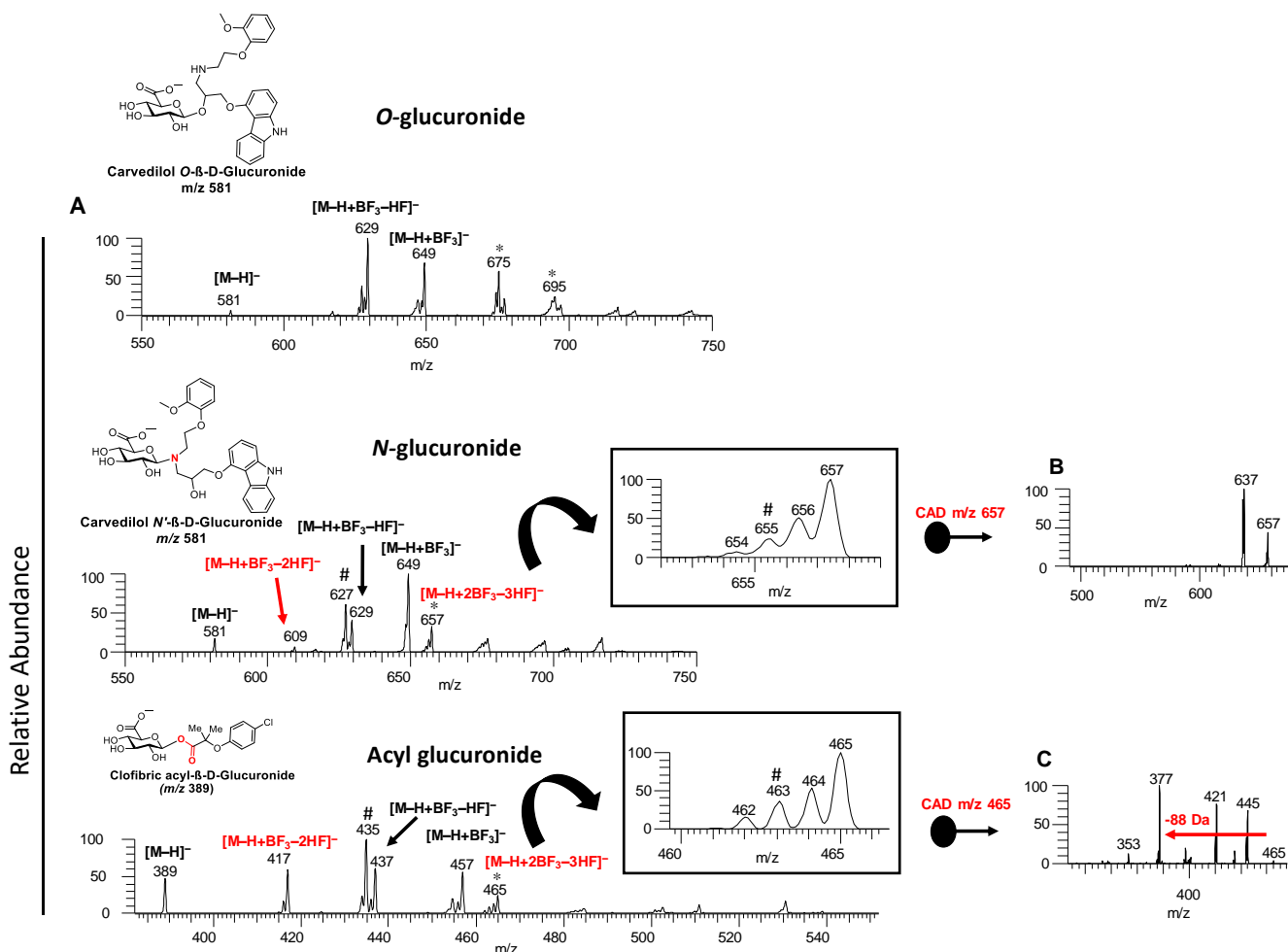


Figure 3.1 (A) Mass spectra measured for after 200 ms reaction of a deprotonated *O*-, *N*-, and acyl glucuronide with  $\text{BF}_3$ . Only the deprotonated *N*- and acyl glucuronides formed the diagnostic product ions:  $[\text{M} - \text{H} + \text{BF}_3 - 2\text{HF}]^-$  and  $[\text{M} - \text{H} + 2\text{BF}_3 - 3\text{HF}]^-$ . (B) For the deprotonated *N*-glucuronide, CAD (collision energy 15 arbitrary units) of the  $[\text{M} - \text{H} + 2\text{BF}_3 - 3\text{HF}]^-$  ions yielded a major fragment ion corresponding to elimination of HF (MW 20 Da). (C) For the deprotonated acyl glucuronide, a diagnostic fragment ion was formed via the loss of a molecule with MW 88 Da. # Product ions that are due to hydrolysis of  $[\text{M} - \text{H} + \text{BF}_3 - \text{HF}]^-$  and  $[\text{M} - \text{H} + 2\text{BF}_3 - 3\text{HF}]^-$  product ions to form  $[\text{M} - \text{H} + \text{BF}_3 + \text{H}_2\text{O} - 2\text{HF}]^-$  and  $[\text{M} - \text{H} + 2\text{BF}_3 + \text{H}_2\text{O} - 4\text{HF}]^-$  product ions, respectively, were also observed.\*

Secondary product ions.

Table 3.1 Product ions ( $m/z$ ) with their relative abundances (%) after 100 ms reaction of deprotonated acyl glucuronides with  $\text{BF}_3$  and fragment ions ( $m/z$ ) with their relative abundances (%) formed upon CAD of the product ions  $[\text{M} - \text{H} + 2 \text{BF}_3 - 3 \text{HF}]^-$  at a collision energy of 15 (arbitrary units)

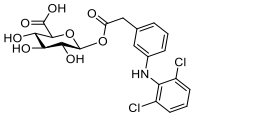
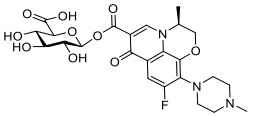
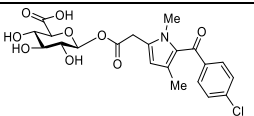
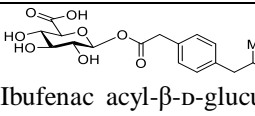
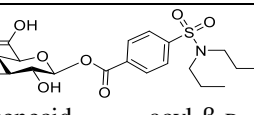
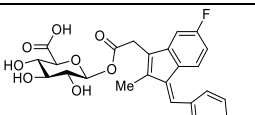
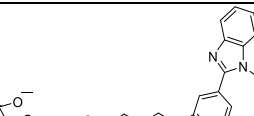
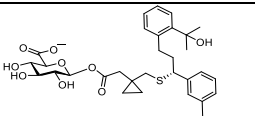
Acyl glucuronides ( $m/z$ of deprotonated analyte)	Major product ions ( $m/z$ ) and their relative abundances (%)	Acyl glucuronides ( $m/z$ of deprotonated analyte)	Major product ions ( $m/z$ ) and their relative abundances (%)
	Major CAD fragment ions ( $m/z$ ) of $[\text{M} - \text{H} + 2 \text{BF}_3 - 3 \text{HF}]^-$ and their relative abundances (%)		Major CAD fragment ions ( $m/z$ ) of $[\text{M} - \text{H} + 2 \text{BF}_3 - 3 \text{HF}]^-$ and their relative abundances (%)
 Diclofenac glucuronide (470)	$[\text{M} - \text{H} + \text{BF}_3]^-$ (538) 60 % $[\text{M} - \text{H} + \text{BF}_3 - \text{HF}]^-$ (518) 47 % $[\text{M} - \text{H} + \text{BF}_3 - 2\text{HF}]^-$ (498) 23 % $[\text{M} - \text{H} + 2\text{BF}_3 - 3\text{HF}]^-$ (556) 25 % $[\text{M} - \text{H} + 2\text{BF}_3 - 4\text{HF}]^-$ (526) 10 % $[\text{MH} + 2 \text{BF}_3 - 3 \text{HF} - \text{CO}_2]^-$ (492) 5 %	 Levofloxacin glucuronide (536)	$[\text{M} - \text{H} + \text{BF}_3]^-$ (604) 78 % $[\text{M} - \text{H} + \text{BF}_3 - \text{HF}]^-$ (584) 100 % $[\text{M} - \text{H} + \text{BF}_3 - 2\text{HF}]^-$ (564) 5 % $[\text{M} - \text{H} + 2\text{BF}_3 - 3\text{HF}]^-$ (612) 36 % $[\text{M} - \text{H} + 2\text{BF}_3 - 4\text{HF}]^-$ (592) 10 % $[\text{M} - \text{H} + 2\text{BF}_3 - 3\text{HF} - \text{CO}_2]^-$ (568) 42 % $[\text{M} - \text{H} + 2\text{BF}_3 - 3\text{HF} - \text{C}_2\text{H}_2\text{O}_2\text{BF}]^-$ (524) 100 %
 Zomepirac glucuronide (466)	$[\text{M} - \text{H} + \text{BF}_3]^-$ (514) 100 % $[\text{M} - \text{H} + \text{BF}_3 - \text{HF}]^-$ (494) 55 % $[\text{M} - \text{H} + \text{BF}_3 - 2\text{HF}]^-$ (474) 10 % $[\text{M} - \text{H} + 2\text{BF}_3 - 3\text{HF}]^-$ (442) 22 % $[\text{M} - \text{H} + 2\text{BF}_3 - 4\text{HF}]^-$ (522) 15 % $[\text{M} - \text{H} + 2\text{BF}_3 - 3\text{HF} - \text{CO}_2]^-$ (498) 5 % $[\text{M} - \text{H} + 2\text{BF}_3 - 3\text{HF} - \text{C}_2\text{H}_2\text{O}_2\text{BF}]^-$ (454) 18 %	 Ibuprofen acyl- $\beta$ -D-glucuronide (367)	$[\text{M} - \text{H} + \text{BF}_3]^-$ (435) 100 % $[\text{M} - \text{H} + \text{BF}_3 - \text{HF}]^-$ (415) 74 % $[\text{M} - \text{H} + \text{BF}_3 - 2\text{HF}]^-$ (395) 17 % $[\text{M} - \text{H} + 2\text{BF}_3 - 3\text{HF}]^-$ (443) 32 % $[\text{M} - \text{H} + 2\text{BF}_3 - 4\text{HF}]^-$ (423) 20 % $[\text{M} - \text{H} + 2\text{BF}_3 - 3\text{HF} - \text{CO}_2]^-$ (399) 42 % $[\text{M} - \text{H} + 2\text{BF}_3 - 3\text{HF} - \text{C}_2\text{H}_2\text{O}_2\text{BF}]^-$ (355) 51 %
 Probenecid glucuronide (460)	$[\text{M} - \text{H} + \text{BF}_3]^-$ (528) 60 % $[\text{M} - \text{H} + \text{BF}_3 - \text{HF}]^-$ (508) 47 % $[\text{M} - \text{H} + \text{BF}_3 - 2\text{HF}]^-$ (488) 23 % $[\text{M} - \text{H} + 2\text{BF}_3 - 3\text{HF}]^-$ (536) 25 % $[\text{M} - \text{H} + 2\text{BF}_3 - 4\text{HF}]^-$ (516) 39 % $[\text{M} - \text{H} + 2\text{BF}_3 - 3\text{HF} - \text{CO}_2]^-$ (492) 22 %	 Sulindac acyl- $\beta$ -D-glucuronide (531)	$[\text{M} - \text{H} + \text{BF}_3]^-$ (599) 100 % $[\text{M} - \text{H} + \text{BF}_3 - \text{HF}]^-$ (579) 65 % $[\text{M} - \text{H} + \text{BF}_3 - 2\text{HF}]^-$ (559) 10 % $[\text{M} - \text{H} + 2\text{BF}_3 - 3\text{HF}]^-$ (607) 22 % $[\text{M} - \text{H} + 2\text{BF}_3 - 3\text{HF} - \text{CO}_2]^-$ (563) 15 % $[\text{M} - \text{H} + 2\text{BF}_3 - 3\text{HF} - \text{C}_2\text{H}_2\text{O}_2\text{BF}]^-$ (519) 51 %
 Telmisartan glucuronide (689)	$[\text{M} - \text{H} + \text{BF}_3]^-$ (757) 100 % $[\text{M} - \text{H} + \text{BF}_3 - \text{HF}]^-$ (737) 42 % $[\text{M} - \text{H} + \text{BF}_3 - 2\text{HF}]^-$ (617) 10 % $[\text{M} - \text{H} + 2\text{BF}_3 - 3\text{HF}]^-$ (765) 25 % $[\text{M} - \text{H} + 2\text{BF}_3 - 4\text{HF}]^-$ (745) 12 % $[\text{M} - \text{H} + 2\text{BF}_3 - 3\text{HF} - \text{CO}_2]^-$ (721) 32 % $[\text{M} - \text{H} + 2\text{BF}_3 - 3\text{HF} - \text{C}_2\text{H}_2\text{O}_2\text{BF}]^-$ (677) 28 %	 Montelukast glucuronide (760)	$[\text{M} - \text{H} + \text{BF}_3]^-$ (828) 30 % $[\text{M} - \text{H} + \text{BF}_3 - \text{HF}]^-$ (808) 56 % $[\text{M} - \text{H} + \text{BF}_3 - 2\text{HF}]^-$ (788) 5 % $[\text{M} - \text{H} + 2\text{BF}_3 - 3\text{HF}]^-$ (836) 7 % $[\text{M} - \text{H} + 2\text{BF}_3 - 4\text{HF}]^-$ (816) 6 % $[\text{M} - \text{H} + 2\text{BF}_3 - 3\text{HF} - \text{CO}_2]^-$ (792) 5 % $[\text{M} - \text{H} + 2\text{BF}_3 - 3\text{HF} - \text{C}_2\text{H}_2\text{O}_2\text{BF}]^-$ (728) 20 %

Table 3.1 (Continued)

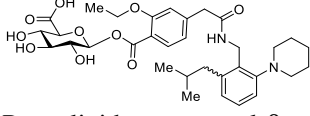
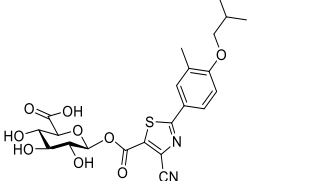
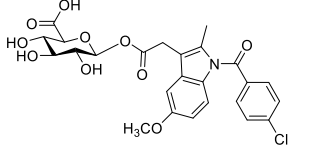
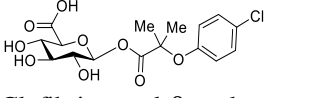
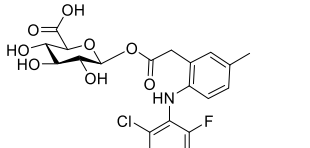
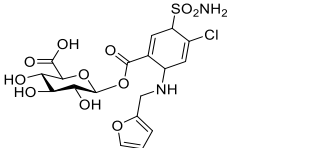
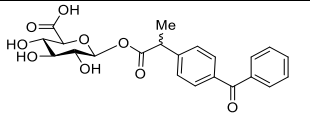
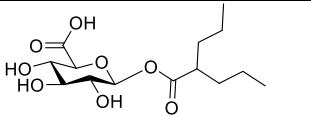
Acyl glucuronides ( <i>m/z</i> of deprotonated analyte)	Major product ions ( <i>m/z</i> ) and their relative abundances (%)	Acyl glucuronides ( <i>m/z</i> of deprotonated analyte)	Major product ions ( <i>m/z</i> ) and their relative abundances (%)
	Major CAD fragment ions ( <i>m/z</i> ) of [ <i>M</i> – <i>H</i> + 2 <i>BF</i> <sub>3</sub> – 3 <i>HF</i> ] <sup>–</sup> and their relative abundances (%)		Major CAD fragment ions ( <i>m/z</i> ) of [ <i>M</i> – <i>H</i> + 2 <i>BF</i> <sub>3</sub> – 3 <i>HF</i> ] <sup>–</sup> and their relative abundances (%)
 Repaglinide glucuronide (627)	$[M-H+BF_3]^-$ (695) 100 % $[M-H+BF_3-HF]^-$ (675) 15 % $[M-H+BF_3-2HF]^-$ (488) 5 % $[M-H+2BF_3-3HF]^-$ (703) 25 % $[M-H+2BF_3-3HF-CO_2]^-$ (659) 65 % $[M-H+2BF_3-3HF-C_2H_2O_2BF]^-$ (615) 100 %	 Febuxostat glucuronide (491)	$[M-H+BF_3]^-$ (559) 100 % $[M-H+BF_3-HF]^-$ (539) 62 % $[M-H+BF_3-2HF]^-$ (519) 15 % $[M-H+2BF_3-3HF]^-$ (567) 19 % $[M-H+2BF_3-4HF]^-$ (547) 5 % $[M-H+2BF_3-3HF-CO_2]^-$ (523) 85 % $[M-H+2BF_3-3HF-C_2H_2O_2BF]^-$ (479) 100 %
 Indomethacin glucuronide (532)	$[M-H+BF_3]^-$ (600) 100 % $[M-H+BF_3-HF]^-$ (580) 39 % $[M-H+BF_3-2HF]^-$ (560) 13 % $[M-H+2BF_3-3HF]^-$ (608) 20 % $[M-H+2BF_3-3HF-CO_2]^-$ (564) 25 % $[M-H+2BF_3-3HF-C_2H_2O_2BF]^-$ (448) 8 %	 Clofibric acid glucuronide (389)	$[M-H+BF_3]^-$ (457) 56 % $[M-H+BF_3-HF]^-$ (437) 61 % $[M-H+BF_3-2HF]^-$ (417) 59 % $[M-H+2BF_3-3HF]^-$ (465) 24 % $[M-H+2BF_3-4HF]^-$ (445) 76 % $[M-H+2BF_3-3HF-CO_2]^-$ (421) 85 % $[M-H+2BF_3-3HF-C_2H_2O_2BF]^-$ (377) 100 %
 Lumiracoxib glucuronide (468)	$[M-H+BF_3]^-$ (536) 65 % $[M-H+BF_3-HF]^-$ (516) 35 % $[M-H+BF_3-2HF]^-$ (496) 4 % $[M-H+2BF_3-3HF]^-$ (544) 100 % $[M-H+2BF_3-4HF]^-$ (524) 39 % $[M-H+2BF_3-3HF-CO_2]^-$ (500) 22 % $[M-H+2BF_3-3HF-C_2H_2O_2BF]^-$ (456) 100 %	 Furosemide glucuronide (505)	$[M-H+BF_3]^-$ (573) 100 % $[M-H+BF_3-HF]^-$ (553) 57 % $[M-H+BF_3-2HF]^-$ (533) 10 % $[M-H+2BF_3-3HF]^-$ (581) 25 % $[M-H+2BF_3-4HF]^-$ (561) 14 % $[M-H+2BF_3-3HF-CO_2]^-$ (537) 10 % $[M-H+2BF_3-3HF-C_2H_2O_2BF]^-$ (493) 12 %
 rac Ketoprofen glucuronide (429)	$[M-H+BF_3]^-$ (497) 100 % $[M-H+BF_3-HF]^-$ (477) 46 % $[M-H+BF_3-2HF]^-$ (457) 5 % $[M-H+2BF_3-3HF]^-$ (505) 55 % $[M-H+2BF_3-3HF-CO_2]^-$ (351) 9 % $[M-H+2BF_3-3HF-C_2H_2O_2BF]^-$ (417) 17 %	 Valproic acid glucuronide (319)	$[M-H+BF_3]^-$ (387) 100 % $[M-H+BF_3-HF]^-$ (367) 46 % $[M-H+BF_3-2HF]^-$ (347) 5 % $[M-H+2BF_3-3HF]^-$ (395) 55 % $[M-H+2BF_3-4HF]^-$ (375) 12 % $[M-H+2BF_3-3HF-CO_2]^-$ (351) 60 % $[M-H+2BF_3-3HF-C_2H_2O_2BF]^-$ (307) 22 %

Table 3.1 (Continued)

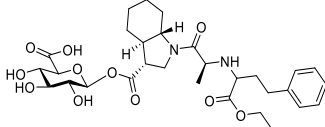
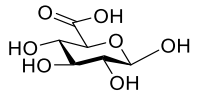
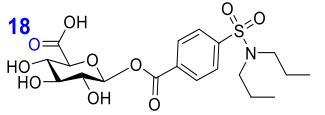
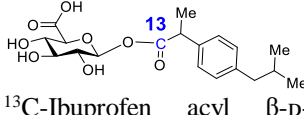
Acyl glucuronides ( <i>m/z</i> of deprotonated analyte)	Major product ions ( <i>m/z</i> ) and their relative abundances (%)	Acyl glucuronides ( <i>m/z</i> of deprotonated analyte)	Major product ions ( <i>m/z</i> ) and their relative abundances (%)
	Major CAD fragment ions ( <i>m/z</i> ) of [M – H + 2 BF <sub>3</sub> – 3 HF] <sup>–</sup> and their relative abundances (%)		Major CAD fragment ions ( <i>m/z</i> ) of [M – H + 2 BF <sub>3</sub> – 3 HF] <sup>–</sup> and their relative abundances (%)
 Trandolapril glucuronide (605)	[M–H+BF <sub>3</sub> ] <sup>–</sup> (673) 100 % [M–H+BF <sub>3</sub> –HF] <sup>–</sup> (653) 35 % [M–H+BF <sub>3</sub> –2HF] <sup>–</sup> (633) 10 % [M–H+2BF <sub>3</sub> –3HF] <sup>–</sup> (681) 32 % [M–H+2BF <sub>3</sub> –4HF] <sup>–</sup> (661) 39 %	 Glucuronic acid (193)	[M–H+BF <sub>3</sub> ] <sup>–</sup> (261) 100 % [M–H+BF <sub>3</sub> –HF] <sup>–</sup> (241) 95 % [M–H+BF <sub>3</sub> –2HF] <sup>–</sup> (221) 10 % [M–H+2BF <sub>3</sub> –3HF] <sup>–</sup> (269) 43 % [M–H+2BF <sub>3</sub> –4HF] <sup>–</sup> (249) 39 %
 <sup>18</sup> O-Probenecid glucuronide (462)	[M–H+BF <sub>3</sub> ] <sup>–</sup> (530) 100 % [M–H+BF <sub>3</sub> –HF] <sup>–</sup> (510) 24 % [M–H+BF <sub>3</sub> –2HF] <sup>–</sup> (490) 20 % [M–H+2BF <sub>3</sub> –3HF] <sup>–</sup> (538) 17 % [M–H+2BF <sub>3</sub> –3HF–C <sup>18</sup> O <sub>2</sub> ] <sup>–</sup> (492) 20 % [M–H+2BF <sub>3</sub> –3HF–C <sub>2</sub> H <sub>2</sub> O <sub>2</sub> BF] <sup>–</sup> (448) 30 %	 <sup>13</sup> C-Ibuprofen glucuronide (382)	[M–H+BF <sub>3</sub> ] <sup>–</sup> (450) 100 % [M–H+BF <sub>3</sub> –HF] <sup>–</sup> (430) 76 % [M–H+BF <sub>3</sub> –2HF] <sup>–</sup> (410) 23 % [M–H+2BF <sub>3</sub> –3HF] <sup>–</sup> (410) 10 % [M–H+2BF <sub>3</sub> –4HF] <sup>–</sup> (438) 12 % [M–H+2BF <sub>3</sub> –3HF–CO <sub>2</sub> ] <sup>–</sup> (414) 100 %

Table 3.2 Product ions ( $m/z$ ) with their relative abundances (%) after 100 ms reaction of deprotonated *N*-glucuronides with  $\text{BF}_3$  and fragment ions ( $m/z$ ) with their relative abundances (%) formed upon CAD of the product ions  $[\text{M} - \text{H} + 2 \text{BF}_3 - 3 \text{HF}]^-$  at a collision energy of 15 (arbitrary units)

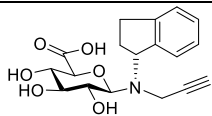
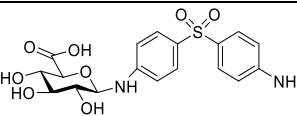
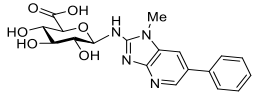
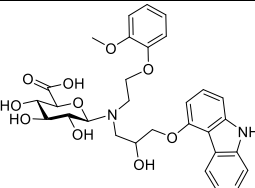
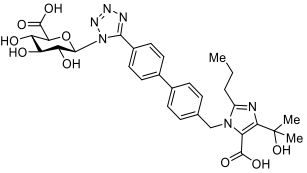
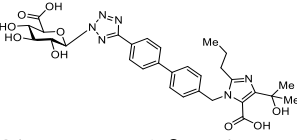
Acyl glucuronides ( $m/z$ of deprotonated analyte)	Major product ions ( $m/z$ ) and their relative abundances in %	Acyl glucuronides ( $m/z$ of deprotonated analyte)	Major product ions ( $m/z$ ) and their relative abundances in %
	Major fragment ions of CAD of $[\text{M} - \text{H} + 2\text{BF}_3 - 3\text{HF}]^-$ and their relative abundances		Major fragment ions of CAD of $[\text{M} - \text{H} + 2\text{BF}_3 - 3\text{HF}]^-$ and their relative abundances
 Rasaglinide <i>N</i> - $\beta$ -D-glucuronide (346)	$[\text{M} - \text{H} + \text{BF}_3]^-$ (414) 100 % $[\text{M} - \text{H} + \text{BF}_3 - \text{HF}]^-$ (394) 37 % $[\text{M} - \text{H} + \text{BF}_3 - 2\text{HF}]^-$ (374) 6 % $[\text{M} - \text{H} + 2\text{BF}_3 - 3\text{HF}]^-$ (422) 45 % <hr/> $[\text{M} - \text{H} + 2\text{BF}_3 - 4\text{HF}]^-$ (402) 42 % $[\text{M} - \text{H} + 2\text{BF}_3 - 3\text{HF} - \text{CO}_2]^-$ (378) 35 %	 Dapsone <i>N</i> - $\beta$ -D-glucuronide (423)	$[\text{M} - \text{H} + \text{BF}_3]^-$ (491) 55 % $[\text{M} - \text{H} + \text{BF}_3 - \text{HF}]^-$ (471) 67 % $[\text{M} - \text{H} + \text{BF}_3 - 2\text{HF}]^-$ (451) 3 % $[\text{M} - \text{H} + 2\text{BF}_3 - 3\text{HF}]^-$ (499) 100 % <hr/> $[\text{M} - \text{H} + 2\text{BF}_3 - 4\text{HF}]^-$ (455) 100 % $[\text{M} - \text{H} + 2\text{BF}_3 - 3\text{HF} - \text{CO}_2]^-$ (431) 7 %
 PhIP- <i>N</i> - $\beta$ -D-glucuronide (399)	$[\text{M} - \text{H} + \text{BF}_3]^-$ (467) 100 % $[\text{M} - \text{H} + \text{BF}_3 - \text{HF}]^-$ (447) 47 % $[\text{M} - \text{H} + \text{BF}_3 - 2\text{HF}]^-$ (427) 3 % $[\text{M} - \text{H} + 2\text{BF}_3 - 3\text{HF}]^-$ (475) 25 % <hr/> $[\text{M} - \text{H} + 2\text{BF}_3 - 4\text{HF}]^-$ (455) 85 % $[\text{M} - \text{H} + 2\text{BF}_3 - 3\text{HF} - \text{CO}_2]^-$ (431) 5 %	 Carvedilol <i>N</i> - $\beta$ -D-glucuronide (581)	$[[\text{M} - \text{H} + \text{BF}_3]^-$ (649) 100 % $[\text{M} - \text{H} + \text{BF}_3 - \text{HF}]^-$ (629) 37 % $[\text{M} - \text{H} + \text{BF}_3 - 2\text{HF}]^-$ (609) 13 % $[\text{M} - \text{H} + 2\text{BF}_3 - 3\text{HF}]^-$ (657) 22 % <hr/> $[\text{M} - \text{H} + 2\text{BF}_3 - 4\text{HF}]^-$ (637) 100 %
 Olmesartan <i>N</i> 1- $\beta$ -D-glucuronide (621)	$[\text{M} - \text{H} + \text{BF}_3]^-$ (689) 33 % $[\text{M} - \text{H} + \text{BF}_3 - \text{HF}]^-$ (669) 92 % $[\text{M} - \text{H} + \text{BF}_3 - 2\text{HF}]^-$ (649) 100 % $[\text{M} - \text{H} + 2\text{BF}_3 - 3\text{HF}]^-$ (697) 5 % <hr/> $[\text{M} - \text{H} + 2\text{BF}_3 - 4\text{HF}]^-$ (677) 100 %	 Olmesartan <i>N</i> 1- $\beta$ -D-glucuronide (621)	$[\text{M} - \text{H} + \text{BF}_3]^-$ (689) 33 % $[\text{M} - \text{H} + \text{BF}_3 - \text{HF}]^-$ (669) 100 % $[\text{M} - \text{H} + \text{BF}_3 - 2\text{HF}]^-$ (649) 46 % $[\text{M} - \text{H} + 2\text{BF}_3 - 3\text{HF}]^-$ (697) 5 % <hr/> $[\text{M} - \text{H} + 2\text{BF}_3 - 4\text{HF}]^-$ (677) 100 %



Table 3.2 (Continued)

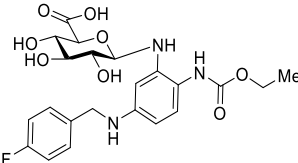
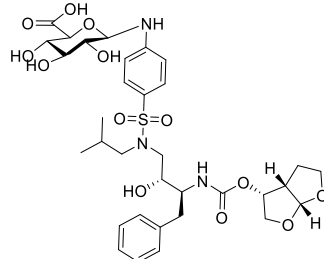
Acyl glucuronides ( <i>m/z</i> of deprotonated analyte)	Major product ions ( <i>m/z</i> ) and their relative abundances in %		Acyl glucuronides ( <i>m/z</i> of deprotonated analyte)	Major product ions ( <i>m/z</i> ) and their relative abundances in %	
	Major fragment ions of CAD of [M-H+2BF <sub>3</sub> -3HF] <sup>-</sup> and their relative abundances			Major fragment ions of CAD of [M-H+2BF <sub>3</sub> -3HF] <sup>-</sup> and their relative abundances	
 Retigabine <i>N</i> -β-D- glucuronide (478)	[M-H+BF <sub>3</sub> ] <sup>-</sup> (546)	100 %	 Darunavir <i>N</i> -β-D-glucuronide (722)	[M-H+BF <sub>3</sub> ] <sup>-</sup> (790)	63 %
	[M-H+BF <sub>3</sub> -HF] <sup>-</sup> (526)	37 %		[M-H+BF <sub>3</sub> -HF] <sup>-</sup> (770)	100 %
	[M-H+BF <sub>3</sub> -2HF] <sup>-</sup> (506)	13 %		[M-H+BF <sub>3</sub> -2HF] <sup>-</sup> (750)	36 %
	[M-H+2BF <sub>3</sub> -3HF] <sup>-</sup> (554)	22 %		[M-H+2BF <sub>3</sub> -3HF] <sup>-</sup> (798)	10 %
	[M-H+2BF <sub>3</sub> -4HF] <sup>-</sup> (534)	100 %		[M-H+2BF <sub>3</sub> -4HF] <sup>-</sup> (778)	100 %
	[M-H+2BF <sub>3</sub> -3HF-CO <sub>2</sub> ] <sup>-</sup> (514)	5 %			

Table 3.3 Product ions ( $m/z$ ) and their relative abundance (%) observed after 100 ms reaction time between deprotonated *O*-glucuronides with BF<sub>3</sub>

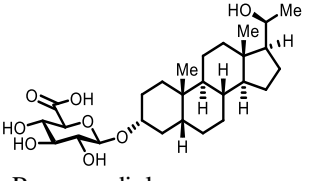
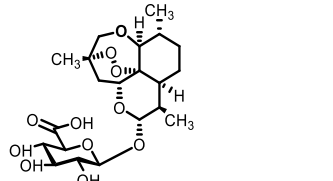
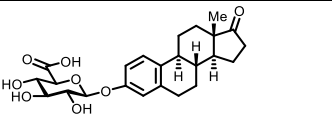
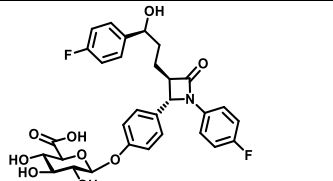
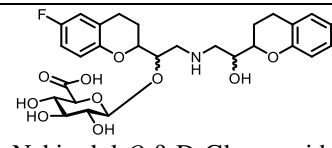
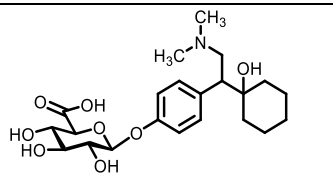
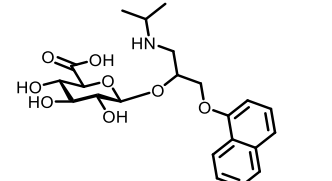
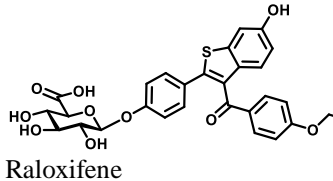
Acyl glucuronides ( $m/z$ of deprotonated analyte)	Major product ions ( $m/z$ ) and their relative abundances in %	Acyl glucuronides ( $m/z$ of deprotonated analyte)	Major product ions ( $m/z$ ) and their relative abundances in %
 Pregnanediol 3a- <i>O</i> -β-D-Glucuronide (346)	[M-H+BF <sub>3</sub> ] <sup>-</sup> (563) 100 % [M-H+BF <sub>3</sub> -HF] <sup>-</sup> (544) 35 %	 Dihydroartemisinin <i>O</i> -β-D-Glucuronide (459)	[M-H+BF <sub>3</sub> ] <sup>-</sup> (527) 100 % [M-H+BF <sub>3</sub> -HF] <sup>-</sup> (507) 10 %
 Estrone <i>O</i> -β-D-Glucuronide (445)	[M-H+BF <sub>3</sub> ] <sup>-</sup> (513) 100 % [M-H+BF <sub>3</sub> -HF] <sup>-</sup> (493) 37 %	 Ezetimibe Phenoxy <i>O</i> -β-D-Glucuronide (584)	[M-H+BF <sub>3</sub> ] <sup>-</sup> (652) 100 % [M-H+BF <sub>3</sub> -HF] <sup>-</sup> (632) 18 %
 Nebivolol <i>O</i> -β-D-Glucuronide (580)	[M-H+BF <sub>3</sub> ] <sup>-</sup> (648) 100 % [M-H+BF <sub>3</sub> -HF] <sup>-</sup> (628) 7 %	 Desmethyl Venlafaxine <i>O</i> -β-D-Glucuronide (438)	[M-H+BF <sub>3</sub> ] <sup>-</sup> (506) 100 % [M-H+BF <sub>3</sub> -HF] <sup>-</sup> (486) 18 %
 Propranolol <i>O</i> -β-D-Glucuronide (516)	[M-H+BF <sub>3</sub> ] <sup>-</sup> (584) 100 % [M-H+BF <sub>3</sub> -HF] <sup>-</sup> (564) 8 %	 Raloxifene <i>O</i> -β-D-Glucuronide (648)	[M-H+BF <sub>3</sub> ] <sup>-</sup> (716) 100 % [M-H+BF <sub>3</sub> -HF] <sup>-</sup> (696) 5 %

Table 3.3 (Continued)

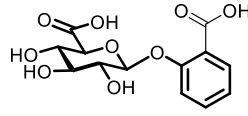
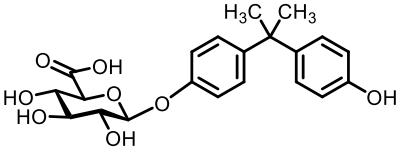
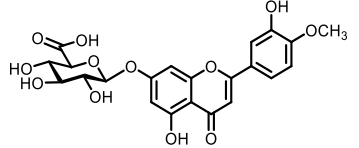
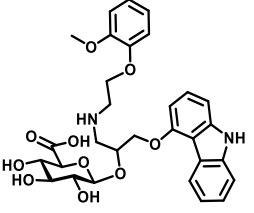
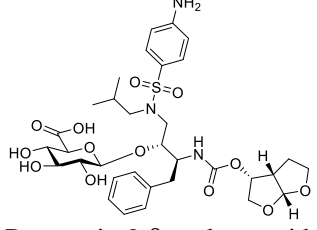
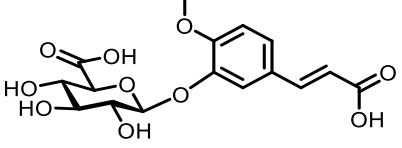
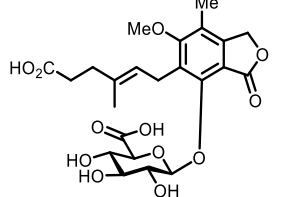
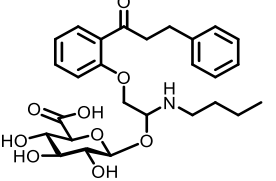
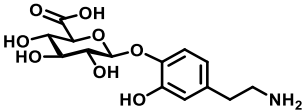
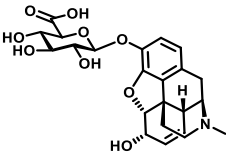
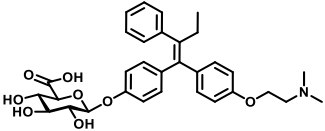
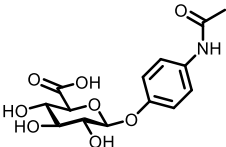
Deprotonated acyl glucuronides ( <i>m/z</i> of deprotonated analyte)	Major product ions ( <i>m/z</i> ) and their relative abundances in %	Acyl glucuronides ( <i>m/z</i> of deprotonated analyte)	Major product ions ( <i>m/z</i> ) and their relative abundances in %
 Salicylic acid <i>O</i> - $\beta$ -D-glucuronide (313)	$[M-H+BF_3]^-$ (381) 100 % $[M-H+BF_3-HF]^-$ (361) 53 %	 Bisphenol A <i>O</i> - $\beta$ -D-glucuronide (403)	$[M-H+BF_3]^-$ (471) 100 % $[M-H+BF_3-HF]^-$ (451) 56 %
 Diosmetim glucuronide (475)	$[M-H+BF_3]^-$ (543) 100 % $[M-H+BF_3-HF]^-$ (523) 5 %	 Carvedilol <i>O</i> - $\beta$ -D-glucuronide (581)	$[M-H+BF_3]^-$ (649) 100 % $[M-H+BF_3-HF]^-$ (629) 28 %
 Darunavir <i>O</i> - $\beta$ -D-glucuronide (599)	$[M-H+BF_3]^-$ (790) 75 % $[M-H+BF_3-HF]^-$ (770) 100 %	 Ferulic acid <i>O</i> - $\beta$ -D-glucuronide (369)	$[M-H+BF_3]^-$ (437) 100 % $[M-H+BF_3-HF]^-$ (417) 35 %
 Mycophenolic acid <i>O</i> - $\beta$ -D-glucuronide (495)	$[M-H+BF_3]^-$ (563) 100 % $[M-H+BF_3-HF]^-$ (543) 54 %	 Propafenone <i>O</i> - $\beta$ -D-glucuronide (517)	$[M-H+BF_3]^-$ (584) 100 % $[M-H+BF_3-HF]^-$ (565) 25 %

Table 3 (Continued)

Deprotonated acyl glucuronides ( <i>m/z</i> of deprotonated analyte)	Major product ions ( <i>m/z</i> ) and their relative abundances in %	Acyl glucuronides ( <i>m/z</i> of deprotonated analyte)	Major product ions ( <i>m/z</i> ) and their relative abundances in %
 Dopamine 4 <i>O</i> -β-D-glucuronide (328)	[M-H+BF <sub>3</sub> ] <sup>-</sup> (381)      40 % [M-H+BF <sub>3</sub> -HF] <sup>-</sup> (361)      42 %	 Morphine <i>O</i> -β-D-glucuronide (460)	[M-H+BF <sub>3</sub> ] <sup>-</sup> (528)      100 % [M-H+BF <sub>3</sub> -HF] <sup>-</sup> (508)      56 %
 Tamoxifen <i>O</i> -β-D-glucuronide (562)	[M-H+BF <sub>3</sub> ] <sup>-</sup> (628)      100 % [M-H+BF <sub>3</sub> -HF] <sup>-</sup> (610)      10 %	 <i>p</i> -Acetamidophenyl <i>O</i> -β-D-glucuronide (326)	[M-H+BF <sub>3</sub> ] <sup>-</sup> (394)      20 % [M-H+BF <sub>3</sub> -HF] <sup>-</sup> (374)      8 %

### 3.3.2 HPLC/MS<sup>3</sup> of Acyl Glucuronides

As stated above, acyl glucuronides can undergo acyl migration at physiological conditions. To determine whether unmigrated 1- $\beta$ -acyl glucuronides and their isomeric migrated acyl glucuronides react similarly with BF<sub>3</sub>, an acyl glucuronide was stored at physiological conditions for four hours to induce migration, and HPLC was then used to separate the unmigrated and migrated acyl glucuronides. The separated isomeric glucuronides were then ionized via (–) ESI and the ionized analytes were isolated and allowed to react with BF<sub>3</sub> in the ion trap for up to 30 ms. Lumiracoxib acyl- $\beta$ -D-glucuronide ( $t_{1/2}$  6.5 h in plasma<sup>34</sup>) was used as a model analyte for these experiments. Because acyl migration occurs most rapidly at neutral to high pH values (pH 7–9),<sup>35,36</sup> the analyte was dissolved in either water containing 0.1 % (v/v) formic acid or 100 mM phosphate buffer at pH 7.4 and stored at room temperature for a variable length of time. Samples were taken at one, two, three, and four hours. The resulting chromatograms for the analyte in acidified water showed only one chromatographic peak over the four hour period, suggesting that acyl migration did not occur (Figure 3.2 A). However, when the analyte was dissolved in the phosphate buffer, multiple peaks with different retention times were observed, suggesting that lumiracoxib acyl- $\beta$ -D-glucuronide had undergone acyl migration (Figure 3.2 B). Based on Figure 3.2, the unmigrated acyl glucuronides eluted at the same time in all experiments. The additional peaks eluting at different times when the analyte was dissolved in the phosphate buffer were assumed to be due to migrated acyl glucuronides.

Following the HPLC separation and ionization of the separated isomeric glucuronides, the ionized analytes ( $m/z$  468) were isolated and allowed to react with BF<sub>3</sub> in the ion trap for up to 30 ms. *All* deprotonated migrated acyl glucuronides were found to form the diagnostic product ions,  $[M - H + BF_3 - 2 HF]^-$  ( $m/z$  496) and  $[M - H + 2 BF_3 - 3 HF]^-$  ( $m/z$  544), while the unmigrated

acyl glucuronides did not (Figures 3.2 C and D). CAD of the  $[M - H + 2 BF_3 - 3 HF]^-$  product ions yielded fragment ions via the loss of a molecule with MW 88 Da (Figure 3.2 D). The same results were obtained when the experiments were replicated with probenecid acyl  $\beta$ -D-glucuronide ( $t_{1/2}$  6.5 0.3 h in phosphate buffer<sup>28</sup>). Probenecid acyl  $\beta$ -D-glucuronide was dissolved either in water or water containing 0.1 % formic acid (v/v). When probenecid acyl  $\beta$ -D-glucuronide was dissolved in pure water, its deprotonated analyte ( $m/z$  460) formed the diagnostic product ions,  $[M - H + BF_3 - 2 HF]^-$  ( $m/z$  488) and  $[M - H + 2 BF_3 - 3 HF]^-$  ( $m/z$  534) after isolation and reactions with  $BF_3$ . However, when it was dissolved in acidified water, which inhibits acyl migration, the diagnostic product ions were not observed. This finding suggests that probenecid acyl  $\beta$ -D-glucuronide underwent acyl migration when it was dissolved in water but not when it was dissolved in acidified water (Figure 3.3). The results obtained for both lumiracoxib acyl- $\beta$ -D-glucuronide and probenecid acyl  $\beta$ -D-glucuronide support the earlier result that acyl migration occurs rapidly at neutral to high pH values (pH 7–9).<sup>35,36</sup> Further, based on these results, it was concluded that only deprotonated migrated acyl glucuronides react with  $BF_3$  to form the diagnostic products ions. Therefore, this methodology can differentiate migrated acyl glucuronides from their unmigrated 1- $\beta$ -acyl glucuronide isomers.

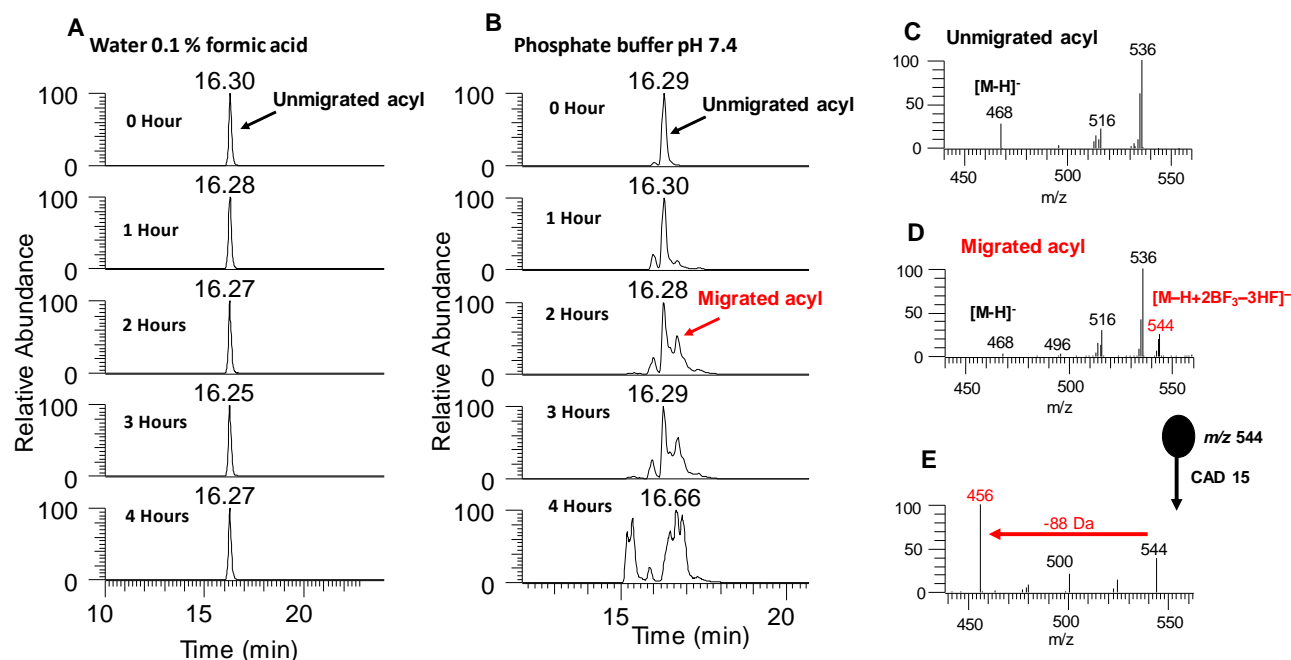


Figure 3.2 Time-course HPLC chromatograms and mass spectra showing gas-phase ion molecule and CAD reactions for lumiracoxib acyl-β-D-glucuronide incubated in 0.1 % formic acid (by volume) in water (pH 2.7) and in phosphate buffer at pH 7.4. (A) After four hours, only one peak was observed in the HPLC chromatogram measured for lumiracoxib acyl-β-D-glucuronide dissolved in acidified water. (B) Multiple peaks due to isomerization via acyl migration were observed in the HPLC chromatogram for lumiracoxib acyl-β-D-glucuronides incubated in phosphate buffer. (C) The deprotonated unmigrated isomer did not form the diagnostic product ions in the mass spectrometer. (D) The migrated isomers formed the diagnostic product ions  $[M - H + BF_3 - 2 HF]^-$  ( $m/z$  496) and  $[M - H + 2 BF_3 - 3 HF]^-$  ( $m/z$  544) after 30 ms reaction. (E) The CAD (collision energy 15 arbitrary units) of the  $[M - H + 2 BF_3 - 3 HF]^-$  product ion ( $m/z$  544) yielded a fragment ion ( $m/z$  456) via loss of molecule with MW 88 Da.

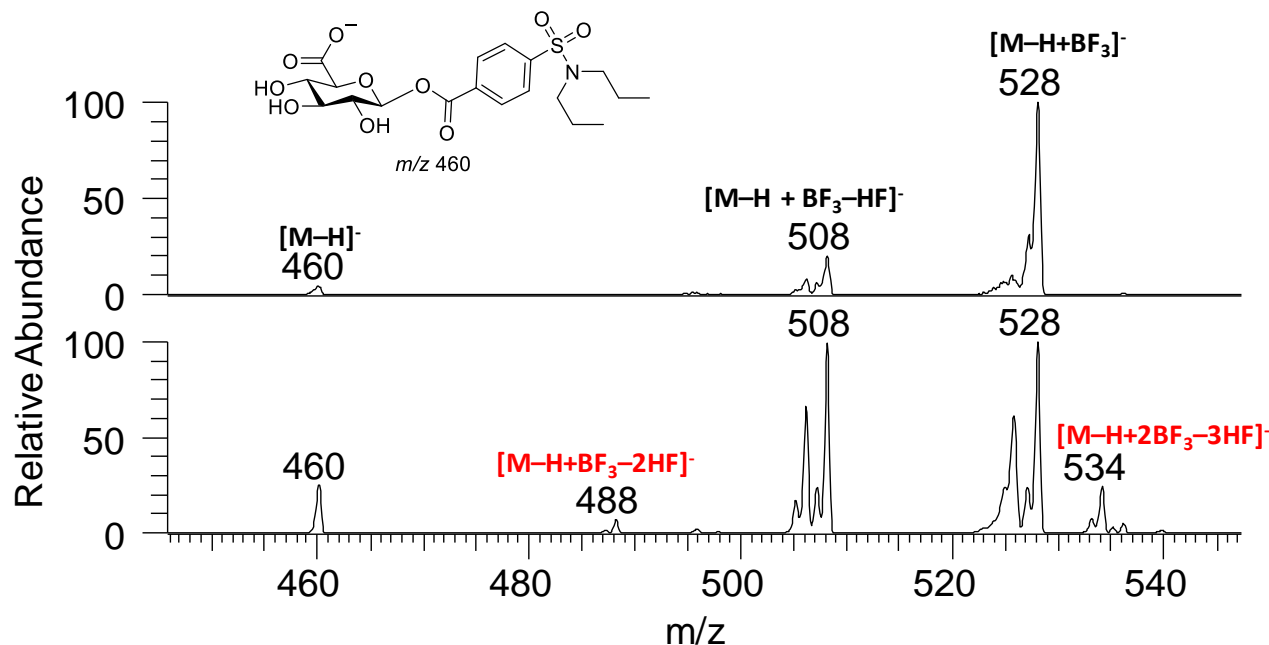


Figure 3.3 Mass spectra measured after 100 ms reaction between deprotonated probenecid acyl  $\beta$ -D-glucuronide and  $BF_3$  when the analyte was dissolved in water containing 0.1 % formic acid (v/v) (top) and when the analyte was dissolved in pure water (bottom).

### 3.3.3 Mechanism for the Formation of the Primary $[M - H + BF_3 - 2 HF]^-$ Diagnostic Product Ions

As discussed above, the formation of the primary  $[M - H + BF_3 - 2 HF]^-$  diagnostic product ions were only observed for reactions between deprotonated migrated acyl or *N*-glucuronides and  $BF_3$ . Deprotonated *O*-glucuronides did not form the diagnostic product ions when they were allowed to react with  $BF_3$ . Similar primary diagnostic product ions have been observed upon gas-phase ion-molecule reactions between deprotonated *N*-glucuronides and trichlorosilane but not between deprotonated *O*-glucuronides and trichlorosilane.<sup>25</sup> Quantum chemical calculations were performed using deprotonated glucuronic acid as a model to explore the mechanism for formation of the diagnostic primary product ions. Deprotonated glucuronic acid formed the same product ions as deprotonated migrated acyl and *N*-glucuronides when allowed to react with  $BF_3$  but it is



smaller than the glucuronides studied and therefore allowed the desired computational results to be obtained in a reasonable amount of time.

As shown in Figure 3.4 A, the formation of the  $[M - H + BF_3 - 2 HF]^-$  product ions involves two steps: ring-opening at the anomeric position of the glucuronic acid and bicyclization. The reaction is initiated by the formation of the adduct ions,  $[M - H + BF_3]^-$ , which are formed when  $BF_3$  covalently binds to the deprotonated carboxylic acid of the glucuronic acid moiety. The resulting  $[M - H + BF_3]^-$  product then undergoes ring-opening at the anomeric position of the glucuronic acid, followed by the loss of one HF molecule to form the  $[M - H + BF_3 - HF]^-$  product ions. Because the ring opens at the anomeric position, these  $[M - H + BF_3 - HF]^-$  product ions become flexible and further react with one hydroxyl group of the glucuronic acid moiety, leading to a loss of another HF molecule. This results in the formation of the bicyclic product ion  $[M - H + BF_3 - 2 HF]^-$ . Based on this mechanism, deprotonated glucuronic acid and deprotonated migrated acyl glucuronides react similarly with  $BF_3$  because both have a free hydroxyl group at the anomeric position, which plays a critical role in the ring-opening and bicyclization steps of the reaction mechanisms (Figure 3.4 B). A similar mechanism can be depicted for the reaction between deprotonated N-glucuronides and  $BF_3$  (Figure 3.4 C). In the case of deprotonated unmigrated acyl glucuronides or deprotonated *O*-glucuronides, this mechanism is not feasible.

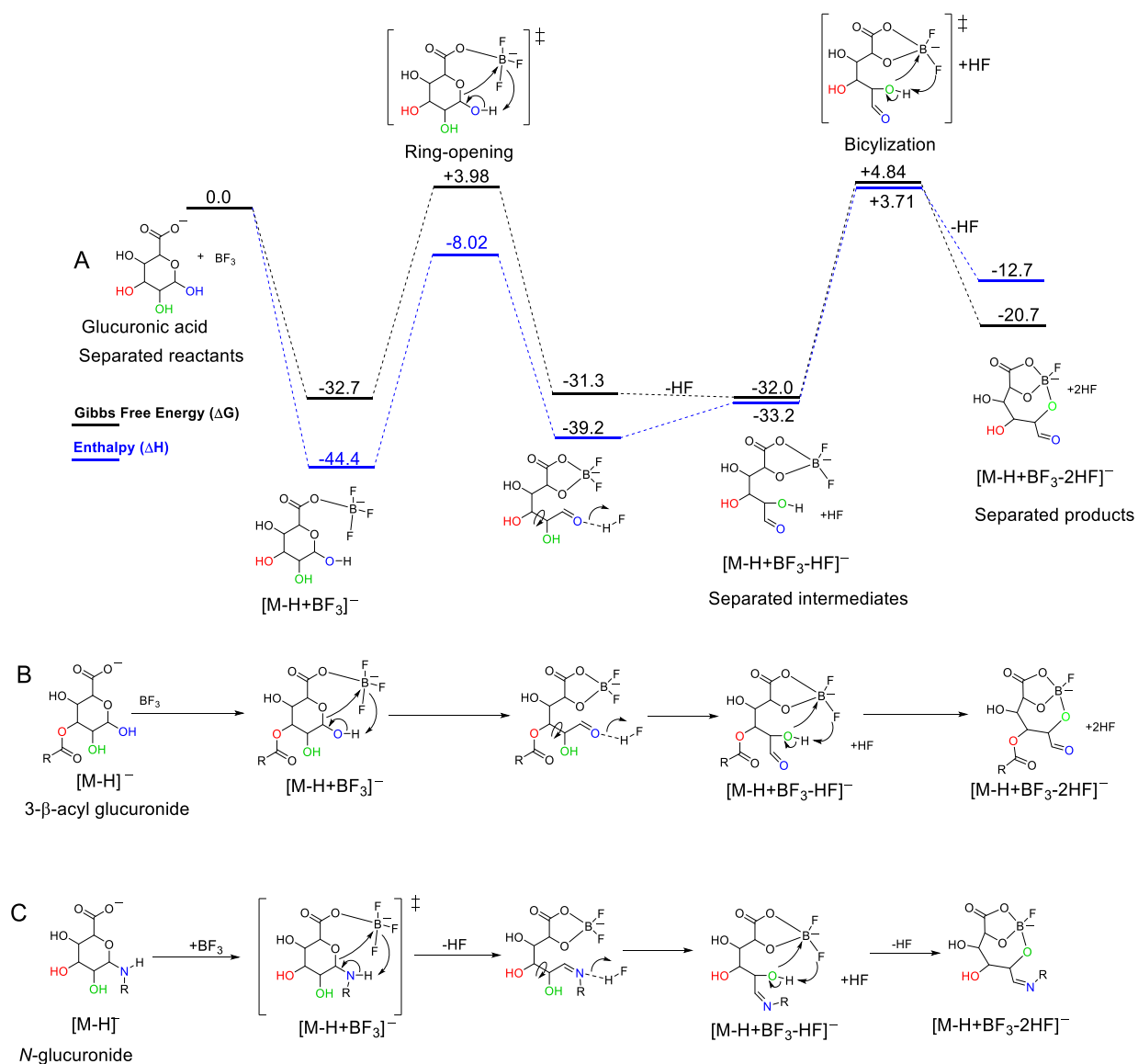


Figure 3.4 (A) Proposed mechanism and potential energy surface calculated for the reaction between deprotonated glucuronic acid and BF<sub>3</sub>. Values shown are  $\Delta G$  (black) and  $\Delta H$  (blue) in kcal/mol calculated relative to the separated reactants. All calculations were performed at the M06-2X/6-311++G(d,p) level of theory. (B) The same mechanism for the formation of the primary diagnostic product ions, [M - H + BF<sub>3</sub> - 2 HF], is proposed for the reaction between BF<sub>3</sub> and (B) a migrated deprotonated migrated (3- $\beta$ -) acyl glucuronide and (C) *N*-glucuronide.

The calculations were done by Dr. McKay W. Easton.

### 3.3.4 Mechanism for the Formation of the Secondary $[M - H + 2 BF_3 - 3 HF]^-$ Diagnostic Product Ions

The secondary diagnostic product ion,  $[M - H + 2 BF_3 - 3 HF]^-$ , is proposed to form from the primary product ion  $[M - H + BF_3 - HF]^-$  (Figure 3.5 A). This is based on the fact that when the  $[M - H + BF_3 - HF]^-$  is isolated and allowed to react with  $BF_3$ , it forms the  $[M - H + 2 BF_3 - 3 HF]^-$  diagnostic product ion. Deprotonated erythronic acid, which forms the same product ions with  $BF_3$  as deprotonated glucuronic acid and deprotonated migrated acyl glucuronides but has a much lower molecular weight, was used for the computational calculations for the formation of the secondary diagnostic product ion. Based on the proposed mechanism in Figure 3.5 A and B, prior to the bicyclization step shown in Figure 3.4, the  $[M - H + BF_3 - HF]^-$  product ion can react with another  $BF_3$  by covalently binding at the 2-, 3- or 4-hydroxyl group of the glucuronic acid moiety of the deprotonated migrated acyl glucuronide, forming  $[M - H + 2 BF_3 - HF]^-$ . These product ions gain solvation energy and can then undergo rearrangement and further reactions, leading to a loss of one HF molecule to form the  $[M - H + 2 BF_3 - 2 HF]^-$  product ions. The  $[M - H + 2 BF_3 - 2 HF]^-$  product ions then react with another hydroxyl group to form the secondary  $[M - H + 2 BF_3 - 3 HF]^-$  diagnostic product ions (Figure 3.5 B). The proposed mechanism for the formation of the  $[M - H + 2 BF_3 - 3 HF]^-$  product ion from reactions of deprotonated erythronic acid and  $BF_3$  is also feasible for reactions of deprotonated migrated acyl glucuronides with  $BF_3$  (Figure 3.5 C). A similar mechanism can also be depicted for deprotonated *N*-glucuronide (Figure 3.5 D).

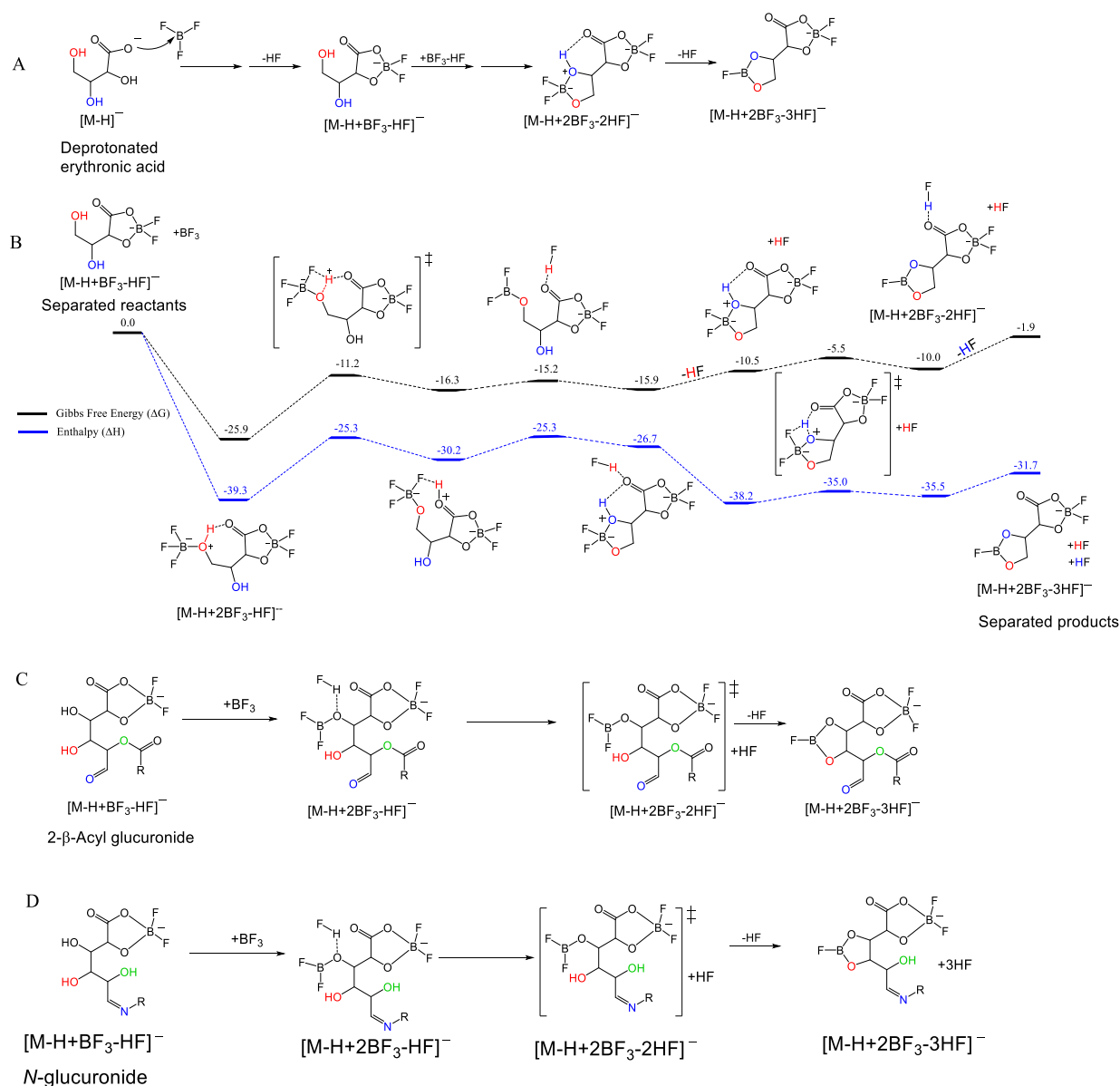


Figure 3.5 (A) Proposed mechanism for the formation of the secondary diagnostic product ions,  $[M - H + 2 BF_3 - 3 HF]^-$ , from deprotonated erythronic acid and  $BF_3$ . (B) Calculated potential energy surfaces for the formation of the secondary diagnostic product ions. Values shown are  $\Delta G$  (black) and  $\Delta H$  (blue) in kcal/mol calculated relative to the separated reactants. All calculations were performed at the M06-2X/6-311++G(d,p) level of theory. The same mechanism for the formation of the secondary diagnostic product ions is proposed for (C) deprotonated migrated 2- $\beta$ -acyl glucuronide and (D) deprotonated *N*-glucuronide with  $BF_3$ . The calculations were performed by Erlu Feng.

### 3.3.5 Mechanism for the Loss of a Molecule with MW 88 Da Upon CAD of the $[M - H + 2 BF_3 - 3 HF]^-$ Product Ions

A molecule with MW 88 Da, proposed to be 2-Fluoro-1,3,2-dioxaborale, is eliminated upon CAD of the  $[M - H + 2 BF_3 - 3 HF]^-$  product ion, which is formed following reactions between migrated acyl glucuronides and  $BF_3$ . 2-Fluoro-1,3,2-dioxaborale is eliminated via a mechanism involving a four-membered transition state that involves the aldehyde moiety formed at the anomeric position (Figure 3.6). Quantum chemical calculations were performed on ions similar to the product ion generated from reactions between deprotonated 4- $\beta$ -acyl glucuronide and  $BF_3$  and the results demonstrated that the proposed mechanism is feasible (Figure 3.6).

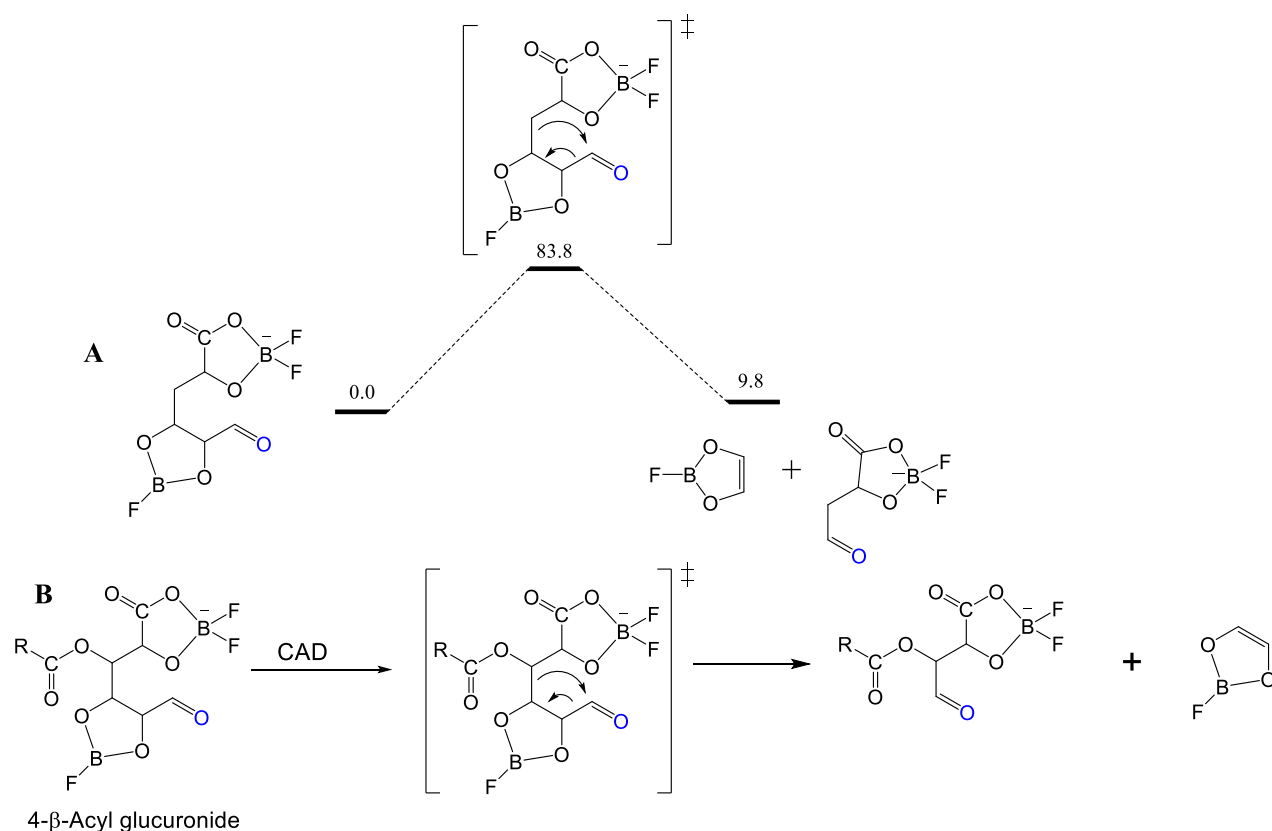


Figure 3.6 (A) Calculated potential energy surfaces for the loss of 2-fluoro-1,3,2-dioxaborale. Values shown are  $\Delta G$  in kcal/mol calculated relative to the separated reactants. All calculations were performed at the M06-2X/6-311++G(d,p) level of theory. (B) Proposed mechanism for the loss of 2-fluoro-1,3,2-dioxaborale upon CAD of the  $[M-H+2BF_3-3HF]^-$  product ion formed between 4- $\beta$ -O-acyl glucuronide and  $BF_3$ . The calculations were performed by Erlu Feng.

The mechanism for the loss of 2-fluoro-1,3,2-dioxaborole generated from deprotonated migrated 3- $\beta$ -acyl and 4- $\beta$ -acyl glucuronides is quite different from that of deprotonated migrated 2- $\beta$ -acyl glucuronide; however, the initial step for each mechanism involves the aldehyde group. (Figure 3.7 B and C).

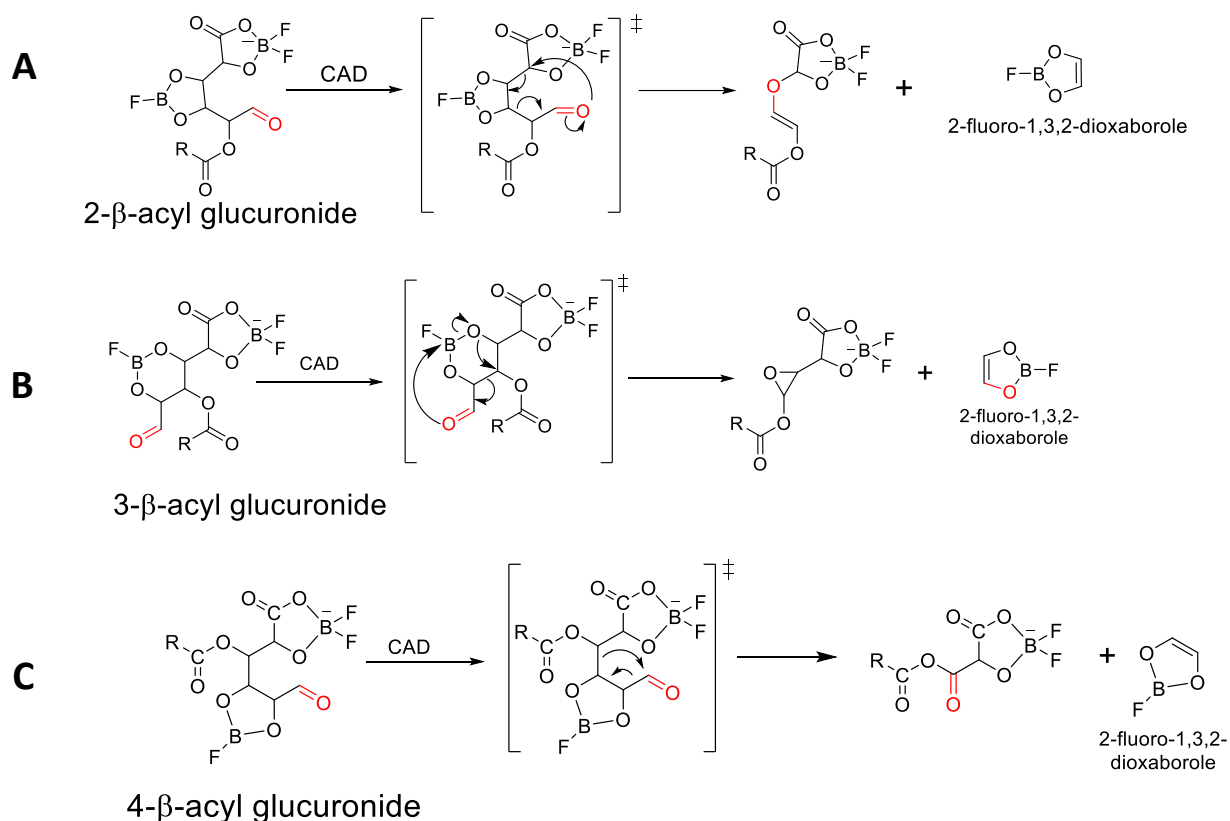


Figure 3.7 Proposed mechanism for the loss of 2-fluoro-1,3,2-dioxaborole (MW 88 Da) upon CAD of the  $[M - H + 2 BF_3 - 3 HF]^-$  product ions formed between  $BF_3$  and deprotonated (A) 2- $\beta$ -acyl glucuronide, (B) 3- $\beta$ -acyl glucuronide and (C) 4- $\beta$ -acyl glucuronide.

Further, the proposed structure of the fragment ions generated from the loss of 2-fluoro-1,3,2-dioxaborole agrees with the relative abundance of boron isotopes. The fragmenting ion contains two boron atoms, which results in a 50 % abundance of  $^{10}B$  relative to  $^{11}B$ . However, in the fragment ions (after the loss of 2-fluoro-1,3,2-dioxaborole), the abundance of  $^{10}B$  is only 25 %

relative to  $^{11}\text{B}$ , suggesting that the fragment ion contains one boron atom while the fragmenting ion contained two boron atom (Figure 3.8).

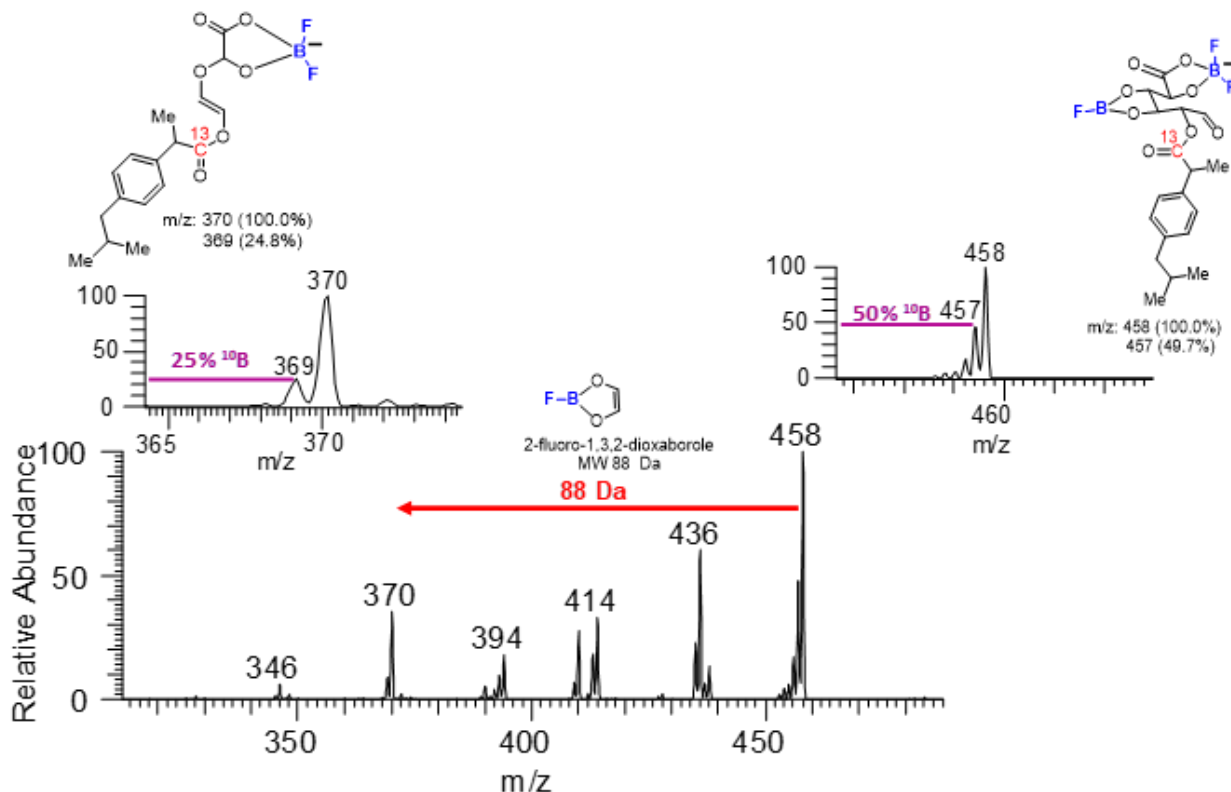


Figure 3.8 CAD mass spectrum ( $\text{MS}^3$ ) measured for the diagnostic secondary  $[\text{M} - \text{H} + 2 \text{BF}_3 - 3 \text{HF}]^-$  product ions ( $m/z$  458) formed upon reactions of  $^{13}\text{C}$ -labeled ibuprofen acyl  $\beta$ -D-glucuronide and  $\text{BF}_3$  and the relative abundances of the  $^{10}\text{B}$ -isotopes in the  $[\text{M} - \text{H} + 2 \text{BF}_3 - 3 \text{HF}]^-$  product ion (top right) and in the fragment ion formed from this product ion via the loss of a molecule with MW 88 Da (top left). These results demonstrate that upon elimination of this molecule, a boron atom was lost.

Although the reactions between deprotonated glucuronic acid or *N*-glucuronides and  $\text{BF}_3$  yield the diagnostic secondary  $[\text{M} - \text{H} + 2 \text{BF}_3 - 3 \text{HF}]^-$  product ions, CAD of these  $[\text{M} - \text{H} + 2 \text{BF}_3 - 3 \text{HF}]^-$  product ions ( $\text{MS}^3$ ) resulted in the elimination of HF to yield  $[\text{M} - \text{H} + 2 \text{BF}_3 - 4 \text{HF}]^-$  fragment ions but not the elimination of 2-fluoro-1,3,2-dioxaborole. This is likely due to the extra hydroxyl group present in above  $[\text{M} - \text{H} + 2 \text{BF}_3 - 3 \text{HF}]^-$  product ions, which facilitates elimination of HF, possibly as shown in Figure 3.9. Because there is no free hydroxyl group in the

$[M - H + 2 BF_3 - 3 HF]^-$  product ion formed between deprotonated migrated acyl glucuronides and  $BF_3$ , the loss of 2-fluoro-1,3,2-dioxaborole is observed.

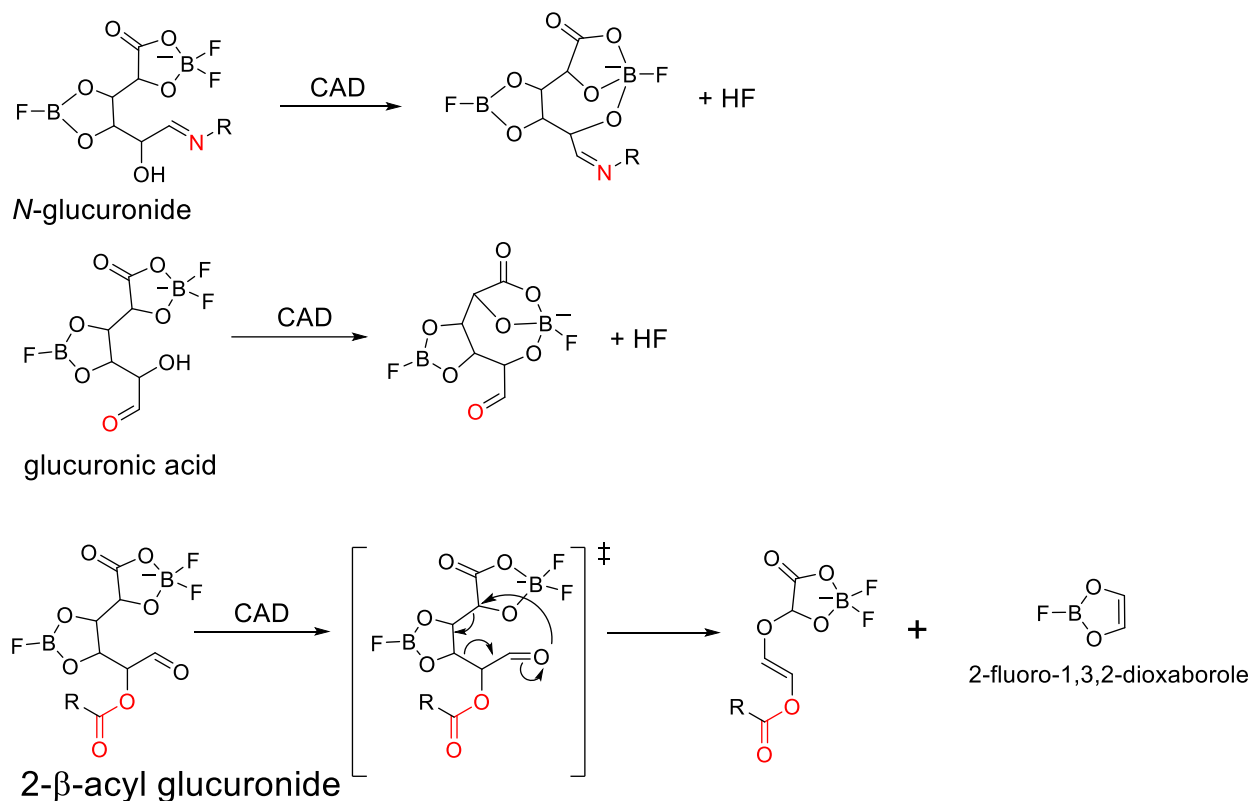


Figure 3.9 Proposed mechanism for the elimination of the HF molecule upon CAD of the  $[M - H + 2 BF_3 - 3 HF]^-$  diagnostic product ion formed between  $BF_3$  and deprotonated *N*-glucuronide or glucuronic acid and the elimination of 2-fluoro-1,3,2-dioxaborole upon CAD of the  $[M - H + 2 BF_3 - 3 HF]^-$  diagnostic product ion formed between  $BF_3$  and deprotonated, migrated acyl 2- $\beta$ -D-glucuronide.

### 3.3.6 Application of this Methodology in Differentiating acyl, *N*-, and *O*-glucuronides in a Mixture

To further demonstrate the utility of above method for differentiating deprotonated *O*-, *N*- and acyl glucuronides, a mixture of telmisartan acyl- $\beta$ -D-glucuronide (denoted acyl), PhIP *N*- $\beta$ -D-glucuronide (denoted *N*-), and ezetimibe *O*- $\beta$ -D-glucuronide (denoted *O*-) was stored in phosphate buffer for 4 hours at room temperature to induce acyl migration prior to HPLC/MS<sup>3</sup> analysis. The structures of these three glucuronides are shown in Figure 3.10. After four hours, telmisartan acyl-



$\beta$ -D-glucuronide and PhIP *N*- $\beta$ -D-glucuronide showed a single chromatographic peak each, while ezetimibe *O*- $\beta$ -D-glucuronide showed two unresolved peaks (Figure 3.11 A) in the HPLC chromatogram. The two peaks for ezetimibe *O*- $\beta$ -D-glucuronide are proposed to correspond to its stereoisomers. It was not surprising that one single peak was observed in the HPLC chromatogram of telmisartan acyl- $\beta$ -D-glucuronide because telmisartan acyl- $\beta$ -D-glucuronide is among the most stable acyl glucuronides.<sup>28,37,38</sup> Furthermore, the degradation of telmisartan acyl- $\beta$ -D-glucuronide has been reported to occur primarily through hydrolysis, not through acyl migration.<sup>39</sup>

Following HPLC separation and ionization of the analytes, the ionized analytes were isolated and allowed to react with  $\text{BF}_3$  in the ion trap. As expected, deprotonated PhIP *N*- $\beta$ -D-glucuronide produced both the  $[\text{M} - \text{H} + \text{BF}_3 - 2 \text{HF}]^-$  and  $[\text{M} - \text{H} + 2 \text{BF}_3 - 3 \text{HF}]^-$  diagnostic product ions (Figure 3.11 B). Although the chromatogram measured for telmisartan acyl- $\beta$ -D-glucuronide consisted of only one peak, suggesting that acyl migration did not occur, ion-molecule reactions revealed that there were multiple unresolved peaks corresponding to ions of different reactivities towards  $\text{BF}_3$ . No diagnostic product ions were observed for the first half of the peak, while the latter half showed diagnostic product ions following reactions with  $\text{BF}_3$  (Figure 3.11 C and D). Because only deprotonated migrated acyl glucuronides form the diagnostic product ions with  $\text{BF}_3$ , this observation suggests that telmisartan acyl- $\beta$ -D-glucuronide underwent partial acyl migration, which was not resolved by the HPLC. Deprotonated ezetimibe *O*- $\beta$ -D-glucuronide, as expected, did not form the diagnostic product ions (Figure 3.11 E). Also as expected, CAD of the  $[\text{M} - \text{H} + 2 \text{BF}_3 - 3 \text{HF}]^-$  product ion yielded a fragment ion via the neutral loss 2-fluoro-1,3,2-dioxaborole only in the case of deprotonated migrated telmisartan acyl- $\beta$ -D-glucuronide, but not for deprotonated PhIP *N*- $\beta$ -D-glucuronide (Figures 3.11 F and G).

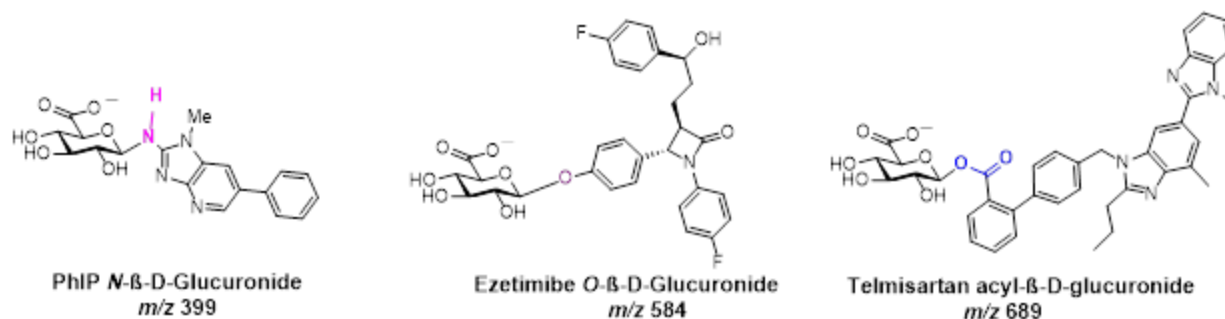


Figure 3.10 Deprotonated glucuronides used to demonstrate the utility of coupling HPLC with tandem mass spectrometry based on ion-molecule reactions followed by CAD.

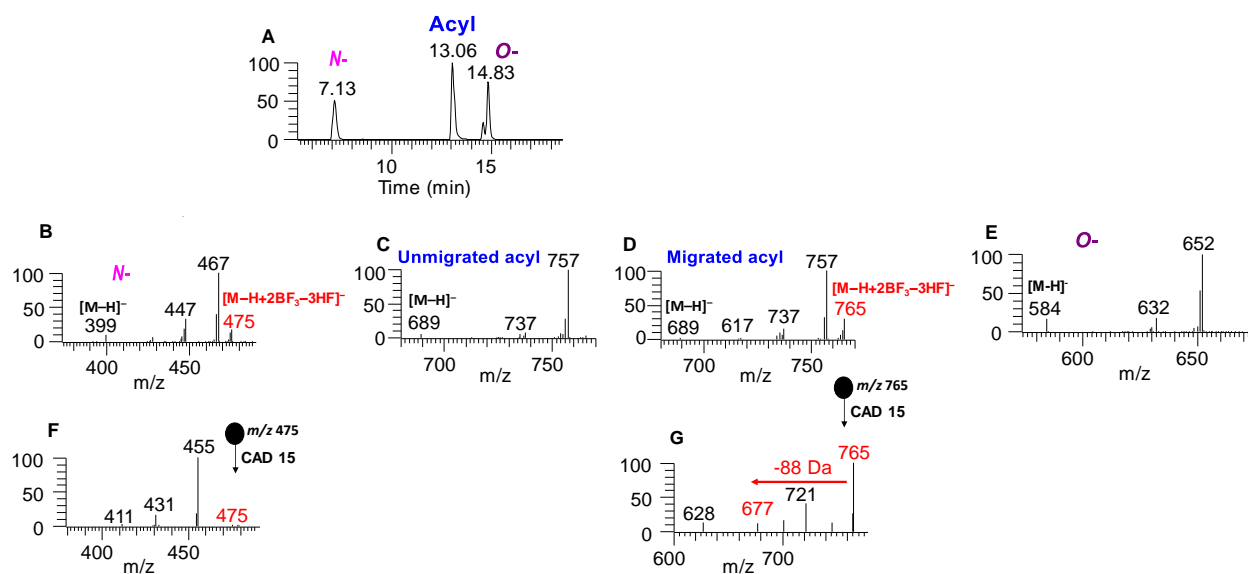


Figure 3.11 (A) HPLC chromatogram measured for a mixture of an *N*-, *O*-, and acyl glucuronide after 4 hours in phosphate buffer (pH 7.4). Mass spectra measured after 30 ms reaction with  $BF_3$  for (B) deprotonated PhIP-*N*-β-D-glucuronide, (C) deprotonated unmigrated telmisartan acyl-β-D-glucuronide, (D) deprotonated migrated telmisartan acyl-β-D-glucuronide, and (E) ezetimibe *O*-β-D-glucuronide. Both deprotonated PhIP-*N*-β-D-glucuronide and deprotonated migrated telmisartan acyl-β-D-glucuronide formed the diagnostic  $[M-H+2BF_3-3HF]^-$  product ions while deprotonated ezetimibe *O*-β-D-glucuronide did not. (F) The CAD (collision energy 15 arbitrary units) mass spectrum measured for the  $[M-H+2BF_3-3HF]^-$  product ions of deprotonated PhIP-*N*-β-D-glucuronide does not show fragment ions corresponding to the loss of 2-fluoro-1,3,2-dioxaborole. (G) The CAD mass spectrum measured for the  $[M-H+2BF_3-3HF]^-$  product ions of deprotonated migrated telmisartan acyl-β-D-glucuronide yielded fragment ions that are due to the loss of the 2-fluoro-1,3,2-dioxaborole (MW 88 Da).

### 3.4 Conclusions

A tandem mass spectrometry methodology based on gas-phase ion-molecule and CAD reactions was developed to differentiate acyl, *N*- and *O*-glucuronide drug metabolites via reactions of their deprotonated forms with  $\text{BF}_3$ . Deprotonated acyl and *N*-glucuronides can be distinguished from deprotonated *O*-glucuronides by the formation of the  $[\text{M} - \text{H} + \text{BF}_3 - 2 \text{HF}]^-$  and  $[\text{M} - \text{H} + 2 \text{BF}_3 - 3 \text{HF}]^-$  product ions, while deprotonated acyl glucuronides can be differentiated from deprotonated *N*-glucuronides by isolating the  $[\text{M} - \text{H} + 2 \text{BF}_3 - 3 \text{HF}]^-$  product ions and subjecting them to CAD. Fragment ions from a loss of 2-fluoro-1,3,2-dioxaborole (MW 88 Da) are formed for deprotonated acyl glucuronides but not for *N*-glucuronides. When ion-molecule reaction methodology was coupled with HPLC, it was also revealed that only migrated acyl glucuronides form the diagnostic  $[\text{M} - \text{H} + \text{BF}_3 - 2 \text{HF}]^-$  and  $[\text{M} - \text{H} + 2 \text{BF}_3 - 3 \text{HF}]^-$  product ions when allowed to react with  $\text{BF}_3$ , while deprotonated unmigrated acyl glucuronides do not, suggesting that this methodology can be used to differentiate unmigrated acyl glucuronides (1- $\beta$ -acyl glucuronides) from their isomeric migrated acyl glucuronides. The reactivity difference observed between deprotonated acyl, *N*- and *O*-glucuronides was computationally explored. The diagnostic product ions formed between  $\text{BF}_3$  and deprotonated *N*- and acyl glucuronides were found to arise due to the ability of these ions to undergo ring-opening at the anomeric position of the glucuronic acid moiety followed by bicyclization. Further, the HPLC/MS<sup>3</sup> measured for telmisartan acyl- $\beta$ -D-glucuronide revealed that in some cases, HPLC/MS alone cannot reliably be used to determine whether an acyl glucuronide has undergone acyl migration. However, this is critically important because the extent of acyl migration for some acyl glucuronides may be underestimated; hence, their IDT may also be underestimated. On the other hand, coupling this ion-molecule reaction methodology with HPLC did demonstrate the practicality of this methodology to rapidly and accurately identify the glucuronidation site in deprotonated acyl, *N*- and *O*-glucuronide drug

metabolites as well as to determine whether acyl migration had occurred for stable acyl glucuronides.

### 3.5 References

- (1) King, C.; Rios, G.; Green, M.; Tephly, T. UDP-Glucuronosyltransferases. *Curr. Drug Metab.* **2000**, *1* (2), 143–161.
- (2) Lemke, T. L.; Williams, D. A.; Roche, V. F.; Zito, W. S. *Foye's Principles of Medicinal Chemistry*, 7th ed.; Lippincott Williams & Wilkins: Baltimore, MD, 2013.
- (3) Kato, Y.; Igarashi, T.; Sugiyama, Y.; Nishino, A. Both CMOAT/MRP2 and Another Unknown Transporter (s) Are Responsible for the Biliary Excretion of Glucuronide Conjugate of the Nonpeptide Angiotensin II Antagonist, Telmisaltan. *Drug Metab. Dispos.* **2000**, *28* (10), 1146–1148.
- (4) Mackenzie, P. I.; Somogyi, A. A.; Miners, J. O. Advances in Drug Metabolism and Pharmacogenetics Research in Australia. *Pharmacol. Res.* **2017**, *116*, 7–19.
- (5) Sabordo, L.; Sallustio, B. C.; Evans, A. M.; Nation, R. L. Hepatic Disposition of the Acyl Glucuronide 1-O-Gemfibrozil- $\beta$ -D-Glucuronide: Effects of Clofibrilic Acid, Acetaminophen, and Acetaminophen Glucuronide. *J. Pharmacol. Exp. Ther.* **2000**, *295* (1), 44–50.
- (6) Mulder, G. J. Pharmacological Effects of Drug Conjugates: Is Morphine 6-Glucuronide an Exception? *Trends Pharmacol. Sci.* **1992**, *13*, 302–304.
- (7) Yi, L.; Dratter, J.; Wang, C.; Tunge, J. A.; Desaire, H. Identification of Sulfation Sites of Metabolites and Prediction of the Compounds' Biological Effects. *Anal. Bioanal. Chem.* **2006**, *386* (3), 666–674.
- (8) Langguth, H. S.; Benet, L. Z. Acyl Glucuronides Revisited: Is the Glucuronidation Process a Toxication as Well as a Detoxification Mechanism? *Drug Metab. Rev.* **1992**, *24* (1), 5–47.
- (9) Bailey, M. J.; Dickinson, R. G. Acyl Glucuronide Reactivity in Perspective: Biological Consequences. *Chem. Biol. Interact.* **2003**, *145* (2), 117–137.
- (10) Regan, S. L.; Maggs, J. L.; Hammond, T. G.; Lambert, C.; Williams, D. P.; Park, B. K. Acyl Glucuronides: The Good, the Bad and the Ugly. *Biopharm. Drug Dispos.* **2010**, *31* (7), 367–395.
- (11) Horng, H.; Spahn-Langguth, H.; Benet, L. Z. Mechanistic Role of Acyl Glucuronides. In *Drug-Induced Liver Disease (Third Edition)*; Elsevier, 2013; pp 35–70.

- (12) Smith, P. C.; Benet, L. Z.; McDonagh, A. F. Covalent Binding of Zomepirac Glucuronide to Proteins: Evidence for a Schiff Base Mechanism. *Drug Metab. Dispos.* **1990**, *18* (5), 639–644.
- (13) Van Breemen, R.; Fenselau, C.; Mogilevsky, W.; Odell, G. Reaction of Bilirubin Glucuronides with Serum Albumin. *J. Chromatogr. B. Biomed. Sci. App.* **1986**, *383*, 387–392.
- (14) Ding, A.; Ojingwa, J. C.; McDonagh, A. F.; Burlingame, A. L.; Benet, L. Z. Evidence for Covalent Binding of Acyl Glucuronides to Serum Albumin via an Imine Mechanism as Revealed by Tandem Mass Spectrometry. *Proc. Natl. Acad. Sci.* **1993**, *90* (9), 3797–3801.
- (15) Qiu, Y.; Burlingame, A.; Benet, L. Mechanisms for Covalent Binding of Benoxaprofen Glucuronide to Human Serum Albumin: Studies by Tandem Mass Spectrometry. *Drug Metab. Dispos.* **1998**, *26* (3), 246–256.
- (16) Smith, D. A.; Hammond, T.; Baillie, T. A. Safety Assessment of Acyl Glucuronides—A Simplified Paradigm. *Drug Metab. Dispos.* **2018**, *46* (6), 908–912.
- (17) Akira, K.; Uchijima, T.; Hashimoto, T. Rapid Internal Acyl Migration and Protein Binding of Synthetic Probenecid Glucuronides. *Chem. Res. Toxicol.* **2002**, *15* (6), 765–772.
- (18) Levsen, K.; Schiebel, H.-M.; Behnke, B.; Dötzer, R.; Dreher, W.; Elend, M.; Thiele, H. Structure Elucidation of Phase II Metabolites by Tandem Mass Spectrometry: An Overview. *J. Chromatogr. A* **2005**, *1067* (1–2), 55–72.
- (19) Lampinen-Salomonsson, M.; Bondesson, U.; Petersson, C.; Hedeland, M. Differentiation of Estriol Glucuronide Isomers by Chemical Derivatization and Electrospray Tandem Mass Spectrometry. *Rapid Commun. Mass Spectrom.* **2006**, *20* (9), 1429–1440.
- (20) Schaefer, W. H.; Politowski, J.; Hwang, B.; Dixon, F.; Goalwin, A.; Gutzait, L.; Anderson, K.; DeBrosse, C.; Bean, M.; Rhodes, G. R. Metabolism of Carvedilol in Dogs, Rats, and Mice. *Drug Metab. Dispos.* **1998**, *26* (10), 958–969.
- (21) Salomonsson, M. L.; Bondesson, U.; Hedeland, M. Structural Evaluation of the Glucuronides of Morphine and Formoterol Using Chemical Derivatization with 1, 2-dimethylimidazole-4-sulfonyl Chloride and Liquid Chromatography/Ion Trap Mass Spectrometry. *Rapid Commun. Mass Spectrom.* **2008**, *22* (17), 2685–2697.
- (22) Vaz, A. D.; Wang, W. W.; Bessire, A. J.; Sharma, R.; Hagen, A. E. A Rapid and Specific Derivatization Procedure to Identify Acyl-glucuronides by Mass Spectrometry. *Rapid Commun. Mass Spectrom.* **2010**, *24* (14), 2109–2121.
- (23) Mareck, U.; Geyer, H.; Opfermann, G.; Thevis, M.; Schänzer, W. Factors Influencing the Steroid Profile in Doping Control Analysis. *J. Mass Spectrom.* **2008**, *43* (7), 877–891.

- (24) Fabregat, A.; Pozo, O. J.; Marcos, J.; Segura, J.; Ventura, R. Use of LC-MS/MS for the Open Detection of Steroid Metabolites Conjugated with Glucuronic Acid. *Anal. Chem.* **2013**, *85* (10), 5005–5014.
- (25) Kong, J. Y.; Yu, Z.; Easton, M. W.; Niyonsaba, E.; Ma, X.; Yerabolu, R.; Sheng, H.; Jarrell, T. M.; Zhang, Z.; Ghosh, A. K.; Kenttämää, H. I. Differentiating Isomeric Deprotonated Glucuronide Drug Metabolites via Ion/Molecule Reactions in Tandem Mass Spectrometry. *Anal. Chem.* **2018**, *90* (15), 9426–9433.
- (26) Niles, R.; Witkowska, H. E.; Allen, S.; Hall, S. C.; Fisher, S. J.; Hardt, M. Acid-Catalyzed Oxygen-18 Labeling of Peptides. *Anal. Chem.* **2009**, *81* (7), 2804–2809.
- (27) Liu, W.; Ren, W.; Li, J.; Shi, Y.; Chang, W.; Shi, Y. A Ligand-Directed Catalytic Regioselective Hydrocarboxylation of Aryl Olefins with Pd and Formic Acid. *Org. Lett.* **2017**, *19* (7), 1748–1751.
- (28) Sawamura, R.; Okudaira, N.; Watanabe, K.; Murai, T.; Kobayashi, Y.; Tachibana, M.; Ohnuki, T.; Masuda, K.; Honma, H.; Kurihara, A. Predictability of Idiosyncratic Drug Toxicity Risk for Carboxylic Acid-Containing Drugs Based on the Chemical Stability of Acyl Glucuronide. *Drug Metab. Dispos.* **2010**, *38* (10), 1857–1864.
- (29) Gronert, S. Estimation of Effective Ion Temperatures in a Quadrupole Ion Trap. *J. Am. Soc. Mass Spectrom.* **1998**, *9* (8), 845–848.
- (30) Gronert, S. Quadrupole Ion Trap Studies of Fundamental Organic Reactions. *Mass Spectrom. Rev.* **2005**, *24* (1), 100–120.
- (31) Habicht, S. C.; Vinueza, N. R.; Archibold, E. F.; Duan, P.; Kenttämää, H. I. Identification of the Carboxylic Acid Functionality by Using Electrospray Ionization and Ion–Molecule Reactions in a Modified Linear Quadrupole Ion Trap Mass Spectrometer. *Anal. Chem.* **2008**, *80* (9), 3416–3421.
- (32) Frisch, M. J.; Trucks, G. W.; Schlegel, H. B.; Scuseria, G. E.; Robb, M. A.; Cheeseman, J. R.; Scalmani, G.; Barone, V.; Petersson, G. A.; Nakatsuji, H.; Li, X.; Caricato, M.; Marenich, A. V.; Bloino, J.; Janesko, B. G.; Gomperts, R.; Mennucci, B.; Hratchian, H. P.; Ortiz, J. V.; Izmaylov, A. F.; Sonnenberg, J. L.; Williams-Young, D.; Ding, F.; Lipparini, F.; Egidi, F.; Goings, J.; Peng, B.; Petrone, A.; Henderson, T.; Ranasinghe, D.; Zakrzewski, V. G.; Gao, J.; Rega, N.; Zheng, G.; Liang, W.; Hada, M.; Ehara, M.; Toyota, K.; Fukuda, R.; Hasegawa, J.; Ishida, M.; Nakajima, T.; Honda, Y.; Kitao, O.; Nakai, H.; Vreven, T.; Throssell, K.; Montgomery, J. A., Jr.; Peralta, J. E.; Ogliaro, F.; Bearpark, M. J.; Heyd, J. J.; Brothers, E. N.; Kudin, K. N.; Staroverov, V. N.; Keith, T. A.; Kobayashi, R.; Normand, J.; Raghavachari, K.; Rendell, A. P.; Burant, J. C.; Iyengar, S. S.; Tomasi, J.; Cossi, M.; Millam, J. M.; Klene, M.; Adamo, C.; Cammi, R.; Ochterski, J. W.; Martin, R. L.; Morokuma, K.; Farkas, O.; Foresman, J. B.; Fox, D. J. *Gaussian 16, Revision B.01*. Gaussian, Inc., Wallingford CT, 2016.

- (33) Zhao, Y.; Truhlar, D. G. The M06 Suite of Density Functionals for Main Group Thermochemistry, Thermochemical Kinetics, Noncovalent Interactions, Excited States, and Transition Elements: Two New Functionals and Systematic Testing of Four M06-Class Functionals and 12 Other Functionals. *Theor. Chem. Acc.* **2008**, *120* (1–3), 215–241.
- (34) Kang, P.; Dalvie, D.; Smith, E.; Renner, M. Bioactivation of Lumiracoxib by Peroxidases and Human Liver Microsomes: Identification of Multiple Quinone Imine Intermediates and GSH Adducts. *Chem. Res. Toxicol.* **2008**, *22* (1), 106–117.
- (35) Shipkova, M.; Armstrong, V. W.; Oellerich, M.; Wieland, E. Acyl Glucuronide Drug Metabolites: Toxicological and Analytical Implications. *Ther. Drug Monit.* **2003**, *25* (1), 1–16.
- (36) Faed, E. M. Properties of Acyl Glucuronides: Implications for Studies of the Pharmacokinetics and Metabolism of Acidic Drugs. *Drug Metab. Rev.* **1984**, *15* (5–6), 1213–1249.
- (37) Ebner, T.; Heinzl, G.; Prox, A.; Beschke, K.; Wachsmuth, H. Disposition and Chemical Stability of Telmisartan 1-O-Acylglucuronide. *Drug Metab. Dispos.* **1999**, *27* (10), 1143–1149.
- (38) Jinno, N.; Ohashi, S.; Tagashira, M.; Kohira, T.; Yamada, S. A Simple Method to Evaluate Reactivity of Acylglucuronides Optimized for Early Stage Drug Discovery. *Biol. Pharm. Bull.* **2013**, *36* (9), 1509–1513.
- (39) Lassila, T.; Hokkanen, J.; Aatsinki, S.-M.; Mattila, S.; Turpeinen, M.; Tolonen, A. Toxicity of Carboxylic Acid-Containing Drugs: The Role of Acyl Migration and CoA Conjugation Investigated. *Chem. Res. Toxicol.* **2015**, *28* (12), 2292–2303.

## **CHAPTER 4. IDENTIFICATION OF PROTONATED PRIMARY CARBAMATES BY USING GAS-PHASE ION-MOLECULE REACTIONS FOLLOWED BY COLLISION-ACTIVATED DISSOCIATION IN TANDEM MASS SPECTROMETRY EXPERIMENTS**

### **4.1 Introduction**

During manufacturing, drugs may gain residual impurities that are generated as synthetic byproducts or from degradation of active pharmaceutical ingredients.<sup>1,2</sup> Some impurities are potentially mutagenic (PMI) and therefore highly regulated because they pose considerable safety concerns.<sup>3,4</sup> The International Council for Harmonization of Technical Requirements for Pharmaceuticals for Human Use (ICH) has issued regulations to control the amounts of these PMIs in pharmaceutical products.<sup>5,6</sup> To ensure that the amounts of these impurities are below the acceptable threshold, robust analytical methods are needed to first identify whether or not PMIs are present. Primary carbamates are one class of such PMIs of interest because some of them, such as ethyl carbamate (urethane), vinyl carbamate, thiocarbamate, and dithiocarbamate, have been reported to be formed as byproducts during pharmaceutical syntheses.<sup>7</sup>

Unfortunately, modern analytical techniques used for identifying primary carbamates are limited in their scope and practicality. For example, X-ray crystallography and NMR spectroscopy require large amounts of pure sample, which limits their use in the analysis of complex mixtures.<sup>8</sup> Although gas chromatography coupled with electron ionization mass spectrometry has been the method of choice for identifying and quantitating different PMIs,<sup>9,10</sup> it often requires derivatizing the analytes, which can be time-consuming. High-performance liquid chromatography coupled with soft ionization mass spectrometry is the commonly used technique for mixture analysis;<sup>6,11,12</sup> however, this methods only provides the molecular weight of the analytes in the mixture. HPLC



coupled with tandem mass spectrometry ( $MS^2$ ) based on collision-activated dissociation (CAD) is the gold standard for identifying analytes in complex mixtures.<sup>13,14</sup> However, in some cases, some isomeric ions fragment in an identical manner and therefore cannot be differentiated.<sup>15</sup> In the case of primary carbamates, their CAD alone do not yield fragment ions that are diagnostic for protonated compounds in this compound class (Figure 4.1)

In contrast,  $MS^2$  based on gas-phase ion-molecule reactions can be used to differentiate many isomeric ions without reference compounds.<sup>16–18</sup> Such ion-molecule reactions have been employed to identify many functional groups,<sup>19</sup> such as *N*-oxide,<sup>20,21</sup> epoxide,<sup>22</sup> *N*-hydroxylamino,<sup>23</sup> and keto groups,<sup>24</sup> in protonated analytes. Trimethoxymethylsilane (TMMS) has been used previously as a neutral reagent in gas-phase ion-molecule reactions to identify carboxylic acid, sulfone, and sulfonamido functionalities in protonated analytes.<sup>26–37</sup> analytes, each containing one or more of 22 different functional groups, were examined, and only protonated carboxylic acid, sulfone, and sulfonamido functionalities were found to react with TMMS to form an adduct ion that had lost methanol,  $[M + H + TMMS - MeOH]^+$ . To differentiate these three functionalities, the  $[M + H + TMMS - MeOH]^+$  product ions were isolated and subjected to CAD ( $MS^3$  experiments). CAD yielded product ions that were diagnostic for each protonated analyte.<sup>26</sup> In this study, the same methodology is presented for identifying protonated primary carbamates by allowing them to react with TMMS. The reactivity of protonated amides towards TMMS is also reported here because of their structural similarity to carbamates. To rationalize the reactions which occurred between protonated amides and TMMS, reaction mechanisms were proposed and explored through quantum chemical calculations.

## 4.2 Experimental

### 4.2.1 Chemicals

TMMS (98 % purity) was purchased from Sigma-Aldrich. Carbamate model compounds (Table 4.1) and amide model compounds (Table 4.2) were also purchased from Sigma-Aldrich. Water (LC/MS grade), methanol (LC/MS grade), and acetonitrile (LC/MS grade) were purchased from Fisher Scientific. All chemicals were used without further purification.

### 4.2.2 Sample Preparation

Stock solutions of all analytes were prepared at a mass fraction of 10 parts-per-million (ppm) in 50:50 (v/v) acetonitrile:water and was then diluted to 1 ppm using the same solvent.

### 4.2.3 Instrumentation

All the mass spectrometry experiments were conducted on a Thermo Scientific LQIT MS equipped with (+) APCI. The fundamental aspects of the LQIT and of APCI are described in chapter 2 of this dissertation. The analyte solutions were injected into the APCI source at a rate of 10  $\mu\text{L}/\text{min}$  with a 500  $\mu\text{L}$  Hamilton syringe. Typical APCI source conditions were as follows: the vaporizer and capillary temperatures were set at 300 and 275  $^{\circ}\text{C}$ , respectively; the discharge current was set at 3.8  $\mu\text{A}$ ; the sheath and auxiliary gas ( $\text{N}_2$ ) flow rates were set at 30 and 10 (arbitrary units), respectively; the capillary voltage was set at 10 V and the tube lens at 40 V.

The LQIT mass spectrometer was equipped with an external reagent mixing manifold that was used to introduce the reagent (TMMS) into the ion trap through a helium buffer gas line, as previously described.<sup>27–29</sup> Briefly, TMMS was introduced into the reagent mixing manifold via a syringe pump at a flow rate of 3  $\mu\text{L}/\text{h}$ . The syringe port and surrounding area were heated to approximately 110  $^{\circ}\text{C}$  to ensure complete evaporation of TMMS. The reagent was then diluted

with a controlled amount of helium before entering the ion trap through a leak valve. To ensure that TMMS was present in the ion trap, a protonated methanol dimer ( $m/z$  65) generated in the APCI source from methanol was isolated with an isolation width of 12  $m/z$  units and allowed to react with TMMS for 300 ms. Protonated TMMS ( $m/z$  137) was observed with an abundance of 30 % relative to the protonated methanol dimer ( $m/z$  65). For gas-phase ion-molecule reactions, the protonated analytes were isolated with an isolation width of two  $m/z$  units and allowed to react with TMMS for 300 ms. For CAD experiments, an  $[M + H + TMMS - MeOH]^+$  product ion generated from the reaction between protonated analytes and TMMS was isolated and subjected to CAD in the ion trap. Typical CAD conditions were as follow: reaction time 30 ms, isolation width of two  $m/z$ -units, activation  $q$  value 0.25, and collision energy 20 (arbitrary units). Some of the mass spectrometry measurements were performed by Judy Liu.

#### 4.2.4 Computational Studies

The proton affinities of selected analytes (Table 4.1) were calculated at the B3LYP/6-311++G(d,p) level of theory. All calculations for the reaction pathways were performed at the M06-2X/6-311++G(d,p) level of theory by using Gaussian 16.<sup>30,31</sup> Transition state structures were ensured to possess one negative frequency corresponding to the reaction coordinate, while minima had no negative frequencies. Intrinsic reaction coordinate calculations were also performed for all transition states to ensure that the optimized transition state structure connected the correct reactants and products. The free energies used to construct the potential energy surfaces were computed using ideal gas statistical mechanics. All calculations were carried out by me with Dr. McKay W. Easton's help.

### 4.3 Results and Discussion

To explore the utility of above approach in the identification of primary carbamates, gas-phase reactions of TMMS with several protonated primary carbamates, one secondary carbamate and one tertiary carbamate, followed by CAD of selected product ions, were performed in LQIT mass spectrometer. Zaikuan Yu, Dr. Zhoupeng Zhang, Dr. Huaming Sheng, Dr. John Kong, Leah F. Easterling, and Jacob Milton contributed to the interpretation of the results and the examination of the reaction mechanisms.

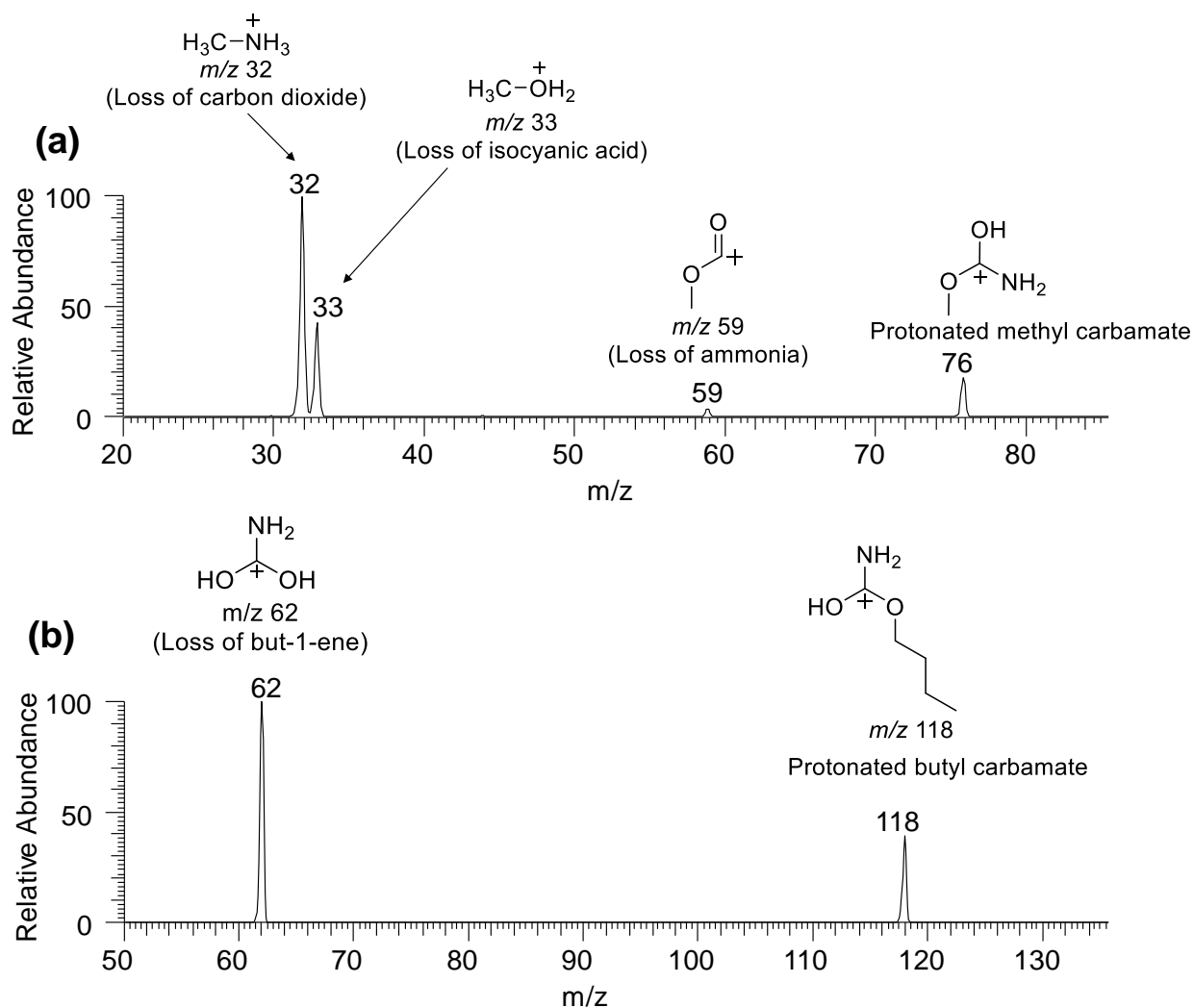


Figure 4.1 MS<sup>2</sup> spectra measured after CAD (collision energy 20 arbitrary units) of two protonated primary carbamates. (a) CAD of pronated methyl carbamate yields a fragment ion via ammonia loss ( $m/z$  59), a fragment ion via isocyanic acid loss ( $m/z$  33), and a fragment ion via carbon dioxide loss ( $m/z$  32). (b) CAD of protonated butyl carbamate only yields a fragment ion via a loss of but-1-ene ( $m/z$  62).

#### 4.3.1 Gas-phase Ion-molecule Reactions Between Protonated Carbamates and TMMS Followed by CAD

The reactivity of several protonated carbamates was tested by isolating them in the ion trap and allowing them to react with TMMS for 300 ms. An example of a mass spectrum collected following such reactions is shown in Figure 4.2. Protonated ethyl carbamate ( $m/z$  90) reacted with TMMS (MW 136 Da) to yield stable adduct ions,  $[M + H + TMMS]^+$  ( $m/z$  226), and adduct ions

that had lost methanol,  $[M + H + \text{TMMS} - \text{MeOH}]^+$  ( $m/z$  194). This spectrum is emblematic of the reactions observed for nearly all of the tested protonated primary carbamates, with the exception of protonated methocarbamol: all tested protonated primary carbamates reacted with TMMS to form stable adduct ions,  $[M + H + \text{TMMS}]^+$ , and adduct ions that had lost methanol,  $[M + H + \text{TMMS} - \text{MeOH}]^+$  (Table 4.1). Additionally, no reactions were observed between either protonated secondary or tertiary carbamates and TMMS.

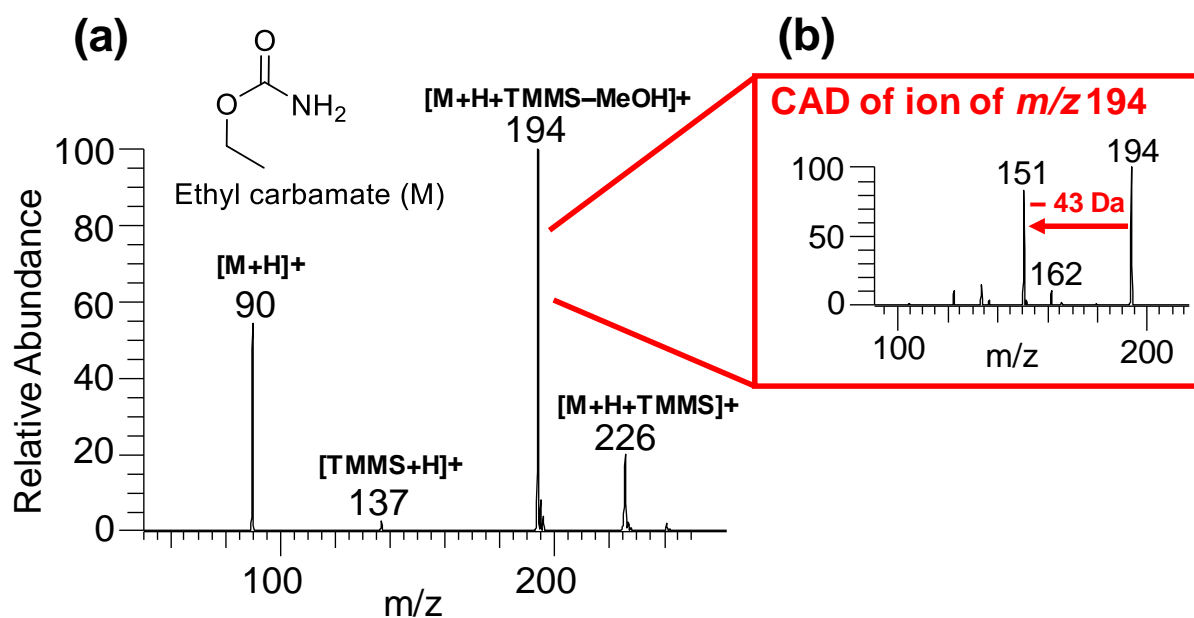


Figure 4.2 (a) MS<sup>2</sup> spectrum measured after 300 ms reaction between protonated ethyl carbamate ( $m/z$  90) and TMMS. The observed product ions are a stable adduct,  $[M + H + \text{TMMS}]^+$  ( $m/z$  226), an adduct that has lost methanol,  $[M + H + \text{TMMS} - \text{MeOH}]^+$  ( $m/z$  194), and protonated TMMS,  $[\text{TMMS} + \text{H}]^+$  ( $m/z$  137). (b) MS<sup>3</sup> spectrum measured after CAD (collision energy 20 arbitrary units) of the  $[M + H + \text{TMMS} - \text{MeOH}]^+$  product ion ( $m/z$  194). The fragment ion with  $m/z$  151 was formed via the loss of isocyanic acid ( $\text{HN}=\text{C}=\text{O}$ ; MW 43 Da), which is diagnostic for protonated primary carbamates. The fragment ion of  $m/z$  162 corresponds to elimination of methanol.

The  $[M + H + \text{TMMS} - \text{MeOH}]^+$  product ion has been previously observed to form in reactions of TMMS with protonated compounds containing a carboxylic acid, sulfone, or sulfonamide functionality.<sup>26</sup> CAD of the  $[M + H + \text{TMMS} - \text{MeOH}]^+$  product ions was used to

differentiate the three functionalities.<sup>26</sup> Thus, to identify protonated primary carbamates, their  $[M + H + \text{TMMS} - \text{MeOH}]^+$  product ions were also subjected to CAD. These experiments revealed a unique fragment ion due to the loss of isocyanic acid ( $\text{HN}=\text{C}=\text{O}$ ; MW 43 Da) which was not observed upon CAD of ions formed upon reactions of protonated carboxylic acids, sulfones, and sulfonamides.<sup>26</sup> Therefore, this methodology can be used to differentiate primary carbamates from these compound groups.

Quantum chemical calculations were performed (M06-2X/6-311++G(d,p) level of theory) to rationalize the mechanisms for the reactions of protonated ethyl carbamate with TMMS and for the elimination of isocyanic acid and methanol upon CAD of the  $[M + H + \text{TMMS} - \text{MeOH}]^+$  product ion. First, the proton affinities for selected primary carbamates were calculated to determine their protonation sites. Based on the proton affinities calculated for ethyl carbamate and phenyl carbamate, the protonation of primary carbamates likely occurs at the carbonyl oxygen because it has the highest proton affinity for these two compounds. For instance, for ethyl carbamate, the proton affinity at the carbonyl oxygen is 205.8 kcal/mol compared to 189.1 kcal/mol at the ether oxygen and 189.7 kcal/mol at the amino group (Table 4.1). Based on these calculations, the adduct ions,  $[M + H + \text{TMMS}]^+$ , formed upon reactions of protonated primary carbamates with TMMS, are stabilized by two hydrogen bonds between two oxygen atoms of TMMS and two hydrogen atoms of the protonated primary carbamate (Figure 4.3). The elimination of methanol from this adduct involves forming a covalent bond between the carbonyl oxygen of the carbamate and the silicon atom of TMMS to form the  $[M + H + \text{TMMS} - \text{MeOH}]^+$  product ion (Figure 4.3).

The elimination of isocyanic acid ( $\text{HN}=\text{C}=\text{O}$ ) upon CAD of the  $[M + H + \text{TMMS} - \text{MeOH}]^+$  ion of the ethyl carbamate is proposed to be initiated by breaking a hydrogen bond between the

NH-group of the carbamate and a methoxy group of TMMS, followed by rotation and transfer of a dimethoxymethylsilyl group from the carbonyl oxygen to the ether oxygen of the carbamate (Figure 4.3). The resulting intermediate produces the  $\text{HN}=\text{C}=\text{O}$  elimination product via a transition state that is 32.5 kcal/mol above the free energy of the  $[\text{M} + \text{H} + \text{TMMS} - \text{MeOH}]^+$  product ions. On the other hand, elimination of methanol from the  $[\text{M} + \text{H} + \text{TMMS} - \text{MeOH}]^+$  product ions is calculated to have a higher barrier (37.6 kcal/mol), which explains why isocyanic acid elimination was observed rather than methanol elimination (Figure 4.2). However, three protonated primary carbamates (protonated *tert*-butyl carbamate, butyl carbamate and allyl carbamate) formed unexpectedly low amounts (4 - 6 % relative abundance) of the fragment ions due to isocyanic acid loss ( $[\text{M} + \text{H} + \text{TMMS} - \text{MeOH} - \text{HNCO}]^+$ ) (Table 1). For protonated *tert*-butyl carbamate and butyl carbamate, the low relative abundance of the  $[\text{M} + \text{H} + \text{TMMS} - \text{MeOH} - \text{HNCO}]^+$  ions is probably due to steric hindrance, which makes the elimination of methanol more favorable than the elimination of isocyanic acid (Figure 4.3). For protonated allyl carbamate, the reasons for this behavior are unknown.



Table 4.1 Product ions ( $m/z$ ) and their relative abundances in % observed after 300 ms reaction of protonated carbamates with TMMS and the fragment ions ( $m/z$ ) and their relative abundances in % formed upon CAD of the  $[M + H + TMMS - MeOH]^+$  product ions. Also shown are the proton affinities (PAs) in kcal/mol for different atoms in two analytes.<sup>a</sup>

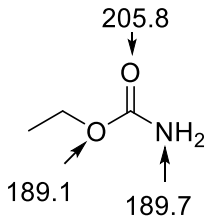
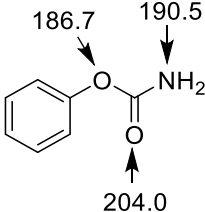
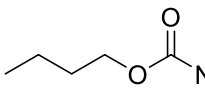
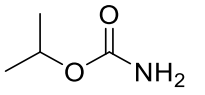
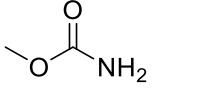
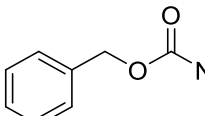
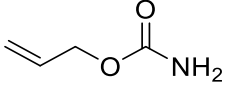
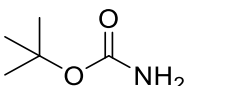
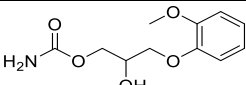
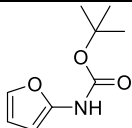
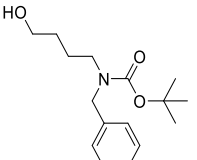
Analyte (M) ( $m/z$ of $[M + H]^+$ ion)	Analyte structure and PA of selected atoms	Products ions ( $m/z$ ) and their relative abundances in % Product ions formed upon CAD <sup>b</sup> of ions of $[M + H + TMMS - MeOH]^+$ and their relative abundances in %
Ethyl carbamate (90)		$[M + H + TMMS]^+$ (226) 24 % $[M + H + TMMS - MeOH]^+$ (194) 100 % $[TMMS + H]^+$ (137) 3 % $[M + H + TMMS - MeOH - MeOH]^+$ (162) 15 % $[M + H + TMMS - MeOH - HNCO]^+$ (151) 100 %
Phenyl carbamate (138)		$[M + H + TMMS]^+$ (274) 6 % $[M + H + TMMS - MeOH]^+$ (242) 100 % $[M + H + TMMS - MeOH - HNCO]^+$ (199) 100 %
Butyl carbamate (118)		$[M + H + TMMS]^+$ (254) 100 % $[M + H + TMMS - MeOH]^+$ (222) 67 % $[M + H + TMMS - MeOH - HNCO]^+$ (179) 5 % $[M + H + TMMS - MeOH - C_4H_8]^+$ (166) 67 % $[M + H + TMMS - 2 MeOH - C_4H_8]^+$ (134) 100 % $([M + H + TMMS - 2 MeOH - C_4H_8 + H_2O]^+)$ (152) 41 %
Isopropyl carbamate (104)		$[M + H + TMMS]^+$ (240) 100 % $[M + H + TMMS - MeOH]^+$ (208) 67 % $[M + H + TMMS - MeOH - HNCO]^+$ (165) 100 % $[M + H + TMMS - 2 MeOH - C_3H_6]^+$ (134) 8 %
Methyl carbamate (76)		$[M + H + TMMS]^+$ (212) 100 % $[M + H + TMMS - MeOH]^+$ (180) 7 % $[TMMS + H]^+$ (137) 12 % $[M + H + TMMS - MeOH - MeOH]^+$ (148) 10 % $[M + H + TMMS - MeOH - HNCO]^+$ (137) 100 %
Benzyl carbamate (152)		$[M + H + TMMS]^+$ (288) 7 % $[M + H + TMMS - MeOH]^+$ (256) 100 % $[M + H + TMMS - MeOH - HNCO]^+$ (213) 100 %

Table 4.1 (Continued)

Analyte (M) ( $m/z$ of $[M + H]^+$ ion)	Analyte structure	Products ions ( $m/z$ ) and their relative abundances in % Product ions formed upon CAD <sup>b</sup> of ions of $[M + H + TMMS - MeOH]^+$ and their relative abundances in %
Allyl carbamate (102)		$[M + H + TMMS]^+$ (238) 100 % $[M + H + TMMS - MeOH]^+$ (206) 86 % $[M + H + TMMS - MeOH - MeOH]^+$ (174) 11 % $[M + H + TMMS - MeOH - HNCO]^+$ (163) 6 % $[M + H + TMMS - 2 MeOH - C_3H_4]^+$ (134) 100 % $[M + H + TMMS - 2 MeOH - C_3H_4 + H_2O]^+$ (152) 48 %
<i>tert</i> -Butyl carbamate (118)		$[M + H + TMMS]^+$ (254) 100 % $[M + H + TMMS - MeOH]^+$ (222) 67 % $[M + H + TMMS - MeOH - MeOH]^+$ (190) 38 % $[M + H + TMMS - MeOH - HNCO]^+$ (179) 4 % $[M + H + TMMS - MeOH - C_4H_8]^+$ (166) 16 % $[M + H + TMMS - 2 MeOH - C_4H_8]^+$ (134) 39 % $[M + H + TMMS - 2 MeOH - C_4H_8 + H_2O]^+$ (152) 19 %
Methocarbamol (242)		No reactions
<i>tert</i> -Butyl- <i>N</i> -(2-furyl)carbamate (184)		No reactions
<i>tert</i> -Butyl-benzyl-(4-hydroxybutyl) carbamate (280)		No reactions

<sup>a</sup> Proton affinities (in kcal/mol) were calculated at the B3LYP/6-311++G(d,p) level of theory.

<sup>b</sup> CAD collision energy 20 arbitrary units.

Among all primary carbamates studied, protonated methocarbamol is the only primary carbamate that did not react with TMMS (Table 4.1). This observation was rationalized by further quantum chemical calculations on protonated 2-hydroxy-3-methoxypropyl carbamate in order to determine its most stable conformer. This cation was chosen as the model compound for the calculations because it has a similar structure as protonated methocarbamol (Figure 4.4). The most stable conformer of protonated 2-hydroxy-3-methoxypropyl carbamate was determined to be a

seven-membered ring conformer stabilized by a hydrogen bond. This conformer is 3.5 kcal/mol more stable than the linear structure (Figure 4.5). It is expected that the most stable conformer of protonated methocarbamol has a similar seven-membered ring structure. As the highest barrier for the reaction of protonated ethyl carbamate with TMMS is only 3 kcal/mol below the total energy level of the system (Figure 4.3), this extra stabilization may prevent its reactions with TMMS.

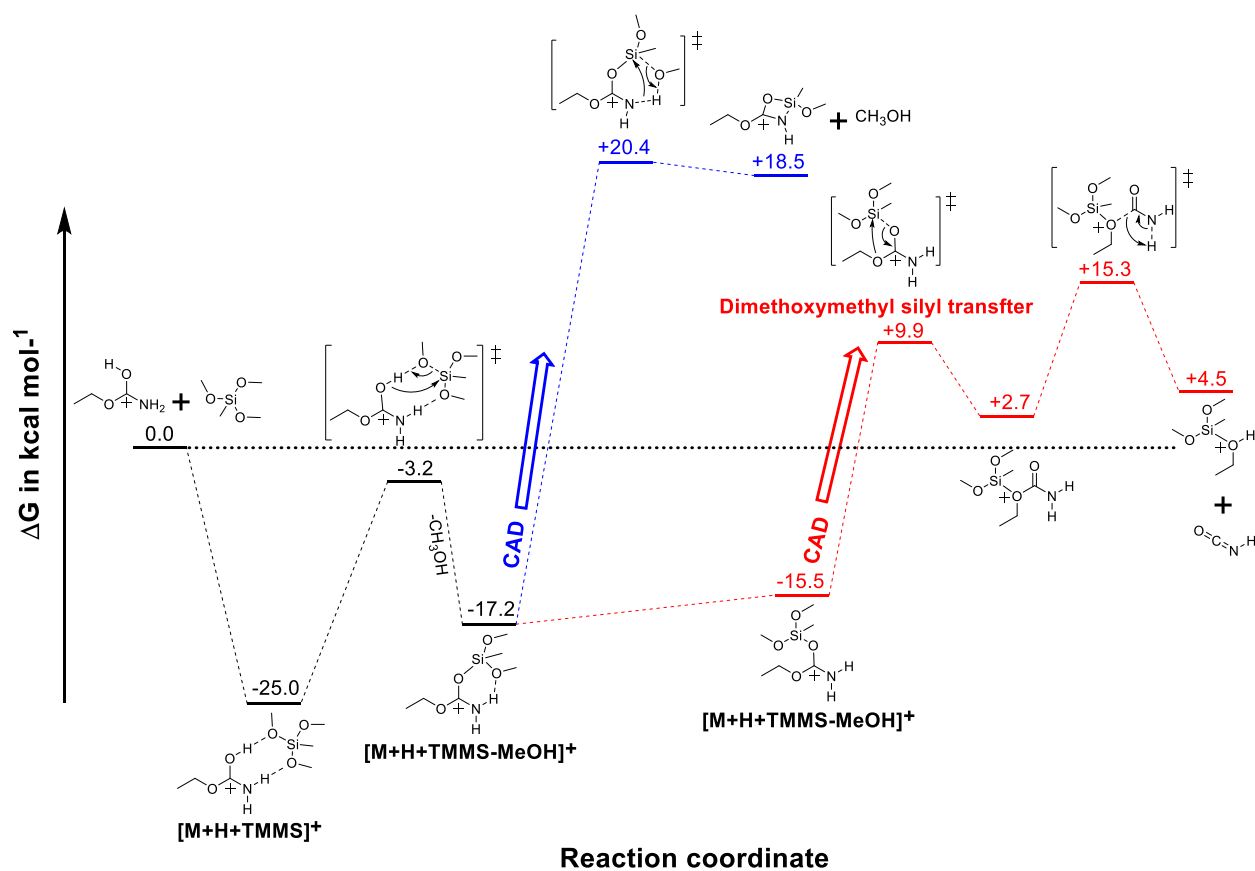


Figure 4.3 Potential energy surface calculated at the M06-2X/6-311++G-(d,p) level of theory for the formation of the ions  $[M + H + TMMS]^+$  and  $[M + H + TMMS - MeOH]^+$  upon reactions of protonated ethyl carbamate with TMMS. Also shown are the potential energy surfaces associated with the formation of fragment ions formed via a loss of isocyanic acid (**red**) and methanol (**blue**) upon CAD of the  $[M + H + TMMS - MeOH]^+$  product ion.

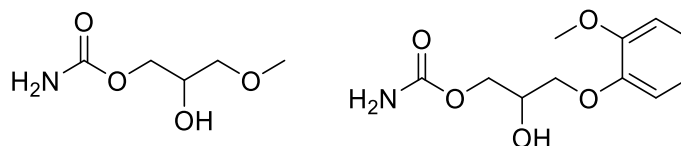


Figure 4.4 2-Hydroxy-3-methoxypropyl carbamate and methocarbamol.

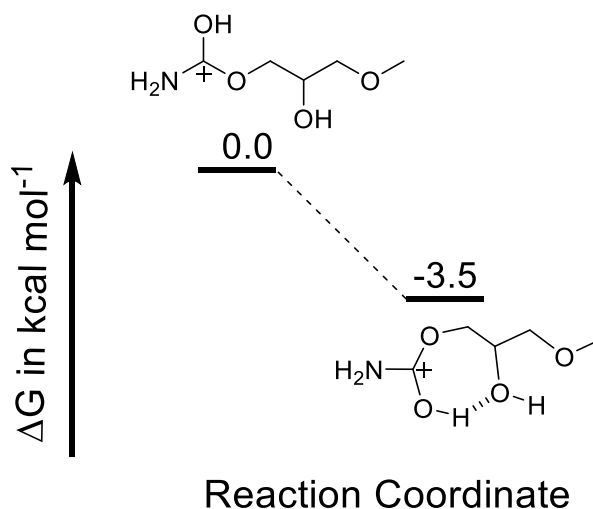


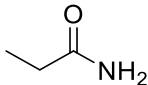
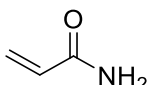
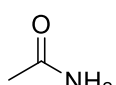
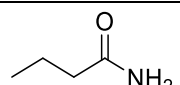
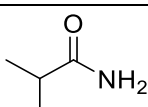
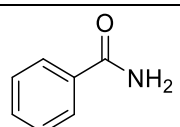
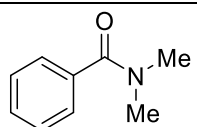
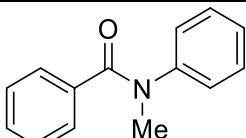
Figure 4.5 Potential energy surface calculated at the M06-2X/6-311++G-(d,p) level of theory for two conformers of protonated 2-hydroxy-3-methoxypropyl carbamate.

#### 4.3.2 Gas-phase Ion-molecule Reactions Between Protonated Amides and TMMS Followed by CAD

Because of the structural similarities between amides and carbamates, several protonated amides were also tested for their reactivity towards TMMS. Among the six primary amides and two tertiary amides studied, only protonated propionamide, protonated acrylamide, and protonated acetamide were found to react with TMMS to form the adduct ion,  $[\text{M} + \text{H} + \text{TMMS}]^+$ , and the adduct ion that had lost methanol,  $[\text{M} + \text{H} + \text{TMMS} - \text{MeOH}]^+$ , (Table 4.2). Upon CAD, the  $[\text{M} + \text{H} + \text{TMMS} - \text{MeOH}]^+$  product ions generated from the three protonated primary amides fragmented via elimination of methanol but not via elimination of isocyanic acid (Figure 4.4). This is not surprising since the mechanism proposed for the isocyanic acid loss for carbamates is not

feasible for amides. Since no elimination of isocyanic acid was observed, the primary amides can be differentiated from primary carbamates.

Table 4.2 Product ions (with their relative abundances) observed after 300 ms reaction of protonated amides and the fragment ions (with their relative abundances) formed upon CAD<sup>a</sup> of the product ions  $[M + H + TMMS - MeOH]^+$ .

Analyte (M) ( $m/z$ of $[M+H]^+$ ion)	Analyte structure	Products ions ( $m/z$ ) and their relative abundances in % Product ions formed upon CAD of ions of $[M + H + TMMS - MeOH]^+$ and their relative abundance in %
Propionamide (74)		$[M + H + TMMS]^+$ (210) 100 % $[M + H + TMMS - MeOH]^+$ (178) 33 % $[M + H + TMMS - 2 MeOH]^+$ (146) 100 % $[M + H + TMMS - 2 MeOH + H_2O]^+$ (164) 6 %
Acrylamide (72)		$[M + H + TMMS]^+$ (208) 100 % $[M + H + TMMS - MeOH]^+$ (176) 85 % $[M + H + TMMS - 2 MeOH]^+$ (144) 100 % $[M + H + TMMS - 2 MeOH + H_2O]^+$ (162) 13 %
Acetamide (60)		$[M + H + TMMS]^+$ (196) 100 % $[M + H + TMMS - MeOH]^+$ (164) 45 % $[M + H + TMMS - 2 MeOH]^+$ (132) 100 % $[M + H + TMMS - 2 MeOH + H_2O]^+$ (150) 24 %
Butyramide (88)		$[M + H + TMMS]^+$ (224) 100 %
Isobutyramide (88)		$[M + H + TMMS]^+$ (224) 100 %
Benzamide (122)		$[M + H + TMMS]^+$ (258) 100 %
<i>N,N</i> -dimethyl- benzamide (150)		No reactions
<i>N</i> -methyl- <i>N</i> - phenylbenzamide (212)		No reactions

<sup>a</sup>CAD collision energy 20 arbitrary units

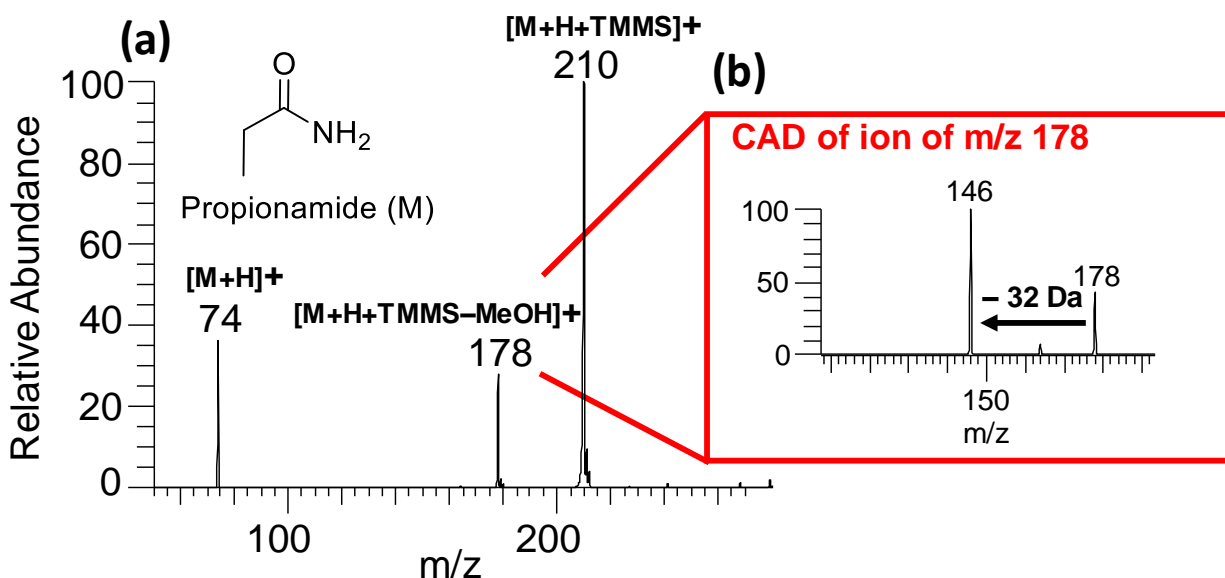


Figure 4.6 (a) MS<sup>2</sup> spectrum measured after 300 ms reaction of protonated propionamide ( $m/z$  74) with TMMS. The observed product ions are a stable adduct,  $[M + H + TMMS]^+$  ( $m/z$  210), and an adduct that has lost methanol,  $[M + H + TMMS - MeOH]^+$  ( $m/z$  178). (b) MS<sup>3</sup> spectrum measured after CAD (collision energy 20 arbitrary units) of the  $[M + H + TMMS - MeOH]^+$  product ion ( $m/z$  178). The major fragment ion observed ( $m/z$  146) corresponds to the loss of methanol. No fragment ion from the loss of isocyanic acid (MW 43 Da) was observed.

Upon CAD of the  $[M + H + TMMS - MeOH]^+$  product ions of protonated carbamates (Table 4.1; Figure 4.7) and protonated amides (Table 4.2), the formation of water adducts was observed. Similar water adduct ions have previously been reported for the CAD of protonated isoquinoline-3-carboxamides.<sup>32</sup> An example of these water adduct ions and how they are likely to be formed is shown in Figure 4.7.

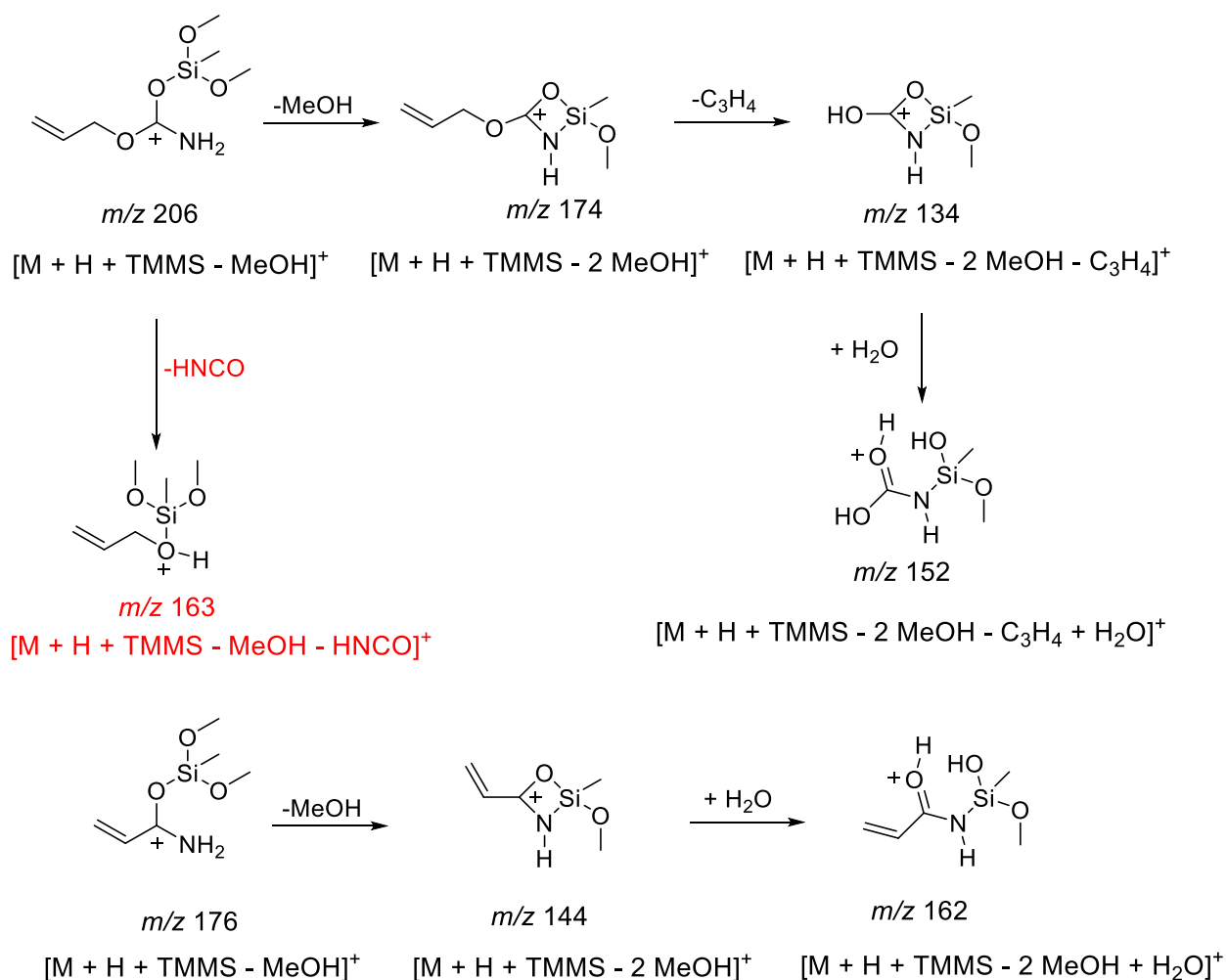


Figure 4.7 Proposed fragmentation pathway for CAD of the  $[\text{M} + \text{H} + \text{TMMS} - \text{MeOH}]^+$  product ion formed between TMMS and protonated allyl carbamate (top) and protonated acrylamide (bottom). CAD of the  $[\text{M} + \text{H} + \text{TMMS} - \text{MeOH}]^+$  product ion of protonated allyl carbamate yields a diagnostic fragment ion via the elimination of isocyanic acid ( $m/z$  163), a fragment ion via elimination of methanol ( $m/z$  174) and a fragment ion via elimination of both methanol and propa-1,2-diene ( $m/z$  134). This fragment ion ( $m/z$  134) reacts with water to form a water adduct ion ( $m/z$  152). CAD of  $[\text{M} + \text{H} + \text{TMMS} - \text{MeOH}]^+$  of protonated acrylamide only yields a fragment ion via elimination of methanol ( $m/z$  144). This fragment ion reacts with water to form a water adduct ion ( $m/z$  162).

#### 4.4 Conclusions

Primary carbamates were found to react with TMMS in the gas phase to form adduct ions,  $[\text{M} + \text{H} + \text{TMMS}]^+$ , and adduct ions that had lost methanol,  $[\text{M} + \text{H} + \text{TMMS} - \text{MeOH}]^+$ . These product ions were observed for protonated primary carbamates, some primary amides, and for



protonated carboxylic acids, sulfones, and sulfonamides, as previously reported.<sup>26</sup> CAD of these ions generated for primary carbamates yields a fragment ion due to isocyanic acid loss. This loss was not observed for analogous ions generated for carboxylic acids, sulfones, sulfonamide, or amides. Therefore, this loss is diagnostic for protonated primary carbamates. The elimination of isocyanic acid upon CAD of the  $[M + H + \text{TMMS} - \text{MeOH}]^+$  product ions is proposed to be initiated by breaking a hydrogen bond between the NH-group of the carbamate and a methoxy group of TMMS in the  $[M + H + \text{TMMS} - \text{MeOH}]^+$  ions, followed by rotation and transfer of the dimethoxymethylsilyl group from the carbonyl oxygen to the ether oxygen of the carbamate. This intermediate yields the  $[M + H + \text{TMMS} - \text{MeOH} - \text{HNCO}]^+$  ions via the loss of isocyanic acid. This method shows considerable promise for identifying primary carbamates.

#### 4.5 References

- (1) Callis, C. M.; Bercu, J. P.; DeVries, K. M.; Dow, L. K.; Robbins, D. K.; Varie, D. L. Risk Assessment of Genotoxic Impurities in Marketed Compounds Administered over a Short-Term Duration: Applications to Oncology Products and Implications for Impurity Control Limits. *Org. Process Res. Dev.* **2010**, *14* (4), 986–992.
- (2) Lee, C.; Helmy, R.; Strulson, C.; Plewa, J.; Kolodziej, E.; Antonucci, V.; Mao, B.; Welch, C. J.; Ge, Z.; Al-Sayah, M. A. Removal of Electrophilic Potential Genotoxic Impurities Using Nucleophilic Reactive Resins. *Org. Process Res. Dev.* **2010**, *14* (4), 1021–1026.
- (3) Bercu, J. P.; Hoffman, W. P.; Lee, C.; Ness, D. K. Quantitative Assessment of Cumulative Carcinogenic Risk for Multiple Genotoxic Impurities in a New Drug Substance. *Regul. Toxicol. Pharmacol.* **2008**, *51* (3), 270–277.
- (4) Cimarosti, Z.; Bravo, F.; Stonestreet, P.; Tinazzi, F.; Vecchi, O.; Camurri, G. Application of Quality by Design Principles to Support Development of a Control Strategy for the Control of Genotoxic Impurities in the Manufacturing Process of a Drug Substance. *Org. Process Res. Dev.* **2010**, *14* (4), 993–998.

- (5) Kroes, R.; Renwick, A. G.; Cheeseman, M.; Kleiner, J.; Mangelsdorf, I.; Piersma, A.; Schilter, B.; Schlatter, J.; van Schothorst, F.; Vos, J.; Würtzen, G. Structure-Based Thresholds of Toxicological Concern (TTC): Guidance for Application to Substances Present at Low Levels in the Diet. *Food Chem. Toxicol.* **2004**, *42* (1), 65–83.
- (6) Teasdale, A.; Elder, D. P. Analytical Control Strategies for Mutagenic Impurities: Current Challenges and Future Opportunities? *TrAC Trends Anal. Chem.* **2018**, *101*, 66–84.
- (7) Galloway, S. M.; Reddy, M. V.; McGettigan, K.; Gealy, R.; Bercu, J. Potentially Mutagenic Impurities: Analysis of Structural Classes and Carcinogenic Potencies of Chemical Intermediates in Pharmaceutical Syntheses Supports Alternative Methods to the Default TTC for Calculating Safe Levels of Impurities. *Regul. Toxicol. Pharmacol.* **2013**, *66* (3), 326–335.
- (8) Peiris, D. M.; Lam, W.; Michael, S.; Ramanathan, R. Distinguishing N-oxide and Hydroxyl Compounds: Impact of Heated Capillary/Heated Ion Transfer Tube in Inducing Atmospheric Pressure Ionization Source Decompositions. *J. Mass Spectrom.* **2004**, *39* (6), 600–606.
- (9) Liu, X.-W.; Zhang, W.-P.; Han, H.-Y.; Sun, L.; Chen, D.-Y. Trace Determination of Mutagenic Alkyl Toluenesulfonate Impurities via Derivatization Headspace–GC/MS in an Active Pharmaceutical Ingredient of a Candidate Drug. *J. Pharm. Biomed. Anal.* **2018**, *155*, 104–108.
- (10) Loda, C.; Bernabe, E.; Nicoletti, A.; Bacchi, S.; Dams, R. Determination of Epichlorohydrin in Active Pharmaceutical Ingredients by Gas Chromatography–Mass Spectrometry. *Org. Process Res. Dev.* **2011**, *15* (6), 1388–1391.
- (11) Yang, R.-S.; Beard, A.; Sheng, H.; Zhang, L.-K.; Helmy, R. Applications of TiCl<sub>3</sub> as a Diagnostic Reagent for the Detection of Nitro- and N-Oxide-Containing Compounds as Potentially Mutagenic Impurities Using Ultrahigh-Performance Liquid Chromatography Coupled with High-Resolution Mass Spectrometry. *Org. Process Res. Dev.* **2015**, *20* (1), 59–64.
- (12) Yuabova, Z. Y.; Holschlag, D. R.; Rodriguez, S. A.; Qin, C.; Papov, V. V.; Qiu, F.; McCaffrey, J. F.; Norwood, D. L. Genotoxic Impurities: A Quantitative Approach. *J. Liq. Chromatogr. Relat. Technol.* **2008**, *31* (15), 2318–2330.
- (13) Ma, S.; Chowdhury, S. K. Data Acquisition and Data Mining Techniques for Metabolite Identification Using LC Coupled to High-Resolution MS. *Bioanalysis* **2013**, *5* (10), 1285–1297.
- (14) Wen, B.; Zhu, M. Applications of Mass Spectrometry in Drug Metabolism: 50 Years of Progress. *Drug Metab. Rev.* **2015**, *47* (1), 71–87.

- (15) Kong, J. Y.; Yu, Z.; Easton, M. W.; Niyonsaba, E.; Ma, X.; Yerabolu, R.; Sheng, H.; Jarrell, T. M.; Zhang, Z.; Ghosh, A. K. Differentiating Isomeric Deprotonated Glucuronide Drug Metabolites via Ion/Molecule Reactions in Tandem Mass Spectrometry. *Anal. Chem.* **2018**, *90* (15), 9426–9433.
- (16) Sheng, H.; Tang, W.; Yerabolu, R.; Max, J.; Kotha, R. R.; Riedeman, J. S.; Nash, J. J.; Zhang, M.; Kenttämä, H. I. Identification of N-Oxide and Sulfoxide Functionalities in Protonated Drug Metabolites by Using Ion–Molecule Reactions Followed by Collisionally Activated Dissociation in a Linear Quadrupole Ion Trap Mass Spectrometer. *J. Org. Chem.* **2016**, *81* (2), 575–586.
- (17) Fu, M.; Duan, P.; Li, S.; Habicht, S. C.; Pinkston, D. S.; Vinueza, N. R.; Kenttämä, H. I. Regioselective Ion–Molecule Reactions for the Mass Spectrometric Differentiation of Protonated Isomeric Aromatic Diamines. *The Analyst* **2008**, *133* (4), 452.
- (18) Bjarnason, A.; Taylor, J. W.; Kinsinger, J. A.; Cody, R. B.; Weil, D. A. Isomer Discrimination of Disubstituted Benzene Derivatives through Gas-Phase Iron(I) Ion Reactions in a Fourier-Transform Mass Spectrometer. *Anal. Chem.* **1989**, *61* (17), 1889–1894.
- (19) Osburn, S.; Ryzhov, V. Ion–Molecule Reactions: Analytical and Structural Tool. *Anal. Chem.* **2013**, *85* (2), 769–778.
- (20) Duan, P.; Gillespie, T. A.; Winger, B. E.; Kenttämä, H. I. Identification of the Aromatic Tertiary N -Oxide Functionality in Protonated Analytes via Ion/Molecule Reactions in Mass Spectrometers. *J. Org. Chem.* **2008**, *73* (13), 4888–4894.
- (21) Duan, P.; Fu, M.; Gillespie, T. A.; Winger, B. E.; Kenttämä, H. I. Identification of Aliphatic and Aromatic Tertiary N-Oxide Functionalities in Protonated Analytes via Ion/Molecule and Dissociation Reactions in an FT-ICR Mass Spectrometer. *J. Org. Chem.* **2009**, *74* (3), 1114–1123.
- (22) Eismin, R. J.; Fu, M.; Yem, S.; Widjaja, F.; Kenttämä, H. I. Identification of Epoxide Functionalities in Protonated Monofunctional Analytes by Using Ion/Molecule Reactions and Collision-Activated Dissociation in Different Ion Trap Tandem Mass Spectrometers. *J. Am. Soc. Mass Spectrom.* **2012**, *23* (1), 12–22.
- (23) Sheng, H.; Tang, W.; Yerabolu, R.; Kong, J. Y.; Williams, P. E.; Zhang, M.; Kenttämä, H. I. Mass Spectrometric Identification of the N-monosubstituted N-hydroxylamino Functionality in Protonated Analytes via Ion/Molecule Reactions in Tandem Mass Spectrometry. *Rapid Commun. Mass Spectrom.* **2015**, *29* (8), 730–734.
- (24) Moraes, L.; Eberlin, M. N. Structurally Diagnostic Ion–Molecule Reactions: Acylium Ions with A-, B- and  $\Gamma$ -hydroxy Ketones. *J. Mass Spectrom.* **2002**, *37* (2), 162–168.
- (25) Robinson, D. I. Control of Genotoxic Impurities in Active Pharmaceutical Ingredients: A Review and Perspective. *Org. Process Res. Dev.* **2010**, *14* (4), 946–959.

- (26) Yerabolu, R.; Kong, J.; Easton, M.; Kotha, R. R.; Max, J.; Sheng, H.; Zhang, M.; Gu, C.; Kenttamaa, H. I. Identification of Protonated Sulfone and Aromatic Carboxylic Acid Functionalities in Organic Molecules by Using Ion–Molecule Reactions Followed by Collisionally Activated Dissociation in a Linear Quadrupole Ion Trap Mass Spectrometer. *Anal. Chem.* **2017**, 89 (14), 7398–7405.
- (27) Gronert, S. Estimation of Effective Ion Temperatures in a Quadrupole Ion Trap. *J. Am. Soc. Mass Spectrom.* **1998**, 9 (8), 845–848.
- (28) Gronert, S. Quadrupole Ion Trap Studies of Fundamental Organic Reactions. *Mass Spectrom. Rev.* **2005**, 24 (1), 100–120.
- (29) Habicht, S. C.; Vinueza, N. R.; Archibold, E. F.; Duan, P.; Kenttämä, H. I. Identification of the Carboxylic Acid Functionality by Using Electrospray Ionization and Ion–Molecule Reactions in a Modified Linear Quadrupole Ion Trap Mass Spectrometer. *Anal. Chem.* **2008**, 80 (9), 3416–3421.
- (30) Zhao, Y.; Truhlar, D. G. Density Functionals with Broad Applicability in Chemistry. *Acc. Chem. Res.* **2008**, 41 (2), 157–167.
- (31) Frisch, M. J.; Trucks, G. W.; Schlegel, H. B.; Scuseria, G. E.; Robb, M. A.; Cheeseman, J. R.; Scalmani, G.; Barone, V.; Petersson, G. A.; Nakatsuji, H.; Li, X.; Caricato, M.; Marenich, A. V.; Bloino, J.; Janesko, B. G.; Gomperts, R.; Mennucci, B.; Hratchian, H. P.; Ortiz, J. V.; Izmaylov, A. F.; Sonnenberg, J. L.; Williams-Young, D.; Ding, F.; Lipparini, F.; Egidi, F.; Goings, J.; Peng, B.; Petrone, A.; Henderson, T.; Ranasinghe, D.; Zakrzewski, V. G.; Gao, J.; Rega, N.; Zheng, G.; Liang, W.; Hada, M.; Ehara, M.; Toyota, K.; Fukuda, R.; Hasegawa, J.; Ishida, M.; Nakajima, T.; Honda, Y.; Kitao, O.; Nakai, H.; Vreven, T.; Throssell, K.; Montgomery, J. A., Jr.; Peralta, J. E.; Ogliaro, F.; Bearpark, M. J.; Heyd, J. J.; Brothers, E. N.; Kudin, K. N.; Staroverov, V. N.; Keith, T. A.; Kobayashi, R.; Normand, J.; Raghavachari, K.; Rendell, A. P.; Burant, J. C.; Iyengar, S. S.; Tomasi, J.; Cossi, M.; Millam, J. M.; Klene, M.; Adamo, C.; Cammi, R.; Ochterski, J. W.; Martin, R. L.; Morokuma, K.; Farkas, O.; Foresman, J. B.; Fox, D. J. *Gaussian 16, Revision B.01*. Gaussian, Inc., Wallingford CT, 2016.
- (32) Beuck, S.; Schwabe, T.; Grimme, S.; Schlörer, N.; Kamber, M.; Schänzer, W.; Thevis, M. Unusual Mass Spectrometric Dissociation Pathway of Protonated Isoquinoline-3-Carboxamides Due to Multiple Reversible Water Adduct Formation in the Gas Phase. *J. Am. Soc. Mass Spectrom.* **2009**, 20 (11), 2034–2048.

## **CHAPTER 5. DETERMINATION OF THE CHEMICAL COMPOSITIONS OF HEAVY, MEDIUM, AND LIGHT CRUDE OILS BY USING THE DISTILLATION, PRECIPITATION, FRACTIONATION MASS SPECTROMETRY (DPF MS) METHOD**

### **5.1 Introduction**

The depletion of light crude oils has recently increased society's reliance on heavy crude oils.<sup>1-3</sup> Unfortunately, heavier crude oils have a lower economic value because they are more difficult to process.<sup>4</sup> Crude oil quality is formally classified as heavy or light based on its American Petroleum Institute (API) gravity value, which is defined as the density of the crude oil relative to water.<sup>5</sup> This value is commonly determined using a reference method detailed in the ASTM D4052 document.<sup>6</sup> Crude oil classified as heavy has an API gravity lower than 22.3 while medium and light crude oils have API gravities between 22.3 and 31.1 and equal to or greater than 31.1, respectively.<sup>7</sup>

Although API gravity is an accepted tool for broadly classifying crude oils, crude oils with the same API gravities can exhibit different physical properties,<sup>8</sup> indicating that they have different chemical compositions. However, variations in crude oil compositions directly impact refinery processes.<sup>9</sup> To improve the refinery processes, a more accurate method of classing crude oils is needed. The first step in this direction is to establish correlations between the chemical composition of crude oils and their physical properties, including API gravity.

High-resolution mass spectrometry has revealed a great amount of information on the elemental composition of crude oils.<sup>10-12</sup> However, because of the exceeding complexity of crude oil, using mass spectrometry with only one ionization method to directly analyze the crude oil provides an inaccurate representation of its chemical compositions. This is because no single ionization method efficiently ionizes all the different types of compounds in crude oil without

extensive fragmentation.<sup>13</sup> In spite of these limitations, mass spectrometric methods have been used to correlate the API gravity of crude oils to their chemical compositions. For example, twenty crude oils of different API gravity were studied by using (+) atmospheric pressure photoionization (APPI) and a correlation was found between the API gravity and the concentration of aromatic compounds containing either one nitrogen or one nitrogen and one oxygen<sup>14</sup> However, only a weak correlation was found between the total nitrogen content and API gravity. This discrepancy may be due to the inability of the APPI method to detect nonaromatic nitrogen-compounds.

In other studies, crude oil samples were subjected to SARA fractionation prior to MS analysis. SARA is a common separation method that separates crude oils into four fractions: saturated compounds, asphaltenes, resins and asphaltenes.<sup>15,16</sup> In one such study, a correlation was found between the API gravities of three crude oils and the average ring and double bond equivalence (RDBE) for compounds containing one nitrogen atom in the resin and asphaltene fractions.<sup>7</sup> However, the mass spectrometric analysis method used (+) ESI which only ionizes basic compounds in the crude oil. In another study, API gravity was found to be inversely related to the average RDBE for compounds in the aromatic fraction.<sup>17</sup> However, it should be noted that the fractions obtained by SARA are still complex mixtures of compounds and not separate chemical classes. For example, the SARA fraction referred to as saturated compounds contains a substantial amount of aromatic compounds.<sup>18</sup>

Previously, we have demonstrated the benefits of a new approach referred to as distillation, precipitation, fractionation mass spectrometry (DPF MS) for the molecular profiling of crude oils.<sup>18</sup> This method involves fractionating crude oil into six major classes of compounds: volatile saturated hydrocarbons, asphaltenes, heavy saturated hydrocarbons, alkyl aromatic hydrocarbons, heteroaromatic compounds, and polar compounds. To uniformly ionize the compounds within

each class while inducing minimal fragmentation, optimized ionization and mass spectrometric analysis methods are used to analyze each compound class.<sup>18</sup> This method has been shown to enable the accurate determination of the chemical compositions of crude oils. In this study, the DPF MS method was utilized for molecular profiling of light, medium, and heavy crude oils to draw correlations between the chemical composition and the API gravity of each sample.

## 5.2 Experimental

### 5.2.1 Materials

*n*-Hexane (HPLC grade), dichloromethane (HPLC grade), isopropanol (HPLC grade), and carbon disulfide (> 99.9 %) were purchased from Sigma-Aldrich. All chemicals were used as received without further purification. Whatman PTFE membrane filters (TE 36) were purchased from GE Healthcare Life Sciences. Solid phase extraction kit (Si/CN-S-1.5 g) was purchased from Interchim.

### 5.2.2 Samples

Five samples of different API gravities were used: two light crude oils (API gravities 35.4 and 32.1°), two medium crude oils (API gravities 31.0 and 25.5°), and one heavy crude oil (API gravity 14.2°). The API gravity values were determined using Equation 1:<sup>19</sup>

$$API = \frac{141.5}{d_r(\frac{60}{60})} - 131.5 \quad (1)$$

where  $d_r$  is the relative density of the crude oil with respect to water measured at 60 °F.  $d_r$  was measured with an SVM 3001 Stabinger Viscometer (Anton Paar).

### 5.2.3 Fractionating the Crude Oils into Six Chemical Classes

Using the DPF method, each of the five crude oil samples was fractionated into six chemical classes:<sup>18</sup> volatile saturated hydrocarbons, asphaltenes, heavy saturated hydrocarbons, alkyl aromatic hydrocarbons, heteroaromatic compounds, and polar compounds. The volatile saturated hydrocarbon class was obtained through vacuum distillation at room temperature. During vacuum distillation, a rough pump was used to generate a vacuum at an inlet of the receiving flask, which was connected to the distillation flask via a condenser. The condenser was cooled using water and the receiving flask was kept at a low temperature with dry ice and acetone ( $< -70\text{ }^{\circ}\text{C}$ ) to collect and condense the volatile compounds. The remaining crude oil was weighed and the asphaltenes were precipitated, as previously described.<sup>20</sup> The precipitate was filtered with a  $0.45\text{ }\mu\text{m}$  Whatman PTFE membrane filter, dried, and weighed. The remaining residue, referred to as maltenes, was chromatographically separated with a Combi-flash Rf 200 auto column system (Teledyne Isco, Inc) . The hexane-eluted fraction contained both the heavy saturated hydrocarbon and alkyl aromatic hydrocarbon classes, while the dichloromethane and isopropanol fractions contained the heteroaromatic compound and polar compound classes, respectively. The hexane fraction was further separated into heavy saturated hydrocarbon and alkyl aromatic hydrocarbon classes by solid phase extraction with a Si/CN-S-1.5 g cartridge (Interchim).

### 5.2.4 Elemental Analysis

A Mitsubishi Model TS-100 trace sulfur/nitrogen analyzer was used to determine the total nitrogen content of each crude oil. Each sample was placed in a furnace kept at  $800 - 1000\text{ }^{\circ}\text{C}$ , where nitrogen was oxidized to nitric oxide (NO) in an oxygen atmosphere. The NO was converted to excited nitrogen dioxide ( $\text{NO}_2$ ) by ozone in the furnace. An inert sweep gas (argon) was used to move the  $\text{NO}_2$  to the detector. As the excited  $\text{NO}_2$  decayed, the emitted light was detected by a



chemiluminescence detector (a photomultiplier tube). This procedure followed the ASTM D5762 standard method<sup>21</sup> and was completed in duplicate measurements. The total nitrogen content measurements were performed by Petr Vozka, Pavel Šimáček, and Josef Tomášek.

#### 5.2.5 High-resolution Mass Spectrometry

All compound classes were analyzed separately, as previously described.<sup>18</sup> With the exception of the volatile saturated hydrocarbons, all compound classes were analyzed using a LQIT/orbitrap. For the heavy saturated hydrocarbon class, hexane was used as the solvent and oxygen was used as the sheath and auxiliary gas ((+) APCI/O<sub>2</sub>/hexane). The aromatic hydrocarbon and heteroaromatic compound classes were analyzed with (+) APCI with carbon disulfide (CS<sub>2</sub>) as the solvent and nitrogen as the sheath and auxiliary gas ((+) APCI/N<sub>2</sub>/CS<sub>2</sub>). The polar compound class was analyzed using (+) APCI with a 3:1 methanol:hexane solution as the solvent and APCI reagent and nitrogen as the sheath and auxiliary gas ((+) APCI/N<sub>2</sub>/3:1 methanol:hexane). Each compound class was dissolved in a preselected solvent or solvent system at a concentration of 30 mg/mL and directly infused into the APCI source at a flow rate of 10 µL/min. The operation of the LQIT/orbitrap and APCI are discussed in detail in chapter two of this dissertation. Some of the LQIT/orbitrap MS measurements were performed by Katherine Wehde.

Compounds in the heteroaromatic compound class were also subjected to in-source collision-activated dissociation (ISCAD) to determine whether nitrogen atoms were located in the aromatic core or in the alkyl side chains in these compounds. As discussed in chapter two of this dissertation, ISCAD can be used to cleave all alkyl side chains from alkyl aromatic ions.<sup>22,23</sup> For these experiments, 100 V was applied to both the multipoles and lenses of the ion optics to accelerate all ions formed in the ion source. The accelerated ions collided with atmospheric atoms and molecules in this region and dissociated. Therefore, by monitoring the nitrogen content before

and after ISCAD, the location of the nitrogen atoms (inside or outside the aromatic core) can be determined.

Xcalibur software was used to assign chemical formulas for ions based on the high-resolution mass spectrometric data. A general elemental formula for a compound in crude oil is  $C_cH_hN_nO_oS_s$  where  $c$  and  $h$  are any positive integers except zero and  $n$ ,  $o$ , and  $s$  are any positive integers, including zero. The number of carbon and hydrogen atoms was unlimited while the number of nitrogen, oxygen and sulfur atoms was constrained between zero and five.

RBDE, which represents the number of rings and double bonds in the ions, was determined using Equation 2:

$$RDBE = c - \frac{h}{2} + \frac{n}{2} + 1 \quad (2)$$

where  $c$ ,  $h$ , and  $n$  are the number of carbon, hydrogen, and nitrogen atoms, respectively.

Volatile saturated hydrocarbons were analyzed (by Katherine Wehde) using a two-dimensional gas chromatograph coupled with electron ionization/high-resolution time-of-flight mass spectrometer (GC×GC/(EI) TOF MS) (Leco) as follows. An auto injector (Agilent G4513A) was used to inject 0.5  $\mu$ L of the compound class into a split/splitless injector with a split ratio of 1:20 held at 260 °C at a constant flow of ultra-pure helium carrier gas (1.25 mL/min). The compounds were separated using a reversed column configuration; a polar 60 m capillary column (Rxi-17Sil ms, Restek) followed by a nonpolar 2 m capillary column (Rxi-1 ms, Restek). The conditions selected for the GC×GC/(EI) TOF MS analysis are shown in Table 5.1.

Table 5.1 Optimized conditions for the analysis of volatile saturated hydrocarbons of the four crude oils by using GC×GC/(EI) TOF MS.

<b>GC×GC/(EI) TOF MS</b>	<b>Conditions</b>
Primary oven (polar column)	35 °C to 55 °C at the rate of 1 °C /min 55 °C to 175 °C at the rate of 3 °C /min
Total Modulator time	3.5 s
Modulator stage one	1.75 s
Modulator stage two	1.75 s
Hot jet pulse	0.6 s
Cold jet pulse	1.75 s
Modulator hot jet	+ 80 °C (offset from the temperature of the secondary oven)
Secondary oven (nonpolar column)	+ 45 °C to 65 °C at the rate of 1 °C /min 65 °C to 185 °C at the rate of 3 °C /min
Transfer line	300 °C (constant throughout the analysis)
MS ion source	250 °C (constant throughout the analysis)
EI	70 eV electron kinetic energy
Resolution	25,000 at $m/z$ 219
Acquisition rate	200 Hz
Acquisition delay	300 s
$m/z$ range	45 – 550
Data collection, processing, and analysis	LECO ChromaTOF
Analyte identification	Wiley (2011) and NIST (2011) mass spectral data base
Spectral match	> 800

### 5.3 Results and Discussion

The Distillation, Precipitation, Fractionation Mass Spectrometry (DPF MS) approach<sup>18</sup> was used for molecular profiling of five crude oils with different API gravities. The crude oil samples were fractionated to obtain six major classes of compounds: volatile saturated hydrocarbons, asphaltenes, heavy saturated hydrocarbons, alkyl aromatic hydrocarbons, heteroaromatic compounds, and polar compounds. Optimized ionization and mass spectrometric analysis methods were utilized for the characterization of each compound class. Two different mass spectrometry methods were employed: GC×GC/(EI) TOF MS and (APCI) LQIT/orbitrap.

Correlations between the API gravity and the chemical compositions of the crude oil samples found for both the crude oils as a whole and found for each individual compound class are discussed below. Katherine Wehde and I contributed equally to data analysis. Ravikiran Yerabolu and I collected the data reported for the crude oil with API gravity 32.1°. Some of these data were previously published.<sup>18</sup>

### 5.3.1 Characterization of Crude Oils as a Whole

The five crude oils were fractionated via the DPF methodology<sup>18</sup> to determine the gravimetric weight percent (wt %) of each compound class. In general, the heavier crude oils were found to contain more asphaltenes and heteroaromatic compounds than the lighter crude oils (Table 5.2). Further, the heavier crude oils contained fewer heavy, alkyl aromatic, and saturated hydrocarbons. The heaviest crude oil contained substantially more polar compounds than the other crude oils and contained no volatile saturated hydrocarbons at all. Based on Table 5.2, the weight percent of compounds in the heteroaromatic compound class increases linearly as a function of decreasing API gravity ( $R^2 = 0.931$ ). The wt % was not found to correlate with API gravity for any other compound classes.

Table 5.2 Gravimetric weight percents of different chemical classes obtained using the DPF method for five different crude oil samples. The crude oils are classified as heavy, medium, or light based on their API gravity (in parenthesis).

Chemical Classes	Gravimetric Weight Percents (wt %)				
	Heavy (14.2°)	Medium (25.5°)	Medium (31.0°)	Light (32.1°)	Light (35.4°)
Alkyl Aromatic Hydrocarbons	8.2	12.9	11.1	21.2	17.5
Heteroaromatic Compounds	37.2	23.3	19.6	9.7	9.3
Polar Compounds	17.3	4.7	7.0	8.1	5.2
Heavy Saturated Hydrocarbons	17.3	36.9	47.6	44.3	48.2
Asphaltenes	6.3	4.2	2.2	1.2	1.0
Volatile Saturated Hydrocarbons	0.0	1.1	2.1	8.0	8.1
Loss	13.7	16.9	10.4	7.5	10.7
Total	100.0	100.0	100.0	100.0	100.0

In addition to the gravimetric weight percent of each compound class, DPF MS allows determination of elemental compositions of the compounds in each compound class. The measured elemental compositions were then consolidated using the measured total ion abundance of each chemical class and the gravimetric percent, as shown in Equation 3. Equation 3 provides an approximation of the weight percent of each elemental composition based on the assumption that the compounds in each class are ionized with similar efficiencies and with minimal fragmentation. This assumption has been previously tested using model mixtures and found to be true for the model compounds studied.<sup>18</sup>

*Approximate weight percentage of each consolidated elemental composition =*

$$\sum_{x=1}^6 \left( \frac{\sum i_x \text{ abundance}}{\sum x \text{ abundance}} * \text{wt \% } (x) \right) \quad (3)$$

where  $i$  is the specific elemental composition of an ionized compound,  $x$  is the number of the compound class (1 – 6),  $\sum x \text{ abundance}$  is the total ion abundance measured for the compound class, and  $wt \% (x)$  is the gravimetric percentage of the compound class.

The consolidated elemental compositions are shown in Table 5.3. The heaviest crude oil appears to contain a much greater amount of compounds with elemental compositions of  $C_cH_hN$ ,  $C_cH_hN_2$  and  $C_cH_hN_2S_2$ , with the  $C_cH_hN$  compounds being the most abundant. On the other hand compounds with the elemental composition  $C_cH_hO_o$  were most abundant (17%) in the lightest crude oil. Meanwhile, the medium heavy crude oils contained more compounds with the elemental composition  $C_cH_hS$  (12 – 18%) than any other crude oil (2 – 7%). Although one of the medium crude oils (31.0°) and one of the light crude oils (32.1°) had similar API gravity values, they were found to contain different amounts of many compounds, such as those with elemental compositions  $C_cH_hS$  (12 vs. 7%) and  $C_cH_hNS$  (0.5 vs. 8.8%). This finding suggests that crude oils with similar API gravities do not necessarily contain similar molecular compositions. Further, no obvious correlations were found between the amounts of compounds with different elemental compositions in the whole crude oil and API gravity. The same applies to the total nitrogen content (Table 5.4): a correlation with the API gravity was found only for the three heaviest crude oils.

Table 5.3 Approximate weight percents of compounds with different elemental compositions (consolidated data) for each crude oil sample (API gravity shown in parenthesis). Elemental compositions are listed as  $C_cH_hN_nO_oS_s$ , where c and h are any non-zero positive integer and n, o, and s are any positive integer between zero and five.

Consolidated Elemental Compositions as Approximate Weight Percentages for the Crude Oil Samples					
Elemental compositions	Heavy (14.2°)	Medium (25.5°)	Medium (31.0°)	Light (32.1°)	Light (35.4°)
$C_cH_h$	29.89	37.48	55.10	57.29	45.80
$C_cH_hN$	35.89	14.59	14.45	13.42	10.70
$C_cH_hN_2$	1.72	0.31	0.19	0.11	0.14
$C_cH_hO_o$ (o = 1-5)	4.62	2.05	0.72	3.42	17.30
$C_cH_hS$	2.39	17.59	11.89	6.91	5.48
$C_cH_hS_2$	0.15	0.82	0.07	0.01	0.00
$C_cH_hNO$	3.29	1.61	1.77	0.41	1.86
$C_cH_hNS$	0.70	3.32	0.50	8.75	0.34
$C_cH_hN_2S_2$	1.90	0.14	0.25	0.01	0.07
$C_cH_hOS$	0.07	1.38	1.06	0.00	0.18
$C_cH_hNSO$	0.04	0.25	0.01	0.05	0.01
Others	5.63	3.56	3.60	2.11	7.43
Total	100.00	100.00	100.01	100.00	100.00

Table 5.4 The average nitrogen content in ppm determined via elemental analysis (for the five crude oils of different API gravity (shown in parenthesis). The total nitrogen content analysis was performed by Petr Vozka, Pavel Šimáček, and Josef Tomášek.

Crude Oil	Average Nitrogen Content (ppm)
Heavy (14.2°)	8600
Medium (25.5°)	3550
Medium (31.0°)	2100
Light (32.1°)	2150
Light (35.4°)	2500

### 5.3.2 Characterization of the Compound Classes Derived from the Five Crude Oils

In addition to comparing the crude oils as a whole, the molecular compositions of the individual compound classes were also compared for each crude oil. The ionized compounds with different elemental compositions and their relative mass spectrometric abundances are shown in

Tables 5.5 through 5.10. The approximated weight percentage (as determined by Equation 3) of the most abundant nitrogen-containing compounds in the heteroaromatic compound class of all crude oil samples was found to decrease as a function with increasing API gravity ( $R^2 > 0.96$ ; Figure 1). The heteroaromatic compound class contained the majority of the  $C_cH_hN$  compounds for every crude oil studied (Figure 2).

As described above, the medium crude oil (31.0 °) and one of the light crude oils (32.1°) contained different amounts of many compounds (Tables 5.2 and 5.3) but had similar API gravities. This conclusion was confirmed by examining the individual chemical classes (Tables 5.5 through 5.10). For example, based on mass spectrometric ion abundances, the alkyl aromatic compound class in the medium crude oil contained a substantially greater amount of sulfur-containing compounds than the same class in the light crude oil (40% vs. 12%, respectively). These findings further suggest that similar API gravities do not imply similar molecular compositions for crude oils.

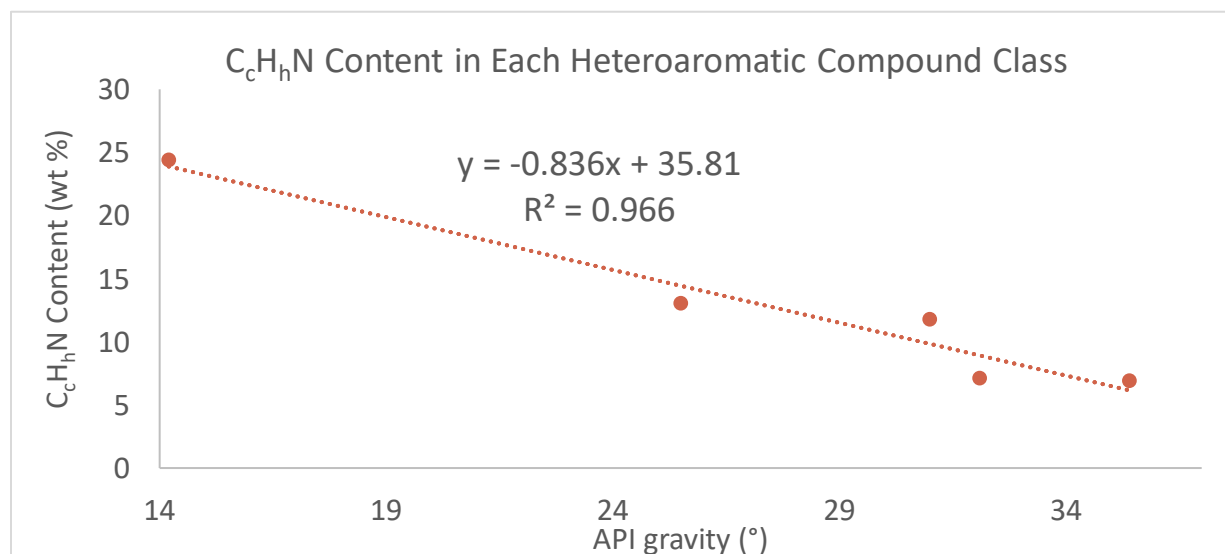


Figure 5.1 The approximate weight percent of compounds with the elemental composition  $C_cH_hN$  in the heteroaromatic compound class as a function of API gravity for five crude oils.



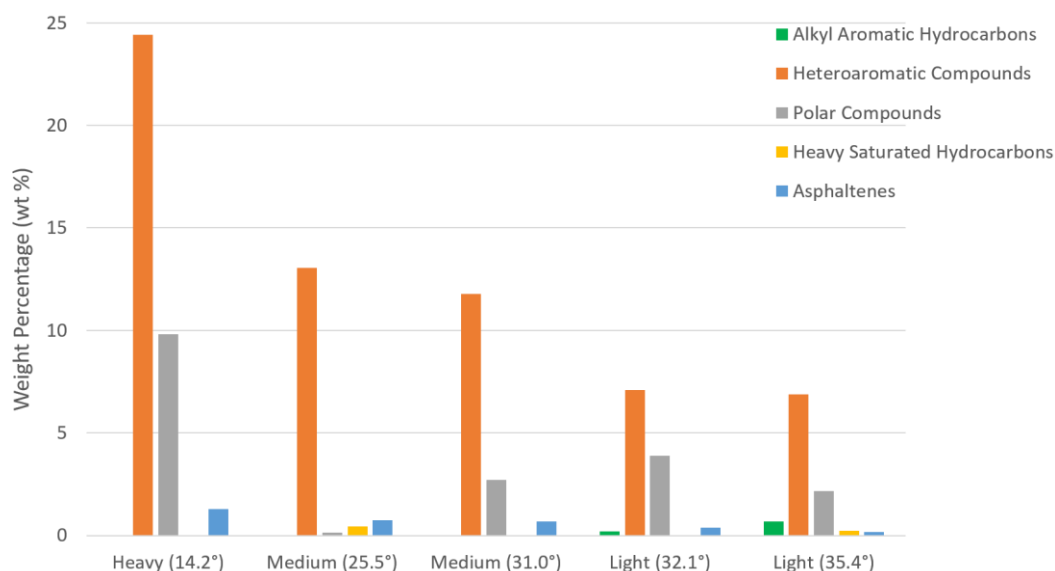


Figure 5.2 Approximate weight percentages of  $C_cH_hN$  compounds in five compound classes derived from each crude oil (API gravity given in parenthesis). Volatile saturated hydrocarbons are not included as they contained no nitrogen-containing compounds (Table 4).

The structures of the  $C_cH_hN$  compounds in the heteroaromatic compound classes of the five crude oils were further examined to determine the location of the nitrogen atoms – in the aromatic cores or in the alkyl chains. As mentioned above, if nitrogen atoms are located in ions outside of aromatic cores, they will be lost upon ISCAD. Comparison of the abundances of the  $C_cH_hN$  ions before and after ISCAD revealed a substantial decrease for the heavier crude oils but not for the lightest ones (Figure 3). This finding indicates that many nitrogen atoms (about half, Figure 3) in the heavier crude oils reside outside the aromatic cores while most nitrogen atoms in the lighter crude oils reside within the aromatic cores. The ratio of the relative abundances of  $C_cH_hN$  and  $C_cH_h$  ions is used to illustrate this relative change in nitrogen content (Figure 3, Table 5.11). The changes in the  $C_cH_hN/C_cH_h$  ion ratios upon ISCAD are smaller for crude oils with greater API gravity. Therefore, the heteroaromatic compound class of heavier crude oils appears to contain more compounds with nitrogen atoms outside the aromatic cores than in the aromatic cores compared to the lighter crude oils. However, it should be noted that if the compounds contain

multiple aromatic cores connected by alkyl chains, some with a nitrogen atom in the chain, then ISCAD could cause a decrease in the nitrogen content via a cleavage of the chain between the cores. Therefore, the observation of a large decreases in the N-content upon ISCAD for the heavier crude oils may indicate the presence of larger amounts of compounds with more than one nitrogen-containing aromatic core.

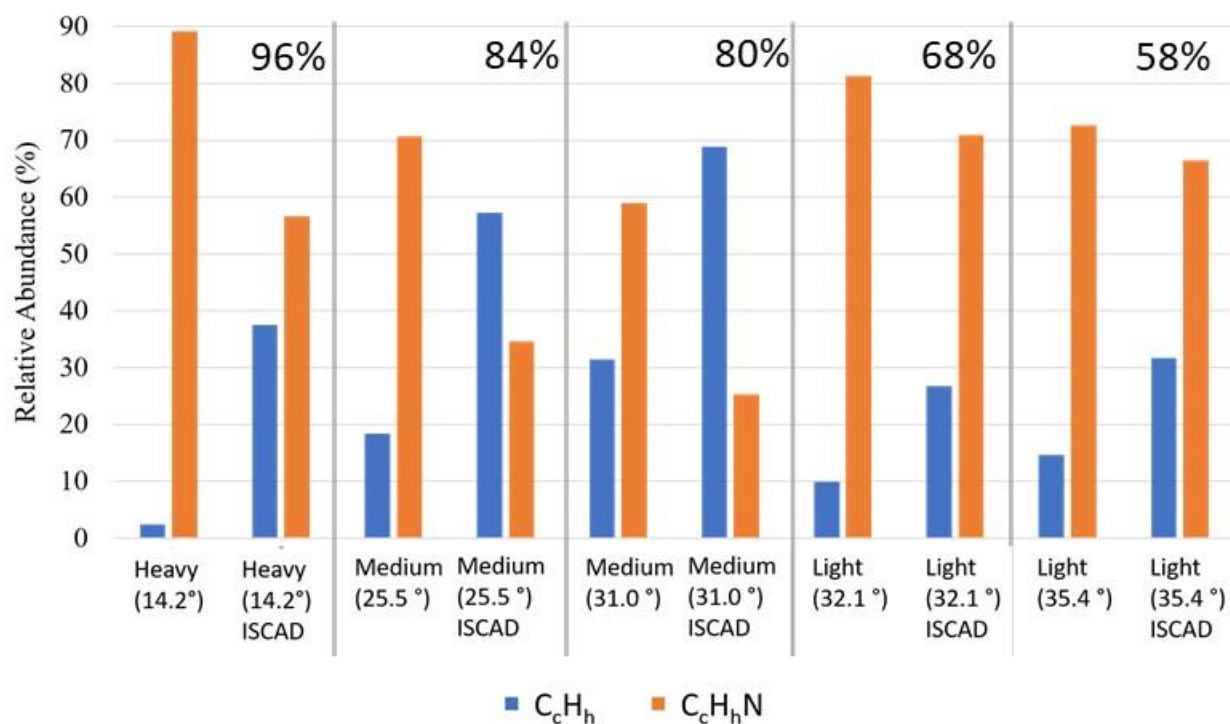


Figure 5.3 Relative abundances of ions with the elemental compositions  $C_cH_h$  and  $C_cH_hN$  in the mass spectra measured before and after ISCAD (marked as ISCAD above) for the heteroaromatic compound class for each crude oil sample (API gravity given in parenthesis). The percent change in the ratio of the  $C_cH_hN/C_cH_h$  ion abundances is also given above (obtained from Table 10).

Table 5.5 Elemental compositions of the compounds in the volatile saturated hydrocarbon class derived from four different crude oils and the relative abundances of the ionized compounds measured by using GC×GC/(EI) TOF MS. The heaviest crude oil sample is not included as it contained no detectable volatile compounds. The data were collected by Katherine Wehde.

Elemental Compositions	Relative Ion Abundances (%)			
	Medium (25.5°)	Medium (31.0°)	Light (32.1°)	Light (35.4°)
C <sub>c</sub> H <sub>h</sub>	93.56	96.61	87.09	93.76
C <sub>c</sub> H <sub>h</sub> N	0.00	0.33	1.00	0.41
C <sub>c</sub> H <sub>h</sub> N <sub>2</sub>	0.00	0.54	1.29	0.37
C <sub>c</sub> H <sub>h</sub> O <sub>o</sub> (o = 1-5)	5.76	1.30	7.53	2.23
C <sub>c</sub> H <sub>h</sub> S	0.00	0.00	0.00	0.00
C <sub>c</sub> H <sub>h</sub> S <sub>2</sub>	0.00	0.00	0.00	0.00
C <sub>c</sub> H <sub>h</sub> NO	0.00	0.02	0.00	0.09
C <sub>c</sub> H <sub>h</sub> NS	0.00	0.00	0.00	0.13
C <sub>c</sub> H <sub>h</sub> N <sub>2</sub> S <sub>2</sub>	0.00	0.00	0.00	0.00
C <sub>c</sub> H <sub>h</sub> OS	0.00	0.01	0.00	0.00
C <sub>c</sub> H <sub>h</sub> NSO	0.00	0.00	0.00	0.00
Others	0.68	1.19	3.09	3.00
Total	100.00	100.00	100.00	100.00

Table 5.6 Elemental compositions of the compounds in the alkyl aromatic compound class derived from five different crude oils and the relative abundances of the ionized compounds measured by using (APCI) LQIT/orbitrap.

Elemental Compositions	Relative Ion Abundances (%)				
	Heavy (14.2°)	Medium (25.5°)	Medium (31.0°)	Light (32.1°)	Light (35.4°)
C <sub>c</sub> H <sub>h</sub>	77.89	54.55	45.17	81.56	48.58
C <sub>c</sub> H <sub>h</sub> N	0.00	0.00	0.00	0.96	3.94
C <sub>c</sub> H <sub>h</sub> N <sub>2</sub>	0.00	0.00	0.00	0.00	0.00
C <sub>c</sub> H <sub>h</sub> O <sub>o</sub> (o = 1-5)	1.50	0.94	0.86	4.17	3.96
C <sub>c</sub> H <sub>h</sub> S	7.21	34.59	39.89	11.93	11.01
C <sub>c</sub> H <sub>h</sub> S <sub>2</sub>	0.00	0.00	0.00	0.00	0.00
C <sub>c</sub> H <sub>h</sub> NO	0.00	0.00	0.00	0.03	0.00
C <sub>c</sub> H <sub>h</sub> NS	0.00	0.00	0.00	1.30	1.15
C <sub>c</sub> H <sub>h</sub> N <sub>2</sub> S <sub>2</sub>	0.00	0.00	0.00	0.00	0.00
C <sub>c</sub> H <sub>h</sub> OS	0.36	0.00	0.00	0.00	0.00
C <sub>c</sub> H <sub>h</sub> NSO	0.00	0.00	0.00	0.05	0.06
Others	13.04	9.92	14.08	0.00	31.29
Total	100.00	100.00	100.00	100.00	100.00

Table 5.7 Elemental compositions of the compounds in the heteroaromatic compound class derived from five different crude oils and the relative abundances of the ionized compounds measured by using (APCI) LQIT/orbitrap.

Elemental Compositions	Relative Ion Abundances (%)				
	Heavy (14.2°)	Medium (25.5°)	Medium (31.0°)	Light (32.1°)	Light (35.4°)
C <sub>c</sub> H <sub>h</sub>	19.08	11.82	26.53	10.53	8.69
C <sub>c</sub> H <sub>h</sub> N	66.00	56.75	56.04	78.96	76.58
C <sub>c</sub> H <sub>h</sub> N <sub>2</sub>	1.64	1.03	0.00	0.02	0.89
C <sub>c</sub> H <sub>h</sub> O <sub>o</sub> (o = 1-5)	4.85	0.65	0.70	3.05	4.69
C <sub>c</sub> H <sub>h</sub> S	2.72	10.59	12.33	0.16	0.83
C <sub>c</sub> H <sub>h</sub> S <sub>2</sub>	0.40	3.45	0.32	0.00	0.00
C <sub>c</sub> H <sub>h</sub> NO	3.52	1.11	0.17	1.76	3.48
C <sub>c</sub> H <sub>h</sub> NS	0.83	12.78	2.05	0.56	0.90
C <sub>c</sub> H <sub>h</sub> N <sub>2</sub> S <sub>2</sub>	0.22	0.55	0.14	0.00	0.39
C <sub>c</sub> H <sub>h</sub> OS	0.06	0.61	1.75	0.04	0.40
C <sub>c</sub> H <sub>h</sub> NSO	0.00	0.00	0.00	0.00	0.00
Others	0.69	0.66	0.00	4.91	3.15
Total	100.00	100.00	100.04	100.00	100.00

Table 5.8 Elemental compositions of the compounds in the polar compound class derived from five different crude oils and the relative abundances of the ionized compounds measured by using (APCI) LQIT/orbitrap.

Elemental Compositions	Relative Ion Abundances (%)				
	Heavy (14.2°)	Medium (25.5°)	Medium (31.0°)	Light (32.1°)	Light (35.4°)
C <sub>c</sub> H <sub>h</sub>	0.00	5.27	0.14	10.87	0.81
C <sub>c</sub> H <sub>h</sub> N	57.70	2.99	38.76	64.99	43.35
C <sub>c</sub> H <sub>h</sub> N <sub>2</sub>	3.72	0.00	0.44	0.00	0.00
C <sub>c</sub> H <sub>h</sub> O <sub>o</sub> (o = 1-5)	13.88	22.51	5.46	7.09	19.87
C <sub>c</sub> H <sub>h</sub> S	0.00	0.00	0.00	0.06	0.00
C <sub>c</sub> H <sub>h</sub> S <sub>2</sub>	0.00	0.00	0.00	0.00	0.00
C <sub>c</sub> H <sub>h</sub> NO	8.08	22.91	22.30	2.48	7.27
C <sub>c</sub> H <sub>h</sub> NS	0.33	0.38	0.58	0.07	0.00
C <sub>c</sub> H <sub>h</sub> N <sub>2</sub> S <sub>2</sub>	10.42	0.00	3.10	0.07	0.51
C <sub>c</sub> H <sub>h</sub> OS	0.04	24.32	10.18	0.00	0.2.66
C <sub>c</sub> H <sub>h</sub> NSO	0.15	4.23	0.00	0.00	0.08
Others	5.68	17.39	19.04	14.36	25.44
Total	100.00	100.00	100.00	100.00	100.00

Table 5.9 Elemental compositions of the compounds in the heavy saturated hydrocarbons class derived from five different crude oils and the relative abundances of the ionized compounds measured by using (APCI) LQIT/orbitrap.

Elemental Compositions	Relative Ion Abundances (%)				
	Heavy (14.2°)	Medium (25.5°)	Medium (31.0°)	Light (32.1°)	Light (35.4°)
C <sub>c</sub> H <sub>h</sub>	93.87	70.21	89.58	68.89	58.87
C <sub>c</sub> H <sub>h</sub> N	0.00	1.18	0.00	0.46	0.00
C <sub>c</sub> H <sub>h</sub> N <sub>2</sub>	0.00	0.00	0.00	0.00	0.00
C <sub>c</sub> H <sub>h</sub> O <sub>o</sub> (o = 1-5)	0.10	0.76	0.00	2.36	30.94
C <sub>c</sub> H <sub>h</sub> S	4.27	27.44	10.42	9.79	7.21
C <sub>c</sub> H <sub>h</sub> S <sub>2</sub>	0.00	0.00	0.00	0.00	0.00
C <sub>c</sub> H <sub>h</sub> NO	0.00	0.40	0.00	0.04	2.32
C <sub>c</sub> H <sub>h</sub> NS	1.76	0.00	0.00	18.92	0.10
C <sub>c</sub> H <sub>h</sub> N <sub>2</sub> S <sub>2</sub>	0.00	0.00	0.00	0.00	0.00
C <sub>c</sub> H <sub>h</sub> OS	0.00	0.00	0.00	0.00	0.00
C <sub>c</sub> H <sub>h</sub> NSO	0.00	0.00	0.00	0.00	0.00
Others	0.00	0.00	0.00	0.00	0.11
Total	100.00	100.00	100.00	100.00	100.00

Table 5.10 Elemental compositions of the compounds in the asphaltene compound class derived from five different crude oils and the relative abundances of the ionized compounds measured by using (APCI) LQIT/orbitrap.

Elemental Compositions	Relative Ion Abundances (%)				
	Heavy (14.2°)	Medium (25.5°)	Medium (31.0°)	Light (32.1°)	Light (35.4°)
C <sub>c</sub> H <sub>h</sub>	2.68	11.89	9.34	50.87	47.24
C <sub>c</sub> H <sub>h</sub> N	21.62	18.87	34.08	18.00	37.62
C <sub>c</sub> H <sub>h</sub> N <sub>2</sub>	7.39	1.75	6.60	0.00	2.63
C <sub>c</sub> H <sub>h</sub> O <sub>o</sub> (o = 1-5)	4.41	8.86	3.36	1.27	4.12
C <sub>c</sub> H <sub>h</sub> S	0.84	12.76	3.74	2.21	0.05
C <sub>c</sub> H <sub>h</sub> S <sub>2</sub>	0.03	0.27	0.34	1.08	0.00
C <sub>c</sub> H <sub>h</sub> NO	9.21	3.06	8.01	0.97	3.55
C <sub>c</sub> H <sub>h</sub> NS	0.53	7.82	2.56	3.05	0.19
C <sub>c</sub> H <sub>h</sub> N <sub>2</sub> S <sub>2</sub>	0.25	0.22	0.38	0.08	0.25
C <sub>c</sub> H <sub>h</sub> OS	0.16	2.26	0.22	0.11	0.14
C <sub>c</sub> H <sub>h</sub> NSO	0.15	1.20	0.28	3.40	0.01
Others	52.73	31.04	31.10	18.95	4.22
Total	100.00	100.00	100.00	100.00	100.00

Table 5.11 The change (%) in the  $C_cH_hN/C_cH_h$  relative ion abundances for the heteroaromatic compound class derived from the five crude oils. The crude oils are classified as heavy, medium, or light based on their API gravity (shown in parenthesis).

Samples	Mass spectra measured	Ratio of $C_cH_hN/C_cH_h$ ion abundances	Relative change (%)
Heavy (14.2°)	Before ISCAD	37.39	96
	After ISCAD	1.51	
Medium (25.5°)	Before ISCAD	3.83	84
	After ISCAD	0.61	
Medium (31.0°)	Before ISCAD	1.87	80
	After ISCAD	0.37	
Light (32.1°)	Before ISCAD	8.19	68
	After ISCAD	2.64	
Light (35.4°)	Before ISCAD	4.97	58
	After ISCAD	2.10	

The DPF MS method was also used to determine average ring and double bond equivalence (RDBE) values (Equation 2) for compounds in all compound classes in the five crude oils (Table 5.13). The levels of unsaturation and number of rings in each compound class of the five crude oils were then compared. Based on the average RDBE data (Table 5.13), asphaltenes and volatile compounds contain the highest and the lowest average RDBE, respectively, for all the five crude oils. However, only the average RDBE in the heteroaromatic compound class correlated with the API gravity of the crude oil. For this class, the average RDBE value was observed to increase as a function of decreasing API gravity ( $R^2 > 0.93$ , Figure 4). This finding suggests that the aromatic core size for compounds in the heteroaromatic compound class may be larger for the heavier crude oils than the lighter crude oils.

Table 5.12 Average RDBE values for the compounds in each of the six compound classes derived from the five different crude oil samples.

Average RDBE of Compounds in Each Compound Class						
Samples	Volatile Saturated Compounds	Asphaltenes	Heavy Saturated Compounds	Polar Compounds	Alkyl Aromatic Hydrocarbons	Hetero aromatic Compounds
Light (35.4°)	1.1	14.0	6.2	6.7	9.8	11.9
Light (32.1°)	0.6	12.6	3.0	3.6	8.6	12.0
Medium (31.0°)	1.2	15.6	3.9	5.0	8.2	12.6
Medium (25.5°)	0.5	15.1	5.2	5.3	7.8	12.6
Heavy (14.2°)	- <sup>a</sup>	15.0	4.9	8.9	9.2	14.3

<sup>a</sup>No volatile compounds were found in the heaviest crude oil (API gravity 14.2°)

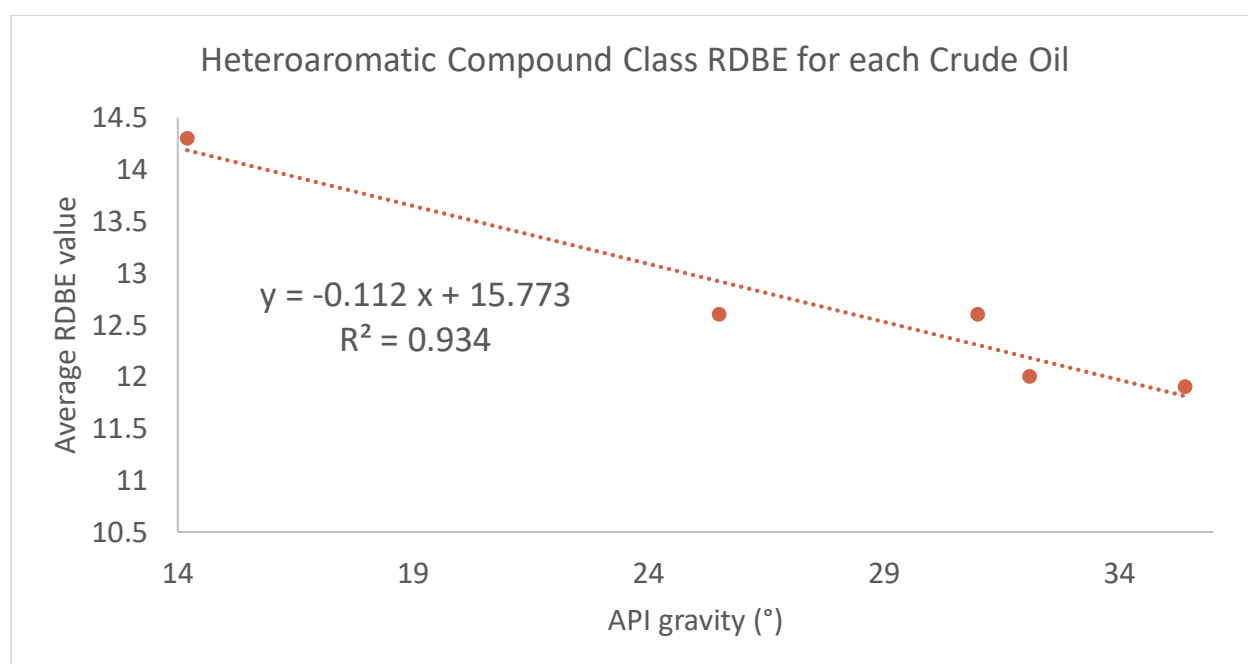


Figure 5.4 The RDBE values for compounds in the heteroaromatic compound class as a function of API gravity for five crude oils.

## 5.4 Conclusions

The DPF MS methodology<sup>18</sup> was used to characterize the chemical compositions of heavy, medium, and light crude oil samples with different API gravities. First, the crude oil was fractionated into six compound classes. Each fraction was then analyzed via an optimized high-



resolution mass spectrometry method. The gravimetric percentages of the six compound classes within each crude oil sample were also determined. Based on the gravimetric weight percentages of the six compound classes, the heavier crude oils contained more asphaltenes and heteroaromatic compounds and fewer heavy, alkyl aromatic, and volatile saturated hydrocarbons than the lighter crude oils. Although these crude oils contained different amounts of each compound class, only the gravimetric weight percentage of the heteroaromatic compound class correlated with the API gravity: the amount of heteroaromatic compounds increased as a function of decreasing API gravity. Further, elemental compositions of each compound class were obtained and consolidated to examine the chemical composition of each crude oil. Compounds with the elemental compositions  $C_cH_h$  or  $C_cH_hN$  were found to be the most abundant compounds in all crude oil samples.  $C_cH_h$  compounds were dominant in all crude oil samples except the heaviest, where  $C_cH_hN$  dominated. No obvious correlations were found between API gravity and the amounts of the compounds with different elemental compositions in the whole crude oils. The same applies to the total nitrogen content of each crude oil sample, which was determined through a controlled combustion experiment.

Examination of the molecular compositions of the different compound classes in each crude oil provided more definitive information. For example, a linear correlation was found for the API gravity and the gravimetric percentage of the most abundant nitrogen-containing compounds ( $C_cH_hN$  elemental composition) in the heteroaromatic compound class. Additionally, the average RDBE values measured for compounds in the heteroaromatic compound class increased as the API gravity decreased, suggesting that the aromatic core size may be greater for heteroaromatic compounds in heavier crude oils. Finally, further examination of the location of nitrogen atom in the  $C_cH_hN$  compounds in the heteroaromatic compound class revealed that

heavier crude oils contained more nitrogen atoms outside the aromatic core compared to lighter crude oils. This finding could facilitate the design of optimal upgrading techniques for nitrogen removal in different types of crude oils based on their API gravity.<sup>24</sup> No other correlations were found between the chemical compositions of the different compound classes in the five crude oils and their API gravity. Therefore, the chemical composition of only one compound class, the heteroaromatic compound class, was found to correlate with API gravity.

## 5.5 References

- (1) Gaspar, A.; Zellermann, E.; Lababidi, S.; Reece, J.; Schrader, W. Characterization of Saturates, Aromatics, Resins, and Asphaltenes Heavy Crude Oil Fractions by Atmospheric Pressure Laser Ionization Fourier Transform Ion Cyclotron Resonance Mass Spectrometry. *Energy Fuels* **2012**, *26* (6), 3481–3487.
- (2) Swain, E. J. Sulfur, Coke, and Crude Quality--Conclusion: US Crude Slate Continues to Get Heavier, Higher in Sulfur. *Oil Gas J.* **1995**, *93* (2), 37–42.
- (3) Altgelt, K. H. *Composition and Analysis of Heavy Petroleum Fractions*; CRC Press: Boca Raton, FL, 2016.
- (4) Weissman, J. G.; Kessler, R. V. Downhole Heavy Crude Oil Hydroprocessing. *Appl. Catal. Gen.* **1996**, *140* (1), 1–16.
- (5) Santos, J. M.; Wisniewski Jr., A.; Eberlin, M. N.; Schrader, W. Comparing Crude Oils with Different API Gravities on a Molecular Level Using Mass Spectrometric Analysis. Part 1: Whole Crude Oil. *Energies* **2018**, *11* (10), 2766. <https://doi.org/10.3390/en11102766>.
- (6) ASTM Standard D4052, 2018. *Test Method for Density, Relative Density, and API Gravity of Liquids by Digital Density Meter*; ASTM International, West Conshohocken, PA, 2018.
- (7) Santos, J.; Vetere, A.; Wisniewski, A.; Eberlin, M.; Schrader, W. Comparing Crude Oils with Different API Gravities on a Molecular Level Using Mass Spectrometric Analysis. Part 2: Resins and Asphaltenes. *Energies* **2018**, *11* (10), 2767.
- (8) Hinkle, A.; Shin, E.; Liberatore, M.; Herring, A.; Batzle, M. Correlating the Chemical and Physical Properties of a Set of Heavy Oils from around the World. *Fuel* **2008**, *87* (13–14), 3065–3070.

- (9) Qian, K.; Rodgers, R. P.; Hendrickson, C. L.; Emmett, M. R.; Marshall, A. G. Reading Chemical Fine Print: Resolution and Identification of 3000 Nitrogen-Containing Aromatic Compounds from a Single Electrospray Ionization Fourier Transform Ion Cyclotron Resonance Mass Spectrum of Heavy Petroleum Crude Oil. *Energy Fuels* **2001**, *15* (2), 492–498.
- (10) Rodgers, R. P.; McKenna, A. M. Petroleum Analysis. *Anal. Chem.* **2011**, *83* (12), 4665–4687.
- (11) Niyonsaba, E.; Manheim, J. M.; Yerabolu, R.; Kenttämää, H. I. Recent Advances in Petroleum Analysis by Mass Spectrometry. *Anal. Chem.* **2019**, *91* (1), 156–177.
- (12) Marshall, A. G.; Rodgers, R. P. Petroleomics: The next Grand Challenge for Chemical Analysis. *Acc. Chem. Res.* **2004**, *37* (1), 53–59.
- (13) Tawara, H.; Kato, T. Total and Partial Ionization Cross Sections of Atoms and Ions by Electron Impact. *At. Data Nucl. Data Tables* **1987**, *36* (2), 167–353.
- (14) Hur, M.; Yeo, I.; Kim, E.; No, M.; Koh, J.; Cho, Y. J.; Lee, J. W.; Kim, S. Correlation of FT-ICR Mass Spectra with the Chemical and Physical Properties of Associated Crude Oils. *Energy Fuels* **2010**, *24* (10), 5524–5532.
- (15) Jewell, D. M.; Weber, J. H.; Bunger, J. W.; Plancher, H.; Latham, D. R. Ion-Exchange, Coordination, and Adsorption Chromatographic Separation of Heavy-End Petroleum Distillates. *Anal. Chem.* **1972**, *44* (8), 1391–1395.
- (16) Kharrat, A. M.; Zacharia, J.; Cherian, V. J.; Anyatonwu, A. Issues with Comparing SARA Methodologies. *Energy Fuels* **2007**, *21* (6), 3618–3621.
- (17) Rüger, C. P.; Neumann, A.; Sklorz, M.; Schwemer, T.; Zimmermann, R. Thermal Analysis Coupled to Ultrahigh Resolution Mass Spectrometry with Collision Induced Dissociation for Complex Petroleum Samples: Heavy Oil Composition and Asphaltene Precipitation Effects. *Energy Fuels* **2017**, *31* (12), 13144–13158.
- (18) Yerabolu, R.; Kotha, R. R.; Niyonsaba, E.; Dong, X.; Manheim, J. M.; Kong, J.; Riedeman, J. S.; Romanczyk, M.; Johnston, C. T.; Kilaz, G.; Kenttämää, H. I. Molecular Profiling of Crude Oil by Using Distillation Precipitation Fractionation Mass Spectrometry (DPF-MS). *Fuel* **2018**, *234*, 492–501.
- (19) Santos, R. G.; Loh, W.; Bannwart, A. C.; Trevisan, O. V. An Overview of Heavy Oil Properties and Its Recovery and Transportation Methods. *Braz. J. Chem. Eng.* **2014**, *31* (3), 571–590.
- (20) Buenrostro-Gonzalez, E.; Lira-Galeana, C.; Gil-Villegas, A.; Wu, J. Asphaltene Precipitation in Crude Oils: Theory and Experiments. *AIChE J.* **2004**, *50* (10), 2552–2570.

- (21) ASTM Standard D5725, 2018. *Test Method for Nitrogen in Liquid Hydrocarbons, Petroleum and Petroleum Products by Boat-Inlet Chemiluminescence*; ASTM International, West Conshohocken, PA, 2018.
- (22) Fan, X.; Li, G.-S.; Dong, X.; Jiang, J.; Wei, X.-Y.; Kenttämä, H. I. Tandem Mass Spectrometric Evaluation of Core Structures of Aromatic Compounds after Catalytic Deoxygenation. *Fuel Process. Technol.* **2018**, *176*, 119–123.
- (23) Dong, X.; Zhang, Y.; Milton, J.; Yerabolu, R.; Easterling, L.; Kenttämä, H. I. Investigation of the Relative Abundances of Single-Core and Multicore Compounds in Asphaltenes by Using High-Resolution in-Source Collision-Activated Dissociation and Medium-Energy Collision-Activated Dissociation Mass Spectrometry with Statistical Considerations. *Fuel* **2019**, *246*, 126–132.
- (24) Prado, G. H. C.; Rao, Y.; de Klerk, A. Nitrogen Removal from Oil: A Review. *Energy Fuels* **2017**, *31* (1), 14–36.

## VITA

Edouard Niyonsaba was born in Nyabihu, Rwanda, on October 13, 1990. Edouard developed a passion for chemistry in high school when he first learned how to make soaps from triglycerides. After graduating from high school in 2010, Edouard was awarded a Rwanda Presidential Scholarship to pursue his undergraduate studies in the United States. He enrolled at the University of Central Arkansas where he obtained a B.S. in Biochemistry with a minor in Mathematics in 2015. At the University of Central of Arkansas, he was fortunate to be able to perform undergraduate research in the Biology Department under the guidance of Professor Brent Hill for 2 years. During that time, he gained a greater love for research and decided to apply for graduate school in order to continue his studies. He was accepted at Purdue University for the Purdue University Life Science Interdisciplinary Program (PULSe). After rotating in multiple laboratories, he found his home in Professor Kenttämä's research group. His research has focused on the development of mass spectrometric methods for identification of drug metabolites and drug impurities and for molecular profiling of crude oils. He defended his thesis in July 2019 and accepted a position as a Senior Chemist with DuPont.

## **PUBLICATIONS**

# Identification of Protonated Primary Carbamates by Using Gas-Phase Ion–Molecule Reactions Followed by Collision-Activated Dissociation in Tandem Mass Spectrometry Experiments

Edouard Niyonsaba,<sup>†</sup> McKay W. Easton,<sup>†</sup> Judy K.Y. Liu,<sup>†</sup> Zaikuan Yu,<sup>†</sup> Huaming Sheng,<sup>‡</sup> John Y. Kong,<sup>‡</sup> Zhoupeng Zhang,<sup>§</sup> Leah F. Easterling,<sup>†</sup> Jacob Milton,<sup>†</sup> and Hilkka I. Kenttämä<sup>\*,†</sup>

<sup>†</sup>Department of Chemistry, Purdue University, West Lafayette, Indiana 47907, United States

<sup>‡</sup>Department of Analytical Research & Development, Merck & Co., Inc., Rahway, New Jersey 07065, United States

<sup>§</sup>Department of Pharmacokinetics, Pharmacodynamics & Drug Metabolism, Merck & Co., Inc., West Point, Pennsylvania 19486, United States

## Supporting Information

**ABSTRACT:** The levels of potentially mutagenic impurities (PMIs) in active pharmaceutical ingredients are highly regulated and must be below a critical safety threshold. One class of PMIs is primary carbamates, which are formed during drug manufacturing and formulation. To comply with safety regulations, it is critically important to develop analytical techniques that enable the identification of primary carbamates during the drug development process. In this study, tandem mass spectrometry combined with gas-phase ion–molecule reactions as well as collision-activated dissociation (CAD) is demonstrated to enable the identification of protonated primary carbamates. Primary carbamates were protonated via atmospheric pressure chemical ionization (APCI) in a linear quadrupole ion trap mass spectrometer, isolated, and allowed to react with trimethoxymethylsilane (TMMS) introduced into the ion trap via an external reagent mixing manifold. Protonated primary carbamates reacted with TMMS to form an adduct ion,  $[M + H + TMMS]^+$ , and an adduct ion that had lost methanol,  $[M + H + TMMS - MeOH]^+$ . Upon CAD, the  $[M + H + TMMS - MeOH]^+$  product ions generated a diagnostic fragment ion via loss of isocyanic acid. Quantum chemical calculations were employed to explore the possible mechanisms for the formation of the product ions upon ion–molecule reactions and for the fragmentation of the  $[M + H + TMMS - MeOH]^+$  product ion.

**KEYWORDS:** potentially mutagenic impurities, carbamates, ion–molecule reactions, collision-activated dissociation, isocyanic acid

## INTRODUCTION

After manufacturing, drugs often contain residual impurities generated as synthetic byproducts or upon degradation of active pharmaceutical ingredients.<sup>1,2</sup> These impurities, including potentially mutagenic impurities (PMIs), can pose considerable safety concerns.<sup>3,4</sup> The PMIs of interest here are those containing the primary carbamate functionality. Ethyl carbamate (urethane), vinyl carbamate, thiocarbamate, and dithiocarbamate have all been reported to form as byproducts or degradation products in pharmaceutical syntheses.<sup>5</sup> This is of concern as some primary carbamates are classified as potentially mutagenic.<sup>6</sup> The International Council for Harmonization of Technical Requirements for Pharmaceuticals for Human Use (ICH) has issued guidelines limiting mutagenic impurity intake to less than 1.5  $\mu\text{g}$  per person per day.<sup>7–9</sup> To ensure that the consumption of impurities is below this threshold, robust analytical methods are needed to identify and quantitate low-level PMIs, such as primary carbamates, during drug development.

Unfortunately, the analytical techniques currently employed for the identification of PMIs, including primary carbamates, are limited in the scope and practicality. NMR spectroscopy and X-ray crystallography require large amounts of samples with high purity, which limits their use for identification of minor components in complex mixtures.<sup>10</sup> Gas chromatog-

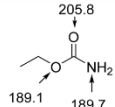
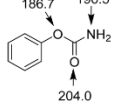
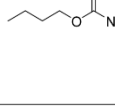
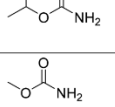
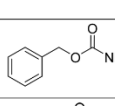
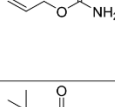
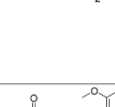
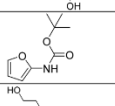
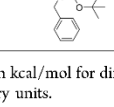
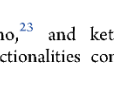

raphy coupled with electron ionization mass spectrometry (MS) has been commonly used to identify and quantitate different PMIs in complex mixtures.<sup>11,12</sup> However, this method often requires derivatization of the compounds, which is time-consuming and can lead to complications. Although high-performance liquid chromatography coupled with soft ionization mass spectrometry has become the gold standard for mixture analysis,<sup>8,13,14</sup> authentic compounds are required to unambiguously identify the compounds in the mixture.

Tandem mass spectrometry (MS<sup>2</sup>) based on collision-activated dissociation (CAD) is a powerful method for identification of previously unknown, ionized analytes in complex mixtures. However, in the case of primary carbamates, CAD does not yield fragment ions that are diagnostic for the compound class (Figure S1). Furthermore, CAD mass spectra of isomeric ions are sometimes uninformative and usually require comparison to CAD mass spectra measured for ionized, authentic compounds.<sup>15</sup> In contrast, MS<sup>2</sup> based on gas-phase ion–molecule reactions can often be used to differentiate isomeric ions without reference compounds.<sup>16–18</sup> Such ion–molecule reactions have been developed for the identification of many functional groups,<sup>19</sup> such as *N*-

Received: February 17, 2019

Published: May 28, 2019

**Table 1. Product Ions (with Their Relative Abundances) Observed after 300 ms Reaction of Protonated Primary, Secondary, and Tertiary Carbamates with TMMS (Proton Affinity<sup>26</sup> (PA) 202 kcal/mol) and the Fragment Ions (with Their Relative Abundances) Formed Upon CAD of the Product Ions  $[M + H + TMMS - MeOH]^+$ <sup>a,c</sup>**

Analyte (M) ( $m/z$ of $[M + H]^+$ ion)	Analyte structure and PA of selected atoms	Products ions ( $m/z$ ) and their relative abundances in % Product ions formed upon CAD <sup>b</sup> of ions of $[M + H + TMMS - MeOH]^+$ and their relative abundances in %
Ethyl carbamate (90)		$[M + H + TMMS]^+$ (226) 24 % $[M + H + TMMS - MeOH]^+$ (194) 100 % $[TMMS + H]^+$ (137) 3 % $[M + H + TMMS - MeOH - MeOH]^+$ (162) 15 % $[M + H + TMMS - MeOH - HNCO]^+$ (151) 100 %
Phenyl carbamate (138)		$[M + H + TMMS]^+$ (274) 6 % $[M + H + TMMS - MeOH]^+$ (242) 100 % $[M + H + TMMS - MeOH - HNCO]^+$ (199) 100 %
Butyl carbamate (118)		$[M + H + TMMS]^+$ (254) 100 % $[M + H + TMMS - MeOH]^+$ (222) 67 % $[M + H + TMMS - MeOH - HNCO]^+$ (179) 5 % $[M + H + TMMS - MeOH - C_4H_9]^+$ (166) 67 % $[M + H + TMMS - 2 MeOH - C_4H_9]^+$ (134) 100 % $[M + H + TMMS - 2 MeOH - C_4H_9 + H_2O]^+$ (152) 41 %
Isopropyl carbamate (104)		$[M + H + TMMS]^+$ (240) 100 % $[M + H + TMMS - MeOH]^+$ (208) 67 % $[M + H + TMMS - MeOH - HNCO]^+$ (165) 100 % $[M + H + TMMS - 2 MeOH - C_3H_7]^+$ (134) 8 %
Methyl carbamate (76)		$[M + H + TMMS]^+$ (212) 100 % $[M + H + TMMS - MeOH]^+$ (180) 7 % $[TMMS + H]^+$ (137) 12 % $[M + H + TMMS - MeOH - MeOH]^+$ (148) 10 % $[M + H + TMMS - MeOH - HNCO]^+$ (137) 100 %
Benzyl carbamate (152)		$[M + H + TMMS]^+$ (288) 7 % $[M + H + TMMS - MeOH]^+$ (256) 100 % $[M + H + TMMS - MeOH - HNCO]^+$ (213) 100 %
Allyl carbamate (102)		$[M + H + TMMS]^+$ (238) 100 % $[M + H + TMMS - MeOH]^+$ (206) 86 % $[M + H + TMMS - MeOH - MeOH]^+$ (174) 11 % $[M + H + TMMS - MeOH - HNCO]^+$ (163) 6 % $[M + H + TMMS - 2 MeOH - C_3H_5]^+$ (134) 100 % $[M + H + TMMS - 2 MeOH - C_3H_5 + H_2O]^+$ (152) 48 %
<i>tert</i> -Butyl carbamate (118)		$[M + H + TMMS]^+$ (254) 100 % $[M + H + TMMS - MeOH]^+$ (222) 67 % $[M + H + TMMS - MeOH - MeOH]^+$ (190) 38 % $[M + H + TMMS - MeOH - HNCO]^+$ (179) 4 % $[M + H + TMMS - MeOH - C_4H_9]^+$ (166) 16 % $[M + H + TMMS - 2 MeOH - C_4H_9]^+$ (134) 39 % $[M + H + TMMS - 2 MeOH - C_4H_9 + H_2O]^+$ (152) 19 %
Methocarbamol (242)		No reactions
<i>tert</i> -Butyl- <i>N</i> -(2-furyl)carbamate (184)		No reactions
<i>tert</i> -Butyl-benzyl-(4-hydroxybutyl) carbamate (280)		No reactions

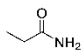
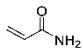
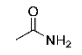
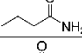
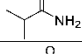
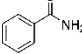
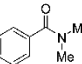
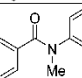
<sup>a</sup>Also shown are the proton affinities (PAs) in kcal/mol for different atoms in two analytes. PAs were calculated at the B3LYP/6-311++G(d,p) level of theory. <sup>b</sup>CAD collision energy 20 arbitrary units.

oxide,<sup>20,21</sup> epoxide,<sup>22</sup> *N*-hydroxylamino,<sup>23</sup> and keto,<sup>24</sup> in protonated analytes. All these are functionalities commonly found in PMIs.<sup>25</sup>

MS<sup>2</sup> based on gas-phase ion–molecule reactions with trimethoxymethyl silane (TMMS) followed by CAD (MS<sup>3</sup> experiment) of a diagnostic product ion (an adduct ion that



**Table 2.** Product Ions (with Their Relative Abundances) Observed after 300 ms Reaction of Protonated Amides and the Fragment Ions (with Their Relative Abundances) Formed Upon CAD<sup>a</sup> of the Product Ions  $[M + H + TMMS - MeOH]^+$ 

Analyte (M) ( <i>m/z</i> of $[M+H]^+$ ion)	Analyte structure	Products ions ( <i>m/z</i> ) and their relative abundances in %
Propionamide (74)		Product ions formed upon CAD of ions of $[M + H + TMMS - MeOH]^+$ and their relative abundance in % $[M + H + TMMS]^+$ (210) 100 % $[M + H + TMMS - MeOH]^+$ (178) 33 % $[M + H + TMMS - 2 MeOH]^+$ (146) 100 % $[M + H + TMMS - 2 MeOH + H_2O]^+$ (164) 6 %
Acrylamide (72)		$[M + H + TMMS]^+$ (208) 100 % $[M + H + TMMS - MeOH]^+$ (176) 85 % $[M + H + TMMS - 2 MeOH]^+$ (144) 100 % $[M + H + TMMS - 2 MeOH + H_2O]^+$ (162) 13 %
Acetamide (60)		$[M + H + TMMS]^+$ (196) 100 % $[M + H + TMMS - MeOH]^+$ (164) 45 % $[M + H + TMMS - 2 MeOH]^+$ (132) 100 % $[M + H + TMMS - 2 MeOH + H_2O]^+$ (150) 24 %
Butyramide (88)		$[M + H + TMMS]^+$ (224) 100 %
Isobutyramide (88)		$[M + H + TMMS]^+$ (224) 100 %
Benzamide (122)		$[M + H + TMMS]^+$ (258) 100 %
<i>N,N</i> -dimethylbenzamide (150)		No reactions
<i>N</i> -methyl- <i>N</i> -phenylbenzamide (212)		No reactions

<sup>a</sup>CAD collision energy 20 arbitrary units.

had lost methanol,  $[M + H + TMMS - MeOH]^+$  has been previously employed to identify carboxylic acid, sulfone, and sulfonamido functionalities in protonated analytes.<sup>26</sup> A total of 37 analytes containing one or more of 22 different functional groups were explored. Only protonated carboxylic acids, protonated sulfones, and protonated sulfonamides were found to form the  $[M + H + TMMS - MeOH]^+$  product ion. These three compound groups were differentiated from each other based on diagnostic CAD products of the  $[M + H + TMMS - MeOH]^+$  product ion. In this report, the same approach is presented for the identification of protonated primary carbamates. The reactivity of protonated amides toward TMMS is also reported here because of the structural similarities of amides and carbamates. Quantum chemical calculations were employed to explore relevant reaction mechanisms.

## EXPERIMENTAL SECTION

**Chemicals.** TMMS (98% purity) was purchased from Sigma-Aldrich. Carbamate model compounds (Table 1) and amide model compounds (Table 2) were also purchased from Sigma-Aldrich. Water (LC/MS grade), methanol (LC/MS grade), and acetonitrile (LC/MS grade) were purchased from Fisher Scientific. All chemicals were used as received without purification.

**Sample Preparation.** Stock solutions of all analytes were prepared at a mass fraction of 10 parts per million (ppm) in 50:50 (v/v) acetonitrile:water. The stock solution was then diluted to 1 ppm using the same solvent.

**Instrumentation.** All experiments were performed with a Thermo Scientific linear quadrupole ion trap (LQIT) mass spectrometer equipped with atmospheric pressure chemical ionization (APCI) operated in positive ion mode. The analytes dissolved in 50:50 (v/v) acetonitrile:water were infused into the APCI source at a rate of 10  $\mu$ L/min with a 500  $\mu$ L Hamilton syringe. Typical APCI source conditions were as follows. The discharge current was set at 3.8  $\mu$ A. The sheath and auxiliary gas ( $N_2$ ) outputs were set at 30 and 10 (arbitrary units), respectively. The vaporizer and capillary temperatures were 300 and 275  $^{\circ}$ C, respectively. The capillary voltage was set at 10 V and the tube lens at 40 V.

An external reagent mixing manifold was used to introduce the reagent, TMMS, into the helium buffer gas line, as previously described.<sup>27–29</sup> Briefly, TMMS was introduced into the reagent mixing manifold via a syringe pump at a flow rate of 3  $\mu$ L/h. The syringe port and surrounding area were heated to approximately 110  $^{\circ}$ C to ensure complete evaporation of TMMS. The reagent was then diluted with a controlled amount of helium before entering the ion trap through a leak valve. To determine whether TMMS was present in the ion trap, a protonated methanol dimer (*m/z* 65) generated in the APCI source from methanol was isolated (isolation width of 12 *m/z* units) and allowed to react with TMMS for 300 ms. Protonated TMMS (*m/z* 137) was observed with an abundance of 30% relative to the protonated methanol dimer (*m/z* 65). Protonated analytes were also isolated and allowed to react with TMMS. For CAD experiments, the  $[M + H + TMMS - MeOH]^+$  product ion was isolated and subjected to CAD in the ion trap. Typical reaction, isolation, and CAD

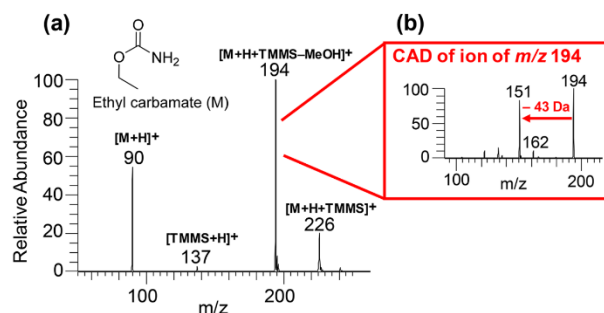


**Figure 1.** (a)  $MS^2$  spectrum measured after 300 ms reaction of protonated ethyl carbamate ( $m/z$  90) with TMMS. The observed product ions are a stable adduct,  $[M + H + TMMS]^+$  ( $m/z$  226), an adduct that has lost methanol,  $[M + H + TMMS - MeOH]^+$  ( $m/z$  194), and protonated TMMS,  $[TMMS + H]^+$  ( $m/z$  137). (b)  $MS^3$  spectrum measured after CAD (collision energy 20 arbitrary units) of the  $[M + H + TMMS - MeOH]^+$  product ion ( $m/z$  194). The fragment ion with  $m/z$  151 formed via the loss of isocyanic acid ( $HN=C=O$ ; MW 43 Da) is diagnostic for protonated primary carbamates. The fragment ion of  $m/z$  162 corresponds to elimination of methanol.

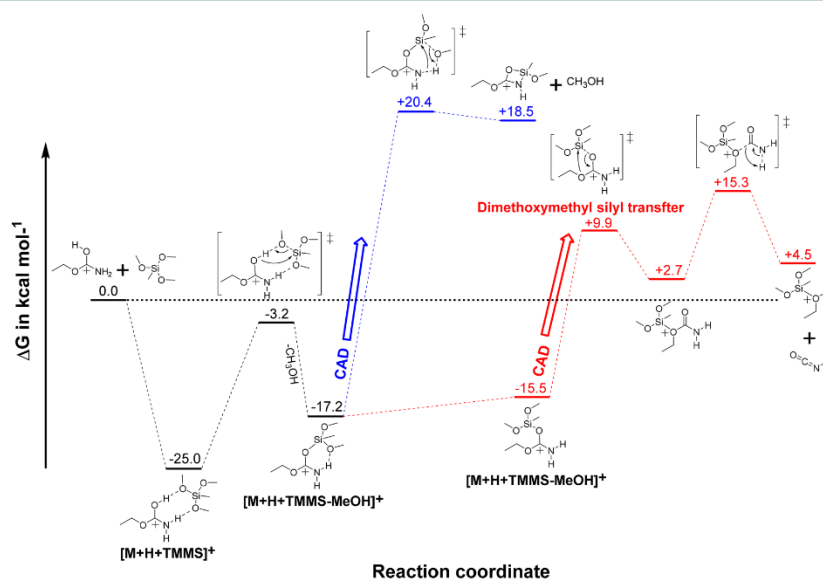


**Figure 2.** Potential energy surface calculated at the M06-2X/6-311++G(d,p) level of theory for the formation of the ions  $[M + H + TMMS]^+$  and  $[M + H + TMMS - MeOH]^+$  upon reactions of protonated ethyl carbamate with TMMS. Also shown are the potential energy surfaces associated with the formation of fragment ions formed via a loss of isocyanic acid (red) and methanol (blue) upon CAD of the  $[M + H + TMMS - MeOH]^+$  product ion.

conditions were as follows: reaction time 300 ms, isolation width of two  $m/z$  units, activation  $q$  value 0.25, and collision energy 20 (arbitrary units).

**Computational Studies.** The proton affinities of ethyl carbamate, phenyl carbamate, and 2-hydroxy-3-methoxypropyl carbamate were calculated at the B3LYP/6-311++G(d,p) level of theory. The quantum chemical calculations were performed at the M06-2X/6-311++G(d,p) level of theory by using Gaussian 16.<sup>30,31</sup> Transition state structures possessed exactly one negative frequency corresponding to the reaction coordinate. Intrinsic reaction coordinate (IRC) calculations

were performed for all transition states to ensure that the optimized structure connected the correct reactants and products. The free energies used to construct the potential energy surfaces were computed using ideal gas statistical mechanics.

## RESULTS AND DISCUSSION

Gas-phase reactivity of several protonated primary carbamates, one secondary carbamate, and one tertiary carbamate toward TMMS, followed by CAD of selected product ions, were studied in a linear quadrupole ion trap (LQIT) mass

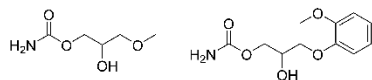


Figure 3. 2-Hydroxy-3-methoxypropyl carbamate and methocarbamol.

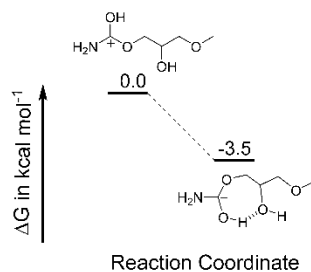


Figure 4. Potential energy surface calculated at the M06-2X/6-311++G(d,p) level of theory for two conformers of protonated 2-hydroxy-3-methoxypropyl carbamate.

spectrometer to explore the utility of this approach in the identification of primary carbamates. The experimental and computational results obtained for the reactions between protonated carbamates and TMMS, and in the following CAD experiments, will be discussed first. After this, the reactivity of protonated amides is considered because of the structural similarities of amides and carbamates.

**Reactions of Protonated Carbamates with TMMS Followed by CAD.** Several primary carbamates, one secondary carbamate, and one tertiary carbamate were protonated via positive ion mode APCI, isolated, and allowed to react with TMMS for 300 ms in a linear quadrupole ion trap (LQIT) mass spectrometer. The protonated secondary and tertiary carbamates did not react with TMMS. However, all tested protonated primary carbamates, with the exception of protonated methocarbamol, reacted with TMMS to form a stable adduct ion,  $[M + H + TMMS]^+$ , and an adduct ion that had lost methanol,  $[M + H + TMMS - MeOH]^+$  (Table 1). The latter product ion has been previously reported for reactions of TMMS only with protonated compounds containing a carboxylic acid, sulfone, or sulfonamide group;

none of the other functionalities examined (22 total) yielded this product ion.<sup>26</sup> These three compound groups were distinguished from each other based on the different CAD products that were detected for the  $[M + H + TMMS - MeOH]^+$  ions.<sup>26</sup> To explore this approach for the identification of protonated primary carbamates, the  $[M + H + TMMS - MeOH]^+$  product ions formed for the protonated carbamates were subjected to CAD. These experiments revealed a unique fragment ion due to the loss of isocyanic acid ( $HN=C=O$ ; MW 43 Da) formed only for primary carbamates. The  $[M + H + TMMS - MeOH]^+$  product ions formed for protonated carboxylic acids, sulfones, and sulfonamides do not fragment via the loss of isocyanic acid upon CAD,<sup>26</sup> which enables the differentiation of primary carbamates from these compound groups. An example of the reactions of protonated carbamates with TMMS is shown in Figure 1. Protonated ethyl carbamate ( $m/z$  90) reacts with TMMS (MW 136 Da) to yield a stable adduct ion,  $[M + H + TMMS]^+$  ( $m/z$  226), and an adduct ion that has lost methanol,  $[M + H + TMMS - MeOH]^+$  ( $m/z$  194). When the  $[M + H + TMMS - MeOH]^+$  product ion ( $m/z$  194) was isolated and subjected to CAD, a unique diagnostic fragment ion of  $m/z$  151 due to the loss of isocyanic acid ( $HN=C=O$ ; MW 43 Da) was formed (Figure 1). Fragment ion of  $m/z$  162 was also observed. This ion corresponds to the loss of a methanol molecule (MW 32 Da).

Quantum chemical calculations were performed at the M06-2X/6-311++G(d,p) level of theory to probe the mechanisms leading to the elimination of methanol upon reactions of protonated ethyl carbamate with TMMS and the following eliminations of isocyanic acid or methanol upon CAD of the  $[M + H + TMMS - MeOH]^+$  product ions. Based on the proton affinities calculated for ethyl carbamate, the protonation of primary carbamates occurs at the carbonyl oxygen because it has a higher proton affinity (205.8 kcal/mol) than the ether oxygen (189.1 kcal/mol) or the amino group (189.7 kcal/mol) (all values for ethyl carbamate: see Table 1). The adduct formed upon interaction of protonated primary carbamates with TMMS,  $[M + H + TMMS]^+$ , is stabilized by two hydrogen bonds between two oxygen atoms of TMMS and two hydrogen atoms of the protonated primary carbamate (Figure 2). Elimination of methanol involves formation of a covalent bond between the carbonyl oxygen of the carbamate and the silicon atom of TMMS to form  $[M + H + TMMS - MeOH]^+$  product ion (Figure 2). This reaction is calculated to

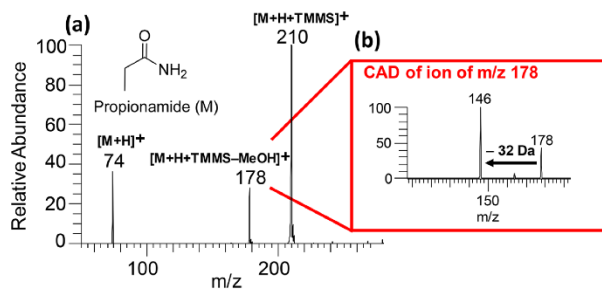
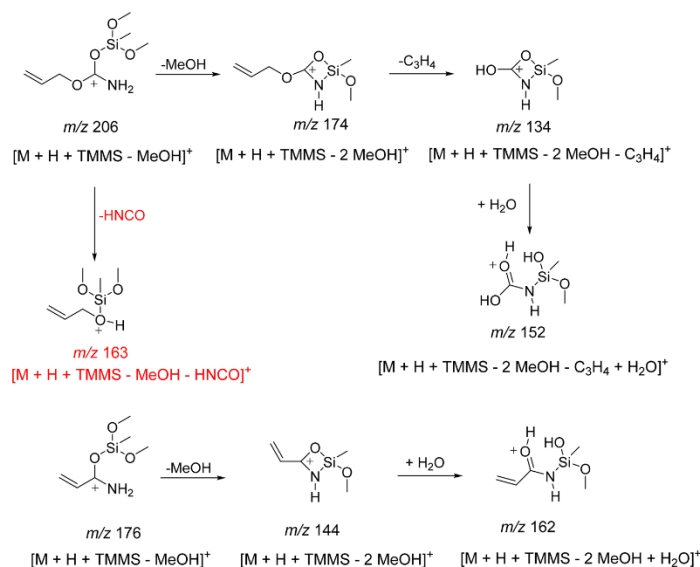


Figure 5. (a)  $MS^2$  spectrum measured after 300 ms reaction of protonated propionamide ( $m/z$  74) with TMMS. The observed product ions are a stable adduct,  $[M + H + TMMS]^+$  ( $m/z$  210), and an adduct that has lost methanol,  $[M + H + TMMS - MeOH]^+$  ( $m/z$  178). (b)  $MS^3$  spectrum measured after CAD (collision energy 20 arbitrary units) of the  $[M + H + TMMS - MeOH]^+$  product ion ( $m/z$  178). The major fragment ion observed ( $m/z$  146) corresponds to the loss of methanol. No fragment ion from the loss of isocyanic acid (MW 43 Da) was observed.



**Figure 6.** Proposed fragmentation pathway for CAD of the  $[M + H + TMMS - MeOH]^+$  product ion formed between TMMS and protonated allyl carbamate (top) and protonated acrylamide (bottom). The CAD of the  $[M + H + TMMS - MeOH]^+$  product ion of protonated allyl carbamate yields a diagnostic fragment ion from the elimination of isocyanic acid ( $m/z\ 163$ ) as well as a fragment ion from elimination of methanol ( $m/z\ 174$ ) and a fragment ion from elimination of methanol and propan-1,2-diene ( $m/z\ 134$ ). This fragment ion reacts with water to form a water adduct ion ( $m/z\ 152$ ), possibly as shown below. CAD of the  $[M + H + TMMS - MeOH]^+$  product ion of protonated acrylamide only yields a fragment ion from elimination of methanol ( $m/z\ 144$ ). This fragment ion reacts with water to form a water adduct ion ( $m/z\ 162$ ), possibly as shown below.

be exothermic by 17 kcal/mol for protonated ethyl carbamate. Based on the calculations, the elimination of isocyanic acid ( $HN=C=O$ ) upon CAD of the  $[M + H + TMMS - MeOH]^+$  product ion of protonated allyl carbamate is initiated by breaking a hydrogen bond between the NH-group of the carbamate and a methoxy group of TMMS, followed by rotation of the dimethoxymethylsilyl group and transfer of this group from the carbonyl oxygen to the ether oxygen of the carbamate (Figure 2). This intermediate will produce the  $HN=C=O$  elimination product via a transition state that is 32.5 kcal/mol above the  $[M + H + TMMS - MeOH]^+$  product ion. On the other hand, elimination of methanol from the CAD of the  $[M + H + TMMS - MeOH]^+$  product ion is calculated to have a barrier that is substantially higher (37.6 kcal/mol). This explains why isocyanic acid elimination is favored over methanol elimination for ethyl carbamate. Three protonated primary carbamates, protonated *tert*-butyl carbamate, butyl carbamate, and allyl carbamate, formed less than 100% relative abundance of the  $[M + H + TMMS - MeOH - HNCO]^+$  fragment ion (4–6% relative abundance). For the first two compounds, this is probably due to steric hindrance, which makes the elimination of methanol more favorable than elimination of isocyanic acid (Figure 2). For allyl carbamate, the reasons for this behavior are not known at this time.

Protonated methocarbamol is the only primary carbamate studied that did not react with TMMS to form the  $[M + H + TMMS]^+$  or  $[M + H + TMMS - MeOH]^+$  product ions (Figure S2). To rationalize this observation, quantum chemical calculations at the M06-2X/6-311++G(d,p) level of theory

were performed on protonated 2-hydroxy-3-methoxypropyl carbamate. This cation was chosen as the model compound for the calculations because it has a similar structure as protonated methocarbamol (Figure 3). The most stable conformer of protonated 2-hydroxy-3-methoxypropyl carbamate was found to contain a seven-membered ring stabilized by a hydrogen bond. This conformer is 3.5 kcal/mol more stable than the linear structure (Figure 4). The most stable conformer of protonated methocarbamol is expected to have a similar seven-membered ring structure. As the highest barrier for the reaction of protonated ethyl carbamate with TMMS is only 3 kcal/mol below the total energy level of the system (Figure 2), this extra stabilization of the carbamate may prevent its reactions with TMMS.

**Reactions of Protonated Amides with TMMS Followed by CAD.** Several protonated amides were also tested for their reactivity toward TMMS because of the structural similarities between amides and carbamates. Only protonated propionamide, protonated acrylamide, and protonated acetamide were found to react with TMMS to form the diagnostic adduct ion that has lost methanol,  $[M + H + TMMS - MeOH]^+$  (Table 2), among the six primary amides and two tertiary amides studied. Upon CAD, the  $[M + H + TMMS - MeOH]^+$  product ions generated from the three protonated primary amides fragmented via loss of methanol (Figure 4). As no elimination of isocyanic acid was observed, the primary amides can be differentiated from primary carbamates. This is not surprising as the mechanism proposed for the loss of isocyanic acid for carbamates is not feasible for amides.

Several unusual product ions due to addition of water to a fragment ion were observed upon CAD of the  $[M + H + TMMS - MeOH]^+$  product ions of protonated carbamates (Table 1) and protonated amides (Table 2; Figure 5). Analogous water adduct ions have been previously observed upon CAD of protonated isoquinoline-3-carboxamides.<sup>32</sup> The pathway for the formation of such a water adduct ion upon CAD of the  $[M + H + TMMS - MeOH]^+$  product ion formed from a protonated primary carbamate and a protonated primary amide is shown in Figure 6.

## CONCLUSIONS

Gas-phase ion–molecule reactions of protonated primary carbamates with TMMS are demonstrated to yield an adduct ion that has lost methanol,  $[M + H + TMMS - MeOH]^+$ . This product ion has only been observed for protonated primary carbamates and three primary amides (among the 8 amides studied), as reported here, as well as for protonated carboxylic acids, sulfones, and sulfonamides, as reported<sup>26</sup> previously (among a total of 24 different functionalities studied thus far). Protonated primary carbamates can be differentiated from the above four compound groups as only the  $[M + H + TMMS - MeOH]^+$  ions formed from protonated primary carbamates yield a fragment ion via the loss of isocyanic acid (HNCO) upon CAD, making this fragment ion diagnostic for protonated primary carbamates. The elimination of isocyanic acid upon CAD of the  $[M + H + TMMS - MeOH]^+$  product ions is proposed to be initiated by breaking a hydrogen bond between the NH-group of the carbamate and a methoxy group of TMMS in the  $[M + H + TMMS - MeOH]^+$  ions, followed by rotation and transfer of the dimethoxymethylsilyl group from the carbonyl oxygen to the ether oxygen of the carbamate. This intermediate yields the  $[M + H + TMMS - MeOH - HNCO]^+$  ion from the loss of isocyanic acid.

## ASSOCIATED CONTENT

### Supporting Information

The Supporting Information is available free of charge on the ACS Publications website at DOI: 10.1021/acs.oprd.9b00080.

MS<sup>2</sup> of selected protonated primary carbamates; Cartesian coordinates and Gibb's free energies of the computational results (PDF)

## AUTHOR INFORMATION

### Corresponding Author

\*E-mail: hilkka@purdue.edu. Tel.: +1 (765) 494 0882. Fax: +1 (765) 494 9421.

### ORCID

Edouard Niyonsaba: 0000-0002-3847-0935

Mckay W. Easton: 0000-0003-2754-4799

Hilkka I. Kenttämä: 0000-0001-8988-6984

### Notes

The authors declare no competing financial interest.

## ACKNOWLEDGMENTS

The authors thank Merck Sharp & Dohme Corp., a subsidiary of Merck & Co., Inc., Kenilworth, NJ, USA, for financial support.

## REFERENCES

- (1) Callis, C. M.; Bercu, J. P.; DeVries, K. M.; Dow, L. K.; Robbins, D. K.; Varie, D. L. Risk Assessment of Genotoxic Impurities in Marketed Compounds Administered over a Short-Term Duration: Applications to Oncology Products and Implications for Impurity Control Limits. *Org. Process Res. Dev.* **2010**, *14* (4), 986–992.
- (2) Lee, C.; Helmy, R.; Strulson, C.; Plewa, J.; Kolodziej, E.; Antonucci, V.; Mao, B.; Welch, C. J.; Ge, Z.; Al-Sayah, M. A. Removal of Electrophilic Potential Genotoxic Impurities Using Nucleophilic Reactive Resins. *Org. Process Res. Dev.* **2010**, *14* (4), 1021–1026.
- (3) Bercu, J. P.; Hoffman, W. P.; Lee, C.; Ness, D. K. Quantitative Assessment of Cumulative Carcinogenic Risk for Multiple Genotoxic Impurities in a New Drug Substance. *Regul. Toxicol. Pharmacol.* **2008**, *51* (3), 270–277.
- (4) Cimarosti, Z.; Bravo, F.; Stonestreet, P.; Tinazzi, F.; Vecchi, O.; Camurri, G. Application of Quality by Design Principles to Support Development of a Control Strategy for the Control of Genotoxic Impurities in the Manufacturing Process of a Drug Substance. *Org. Process Res. Dev.* **2010**, *14* (4), 993–998.
- (5) Galloway, S. M.; Reddy, M. V.; McGettigan, K.; Gealy, R.; Bercu, J. Potentially Mutagenic Impurities: Analysis of Structural Classes and Carcinogenic Potencies of Chemical Intermediates in Pharmaceutical Syntheses Supports Alternative Methods to the Default TTC for Calculating Safe Levels of Impurities. *Regul. Toxicol. Pharmacol.* **2013**, *66* (3), 326–335.
- (6) Snodin, D. J. Genotoxic Impurities: From Structural Alerts to Qualification. *Org. Process Res. Dev.* **2010**, *14* (4), 960–976.
- (7) Kroes, R.; Renwick, A. G.; Cheeseman, M.; Kleiner, J.; Mangelsdorf, I.; Piersma, A.; Schilter, B.; Schlatter, J.; van Schothorst, F.; Vos, J. G.; Würtzen, G. Structure-Based Thresholds of Toxicological Concern (TTC): Guidance for Application to Substances Present at Low Levels in the Diet. *Food Chem. Toxicol.* **2004**, *42* (1), 65–83.
- (8) Teasdale, A.; Elder, D. P. Analytical Control Strategies for Mutagenic Impurities: Current Challenges and Future Opportunities? *TrAC, Trends Anal. Chem.* **2018**, *101*, 66–84.
- (9) Assessment and Control of DNA Reactive (Mutagenic) Impurities in Pharmaceuticals To Limit Potential Carcinogenic Risk M7 (Step 4); 2014; <https://www.fda.gov/downloads/Drugs/GuidanceComplianceRegulatoryInformation/Guidances/UCM347725.pdf>.
- (10) Peiris, D. M.; Lam, W.; Michael, S.; Ramanathan, R. Distinguishing N-oxide and Hydroxyl Compounds: Impact of Heated Capillary/Heated Ion Transfer Tube in Inducing Atmospheric Pressure Ionization Source Decompositions. *J. Mass Spectrom.* **2004**, *39* (6), 600–606.
- (11) Liu, X.-W.; Zhang, W.-P.; Han, H.-Y.; Sun, L.; Chen, D.-Y. Trace Determination of Mutagenic Alkyl Toluene-sulfonate Impurities via Derivatization Headspace–GC/MS in an Active Pharmaceutical Ingredient of a Candidate Drug. *J. Pharm. Biomed. Anal.* **2018**, *155*, 104–108.
- (12) Loda, C.; Bernabe, E.; Nicoletti, A.; Bacchi, S.; Dams, R. Determination of Epichlorohydrin in Active Pharmaceutical Ingredients by Gas Chromatography–Mass Spectrometry. *Org. Process Res. Dev.* **2011**, *15* (6), 1388–1391.
- (13) Yang, R.-S.; Beard, A.; Sheng, H.; Zhang, L.-K.; Helmy, R. Applications of  $TiCl_3$  as a Diagnostic Reagent for the Detection of Nitro- and N-Oxide-Containing Compounds as Potentially Mutagenic Impurities Using Ultrahigh-Performance Liquid Chromatography Coupled with High-Resolution Mass Spectrometry. *Org. Process Res. Dev.* **2016**, *20* (1), 59–64.
- (14) Yuabova, Z. Y.; Holschlag, D. R.; Rodriguez, S. A.; Qin, C.; Papov, V. V.; Qiu, F.; McCaffrey, J. F.; Norwood, D. L. Genotoxic Impurities: A Quantitative Approach. *J. Liq. Chromatogr. Relat. Technol.* **2008**, *31* (15), 2318–2330.
- (15) Kong, J. Y.; Yu, Z.; Easton, M. W.; Niyonsaba, E.; Ma, X.; Yerabolu, R.; Sheng, H.; Jarrell, T. M.; Zhang, Z.; Ghosh, A. K.; Kenttämä, H. I. Differentiating Isomeric Deprotonated Glucuronide

Drug Metabolites via Ion/Molecule Reactions in Tandem Mass Spectrometry. *Anal. Chem.* **2018**, *90* (15), 9426–9433.

(16) Sheng, H.; Tang, W.; Yerabolu, R.; Max, J.; Kotha, R. R.; Riedeman, J. S.; Nash, J. J.; Zhang, M.; Kenttämaa, H. I. Identification of N-Oxide and Sulfoxide Functionalities in Protonated Drug Metabolites by Using Ion–Molecule Reactions Followed by Collisionally Activated Dissociation in a Linear Quadrupole Ion Trap Mass Spectrometer. *J. Org. Chem.* **2016**, *81* (2), 575–586.

(17) Fu, M.; Duan, P.; Li, S.; Habicht, S. C.; Pinkston, D. S.; Vinueza, N. R.; Kenttämaa, H. I. Regioselective Ion–Molecule Reactions for the Mass Spectrometric Differentiation of Protonated Isomeric Aromatic Diamines. *Analyst* **2008**, *133* (4), 452.

(18) Bjarnason, A.; Taylor, J. W.; Kinsinger, J. A.; Cody, R. B.; Weil, D. A. Isomer Discrimination of Disubstituted Benzene Derivatives through Gas-Phase Iron(I) Ion Reactions in a Fourier-Transform Mass Spectrometer. *Anal. Chem.* **1989**, *61* (17), 1889–1894.

(19) Osburn, S.; Ryzhov, V. Ion–Molecule Reactions: Analytical and Structural Tool. *Anal. Chem.* **2013**, *85* (2), 769–778.

(20) Duan, P.; Gillespie, T. A.; Winger, B. E.; Kenttämaa, H. I. Identification of the Aromatic Tertiary N-Oxide Functionality in Protonated Analytes via Ion/Molecule Reactions in Mass Spectrometers. *J. Org. Chem.* **2008**, *73* (13), 4888–4894.

(21) Duan, P.; Fu, M.; Gillespie, T. A.; Winger, B. E.; Kenttämaa, H. I. Identification of Aliphatic and Aromatic Tertiary N-Oxide Functionalities in Protonated Analytes via Ion/Molecule and Dissociation Reactions in an FT-ICR Mass Spectrometer. *J. Org. Chem.* **2009**, *74* (3), 1114–1123.

(22) Eismin, R. J.; Fu, M.; Yem, S.; Widjaja, F.; Kenttämaa, H. I. Identification of Epoxide Functionalities in Protonated Monofunctional Analytes by Using Ion/Molecule Reactions and Collision-Activated Dissociation in Different Ion Trap Tandem Mass Spectrometers. *J. Am. Soc. Mass Spectrom.* **2012**, *23* (1), 12–22.

(23) Sheng, H.; Tang, W.; Yerabolu, R.; Kong, J. Y.; Williams, P. E.; Zhang, M.; Kenttämaa, H. I. Mass Spectrometric Identification of the N-monosubstituted N-hydroxylamino Functionality in Protonated Analytes via Ion/Molecule Reactions in Tandem Mass Spectrometry. *Rapid Commun. Mass Spectrom.* **2015**, *29* (8), 730–734.

(24) Moraes, L.; Eberlin, M. N. Structurally Diagnostic Ion–Molecule Reactions: Acylium Ions with  $\alpha$ -,  $\beta$ - and  $\gamma$ -hydroxy Ketones. *J. Mass Spectrom.* **2002**, *37* (2), 162–168.

(25) Robinson, D. I. Control of Genotoxic Impurities in Active Pharmaceutical Ingredients: A Review and Perspective. *Org. Process Res. Dev.* **2010**, *14* (4), 946–959.

(26) Yerabolu, R.; Kong, J.; Easton, M.; Kotha, R. R.; Max, J.; Sheng, H.; Zhang, M.; Gu, C.; Kenttämaa, H. I. Identification of Protonated Sulfone and Aromatic Carboxylic Acid Functionalities in Organic Molecules by Using Ion–Molecule Reactions Followed by Collisionally Activated Dissociation in a Linear Quadrupole Ion Trap Mass Spectrometer. *Anal. Chem.* **2017**, *89* (14), 7398–7405.

(27) Gronert, S. Estimation of Effective Ion Temperatures in a Quadrupole Ion Trap. *J. Am. Soc. Mass Spectrom.* **1998**, *9* (8), 845–848.

(28) Gronert, S. Quadrupole Ion Trap Studies of Fundamental Organic Reactions. *Mass Spectrom. Rev.* **2005**, *24* (1), 100–120.

(29) Habicht, S. C.; Vinueza, N. R.; Archibold, E. F.; Duan, P.; Kenttämaa, H. I. Identification of the Carboxylic Acid Functionality by Using Electrospray Ionization and Ion–Molecule Reactions in a Modified Linear Quadrupole Ion Trap Mass Spectrometer. *Anal. Chem.* **2008**, *80* (9), 3416–3421.

(30) Zhao, Y.; Truhlar, D. G. Density Functionals with Broad Applicability in Chemistry. *Acc. Chem. Res.* **2008**, *41* (2), 157–167.

(31) Frisch, M. J.; Trucks, G. W.; Schlegel, H. B.; Scuseria, G. E.; Robb, M. A.; Cheeseman, J. R.; Scalmani, G.; Barone, V.; Petersson, G. A.; Nakatsuji, H.; Li, X.; Caricato, M.; Marenich, A. V.; Bloino, J.; Janesko, B. G.; Gomperts, R.; Mennucci, B.; Hratchian, H. P.; Ortiz, J. V.; Izmaylov, A. F.; Sonnenberg, J. L.; Williams-Young, D.; Ding, F.; Lipparini, F.; Egidi, F.; Goings, J.; Peng, B.; Petrone, A.; Henderson, T.; Ranasinghe, D.; Zakrzewski, V. G.; Gao, J.; Rega, N.; Zheng, G.; Liang, W.; Hada, M.; Ehara, M.; Toyota, K.; Fukuda, R.; Hasegawa, J.

Ishida, M.; Nakajima, T.; Honda, Y.; Kitao, O.; Nakai, H.; Vreven, T.; Throssell, K.; Montgomery, J. A., Jr.; Peralta, J. E.; Ogliaro, F.; Bearpark, M. J.; Heyd, J. J.; Brothers, E. N.; Kudin, K. N.; Staroverov, V. N.; Keith, T. A.; Kobayashi, R.; Normand, J.; Raghavachari, K.; Rendell, A. P.; Burant, J. C.; Iyengar, S. S.; Tomasi, J.; Cossi, M.; Millam, J. M.; Klene, M.; Adamo, C.; Cammi, R.; Ochterski, J. W.; Martin, R. L.; Morokuma, K.; Farkas, O.; Foresman, J. B.; Fox, D. J. *Gaussian 16*, Revision B.01. Gaussian, Inc., Wallingford CT, 2016.

(32) Beuck, S.; Schwabe, T.; Grimme, S.; Schlörer, N.; Kamber, M.; Schänzer, W.; Thevis, M. Unusual Mass Spectrometric Dissociation Pathway of Protonated Isoquinoline-3-Carboxamides Due to Multiple Reversible Water Adduct Formation in the Gas Phase. *J. Am. Soc. Mass Spectrom.* **2009**, *20* (11), 2034–2048.



## Recent Advances in Petroleum Analysis by Mass Spectrometry

Edouard Niyonsaba,<sup>†</sup> Jeremy M. Manheim,<sup>†</sup> Ravikiran Yerabolu,<sup>‡</sup> and Hilkkka I. Kenttämä\*<sup>§</sup>

Department of Chemistry, Purdue University, West Lafayette, Indiana 47907, United States

## ■ CONTENTS

Advances in Instrumentation	156
Fourier-Transform Ion Cyclotron Resonance Mass Spectrometry	156
Orbitrap Mass Spectrometry	158
2D Gas Chromatography/Time-of-Flight Mass Spectrometry	158
Ion Mobility Mass Spectrometry	159
Ionization Methods	160
Fractionation	160
Applications	165
Whole Crude Oil	165
Saturated Hydrocarbons	165
Sulfur-Containing Compounds	166
Nitrogen-Containing Compounds	167
Naphthenic Acids	168
Metals	169
Asphaltenes	171
Molecular Weight	171
Island vs Archipelago Structures	171
Geochemistry and Oil Fingerprinting	173
Future Directions	174
Author Information	174
Corresponding Author	174
ORCID	174
Present Address	174
Author Contributions	174
Notes	174
Biographies	174
Acknowledgments	174
References	174

Chemical characterization of petroleum is a challenging task due to its inherently complex nature. For example, crude oil is believed to have as many or more compounds than the number of genes in the human genome.<sup>1</sup> As the depletion of light crude oil has increased the reliance by petroleum industry on heavier crude oils, the ability to carry out detailed chemical analysis of petroleum is essential to improve the efficiency of crude oil recovery from oil wells and its processing.<sup>2</sup> Of the diverse classes of compounds found in petroleum, including saturated hydrocarbons, aromatic hydrocarbons, polar compounds, and asphaltenes, the saturated and aromatic hydrocarbons are the most useful for generation of fuels and other valuable products.<sup>3</sup> Compounds containing heteroatoms, such as nitrogen, oxygen, or sulfur, and metals, including vanadium and nickel, are notorious for their toxicity to the environment and for destroying processing catalysts and decreasing the stability of petroleum products.<sup>4</sup> The asphaltene fraction presents its own unique problems as these compounds

tend to poison catalysts and precipitate out in pipelines, which leads to increased maintenance costs.<sup>5</sup> For more effective recovery and refining of crude oil, more accurate knowledge of the average molecular weight of compounds in petroleum, their molecular structures, and their abundances is crucial.

Mass spectrometry has played a critical role in the characterization of petroleum. The development of very high-resolution instruments has led to a tremendous amount of information on the elemental compositions of the compounds in petroleum samples. Especially, the utilization of a 21 T Fourier-transform ion cyclotron resonance mass spectrometer (21 T FTICR MS) has produced unmatched breadth and depth of compositional information.<sup>6,7</sup> Further, the combination of mass spectrometry and chromatography, including gas chromatography (GC), 2D GC (GC × GC), high-performance liquid chromatography (HPLC), and gel permeation chromatography (GPC), has provided a greater understanding on the types and amounts of certain chemical classes in petroleum. Also, chemometrics is becoming an important analytical tool for determining the origins of unknown petroleum samples as well as differentiating petroleum samples based on mass spectral data. The growing field of petroleomics, defined by Marshall and Rodgers as the characterization of petroleum at the molecular level, has seen many advances in recent years.<sup>8</sup> This review is a continuation to a previous review published by Ryan Rodgers and Amy McKenna,<sup>9</sup> *Petroleum Analysis*, that covers the developments in mass spectrometric characterization of petroleum samples from 2015 until 2018. The most recent advances in mass spectrometry instrumentation, ionization methods, and fractionation methods for petroleum analysis will be first described, followed by discussion on applications of mass spectrometry in the analysis of common petroleum classes, such as asphaltenes, saturated hydrocarbons, naphthenic acids, and metals, and ending with a perspective on future directions for petroleum analysis.

## ■ ADVANCES IN INSTRUMENTATION

**Fourier-Transform Ion Cyclotron Resonance Mass Spectrometry.** FTICR MS is the state-of-the-art for determination of elemental compositions of compounds in complex mixtures due to its ultrahigh resolving power. The basic principles of FTICR MS instrumentation, ionization techniques, and data interpretation were recently reviewed.<sup>10</sup> The need for ultrahigh mass-resolving power for some petroleum samples was demonstrated by Smith et al., who utilized a 21 T FTICR MS and both positive and negative ion

**Special Issue:** Fundamental and Applied Reviews in Analytical Chemistry 2019

**Published:** November 14, 2018

mode ( $\pm$ ) electrospray ionization (ESI) or positive ion mode (+) atmospheric pressure photoionization (APPI) for molecular-level characterization of multiple petroleum samples.<sup>11</sup> For example, the number of assigned peaks was increased by 1.3-fold, and mass resolving power and mass measurement accuracy were improved by 2.2- and 2.6-fold, respectively, for a deasphalted Canadian bitumen heavy distillate (523–593 °C) when using the (–) ESI 21 T FTICR MS instead of using a (–) ESI 9.4 T FTICR MS to analyze the same sample (Figure 1). In addition to these improvements, the authors also

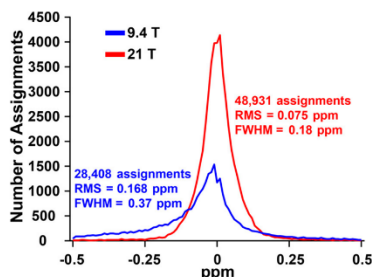


**Figure 1.** Mass error distributions for a deasphalted Canadian bitumen heavy distillate analyzed using (–) ESI and either a 21 T or a 9.4 T FTICR MS. The use of the 21 T FTICR MS improved the mass measurement accuracy and the resolution as demonstrated by the root-mean-square (RMS) and the full width at half-maximum (fwhm) values, respectively. Reproduced from Smith, D. F.; Podgorski, D. C.; Rodgers, R. P.; Blakney, G. T.; Hendrickson, C. L. *Anal. Chem.* **2018**, *90* (3), 2041–2047 (ref 11). Copyright 2018 American Chemical Society.

reported that the 21 T FTICR MS enabled the resolution of unique heteroatoms classes, such as compounds containing one or several oxygen atoms ( $O_x$ ), one or several sulfur as well as oxygen atoms ( $S_xO_x$ ), and one nitrogen atom as well as one or several oxygen atoms ( $NO_x$ ) classes that were previously unresolved.

Cho et al. have evaluated the utility of a 7 T FTICR MS equipped with quadrupolar detection for the analysis of two crude oils obtained from Saudi Arabia and Iraq by using positive ion mode laser desorption/ionization ((+) LDI) and (+) APPI.<sup>12</sup> The use of four electrodes in the quadrupolar detection, instead of two as in the conventional FTICR MS detection, resulted in signals with twice the frequency of the cyclotron resonance frequency; this doubles the resolving-power for a given magnetic field strength. A mass resolving-power of 1.5 million at  $m/z$  400 with a 4 s transient signal was reported. This mass resolving-power is significantly greater than what has been reported for any 7 T FTICR MS using the conventional detection. For instance, Rüger reported<sup>13,14</sup> a resolving power of 280 000 and 300 000 while Benigni reported<sup>15</sup> 424 000 for the analysis of different petroleum samples. Though quadrupolar detection clearly improves the mass resolving-power, Smith et al.<sup>11</sup> pointed out that multiple-frequency detection generally leads to a decrease in sensitivity and induction of signals at unwanted frequencies.

Krajewski et al. reported on mass spectral segmentation when using (+) APPI 9.4 T FTICR MS to characterize a volcanic asphalt petroleum sample.<sup>16</sup> In this approach, the mass spectra were acquired in 20  $m/z$  wide segments from  $m/z$

200 to  $m/z$  1200 that were added together into a single composite mass spectrum. The mass spectral segmentation improved the signal-to-noise ratio (S/N) compared to the measurement of a conventional broad-band mass spectrum. This approach resulted in the identification of the chemical formulas for over 126 000 compounds compared to 59 015 when using traditional measurements. Despite the improved coverage of the sample and improved S/N, the authors emphasized that mass spectral segmentation is time-consuming and it may be only suited for targeted analysis. In another report, Gavard et al. introduced a batch processing algorithm, Themis, to advance the analysis of replicate complex data sets, such as those measured for petroleum samples.<sup>17</sup> An additional benefit of the algorithm, although not the primary focus, was improved differentiation of genuine signals from noise on the basis of consistency of peak positions across replicates, rather than use of a signal-to-noise threshold alone. A light sour crude oil sample and a South American crude oil sample were analyzed using ( $\pm$ ) ESI 12 T FT-ICR MS. Third party software was used for initial peak picking from the raw data, operated with a low signal-to-noise threshold to ensure capture of low intensity signals. The exported peak list for one of these samples contained approximately 16 400 entries (all peaks, including noise). After processing using Themis, 2260 of those peaks were identified as being consistent among the six replicates, and therefore the candidates for data analysis. The authors argued that the advantage of working with replicates is two-fold. Firstly, one can use lower signal-to-noise ratios than when analyzing a single data set, which can help increase the inclusion of low relative abundance peaks. Secondly, by discarding peaks that are not consistent across replicates (reducing data size and computing overheads), one can reduce false positive assignments.

FTICR MS has also been used to evaluate changes in different crude oils. For instance, Martins et al. used (–) ESI 7.2 T FTICR MS to assess the biodegradation level of 30 Brazilian crude oil samples by profiling the changes in relative abundances of compounds in the heteroatom classes, in particular, oxygen-containing compounds.<sup>18</sup> The relative abundance of compounds containing two oxygen atoms ( $O_2$  compounds) were found to increase upon biodegradation. This observation is in agreement with previous findings by the same research group that the relative abundances of compounds containing two, three, or four oxygen atoms increase upon biodegradation of 16 Colombian crude oils.<sup>19</sup> This observation was rationalized by increasing concentration of naphthenic acids upon biodegradation. In another report, Handle et al. used (–) ESI 12 T FTICR MS to compare the chemical compositions of an unaged bitumen sample and its SARA fractions (i.e., Saturated hydrocarbons, Aromatic compounds, Resins, and Asphaltenes) to those of a bitumen sample and its SARA fractions that had been aged in a high-pressure, high-temperature oxidation (aging) vessel.<sup>20</sup> While the aged and unaged bitumen were found to contain similar resins, the aged bitumen sample contained a smaller amount of condensed aromatic hydrocarbons that had been reduced to alicyclic or linear aliphatic hydrocarbons. Furthermore, asphaltenes were found to contain more oxygenated species in aged bitumen than in unaged bitumen. Rüger et al. coupled thermal desorption and pyrolysis with positive ion mode atmospheric pressure chemical ionization ((+) APCI) 7 T FTICR MS to compare the chemical formulas of compounds in five different heavy crude oils and their asphaltene



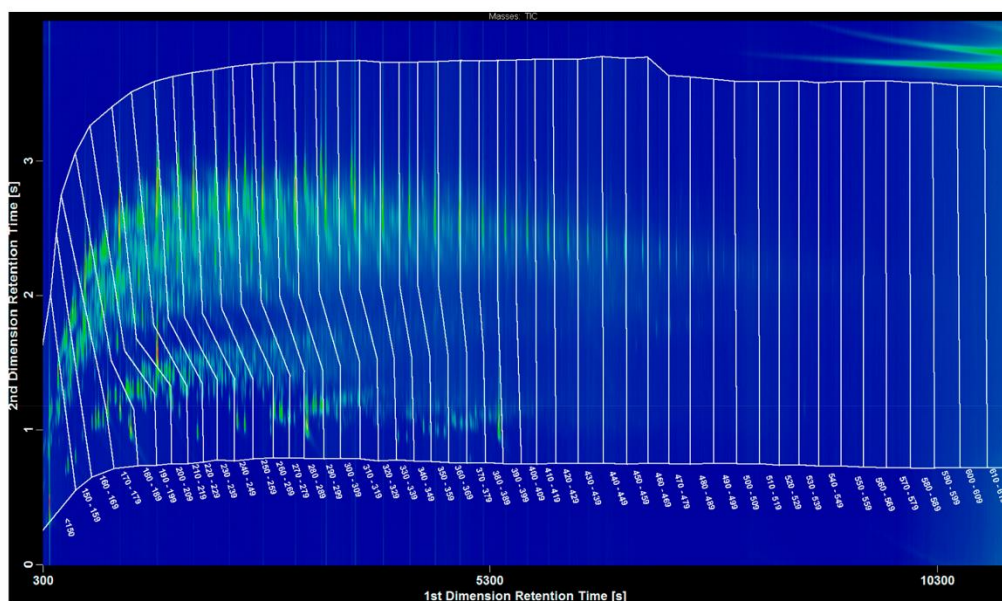


**Figure 2.** Exemplary GC  $\times$  GC/(+) EI TOF MS chromatogram measured for a crude oil distillation fraction with a boiling temperature greater than 150 °C. The temperature template is also shown. Classification areas were drawn so that peaks due to column bleed (above and below the white horizontal lines) were excluded. Reproduced from Jennerwein, M. K.; Eschner, M. S.; Wilharm, T.; Zimmermann, R.; Gröger, T. M. *Energy Fuels* **2017**, *31* (11), 11651–11659 (ref 32). Copyright 2017 American Chemical Society.

fractions.<sup>21</sup> The data indicated that all heavy crude oils and asphaltenes contained dominant CH-, CHS-, and CHN-classes of compounds. Further, the relative abundances of the CHS-class of compounds were found to be positively correlated with the total sulfur content in the tested crude oils.

**Orbitrap Mass Spectrometry.** The capabilities of an Orbitrap mass spectrometer in structural characterization of aromatic fractions of crude oil and shale oil were explored by Cho et al., who compared data obtained using (+) APPI Q Exactive Orbitrap MS, which has a quadrupole in front of an Orbitrap, and (+) APPI 7 T FTICR MS.<sup>22</sup> Plotting the measured ring and double bond equivalence (RDBE) values as a function of the number of carbons for the ionized compounds indicated that (+) APPI FTICR MS detected more ions with greater RDBE values and larger number of carbons than (+) APPI Q Exactive Orbitrap MS. Despite this difference, the distributions of CH, CHN<sub>1</sub>, CHN<sub>1</sub>O, CHO<sub>1</sub>, and CHS<sub>1</sub> classes observed in the (+) APPI Q Exactive Orbitrap mass spectra and FTICR mass spectra were essentially the same. However, the number of peaks that could be assigned based on (+) APPI FTICR MS data (14 000 assigned peaks) was almost twice that of obtained using (+) APPI Orbitrap MS (7 900 assigned peaks) due to the greater resolution and dynamic range of the FTICR MS instrument. Schmidt et al. compared the performance of a modified Orbitrap Elite, which combines a linear quadrupole ion trap (LQIT) to an Orbitrap MS, to that of a 7.2 T FTICR MS for the analysis of Brazilian crude oil.<sup>23</sup> Similar to the results obtained by Cho et al.,<sup>22</sup> the ion distribution was found to have shifted to higher  $m/z$  values for ( $\pm$ ) ESI FTICR MS compared

to the modified ( $\pm$ ) ESI Orbitrap Elite while the class distributions (CHN, CHN<sub>2</sub>, CHNO, CHNS, and CHNOS) were similar for both instruments.

Kostyukovich et al. developed a microprobe coupled to a Q Exactive Orbitrap MS, modified by adding an ion funnel in the front, for analysis of light Siberian crude oil by using thermal desorption at different pressures.<sup>24</sup> The microprobe contained a heating element onto which a crude oil droplet was placed and evaporated. Crude oil vapors were ionized by using a vacuum ultraviolet (VUV) lamp that was operated at different pressures. When the VUV lamp was operated at atmospheric pressure, the major ions detected were protonated nitrogen-containing aromatic compounds. However, when the VUV lamp was operated at lower pressures (5 and 10 Torr), the molecular ions of aromatic hydrocarbons and sulfur-containing aromatic compounds were observed to be dominant compared to the protonated nitrogen-containing aromatic compounds. The appearance of the molecular ions for aromatic hydrocarbons and sulfur-containing aromatic compounds, and the decrease in the relative abundance of the protonated nitrogen-containing aromatic compounds, was rationalized by less H<sup>+</sup> transfer from H<sub>3</sub>O<sup>+</sup> at lower pressures. This method was demonstrated to enable detection of aromatic, nitrogen-containing aromatic, and sulfur-containing aromatic ions without any fractionation.

**2D Gas Chromatography/Time-of-Flight Mass Spectrometry.** The introduction of 2D gas chromatography (GC  $\times$  GC) in 1991 by Zaiyou Liu and John Phillips has enabled significant advances in the chemical characterization of petroleum due to the substantially greater resolution compared

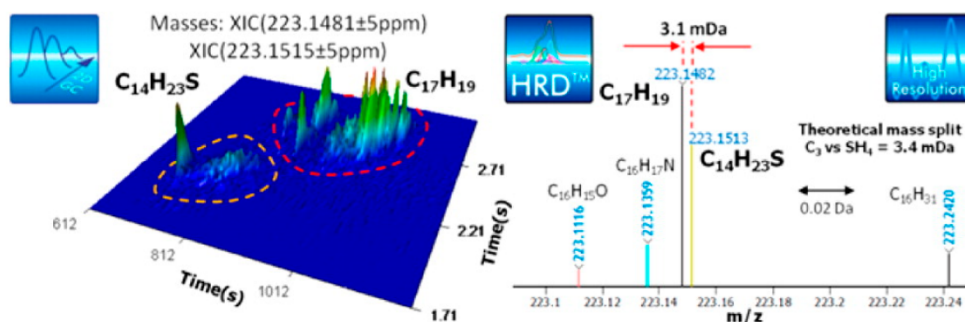


**Figure 3.** (Left) A GC  $\times$  GC/(+) EI TOF MS chromatogram that shows the separation of the isobaric compound classes  $C_{14}H_{23}S$  and  $C_{17}H_{19}$ . (Right) The integrated mass spectrum showing the differentiation of two isobaric ions within a selected  $m/z$  range of 223.10–223.24. Reproduced from Byer, J. D.; Siek, K.; Jobst, K. *Anal. Chem.* **2016**, *88* (12), 6101–6104 (ref 34). Copyright 2016 American Chemical Society.

to conventional GC. The greater resolution has led to a greater sensitivity and an increase in the number of compounds that can be detected.<sup>25</sup> GC  $\times$  GC is often coupled with TOF MS instruments (with positive mode electron ionization ((+) EI)) due to their high scan speeds (100–500 Hz) and medium resolution. Arranging the two columns in the reversed phase manner, i.e., a polar column followed by a nonpolar column, has been demonstrated to improve the separation of saturated and aromatic hydrocarbons in middle distillates by Vendevure et al.<sup>26</sup> and more recently by van der Westhuizen et al.,<sup>27</sup> Prak et al.,<sup>28</sup> and Vozka et al.<sup>29</sup> To achieve even greater separation, Alexandrino et al. developed a time-variable method that changes the cold and hot jet pulses of the GC  $\times$  GC modulator to optimize the separation of the most abundant classes of hydrocarbons in the maltene fraction of crude oil.<sup>30</sup> The times for the hot and cold jets were first optimized for compounds containing 12–22 carbon atoms, followed by optimization for compounds containing 23–31 carbon atoms. The optimized times were then applied to the full range of hydrocarbons (12–31 carbons) to analyze the maltene fraction. This optimization procedure can be applied also to other complex mixtures to enhance the separation capabilities of GC  $\times$  GC.

Potgieter et al. utilized high temperature (>300 °C) GC  $\times$  GC/(+) EI TOF MS to determine the best column configuration for separating compounds in an oxidized heavy saturated hydrocarbon fraction of crude oil.<sup>31</sup> The authors tested seven different column configurations, four reversed phase and three normal phase setups, to determine the column configuration that yielded the best separation. As column temperatures up to 370 °C were used, the most polar columns studied were not highly polar but of midpolarity since highly polar columns have upper temperature limits lower than 340 °C. A reversed phase column setup, which consisted of a midpolarity column with 50% diphenyl–50% dimethyl polysiloxane, 30 m in length, and a 0.25 mm inner diameter followed by a nonpolar column with 100% dimethyl polysiloxane, 1 m in length, and a 0.1 mm inner diameter, was found to achieve the best separation for the oxygenated saturated hydrocarbon fraction. Jennerwein et al. also utilized high temperature GC  $\times$  GC/(+) EI TOF MS to determine the composition of a heavy crude oil and to generate a template that can be used to simulate its distillation.<sup>32</sup> The purpose of a simulated distillation is to predict the amount of petroleum products recovered at different distillation temperatures.<sup>33</sup> In

Figure 2, the GC  $\times$  GC/(+) EI TOF MS chromatogram is sectioned into 10 °C increments from 150 °C to 620 °C. The lines drawn on the GC  $\times$  GC/(+) EI TOF MS chromatogram for each section were determined based on the boiling points of the compounds previously identified based on the NIST library. The compounds in each section were quantitated by generating a calibration plot based on the response factors of linear saturated hydrocarbon model compounds containing 10–60 carbons. The simulated distillation approach based on high temperature GC  $\times$  GC/(+) EI TOF MS was compared to the previously established American Society for Testing Materials (ASTM) D7169 method, which utilizes GC with a flame ionization detector (FID). The simulated distillation results were similar up to 450 °C for both methods. However, GC  $\times$  GC/(+) EI TOF MS can also be used to identify compounds in the heavy crude oil, which is an advantage over the ASTM D7169 method. The one disadvantage of the high temperature GC  $\times$  GC/(+) EI TOF MS simulated distillation approach is that it is not reliable for boiling temperatures above 450 °C.

Byer et al. demonstrated the capabilities of GC  $\times$  GC/(+) EI TOF MS in separation of isomers of  $C_{17}H_{19}$  ( $m/z$  223.1482) and isomers of  $C_{14}H_{23}S$  ( $m/z$  223.1513), in addition to distinguishing these two isobaric compound classes from one another in a Venezuelan crude oil sample (Figure 3).<sup>34</sup> To detect isobaric  $C_{17}H_{19}$  and  $C_{14}H_{23}S$  ions without separation, the MS would have to have at least 66 000 resolving power. However, the use of GC  $\times$  GC to separate these isobaric compounds prior to (+) EI TOF MS analysis at a resolution of  $\sim 25\,000$  enabled their detection.

**Ion Mobility Mass Spectrometry.** Ion mobility (IM), a gas-phase separation technique often used after ionization in mass spectrometry (ion mobility mass spectrometry or IM MS), separates ions based on mobility differences in an electric field. The different types of ion mobility instruments have been recently reviewed.<sup>35–38</sup> Fernandez-Lima et al.<sup>39</sup> have utilized (+) APPI 9.4 T FTICR MS and (+) LDI drift tube IM TOF MS for the characterization of light, medium, and heavy crude oils. While the FTICR MS instrument provided information about the elemental compositions and heteroatom class distributions for the aromatic compounds in the crude oils, the IM MS instrument provided information on the structural diversity of these aromatic compounds.

Lalli et al. demonstrated the ability of (–) ESI traveling-wave ion mobility (TWIM) coupled with TOF MS ((–) ESI TWIM TOF MS) and tandem mass spectrometry (MS/MS) based on collision-activated dissociation (CAD) in the trap cell located after the TWIM to separate and identify ionized isomeric compounds in the  $O_3S_1$  class derived from interfacial petroleum material isolated from Athabasca bitumen and a heavy crude oil.<sup>40</sup> CAD was especially useful in the identification of functional groups, such as carboxylic acid and hydroxyl groups, based on diagnostic neutral fragments such as  $CO_2$  and  $H_2O$ , respectively. The same research group separated and elucidated the structures of isomeric naphthenic acids derived from Athabasca bitumen by using solid-phase extraction followed by (–) ESI TWIM TOF MS.<sup>41</sup> Isomeric steranoic acids containing 28 to 34 carbon atoms and RDBE values equal to 5 were identified. (–) ESI 9.4 T FTICR mass spectral results of the same bitumen sample validated the molecular formula assignments obtained using the (–) ESI TWIM TOF MS. In another study, Santos et al. demonstrated the ability of (–) ESI followed by a uniform-field drift tube IM coupled to Q TOF MS to separate compounds in petroleum samples that are isomers of crude oil contaminants, such as demulsifiers and additives.<sup>42</sup> Analysis of the same contaminated crude oil sample by using (±) ESI 7 T FTICR MS was unsatisfactory due to suppression of ionization of the desired compounds by the demulsifiers and additives.

Due to the relatively low resolving power of IM instruments, multiple isomeric ions may coelute.<sup>43,44</sup> To detect the presence of such isomeric ions, Farenc et al. utilized CAD MS/MS experiments in (+) ESI TWIM Q TOF MS.<sup>45</sup> The CAD mass spectra of isolated ions of the same  $m/z$  value were measured at different drift times under one ion mobility peak. While each CAD mass spectrum showed the same types of fragment ions, their relative abundances varied, suggesting the presence of isomeric fragmenting ions.

Compared to IM TOF MS with moderate resolution, IM coupled with high-resolution MS will provide more accurate elemental composition assignments for ions separated in the IM device. Ibrahim et al. coupled a drift tube-based IM to an Orbitrap MS for the analysis of a heavy fuel oil, a hydrotreated gas oil, ionized by using (+) ESI.<sup>46</sup> To overcome the time scale disparities between the IM device and the Orbitrap MS and to maximize the efficiency of ion transfer into the Orbitrap, a dual grid gating approach was utilized to introduce ions into the drift tube IM and to allow ions of a specific drift time to transfer into the Orbitrap. The results obtained using the (+) ESI drift tube IM Orbitrap MS were compared to results obtained using (+) ESI Orbitrap MS for the same heavy fuel oil. While  $N_1$ ,  $N_1S_1$ ,  $O_1S_1$ , and  $S_1$  classes of compounds were separated and detected using the drift tube IM-Orbitrap MS, this was not the case for the Orbitrap MS. For example, two isobaric ions with the elemental compositions  $C_{22}H_{26}N$  ( $m/z$  304.20584) and  $C_{19}H_{30}NS$  ( $m/z$  304.20917) were resolved in the IM but only poorly resolved by the Orbitrap MS.

## ■ IONIZATION METHODS

An especially challenging aspect in successfully using mass spectrometry for petroleum characterization is the selection of an appropriate ionization method. This is demonstrated, for example, by a study by Panda et al., who showed that the mass spectra measured for a sample of Iranian vacuum gas oil by using five different soft ionization methods were entirely different.<sup>47</sup> Similarly, when Gasper et al. evaluated the impact

of using different ionization methods for the characterization of asphaltenes,<sup>48</sup> they found that the end result of the analysis depended on the ionization method selected. No single ionization method is capable of unbiased ionization of the different compound classes present in many petroleum samples.<sup>49</sup> To overcome this challenge, especially complex petroleum samples, such as crude oil, are preferably characterized after separation into different compound classes. This enables the selection of a soft ionization method specifically suited for each individual compound class. The most desirable ionization methods for mixture analysis would induce no fragmentation of ionized analytes and produce only one ion type, containing the intact analyte molecule (for MW determination), for each analyte (generation of multiple ion types or fragment ions for a single analyte complicates the mass spectrum).

The greatest challenge in ionization of compounds in petroleum is presented by large saturated hydrocarbons. They are not volatile and lack easily ionizable functional groups, posing a great challenge for ionization by using methods such as ESI and matrix-assisted laser desorption/ionization (MALDI). These methods are limited to ionization via deprotonation, protonation, and cation attachment reactions and therefore cannot be used to efficiently ionize saturated hydrocarbons. Alternative ionization methods, such as field desorption (FD),<sup>50</sup> field ionization (FI),<sup>51</sup> and APCI,<sup>52,53</sup> have been proposed for ionization of large saturated hydrocarbons. Although several ionization methods have been reported in the literature for the characterization of petroleum, one should always critically evaluate and, if possible, tailor the ionization conditions to be most suitable for the petroleum sample being analyzed. Usually, this can be performed by using model systems. For example, Yerabolu et al. optimized ionization methods for several crude oil fractions by using model compounds representative of each fraction.<sup>54</sup>

Recent advances in the mass spectrometric ionization methods achieved during the last 3 years for various compound classes in petroleum are briefly summarized in Table 1. Ionization of aromatic, polyaromatic, and polar hydrocarbons has been substantially improved by introduction of different ambient ionization methods. However, ionization of some analyte classes, such as saturated hydrocarbons, remains a challenge and needs further development.

## ■ FRACTIONATION

Due to the complexity of petroleum samples, such as crude oil, it has become evident that their fractionation prior to mass spectrometric analysis facilitates their chemical characterization.<sup>70</sup> Bissada et al. reported that automated multidimensional-high-performance liquid chromatography (AMD-HPLC) can be used to separate crude oil into SARA-like fractions with high efficiency and minimum cross-contamination.<sup>71</sup> The AMD-HPLC instrument was equipped with two columns, a cyano column that was able to retain asphaltenes and resins and a silica column that retained moderately polar organic compounds, such as aromatic compounds. Mixtures of methanol, hexane, and chloroform were used as the eluents. Evaporative light scattering detection (ELSD) enabled quantitation of the fractions. Repeated quantitation demonstrated that the AMD-HPLC/ELSD analysis is highly reproducible. The identities of volatile compounds in the fractions were explored by using GC/(+) EI Q MS. However, these results may not be reliable because their GC method

Table 1. Summary of Ionization Methods Recently Utilized on Petroleum Samples

anlyte class	instrument (mode) ionization method/nebulizer gas/reagent	analytes	details and strengths	weaknesses	ref
Saturated hydrocarbons	Braker 9.4 T Q-FTICR MS hybrid ion trap MS (+) APCI/N <sub>2</sub> /isooctane (other ionization reagents evaluated were <i>n</i> -pentane, <i>n</i> -hexane, <i>n</i> -heptane and cyclohexane)	Saturated linear, branched and cyclic hydrocarbon model compounds, base oils, other petroleum samples	Isooctane as a reagent resulted in greater ionization efficiencies than other ionization reagents evaluated. [M-H] <sup>+</sup> ions were generated without fragmentation.	Saturated hydrocarbon and petroleum samples precipitated from isooctane at higher concentrations. Authors used a mixture of isooctane and CS <sub>2</sub> solvents to address this issue.	55
	Thermo LTQ XL linear quadrupole ion trap MS (+) APCI/O <sub>2</sub> /hexane	Saturated linear, branched and cyclic hydrocarbon model compounds (1 and 4 rings), lubricant base oils	[M-H] <sup>+</sup> ions generated with minimal to no fragmentation; developed as an alternative to field ionization (FI); more robust and easier to maintain than FI; can be automated. This method is well suited for the analysis of low-viscosity base oils unlike FI.	Sometimes fragmentation took place.	56
	Homemade reflectron TOF MS	Linear saturated hydrocarbon model compounds (C <sub>3</sub> –C <sub>10</sub> )	Atomic Au <sup>+</sup> ions generated by laser ablation in the ion source were transported by a carrier gas via pulsed valves into the fast flow reactor region, where they caused ionization of linear saturated hydrocarbons by hydride abstraction. The ionized hydrocarbons were analyzed by the reflectron TOF MS.	Fragmentation was observed for saturated hydrocarbons with more than 10 carbon atoms. Sophisticated instrumentation required.	57
	(+) Laser ablation/supersonic expansion ion source coupled with a fast flow reactor			No results on branched or cyclic saturated hydrocarbons were provided. Only hydrocarbons that can be introduced into the fast flow reactor can be analyzed. Separation of the analytes by chromatography not possible prior to MS analysis.	58
Sulfur containing compounds	Waters Synapt G2S Ion Mobility TOF MS (+) Atmospheric pressure solids analysis probe (ASAP)/N <sub>2</sub> GC/(+) APCI/N <sub>2</sub> (APGC) In APGC, GC eluents are ionized at the corona discharge tip before entering the mass spectrometer.	Linear, branched and cyclic saturated hydrocarbon model compounds, saturated hydrocarbon fraction of petroleum vacuum residue	Both ASAP and APGC methods ionize linear and branched saturated hydrocarbons by addition of a N <sup>+</sup> ion from an N <sub>3</sub> <sup>+</sup> reagent ion. The mechanism was hypothesized to be similar to field-assisted nitrogen fixation: C–C activation and nitrogen fixation to form an iminium ion.	More than one ion type per analyte were generated.	59
	Braker Apex ultra FTICR MS (+) Direct analysis in real time (DART)/N <sub>2</sub> /methanol and toluene mixture, ammonium hydroxide dopant	Aliphatic and aromatic sulfide model compounds, crude oils with high sulfur content	Sulfides (S) were selectively converted to sulfoxide (SO) cations ([SO + H] <sup>+</sup> ).	Thiophenic compounds could not be detected. Sulfoxides that originally existed in the crude oil could not be differentiated from the sulfoxides generated from sulfides during ionization.	60
	Thermo Q-Exactive orbitrap high resolution MS (-) Paper spray chemical ionization (PSCI)/toluene and toluene and methanol (50:50 v/v), 1% formic acid dopant	Sulfur containing aromatic model compounds, soil contaminated with oil	PSCI, like APCI, ionized nonpolar sulfur-containing aromatic compounds better than paper spray ionization (PSI) or ESI. PSCI required 10 times less sample than APCI/APCI.	PSCI suffers from instability of spray.	61
	Thermo linear quadrupole ion trap (LQIT) MS (+) APCI/N <sub>2</sub> /CS <sub>2</sub>	17 aromatic sulfur containing model compounds	The use of CS <sub>2</sub> reagent resulted in the generation of stable molecular ions for most of the model compounds with no fragmentation.	Major fragmentation occurred for three sulfides.	61



Table 1. continued

analyte class	instrument (mode) ionization method/nebulizer gas/reagent	analytes	details and strengths	weaknesses	ref
Naphthenic acids	Braker Apex-ultra FTICR MS	Equimolar mixture of decanoic acid and carbazole, vacuum distillation gas oil (VGO) fractions, crude oils with different total acid number values	(-) DART was found to be more sensitive to carboxylic acids than neutral, nitrogen-containing compounds. Results obtained for crude oils demonstrated that (-) DART can detect more heteroatom classes with better sensitivity than (-) ESI.	Only one model compound was studied.	59
	(+) Direct analysis in real time (DART)/N <sub>2</sub> /methanol and toluene mixture, ammonium hydroxide dopant				
	(-) ESI/N <sub>2</sub> /methanol				
Naphthalene	Braker Ultrafretreme TOF-TOF MS	Naphthenic acid standard mixture, naphthenic acids extracted from a heavy crude oil	[M - H] <sup>-</sup> ions were generated. Provided molecular weight distributions identical to (-) ESI.	Extensive sample preparation required.	62
	(-) UV-MALDI/acetone/water (1:1), 9-aminocadine (9-AA) and 1,8 bis(dimethylamino) naphthalene (DMAN) as matrices		Highly basic compounds such as DMAN, in the matrix act as a proton sponge, reducing the formation of clusters and aggregates, thereby resulting in a cleaner mass spectrum.		
Aromatic and polycyclic aromatic hydrocarbons	Waters Synapt G2S Ion Mobility TOF MS	Chrysene, coronene, alkylbenzenes	Aromatic compounds primarily ionized by electron abstraction. In APGC, the GC eluents are ionized at the corona discharge tip before entering the mass spectrometer.	Generated more than one ion type per analyte ([M <sup>+</sup> ], [M + N] <sup>+</sup> and [M + H] <sup>+</sup> ).	58
	(+) Atmospheric pressure solids analysis probe (ASAP)/N <sub>2</sub> GC/(+) APPI/N <sub>2</sub> (APGC)				
	Waters Synapt G2S IM TOF MS	Aromatic model compounds, crude oil	(+) ASAP efficiently ionized large aromatic analytes (MW > 1000 Da) along with small aromatic molecules, to produce [M - H] <sup>+</sup> and (M <sup>+</sup> ) ions unlike ESI, APPI, DART, or DESI.	Generated more than one ion type per analyte ([M <sup>+</sup> ], [M + H] <sup>+</sup> ).	63
Thermo Orbitrap Elite MS equipped with FAIMS	(+) Atmospheric pressure solids analysis probe (ASAP)/N <sub>2</sub>	Aromatic model compounds, heavy crude oil	FAIMS unit was modified to enable insertion of APPI and APPI ionization sources. Ionization and online separation of ionized analytes.	Unlike for APPI, ionization efficiency of APPI was found to decrease with the decrease in the number of aromatic rings in the analytes.	64
	(+) APPI/N <sub>2</sub> /toluene (one photon VUV ionization)				
	(+) APPI/N <sub>2</sub> /toluene (two photon ionization using laser radiation of 248 nm)				
Braker Apex-ultra FTICR MS	(+) ESI/toluene and methanol mixture (1:3 v/v), ammonium formate dopant	Aromatic and heteroaromatic hydrocarbons extracted from diesel obtained by fluid catalytic cracking (FCC), FCC slurry oil	Aromatic and heteroaromatic hydrocarbons were ionized to generate [M + H] <sup>+</sup> ions. (+) ESI is complementary method to (+) APPI.	Relative ionization efficiencies of aromatic and heteroaromatic hydrocarbons in the presence of polar nonaromatic compounds was not evaluated.	65
	(+) APPI/toluene				
Thermo LTQ XL ion trap MS	(±) Laser-assisted paper spray ionization (LAPSI)/N <sub>2</sub> /methanol and toluene mixture	Naphthalene, pyrene, benzanthracene	N <sub>2</sub> , O <sub>2</sub> , N <sub>2</sub> O, and O <sub>2</sub> class compounds were ionized more efficiently than via (+) APPI. Molecular ions were generated. Better sensitivity than ESI and conventional paper spray. Capable of detecting analytes at 1 nM concentrations.	Different classes of aromatic model compounds, such as aromatic compounds containing alkyl chains or heteroatoms, have to be studied to verify the capabilities of the ionization method to ionize different types of aromatic compounds.	66
	GC/Thermo TSQ Quantum Discovery Max MS	Aromatic model compounds with up to 3–6 aromatic rings	Greater sensitivity than HPLC/(+) ESI MS or HPLC/(+) APPI MS using similar solvents on the same instrument.	Sensitivity was found to depend on the size of the analyte.	67
	(+) ESI/N <sub>2</sub> /acetone/water and/or methanol			Not applicable for large analytes (MW > 300 Da).	
Home-built linear time-of-flight (TOF) MS		Aromatic model compounds, including polycyclic aromatic hydrocarbons (PAHs),	The first IR laser pulse caused thermal desorption of the analytes, the second laser pulse ionized the desorbed analytes via single photon ionization.	The mass resolution and mass accuracy of the home-built TOF-MS were low.	68

Table 1. continued

analyzer class	instrument (mode) ionization method/nebulizer gas/reagent	analytes	details and strengths	weaknesses	ref
	(+) Laser desorption laser ionization (L-MS) (single photon ionization)	alkylated PAHs, heteroatom-containing PAHs, porphyrins, asphaltene	Ionization of different asphaltene occurred with similar ionization efficiencies with minimal formation of multiply charged ions, (<10%), fragment ions (<10%), or aggregates (0%), thereby providing semiquantitative information.	The outcome of the mass spectral data can be influenced by variations in laser power and sample concentration.	
Polar compounds	Thermo Q Exactive Orbitrap MS (+) In-source APPI hydrogen/deuteronium exchange with D <sub>2</sub> O	31 Nitrogen, oxygen, or sulfur-containing model compounds, polar fraction of a crude oil	Polar analytes (containing at least one exchangeable H atom) could be easily detected in complex mixtures.	Generated more than one ion type per analyte. Limited structural information.	69

could not separate the compounds in the polar and asphaltene fractions and the MS method had poor resolution as well as poor mass accuracy. The same research group reported separation of a saturated hydrocarbon fraction of crude oil into linear, cyclic, and branched saturated hydrocarbons by using the AMD-HPLC/ELSD device equipped with two columns, a silicon S<sub>115</sub> column and another silicon column filled with a mixture of 50% S<sub>115</sub> and 50% S<sub>130</sub>, operated at different temperatures.<sup>72</sup> Combinations of isooctane and *n*-octane solvents were used as eluents. The identities of the compounds in each fraction were verified by using GC/(+) EI Q-MS. However, no model compounds were used to verify the reliability of this analysis.

A separation method based on ion exchange and normal phase chromatography has been developed by Robson et al. to fractionate Alaska north slope crude oil.<sup>73</sup> The crude oil was first introduced onto a strong cation-exchange (SCX) solid phase extraction (SPE) cartridge. The compound classes retained in the SCX SPE cartridge included asphaltene, sulfoxides, and quinoline, which were released separately from the cartridge by using different solvents. The initially eluted fraction was then introduced onto a strong anion exchange (SAX) SPE cartridge. The compound classes retained by the SAX SPE cartridge included sulfones and carbazoles, which were released separately by using different solvents. The initially eluted fraction was introduced onto a silica column and further separated into five compound classes by using different solvents in the following order: saturated hydrocarbons (hexane-eluted fraction), aromatic compounds (20% dichloromethane and 80% hexane-eluted fraction), fluorenes (50% dichloromethane and 50% hexane-eluted fraction), xanthenes (dichloromethane-eluted fraction), and thiophenes (tetrahydrofuran-eluted fraction). The feasibility of this method was tested using a mixture of 19 model compounds representing 12 different compound classes. The individual compound classes were characterized by using GC × GC/(+) EI TOF MS and ultra HPLC (uHPLC) coupled to a Q Exactive Orbitrap MS equipped with a heated (+) ESI ((+) HESI) source.

A newly developed HPLC-3 system containing two columns, a dinitroanilinopropyl (DNAP) column and an SCX column that was functionalized with silver cations, was utilized by Putnam et al. to separate crude oil into specific compound classes, including saturated hydrocarbons, six classes corresponding to compounds containing one, two, three, four, or five or more aromatic rings, polar compounds, and sulfides.<sup>74</sup> The HPLC-3 design (Figure 4) utilized both a photodiode array (PDA) detector and an ELSD to determine when saturated hydrocarbons, compounds with different numbers of aromatic rings, polar compounds, and sulfides eluted. A model compound study demonstrated the success of the separation.

A combination of an extraction method and a column chromatography method (extrography) has been reported by Giraldo-Dávila for fractionation of crude oil samples. Extrography was combined with (+) APPI 15 T FTICR MS to characterize compounds in a Colombian heavy crude oil.<sup>75</sup> The fractionation method involved adsorbing the crude oil on neutral alumina followed by Soxhlet extraction by using acetonitrile, methanol, *n*-heptane, and toluene eluents, resulting in fractions enriched in metal complexes, polar compounds, maltenes, and asphaltene, respectively. Polar compounds were fractionated further by using silica gel column chromatography and different combinations of *n*-

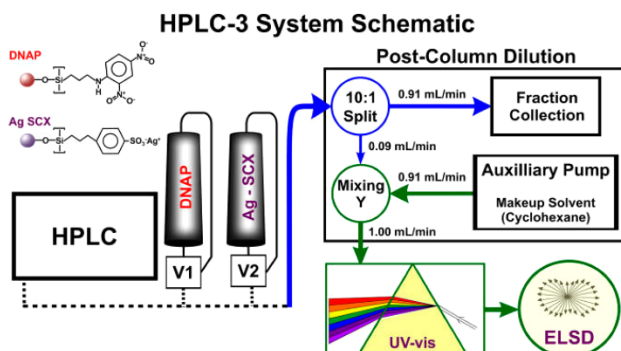


**Figure 4.** Schematic representation of the HPLC-3 system configuration and stationary phase structures. Reproduced from Putman, J. C.; Rowland, S. M.; Podgorski, D. C.; Robbins, W. K.; Rodgers, R. P. *Energy Fuels* 2017, 31 (11), 12064–12071 (ref 74). Copyright 2017 American Chemical Society.

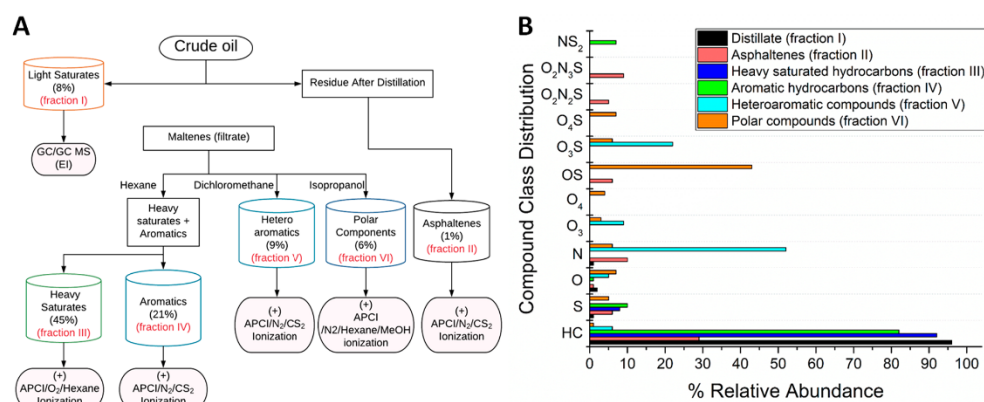


**Figure 5.** (A) DPF MS method developed for the separation of crude oil into six distinct fractions and the ionization methods and mass spectrometric techniques used for the analysis of each fraction. (B) The compound class distributions and their percentage relative abundances in all fractions. Reproduced from *Fuel*, volume 234, Yerabolu, R.; Kotha, R. R.; Niyonsaba, E.; Dong, X.; Manheim, J. M.; Kong, J.; Riedeman, J. S.; Romanczyk, M.; Johnston, C. T.; Kilaz, G.; Kenttämä, H.I. *Molecular Profiling of Crude Oil by Using Distillation Precipitation Fractionation Mass Spectrometry (DPF-MS)*, pp 492–501 (ref 54). Copyright 2018, with permission from Elsevier.

hexane, dichloromethane, and trichloromethane solvents to obtain six subfractions. A total of 11 800 compounds were detected in all fractions compared to 3 700 detected in the unfractionated crude oil, highlighting the importance of fractionation of crude oil prior to mass spectrometric analysis. However, it should be noted here that (+) APPI cannot efficiently ionize all crude oil components, such as saturated hydrocarbons.

More recently, Yerabolu et al. developed a method for molecular profiling of crude oil that was based on fractionating crude oil into six distinct fractions containing different types of compounds and then optimizing the ionization method and mass spectrometry technique for the analysis of each fraction (Figure 5).<sup>49</sup> The method, called Distillation Precipitation Fractionation Mass Spectrometry (DPF MS), involved initial distillation of volatile compounds followed by precipitation of asphaltenes. The remaining maltene fraction was further separated into saturated hydrocarbons, alkyl aromatic com-

pounds, heteroaromatic compounds, and polar compounds by using auto column flash chromatography and SPE. The volatile compounds were analyzed by using GC × GC/(+) EI TOF MS. All the remaining fractions were analyzed using (+) APCI with different APCI reagents coupled with a LQIT Orbitrap MS. The nonvolatile saturated hydrocarbons were ionized by using hexane as the APCI reagent and oxygen as the nebulizer gas. The polar fraction was analyzed by using a mixture of 25% hexane and 75% methanol as the APCI solvents and nitrogen as the nebulizer gas, while alkyl aromatic compounds and heteroaromatic compounds were analyzed by using CS<sub>2</sub> as the APCI reagent and nitrogen as the nebulizer gas. This approach provided the gravimetric percentage of each fraction in the crude oil. Further, the compound class distributions were obtained for each fraction and for the original crude oil. Also, an accurate average molecular weight of the crude oil was obtained by consolidating the average molecular weight and the mass of each fraction.

## ■ APPLICATIONS

**Whole Crude Oil.** Analysis of whole crude oil without fractionation is desirable because it is cheaper and faster than fractionation of the crude oil followed by separate analysis of each fraction. However, the only ionization method that can ionize all the different compound types in crude oil is electron ionization and it causes extensive fragmentation to many of the compounds in crude oil.<sup>76</sup> All other ionization methods possess biases toward specific compound classes. However, specific compound classes in crude oil can be characterized by carefully selected ionization methods without fractionation. ( $\pm$ ) APPI and ( $-$ ) HESI were utilized by Huba et al. to compare the chemical compositions of unweathered and weathered whole crude oil samples by using a Q Exactive Orbitrap MS.<sup>77</sup> ( $+$ ) APPI results demonstrated that the weathered oil samples contained more aromatic compounds with three to five oxygen atoms than the unweathered oil. However, neither of these ionization methods could be used to ionize saturated hydrocarbons, which is one of the most important compound classes in crude oil.

Otto et al. coupled a GC to both ( $+$ ) resonance-enhanced multiphoton ionization (REMPI) TOF MS and ( $+$ ) EI Q MS to analyze volatile compounds in whole crude oil.<sup>78</sup> Whole crude oil was subjected to thermal desorption at 300 °C for 1 min. The ( $+$ ) EI Q MS results obtained for the desorbed compounds suggested that this method is appropriate for the identification of many of the small linear and branched saturated hydrocarbons, while ( $+$ ) REMPI TOF MS appeared to be appropriate for the identification of aromatic compounds. Polycyclic aromatic sulfur-containing compounds were detected with both techniques; however, the signal intensities were much greater for ( $+$ ) REMPI TOF MS than ( $+$ ) EI Q MS. Identification of nitrogen- and oxygen-containing compounds was not discussed.

Vanini et al. utilized GC  $\times$  GC/( $+$ ) EI TOF MS with a reversed phase column setup to analyze volatile hydrocarbons in several whole crude oil samples with different American Petroleum Institute gravities ( $^{\circ}$ API) and ( $-$ ) ESI 9.4 T FTICR MS to analyze acidic compounds in the same whole crude oil samples.<sup>79</sup> Several classes of compounds were identified by using GC  $\times$  GC/( $+$ ) EI TOF MS, including linear, branched, and cyclic saturated hydrocarbons, alkylbenzenes, alkyl-naphthalenes, alkylindanes, pyrenes, and fluorenes. Based on the ( $-$ ) ESI FTICR MS data, the heavier crude oils contained more compounds with two oxygen atoms than the lighter crude oils, suggesting that heavier crude oils may contain more acidic compounds.

**Saturated Hydrocarbons.** Saturated hydrocarbons are one of the most important classes of compounds in crude oil because they are the basis of fuels. After separation of crude oil into different boiling cuts, chemical analysis of the sizes and structures of the hydrocarbons in each fraction is important to be able to effectively convert them to fuel.<sup>32</sup> Unfortunately, the mass spectrometric characterization of saturated hydrocarbons is challenging (unless they are volatile enough for GC/( $+$ ) EI or GC  $\times$  GC/( $+$ ) EI MS) as they do not contain ionizable functional groups. Furthermore, even when they can be ionized, they often fragment extensively (also applies to ( $+$ ) EI). Recent studies aimed at improving MS characterization of saturated hydrocarbons have focused on the use of GC  $\times$  GC coupled with TOF MS and various ionization methods.

Wim Genuit and Hassan Chaabani utilized positive mode field ionization (( $+$ ) FI) TOF MS to ionize and detect saturated hydrocarbons in a middle distillate petroleum fraction (boiling point range 165–265 °C) after separation using a normal phase GC  $\times$  GC setup.<sup>80</sup> The presence of molecular ions in the mass spectra enabled the differentiation of classes of compounds that eluted at similar times from GC  $\times$  GC. For example, di-, tri-, and pentacyclic saturated hydrocarbons have similar retention times in the GC  $\times$  GC. However, their ( $+$ ) FI mass spectra showed molecular ions, which allowed the differentiation of these three classes of compounds. Two drawbacks relating to the use of ( $+$ ) FI were reported: low signal for heavier compounds and lack of reproducibility due to sample adsorption on the FI emitter.

Shuifu Li et al. analyzed a saturated hydrocarbon fraction of crude oil by using reversed phase GC  $\times$  GC/( $+$ ) EI TOF MS.<sup>81</sup> The reversed phase setup was found to provide greater resolution than the more traditional normal phase setup. For example, mixtures of branched saturated hydrocarbons and sesquiterpanes (a class of cyclic biomarkers) were poorly separated utilizing a normal phase setup, whereas the reversed phase column configuration enabled complete separation of these two classes. Despite the disadvantages of extensive fragmentation by EI, the enhanced separation by using the reversed phase column configuration enabled the grouping of all the saturated hydrocarbon classes.

Nonvolatile saturated hydrocarbons cannot be readily analyzed using GC  $\times$  GC. Xin Li et al.<sup>82</sup> reported on the use of a nitrogen fixation method that was previously developed by Guangtao Li et al.<sup>83</sup> for the ionization of commercially available large linear, branched, and cyclic saturated hydrocarbons and mixtures containing saturated and aromatic hydrocarbons. The nitrogen fixation method involved generation of  $N_3^+$  ions from heated  $N_2$  gas that interacted with a piece of paper connected to a high voltage source. The reactions of  $N_3^+$  ions with neutral saturated hydrocarbons (M) were proposed to occur via insertion of a  $N^+$  ion into carbon–carbon or carbon–hydrogen bonds to form  $[M + N]^+$  ions. Xin Li et al. used a LQIT Orbitrap MS to detect primarily  $[M + N]^+$  ions, in addition to minor  $[2M + N - 2H]^+$  and  $[M + N - 2H]^+$  ions, with insignificant levels of fragmentation for the saturated hydrocarbon model compounds. Upon examination of an equimolar mixture of two saturated hydrocarbons and one aromatic hydrocarbon, higher relative abundances were observed for the saturated hydrocarbons than the aromatic hydrocarbon. Unlike conventional ionization methods, which preferentially ionize aromatic hydrocarbons, the nitrogen fixation method is a beneficial complementary ionization method to selectively ionize saturated hydrocarbons. However, the generation of multiple types of ions per analyte was observed, which can complicate the analysis of unknown samples.

Jin et al. utilized oxygen instead of the commonly used nitrogen as the nebulizer gas and hexane as the solvent in ( $+$ ) APCI experiments on commercially available saturated hydrocarbons.<sup>56</sup> The use of  $O_2$  and hexane produced only  $[M-H]^+$  ions for all classes of saturated hydrocarbons studied whereas the use of  $N_2$  gas and hexane produced both  $[M-H]^+$  and  $M^{+*}$  ions for cyclic saturated hydrocarbons. In addition, this approach resulted in significantly lower levels of fragmentation for a mixture of saturated hydrocarbons compared to the approach based on  $N_2$  gas and hexane solvent. Comparison of the ( $+$ ) APCI/ $O_2$ /hexane method to ( $+$ ) FI for ionization of



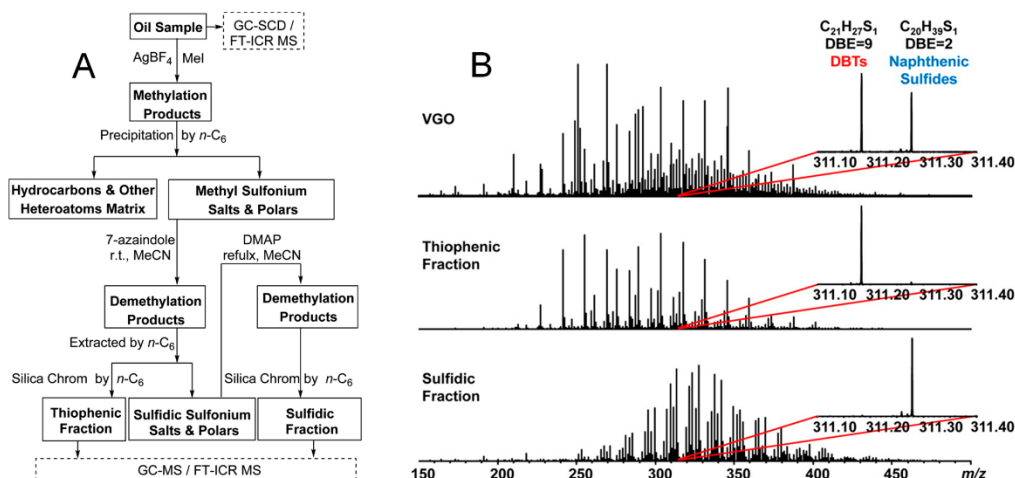


**Figure 6.** (A) Scheme for separation of thiophenes and sulfides from petroleum. DMAP: 4-dimethylaminopyridine. (B) (+) ESI 9.4 T FTICR mass spectra measured for unfractionated vacuum distillation gas oil (VGO) and its thiophene and sulfide fractions. A selected region at *m/z* 313 shows that thiophenes and sulfides were separated into respective fractions. DBTs: dibenzothiophenes. Reproduced from Wang, M.; Zhao, S.; Chung, K. H.; Xu, C.; Shi, Q. *Anal. Chem.* 2015, 87 (2), 1083–1088 (ref 96). Copyright 2014 American Chemical Society.

three base oils with different viscosities revealed comparable performance; however, the (+) APCI/O<sub>2</sub>/hexane method was found to be much more user-friendly and reproducible.

**Sulfur-Containing Compounds.** Determination of the sulfur content in crude oil is critically important because sulfur affects the price of the crude oil. Crude oil containing a lower amount of sulfur, called “sweet” crude oil, is preferred over crude oil with higher sulfur content, called “sour” crude oil,<sup>84</sup> because sulfur-containing compounds deactivate catalysts during crude oil refinery. Han et al. recently reviewed analytical techniques used for total sulfur content determination in crude oils and molecular-level characterization of sulfur-containing compounds.<sup>85</sup> In this review, only recent mass spectrometric techniques employed for above tasks are discussed. Corilo et al. reported on the use of (+) APPI 9.4 T FTICR MS to determine the sulfur content in several crude oils and to build a prediction model for sulfur content in crude oils.<sup>86</sup> Because APPI can ionize aromatic compounds effectively,<sup>87</sup> the ratios of the percent relative abundances of nonsulfur- and sulfur-containing aromatic compounds in the (+) APPI FTICR MS mass spectra of 30 crude oils were used to build a simple multiple regression to predict the sulfur content in crude oils. To test the accuracy of the model, predicted sulfur content was compared to experimental sulfur content obtained by bulk analysis. Predicted sulfur content differed on average by 0.36% from the experimentally obtained total sulfur content, suggesting that the multiple regression model is successful at predicting sulfur content in crude oils. This finding also suggests that most sulfur in crude oil is in aromatic rather than aliphatic compounds as measurement of only aromatic compounds gave a result very close to the total sulfur content.

Silver cationization of sulfur-containing compounds prior to mass spectrometric analysis has been widely used for molecular-level characterization of sulfur-containing compounds in petroleum samples.<sup>88</sup> Maleki et al. compared the ionization efficiency of sulfur-containing compounds in a Saudi

crude oil treated with 1% acetic acid or silver triflate before analysis using (+) nano-ESI drift tube IM LQIT MS.<sup>89</sup> The attachment of a silver cation to sulfur-containing compounds in the silver triflate-treated sample was reported to facilitate the detection of sulfur-containing compounds compared to the acetic acid-treated sample. Lobodin et al. reported on the use of silver-modified SCX SPE and different solvents to separate crude oils and crude oil distillates into three fractions, one containing “unreactive” sulfur-compounds (thiophenes), another containing “reactive” sulfur-compounds (sulfides and disulfides), and a third fraction that contained thiols.<sup>90</sup> As no other fractionation was performed, these fractions also contained numerous abundant compounds that contained no sulfur atoms. The fractions were examined using GC/(+) EI Q MS. Examination of a model compound mixture supported the feasibility of the separation. Further, results obtained for crude oil samples spiked with sulfur-containing compounds suggested that the crude oil matrix did not affect the separation of the unreactive and reactive sulfur-containing compounds. The crude oil fractions were then doped with silver triflate and subjected to analysis using (+) ESI 9.4 T FTICR MS to obtain elemental compositions and RDBE values for compounds in them. The drawback of this approach is that silver ion attachment occurs for both sulfur-containing compounds and aromatic compounds.<sup>91,92</sup> High-resolution MS would be required to differentiate such isobaric ions.

Acter et al. developed a method based on (+) APPI coupled with in-source hydrogen–deuterium exchange (HDX) and 7 T FTICR MS for differentiation of thiols from other sulfur-containing compounds, such as thiophenes and sulfides.<sup>93</sup> Examination of model compounds confirmed that only thiols underwent deuterium exchange. The method was applied to a high-sulfur content Iranian crude oil that was fractionated using a method published by Lobodin et al.<sup>90</sup> The three fractions (thiophenes, sulfides, and thiols) obtained were treated with deuterated methanol prior to MS analysis. Based

on the mass spectra measured,  $M^{+•}$  ions were predominantly formed upon ionization of the first two fractions that contained thiophenes and sulfides. However, despite the low abundance of thiols in this crude oil,  $[M^{+•} - H + D]$  ions were predominantly generated upon ionization of the third fraction that contained thiols. In another publication, Bjerk et al. reported on using silica gel containing silver cations adsorbed to (3-mercaptopropyl)trimethoxysilane to isolate aromatic sulfur-containing compounds from Arabic heavy gas oil followed by analysis with GC  $\times$  GC/(+) EI TOF MS.<sup>94</sup> A total of 168 such compounds were reported to be isolated and tentatively identified. However, no model compounds were studied to test the reliability of this method.

Wang et al. developed an analysis method based on Michael addition reaction followed by (+) ESI 9.4 T FTICR MS for the molecular-level characterization of thiols in five different petroleum samples that included crude oils and fossil fuels.<sup>95</sup> To test the reliability of this method, nine thiol model compounds were dissolved in dichloromethane followed by addition of phenylvinylsulfone and 4-dimethylaminopyridine. The products were analyzed and quantified using (+) ESI 9.4 T FTICR MS and GC coupled with a sulfur chemiluminescence detector (SCD), respectively. Based on the SCD results, the conversion of thiols was greater than 98.5%. The same procedure was performed for petroleum samples. Thiols in the petroleum samples were expected to selectively react with phenylvinylsulfone. The products were isolated through silica gel column chromatography prior to (+) ESI 9.4 T FTICR MS analysis. Unsaturated thiols with alkyl chains containing up to 30 carbon atoms and RDBE values of up to 9 were identified. In another study, the same group developed a method for the characterization of sulfur-containing compounds in fluid catalytic cracking diesel and in a vacuum distillation gas oil fraction obtained from Kuwait heavy crude oil.<sup>96</sup> The characterization was based on selective separation of thiophenes and sulfides from the petroleum samples via a methylation/demethylation procedure. This procedure was first applied to model compounds and then to two petroleum samples. The procedure involved methylating thiophenes and sulfides by using methyl iodide ( $CH_3I$ ) and silver tetrafluoroborate ( $AgBF_4$ ) to form methyl sulfonium salts. This was followed by their separation from the petroleum matrix via precipitation by using *n*-hexane. *n*-Hexane supernatant containing hydrocarbons and other petroleum matrix was discarded while the precipitant containing methyl sulfonium salts and polar compounds was treated with acetonitrile and 7-azaindole. In this step, thiophenes and sulfides were demethylated to regenerate the original thiophenes and sulfides. These compounds were extracted from the mixture by using *n*-hexane and subjected to silica gel chromatography to separate thiophenes, sulfides, and polar compounds from each other (Figure 6). Thiophenes and sulfides were characterized by using (+) ESI 9.4 T FTICR MS. The results suggested that thiophenes and sulfides had been successfully separated into different fractions. The same research group also used this approach to study sulfur-containing compounds in two crude oils obtained from Tarim Basin, China.<sup>97</sup> These two crude oils were concluded to contain different biomarker-like sulfur compounds, such as 1,1-dimethylhexahydro-dibenzo-thiophenes and thiadiazolones. More recently, based on results obtained using (+) ESI Orbitrap Fusion, Wang et al. reported that methylation of sulfides and thiophenes into methyl sulfonium salts forms side products that could lead to

incorrect assignment of sulfur-containing compounds.<sup>98</sup> For instance, toluene can be methylated in the presence of  $CH_3I$  and  $AgBF_4$  to form multiple products. Wang and Schrader reported on selective alkylation and thereby speciation of sulfur-containing compounds in a heavy crude oil by using iodomethane- $d_3$  or iodoethane- $d_5$ .<sup>99</sup> Results obtained studying model compounds supported the success of their method. The alkylated sulfur compounds were analyzed by using (+) ESI LQIT Orbitrap Elite MS and (+) ESI 7 T FTICR MS. Zhu et al. reported on the identification of organic polysulfanes with three to six sulfur atoms in a petroleum sample from Tarim Basin, China, by using GC  $\times$  GC/(+) EI TOF MS.<sup>100</sup> On the other hand, Dijkmans et al. used GC  $\times$  GC/(+) EI TOF MS and GC  $\times$  GC/SCD for the characterization and quantitation, respectively, of sulfur-containing compounds in shale oil.<sup>101</sup> Thiols, benzothiophenes, dibenzothiophenes, and naphthobenzothiophenes were found to be the major sulfur-containing compounds in the shale oil.

Ha et al.<sup>102</sup> conducted MS/MS experiments based on medium-energy CAD (MCAD, herein defined as the CAD experiment performed in the octopole placed after the C-trap (occasionally referred to as the HCD cell in the literature)), by using (+) APPI Q Exactive Orbitrap MS to investigate the structures of sulfur-containing aromatic compounds in an aromatic fraction of Kuwait crude oil obtained through ring-type HPLC separation described by Kim et al.<sup>103</sup> Structures were proposed for some of the sulfur-containing aromatic compounds with RDBE values of 6–9. It would have been beneficial to substantiate the assigned structures by using model compounds with the proposed structures.

**Nitrogen-Containing Compounds.** Detection of nitrogen-containing compounds in crude oil is of interest because they poison catalysts, corrode equipment, and limit storage time. In particular, Chen et al. proposed that basic compounds containing one nitrogen atom and having RDBE values less than 10 are responsible for the deactivation of catalysts during catalytic cracking processes of crude oil.<sup>104</sup> In addition, Celis-Cornejo et al. suggested that weakly basic nitrogen-containing compounds, such as carbazole and tetrahydrocarbazole, reduce catalytic performance in hydrocracking processes.<sup>105</sup>

For speciation of nitrogen-containing compounds in petroleum samples, Kim and co-workers pioneered the use of (+) APPI<sup>106,107</sup> and (+) APCI<sup>108</sup> coupled with HDX in a Q Exactive Orbitrap MS. This approach involved dissolving nitrogen-containing compounds in deuterated toluene or deuterated methanol prior to APPI or APCI. Model compounds were used to demonstrate that primary amines form  $[M - 2H + 2D]^{+•}$  and  $[(M - 2H + 2D) + D]^+$  ions in above experiments while secondary amines, such as alkylated or phenylated pyrrole, form  $[M - H + D]^{+•}$  and  $[(M - H + D) + D]^+$  ions, and tertiary amines, such as pyridine, form  $[M + D]^+$  ions.<sup>106</sup> (+) APPI coupled with HDX indicated that two nitrogen-containing resin fractions obtained from Qinhuangdao crude oil contained mostly alkylated pyrrole- and N-alkylated pyrrole-like compounds, while a resin fraction obtained from shale oil contained mostly pyridine-like compounds. In another study, HDX coupled with HPLC/(+) APPI 7 T FTICR MS was used to examine three different heavy oil samples.<sup>109</sup> Toluene, ethyl acetate, and methanol were used as the eluents in HPLC. The toluene eluted fraction was determined to mostly contain  $N_1$  and  $N_1S_1$  compounds as well as pyrrole derivatives while ethyl acetate and methanol eluted fractions mostly contained pyridine and pyrrole

derivatives. Even though these methods are promising for speciating nitrogen-containing compounds, they generate multiple ions per analyte, which complicates analysis of complex mixtures.

Vasconcelos et al.<sup>110</sup> employed a SPE method based on sulfonic acid bonded to silica, previously described by Rowland et al.,<sup>111</sup> to fractionate basic nitrogen-containing compounds in Brazilian vacuum residues. (+) ESI 7.2 T FTICR MS was used to analyze the fractions. The nonbasic compounds were removed from the basic nitrogen-containing compounds by using different mixtures of methanol and dichloromethane as eluents on the SPE cartridge. The basic nitrogen-containing compounds were separated into five fractions according to their MWs. The average MWs measured for the five fractions were 623, 737, 912, 1100, and 1203 Da while the average MW of the original Brazilian vacuum residue was determined to be 703 Da. Fractionation enabled the assignment of the elemental compositions for 3 500 compounds compared to 1 393 compounds before fractionation, suggesting that fractionation reduced the complexity of the sample so that more compounds could be detected. Sheng et al. have explored the effects of hydrotreatment (HDT) and fluid catalytic cracking (FCC) on nitrogen-containing compounds in a Venezuelan Mery-16 crude oil vacuum residue by using ( $\pm$ ) ESI 9.4 T FTICR MS.<sup>112</sup> The abundance of the nitrogen-containing compounds was found to be significantly reduced upon both HDT and FCC. These results were in agreement with those of Zhang et al., who employed (+) APPI 9.4 T FTICR MS to show that nitrogen- and sulfur-containing compounds were effectively removed from a shale oil upon HDT using a NiMo-based catalyst.<sup>113</sup>

Models that can predict the total nitrogen content in crude oil before and after a treatment based on measured mass spectra would be useful in determining the efficiencies of different treatments. Terra et al. utilized partial least-squares regression with variable selection based on competitive adaptive reweighted sampling (CARSPLS) to create a model for the prediction of the content of basic nitrogen compounds in crude oils based on data obtained using (+) LDI 9.4 T FTICR MS.<sup>114</sup> The model was built based on the relative abundances of molecular ions of 48 basic nitrogen-containing compounds in the mass spectra measured for 50 crude oils. The predicted content of basic nitrogen compounds in 20 crude oil test samples was in a good agreement with the content of basic nitrogen compounds measured using ASTM D5443-14.

**Naphthenic Acids.** The petroleum community defines the naphthenic acid (NA) fraction of petroleum as a fraction containing carboxylic acids.<sup>115</sup> The need to characterize NAs is driven by environmental and crude oil processing reasons because, despite their low abundance in crude oils, NAs are the main corrosive species in acidic crude oils.<sup>116,117</sup> Additionally, NAs are the major contributor to the total acid number of a crude oil. A high total acid number reduces the value of a crude oil because this causes corrosion and other refinery problems.<sup>118,119</sup> Thermal degradation of crude oil has been reported to reduce its total acid number because this process can decarboxylate NAs.<sup>120</sup> It is possible that decarboxylation of NAs can be improved if NAs are better characterized.

Barros et al.<sup>121</sup> have reported on the use of aminopropyl silica-based SPE (SPS SPE), previously developed by Rowland et al.,<sup>111</sup> for isolation of NAs from crude oil and fractionation of the isolated NAs based on their MWs. This procedure

involves loading a deasphalted crude oil onto the SPS SPE cartridge conditioned with dichloromethane. Nonacidic and moderately acidic compounds eluted from the SPS SPE when 100% dichloromethane followed by 50% dichloromethane and 50% methanol were used as eluents. Carboxylic acids (NAs), that had been retained in the SPS SPE, were eluted from the SPS SPE based on their MWs by using different mixtures of methanol, water, and formic acid in a reversed-phase mechanism. The use of formic acid and aminopropyl functionality in the SPE allowed extraction and fractionation of NAs based on their hydrophobicity (i.e., extent of alkylation or number of carbons) due to their interactions with the aminopropyl functionalities. Because ( $\pm$ ) ESI cannot ionize all NAs across a wide MW range with equal efficiency, fractionation of the sample into groups of compounds with similar MWs improves the ionization efficiency of the NAs.<sup>111,122</sup> In a study carried out by Barros et al.,<sup>121</sup> aminopropyl silica stationary phase and different combinations of dichloromethane, methanol, water, and formic acid eluents were used to isolate and fractionate NAs into six fractions containing compounds with different MWs. Prior fractionation enabled the detection of large NAs (MW 700–1200 Da) by using (–) ESI 9.4 T FTICR MS although these compounds are generally not observed due to ion suppression caused by small NAs.<sup>121</sup> This approach was found to be superior to liquid–liquid extraction (LLE) (introduced by Colati et al.<sup>123</sup>) in the analysis of NAs derived from a Brazilian crude oil before and after thermal degradation as only the SPE approach enabled the detection of large NAs. In another study, Valencia-Dávila et al. compared the efficiency of (–) ESI and (–) MALDI in ionization of NAs that were isolated from a heavy crude oil and fractionated based on their MWs by using the above SPE approach.<sup>124</sup> A 7 T FTICR MS was used for these experiments. (–) MALDI allowed the detection of highly oxidized  $O_x$  species ( $x = 1–9, 11$ ) that were not observed in the (–) ESI mass spectra. More recently, Clingenpeel et al. utilized multiple separation methods followed by analysis using (–) ESI 15 T FTICR MS to increase the dynamic range of the analysis of NAs in crude oil.<sup>125</sup> The crude oil was first distilled into fractions that included vacuum gas oil (VGO) and vacuum residue (VR). The NAs were then isolated from VGO, VR, and the original crude oil by using SPE and fractionated based on their MW by using the SPE method discussed above, followed by analysis using (–) ESI 15 T FTICR MS. Mass spectra measured for the VGO and VR fractions revealed small acidic compounds with two to four oxygens that were not detected in the original crude oil. Therefore, distillation combined with NA isolation and fractionation improves the ability to characterize NAs.

Derivatization of NAs prior to MS analysis is another approach that has been recently utilized. Gutierrez-Villagomez et al. explored the use of pentafluorobenzyl bromide (PFBBR) to derivatize NA model compounds and two oil-extracted NA mixtures.<sup>126</sup> PFBBR, which has been previously reported to selectively react with carboxylic acids in the presence of a weak base,<sup>127</sup> substitutes the acidic hydrogen of the NA carboxylic acid functionality with a pentafluorobenzyl group. Model compound studies showed that derivatized NAs generate the pentafluorobenzyl fragment ion ( $m/z$  181) upon (+) EI Q MS. The oil-extracted NA mixtures containing derivatized NAs were analyzed by using GC/(+) EI Q MS and the NAs were detected based on the observation of the pentafluorobenzyl fragment ion. Derivatization with PFBBR was found to improve

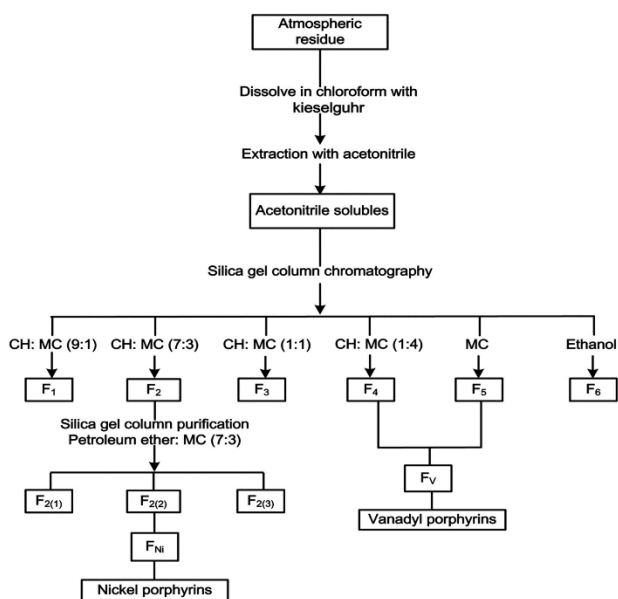


**Figure 7.** Separation scheme of petroporphyrins in heavy crude oil (CH refers to cyclohexane; MC refers to methylene chloride;  $F_1$ – $F_6$  are the corresponding subfractions eluting with certain solvents from acetonitrile extract;  $F_{2(1)}$ ,  $F_{2(2)}$ , and  $F_{2(3)}$  are the three subfractions obtained during further chromatographic purification of  $F_2$ ; the subfractions abundant with Ni-porphyrins and V-porphyrins are labeled as  $F_{Ni}$  and  $F_V$ , respectively). Reproduced from Liu, H.; Mu, J.; Wang, Z.; Ji, S.; Shi, Q.; Guo, A.; Chen, K.; Lu, J. *Energy Fuels* **2015**, 29 (8), 4803–4813 (ref 140). Copyright 2015 American Chemical Society.

the chromatographic resolution and sensitivity compared to other derivatizing reagents, such as boron trifluoride/methanol and *N*-(*t*-butyldimethylsilyl)-*N*-methyltrifluoroacetamide.

Wilde et al. converted NAs to hydrocarbons followed by analysis with GC  $\times$  GC/(+) EI TOF MS in an attempt to structurally identify bicyclic NAs in an unknown commercial petroleum-derived NA mixture.<sup>128</sup> In this approach, the NAs were first converted to methyl esters and then to primary alcohols, which were subsequently converted to tosylates. Finally, the tosylates were reduced to hydrocarbons. Based on a model compound study, 30 individual bicyclic NAs were identified in the petroleum-derived NA mixture. The same research group utilized above approach to identify NAs in oil sands affected-processed water (OSPW) samples.<sup>129</sup> GC  $\times$  GC/(+) EI TOF MS enabled the identification of alicyclic, aromatic, and sulfur-containing hydrocarbons that originated from NAs in the OSPW samples.

**Metals.** Compared to heteroatoms, such as sulfur and nitrogen, metals are found in much lower concentrations in crude oil, ranging from a few hundred parts per million in heavy crude oil to a few parts per billion in lighter crude oil.<sup>130</sup> In spite of their low abundance, metals present tremendous challenges for oil refineries as they poison catalysts and corrode refining columns and turbines.<sup>131</sup> Additionally, the combustion of petroleum products containing metals can have a negative environmental impact, leading to increased air pollution hazards.<sup>132</sup>

To date, the metals identified in crude oil are iron, mercury, molybdenum, palladium, platinum, cobalt, chromium, sodium, potassium, lithium, copper, strontium, silver, tin, lead, titanium,

gold, vanadium, and nickel, with vanadium and nickel the most abundant.<sup>132,133</sup> Identification and quantitation of these metals in crude oil can be conducted via inductively coupled plasma MS (ICPMS). In ICPMS, crude oil is aerosolized and directed into a high temperature (>6000 K) source wherein the crude oil compounds dissociate into free atoms.<sup>134</sup> The gaseous atoms are then ionized by an argon plasma. Metal atoms primarily form metal cations upon ionization. Single quadrupole, triple quadrupole, and double-focusing sector [magnet (B)  $\times$  electrostatic sector (E)] mass spectrometers are typically utilized for the detection of the metal cations.

Crude oil is either dissolved in a solvent and directly injected into the ICPMS or treated to remove as many interfering compounds as possible before ICPMS analysis. The latter approach suffers from poor sample recovery, while the former suffers from low accuracy. To improve the recovery of the metal species in crude oil, Sugiyama and Williams-Jones developed a sample preparation method that combined dry-ashing, chemical oxidation, and acid digestion.<sup>132</sup> Unlike other dry-ashing and acid digestion methods, which suffer from sample contamination and poor sample recovery, this method utilized disposable Pyrex culture tubes capped with quartz wool to reduce sample loss. This approach resulted in highly reproducible and accurate measurements of metal concentrations by using ICP Q MS. When no sample treatment is utilized, the sensitivity and accuracy of the measurements have been reported to improve by using lower sample viscosity and finer primary aerosol as this will introduce a greater amount of analyte into the plasma.<sup>135</sup> However, different results were reported by Poirier et al., who tested the accuracy of



quantitating Fe, Ca, Ni, and V in crude oils of different viscosities via direct injection into ICP Q MS with no sample pretreatment.<sup>136</sup> The crude oil samples were diluted with *o*-xylene to further test whether sample viscosity impacted the quantitation results. Even when the viscosities of the crude oil solutions differed by >30%, no impact was observed on the sensitivity or accuracy of the quantitation measurements. A relative standard deviation below five percent was reported for each of the four metals.

Whether crude oil samples are subjected to extensive pretreatment or directly injected into MS, interferences due to isobaric ions can still be an issue for accurate metal quantitation. For example, many ions with the same nominal mass as  $^{51}\text{V}^+$ , such as  $^{35}\text{Cl}^{16}\text{O}^+$ ,  $^{36}\text{Ar}^{15}\text{N}^+$ , and  $^{37}\text{Cl}^{14}\text{N}^+$ , have been identified as negatively affecting accurate  $^{51}\text{V}^+$  quantitation in crude oils.<sup>137</sup> Although double-focusing MS with a relatively high resolution can resolve many of these interferences, their high price, technical complexity, and low robustness limit their applicability.<sup>138</sup> A low-resolution ICPMS/MS instrument (8800 ICP MS from Agilent) that contains an rf-only octapole reaction chamber (q2) between two quadrupoles (Q1 and Q3) has been reported to enable more accurate quantitation of metals in crude oil.<sup>138</sup> Walkner et al. utilized this ICPMS/MS to test the accuracy of quantitation of 25 trace metals commonly found in crude oil.<sup>137</sup> To eliminate potential interfering ions for the 25 different metal cations in the MS, each metal cation, one at a time, was transferred into q2 by using Q1. The selected metal cation, and any potential interfering isobaric ions, were allowed to react with either  $\text{O}_2$  or  $\text{NH}_3$  gas in q2. Ideally, only the desired metal cation ( $\text{M}^+$ ) reacts with  $\text{O}_2$  or  $\text{NH}_3$  to form  $\text{MO}^+$  or  $\text{M}(\text{NH}_3)_x^+$ , respectively. These product ions were then transferred into Q3 for analysis. The efficiency of this procedure was demonstrated by using model compounds. Interfering compounds were purposefully added into a mixture containing known amounts of Ti, V, Cr, and As. When no gas was introduced into q2, the concentrations measured for each metal were much greater than what was known to be present in the mixture, suggesting that isobaric ions interfered with the quantitation. When  $\text{O}_2$  gas was introduced into q2, the concentrations measured for Ti, V, and As were nearly identical to the amounts present in the mixture. The introduction of  $\text{NH}_3$  gas into q2 enabled accurate quantitation of Cr. Further, two standards, NIST SRM 1634c (trace metals in fuel oil) and NIST SRM1084a (trace metals in lubricant oils), each with the same 25 metals, were studied to evaluate the accuracy of the approach. The quantitation results obtained for all 25 metals in each standard were found to be within the standard deviation of the amounts for each metal in each standard, except for Ag in NIST 1634c and Ti and Ag in NIST SRM 1084a. This finding indicates that ICPMS/MS can be used to accurately quantitate many trace metals in crude oil.

In addition to quantitating the metal content in crude oils, characterizing the structures of the metal-containing compounds is an equally important task. Recent studies on the characterization of metal compounds have focused on  $\text{V}^{4+}$  and  $\text{Ni}^{2+}$  complexes of alkyl porphyrins due to their high abundances in crude oil, their deleterious properties, and their important roles as geochemical markers.<sup>133,139</sup> Additionally, structural characterization of these complexes may facilitate the design of demetallization catalysts for removal of these compounds.<sup>133</sup> Liu et al. have developed a method to concentrate V- and Ni-porphyrins into two fractions from a

heavy crude oil via extraction with chloroform and acetonitrile followed by silica gel chromatography (Figure 7). The compounds in the fractions were identified using (+) ESI 9.4 T FTICR MS.<sup>140</sup> This analysis resulted in the identification of several different types of V-porphyrin compounds with the general formulas  $\text{C}_n\text{H}_m\text{N}_4\text{V}_1\text{O}_1$ ,  $\text{C}_n\text{H}_m\text{N}_4\text{V}_1\text{O}_2$ , and  $\text{C}_n\text{H}_m\text{N}_4\text{V}_1\text{O}_1\text{S}_1$  and with RDBE values of 17–25, 18–20, and 21–27, respectively. The most abundant compounds in the  $\text{C}_n\text{H}_m\text{N}_4\text{V}_1\text{O}_1$  and  $\text{C}_n\text{H}_m\text{N}_4\text{V}_1\text{O}_2$  classes had RDBE values of 17 and 19, respectively, whereas the most abundant compound in the  $\text{C}_n\text{H}_m\text{N}_4\text{V}_1\text{O}_1\text{S}_1$  class had a RDBE value of 24. For the one heavy crude oil that was analyzed, sulfur appears to prefer to incorporate into V-porphyrins with high RDBE values. For the Ni-porphyrins, only one type,  $\text{C}_n\text{H}_m\text{N}_4\text{Ni}$ , was identified. Although many isobaric ions, especially those containing sulfur, can complicate the characterization of Ni-porphyrins, the elemental compositions of the Ni-porphyrins were confirmed by analyzing their isotope distributions. The errors in the measured  $m/z$ -values for the Ni-porphyrins were between 0.01 mDa and –0.23 mDa, suggesting reliable elemental assignments.

Liu et al. have utilized (+) ESI 9.4 T FTICR MS to characterize V-porphyrins in heavy crude oils before and after dehydrometallization.<sup>141</sup> The samples were separated in a Soxhlet extractor into a methanol fraction, a dichloromethane fraction, and a toluene fraction. Each of these three fractions was further separated into seven subfractions by using silica gel chromatography with eluents of varying polarities. Mass spectra measured for the methanol subfractions obtained for the heavy crude oil before and after dehydrometallization revealed  $\text{C}_n\text{H}_m\text{N}_4\text{V}_1\text{O}_1$  porphyrins with RDBE values of 17 to 24; however, their abundances were lower after dehydrometallization. Mass spectra measured for the dichloromethane subfractions revealed mostly  $\text{C}_n\text{H}_m\text{N}_5\text{V}_1\text{O}_2$  porphyrins with RDBE values of 17, 18, 20, and 21. After dehydrometallization, none of these species were observed, suggesting that the dehydrometallization catalyst is more effective at removing  $\text{C}_n\text{H}_m\text{N}_5\text{V}_1\text{O}_2$  porphyrins than  $\text{C}_n\text{H}_m\text{N}_4\text{V}_1\text{O}_1$  porphyrins.

V- and Ni-complexes have been reported to aggregate in crude oil.<sup>142</sup> Determining the sizes of these aggregates is critically important for designing catalysts for their removal.<sup>143</sup> Sama et al. utilized GPC ICP B  $\times$  E MS to determine whether the type of the GPC column or solution storage time can bias the measurement of the size distributions of the aggregates.<sup>144</sup> In brief, GPC is a form of size-exclusion chromatography. The size and the concentration of aggregates can be determined by GPC based on their elution times and the areas of the corresponding peaks, respectively. In this study, the performance of two different GPC columns, Agilent PLgel MIXED-D (Col A) and Waters Styragel (Col W), was tested. The GPC ICP B  $\times$  E MS chromatograms measured by using both columns showed three peaks for  $^{51}\text{V}$  and two peaks for  $^{58}\text{Ni}$ , suggesting the presence of three and two aggregates of different sizes, respectively. A smaller area was observed for the first peak, corresponding to the largest aggregates, for both  $^{51}\text{V}$  and  $^{58}\text{Ni}$  when using Col A compared to Col W. Therefore, Col A was concluded to have higher shear forces than Col W. Larger aggregates have been reported earlier to be prone to breakdown due to shear forces.<sup>145</sup> This could make the amounts of the largest aggregates for V- and Ni-complexes measured using Col A to be too small. Further, aggregate sizes of V- and Ni-complexes were studied after storing the crude oil samples dissolved in tetrahydrofuran for days, weeks, or

months. The observation of a greater area for the first peak eluting from GPC for both  $^{51}\text{V}$  and  $^{58}\text{Ni}$  when the crude oil solutions were stored for over a week compared to when the crude oils were analyzed immediately indicated that V- and Ni-complexes tend to form larger aggregates over time if not properly stored and, therefore, should be analyzed immediately to obtain accurate results for their size distributions.

Single particle (sp) ICPMS is used for determining the size and the concentration of metal particles in a sample. Nelson et al. demonstrated the application of (+) spICP QQQ MS/MS to determine the presence of V, Ni, Mb, and Fe nanoparticles in asphaltenes.<sup>146</sup> In short, spICPMS/MS measures the number of ions of a specified  $m/z$  as a function of time. When a metal nanoparticle enters the argon plasma, all metal atoms are released and are individually ionized. The signal that they produce in MS is proportional to the size of that particle. However, metals that do not exist in large metal nanoparticles, i.e., that exist as individual molecules or small aggregates, do not produce signals larger than the background baseline, and therefore cannot be detected using this method. For the three asphaltene samples studied, signals for  $^{51}\text{V}^+$  and  $^{60}\text{Ni}^+$  were not observed, suggesting that these metals do not form metal nanoparticles or the aggregates formed are too small to be detected by using this technique. These results do not necessarily contradict the results obtained by Sama et al.<sup>144</sup> because the (+) GPC ICP B  $\times$  E MS method does not provide information on the exact size of the V- and Ni-complex aggregates but rather on their relative sizes. On the other hand, numerous signals of varying intensities were observed for  $^{95}\text{Mb}^+$  and  $^{56}\text{Fe}^+$ , suggesting that these two metals exist as nanoparticles of different sizes in asphaltenes.

**Asphaltenes. Molecular Weight.** Determining the MW distribution of asphaltenes is important for the design of economical and efficient crude oil refining processes.<sup>147</sup> For example, more energy is required to break asphaltene molecules with greater MWs into manageable products for refining.<sup>147</sup> Originally thought to have a very wide range of MWs (between 1 000 and 300 000 Da), the largest MWs of asphaltenes have recently been determined by mass spectrometry to be no greater than 1500 Da.<sup>148,149</sup> The most likely cause for the previous discrepancies is the tendency of asphaltenes to aggregate. These aggregates remain intact upon laser desorption in LDI and MALDI experiments, techniques that dominated early asphaltene characterization.<sup>68</sup> The use of two-step laser TOF MS ( $\text{L}^2$  TOF MS) by Pomerantz et al. was one of the first MS studies to demonstrate accurate asphaltene MW distributions.<sup>149</sup> This approach involved desorption of the asphaltenes by using the first laser pulse and then independently ionizing them by using the second laser pulse. Another technique that yields a correct MW distribution for asphaltenes is laser-induced acoustic desorption (LIAD) (+) EI 3 T FTICR MS. Pinkston et al. utilized this technique to desorb neutral asphaltene compounds into the EI source for nonselective ionization.<sup>148</sup>

Although  $\text{L}^2$  TOF MS and LIAD (+) EI FTICR MS are successful techniques for determining the true MW distributions of asphaltenes, these two techniques require more sophisticated setups than LDI and MALDI and are therefore not as commonly employed. Recent analyses of asphaltene MW distributions have utilized LDI and MALDI ionization techniques under carefully controlled conditions to avoid analysis of aggregates.<sup>75,150</sup> Fergoug et al. utilized (+) MALDI TOF MS to measure the MW distributions for asphaltenes in

three different matrixes,  $\alpha$ -cyano-4-hydroxycinnamic acid, 2-(4-hydroxyphenylazo)benzoic acid, and 1,8,9-anthracenetriol. Identical molecular weight distributions in the generally accepted range were measured, suggesting that the type of matrix may not influence these measurements.<sup>150</sup> Results obtained using (+) MALDI TOF MS for neat asphaltenes revealed a much broader MW distribution than the generally accepted range.<sup>151,152</sup> Zheng et al. found no difference between (+) MALDI/TOF mass spectra measured for neat asphaltenes and asphaltenes dissolved in dichloromethane/hexane solvent.<sup>153</sup> A consensus on the ideal way to prepare asphaltenes for MALDI experiments still has not been achieved.

Koolen et al. utilized (+) LDI TWIM TOF MS to determine the MW distributions of asphaltenes.<sup>154</sup> In this experiment, ionized asphaltenes were allowed to collide with nitrogen gas in the ion mobility cell of TWIM to break apart asphaltene aggregates that may have existed in the asphaltene sample or that were formed by LDI. The mass spectra were not sensitive to the laser energy used to desorb the asphaltenes. Asphaltenes with MWs between 150 and 1500 Da were observed, with a maximum at about 300 Da. Riedeman et al. have utilized (+) APCI with  $\text{CS}_2$  as the solvent and APCI reagent and nitrogen gas as the nebulizing gas in LQIT MS to measure the molecular weight distribution of an asphaltene sample.<sup>155</sup> Asphaltene molecules with MWs between 150 and 1050 Da were observed, with an average molecular weight of 497 Da.

**Island vs Archipelago Structures.** It is generally accepted that two types of compounds exist in asphaltenes, those with island structures containing a single aromatic core with alkyl side chains and those with archipelago structures containing multiple aromatic cores, possibly with alkyl side chains, linked via alkyl bridges. However, the relative abundances of the island and archipelago structures in asphaltenes are still controversial in the MS community. Asphaltenes precipitated from different vacuum residues of crude oils by using *n*-heptane were analyzed by Wittrig et al. using (+) APPI 15 T FTICR MS. They subjected the generated  $\text{M}^{+\bullet}$  ions to CAD in order to determine whether island or archipelago structures dominated.<sup>156</sup> All CAD experiments resulted primarily in alkyl radical losses with no change in the RDBE values of the  $\text{M}^{+\bullet}$  ions, demonstrating the presence of only island structures in these asphaltenes. Similarly, Wang et al. also only observed island compounds when utilizing their (+) APPI 15 T FTICR MS to examine CAD of  $\text{M}^{+\bullet}$  ions derived from asphaltenes.<sup>157</sup> Tang et al. also reported the observation of only island structures for six asphaltene samples with different origins.<sup>158</sup> This conclusion was based on experiments wherein the asphaltenes were ionized to generate  $\text{M}^{+\bullet}$  by using (+) APCI with  $\text{CS}_2$  reagent and the  $\text{M}^{+\bullet}$  ions were subjected to CAD in  $\text{MS}^2$  and  $\text{MS}^3$  experiments by using LQIT MS. Fragmentation via losses of large neutral aromatic fragments, as expected for archipelago molecular ions based on model compound studies, were not observed.

Later, Nyadong et al. examined the usefulness of CAD in the ion trap and medium-energy CAD (MCAD) in the octopole of a (+) APPI LQIT Orbitrap MS to determine the relative abundances of island and archipelago compounds in six asphaltene samples based on possible changes in the RDBE values of  $\text{M}^{+\bullet}$  ions.<sup>159</sup> Examination of  $\text{M}^{+\bullet}$  ions of island and archipelago model compounds showed that CAD was inefficient at fragmenting island and archipelago  $\text{M}^{+\bullet}$  ions to single aromatic cores with no alkyl chains attached except methyl groups. MCAD, on the other hand, caused extensive

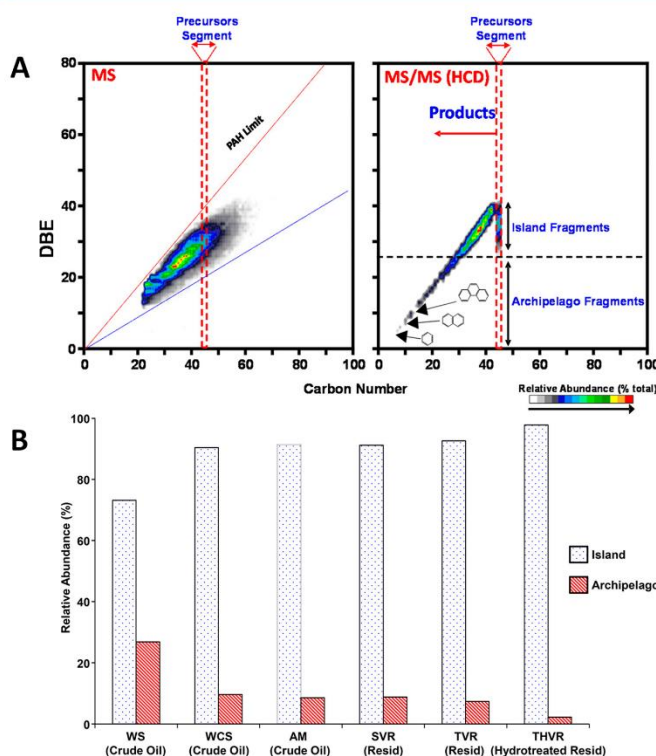


**Figure 8.** (A) Plots showing RDBE (DBE) values as a function of the number of carbon atoms for asphaltenes derived from Eagle Ford crude oil and analyzed using (+) APPI Orbitrap MS. (Left) Data obtained from an APPI mass spectrum. (Right) MCAD (called HCD) mass spectrum for ions with  $m/z$  values in the range of 545–555. (B) Relative proportions of island and archipelago compounds in six asphaltene samples. Reproduced from Nyadong, L.; Lai, J.; Thompson, C.; LaFrancois, C. J.; Cai, X.; Song, C.; Wang, J.; Wang, W. *Energy Fuels* **2018**, 32 (1), 294–305 (ref 159). Copyright 2017 American Chemical Society.

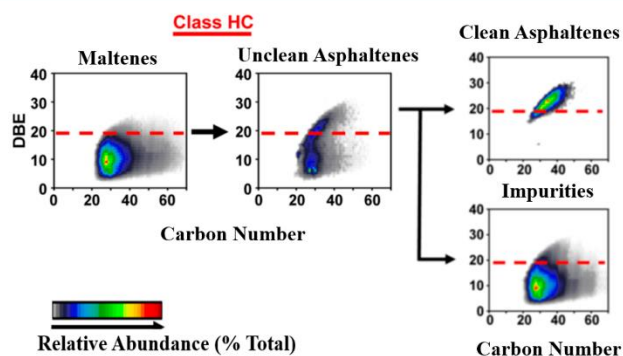


**Figure 9.** Plots of RDBE values as a function of the number of carbons for compounds containing only carbon and hydrogen for maltenes, unclean asphaltenes, asphaltenes after cleaning, and impurities. Modified from Chacón-Patiño, M. L.; Rowland, S. M.; Rodgers, R. P. *Energy Fuels* **2017**, 31 (12), 13509–13518 (ref 160). Copyright 2017 American Chemical Society.

dissociation to both island and archipelago  $M^{+}$  ions, generating single aromatic cores with no larger alkyl groups

than methyl groups attached to them. Due to this great fragmentation efficiency, MCAD enabled the detection of  $M^{+}$

ions of archipelago compounds. Nevertheless, island compounds were found to dominate for all six asphaltene samples. The relative amounts of the archipelago compounds were found to vary from sample to sample (Figure 8).

A recent three-part publication series *Advances in Asphaltene Petroleomics* by Rodgers et al. demonstrated that the relative amounts of island and archipelago compounds depend on the method used to precipitate the asphaltenes and the origin of the asphaltenes.<sup>160–162</sup> In the first study, asphaltenes were extensively cleaned using either *n*-pentane or *n*-heptane from a South American heavy crude oil were analyzed using (+) APPI 9.4 T FTICR MS.<sup>160</sup> Before analysis, the asphaltenes were precipitated using either *n*-pentane or *n*-heptane from a Soxhlet device.<sup>160</sup> Plots of RDBE values as a function of the number of carbon atoms in the asphaltenes before and after cleaning were completely different (Figure 9). On the other hand, the plots generated for maltenes and impurities (removed from the uncleared asphaltenes with the Soxhlet procedure) were similar (Figure 9), suggesting that the uncleared asphaltenes were contaminated with maltenes. Maltenes have been previously determined to mostly contain island compounds.<sup>163</sup> Therefore, analysis of unclean asphaltenes overestimates the relative abundances of island compounds. On the other hand, isolating the  $M^{+•}$  ions of the cleaned asphaltenes and subjecting them to infrared multiphoton dissociation (IRMPD) revealed that the asphaltenes that have been precipitated and cleaned with *n*-heptane contained greater amounts of archipelago compounds than those precipitated and cleaned with *n*-pentane. Overall, island compounds still dominated both asphaltenes. Therefore, asphaltenes should be fractionated into different compound classes in order to accurately determine the relative abundances of the island and archipelago compounds. The second publication reported an extrography fractionation method that was used to separate asphaltenes (precipitated and cleaned with *n*-heptane as described previously<sup>160</sup>) into eight fractions of different polarities.<sup>161</sup> (+) APPI 9.4 T FTICR MS analysis wherein  $M^{+•}$  ions were subjected to IRMPD demonstrated that the original asphaltenes and the first (acetone) fraction of the asphaltenes were similar; both samples predominantly contained island compounds. On the other hand, the other seven fractions contained archipelago compounds that were not identified in the original asphaltenes nor in the first fraction. Even more revealing, the sixth (toluene–tetrahydrofuran) fraction of the asphaltenes, unlike the other seven fractions, contained predominantly archipelago compounds. Therefore, cleaning and fractionation were critical for the detection of archipelago compounds. In the third study, asphaltenes precipitated from Wyoming Deposit and Athabasca bitumen by using *n*-heptane were fractionated using the same extrography method.<sup>161,162</sup> While all fractions obtained for the Wyoming Deposit predominantly contained island compounds based on IRMPD experiments, the fractions obtained for the Athabasca bitumen contained many more archipelago compounds. In agreement with the results obtained by Nyadong et al.,<sup>159</sup> this study indicated that the abundances of island and archipelago compounds vary from sample to sample.

**Geochemistry and Oil Fingerprinting.** Petroleum geochemistry focuses on individual elements or compounds in crude oil that can be used to determine important information about the crude oil, such as its source rock, maturity, and migration. Branched saturated hydrocarbons, hopanes, ster-

anes, isoprenoids, and diamondoids are the most common compounds in crude oil used for geochemical characterization.<sup>164</sup> These compounds are referred to as biomarkers as they originate from biological organisms and are so stable that they can maintain their integrity over time even when subjected to environmental stresses. The analysis of biomarkers may also be utilized to determine the original source of an unknown oil spill, a process typically referred to as oil fingerprinting. Recent MS research has utilized biomarkers for both geochemistry and oil fingerprinting applications.

GC/(+) EI Q MS has been the primary technique utilized for geochemical characterization of crude oil because it is capable of separating saturated hydrocarbon biomarkers. Several recent studies have utilized GC/(+) EI Q MS for the geochemical analysis of crude oils from different oil wells throughout the world.<sup>165–168</sup> However, possible ionization biases or coeluting peaks, which can have a large impact on the accuracy of GC/(+) EI Q MS results, were not discussed.

Improving the reliability of geochemical characterization of petroleum samples by MS has been featured in recent literature. For example, Mogollón et al. utilized GC × GC/(+) EI QqQ MS for the geochemical analysis of two different crude oil samples from the Recôncavo basin in Brazil.<sup>169</sup> Coelution of compounds was found to be problematic when one-dimensional GC was employed due to the inherent complexity of crude oil samples. When GC × GC was used instead, the extent of compound coelution was reduced, leading to more accurate conclusions about the origins of the crude oil samples. Greater amounts of  $\Delta$ -nor-steranes with 19–26 carbons were found in one sample, suggesting that more sponges were present in the environment where this oil was formed compared to the other sample. Additionally, the measured abundances of hopanes, steranes, and terpanes suggested that one sample was formed under oxygen-rich conditions while the other was formed under nonoxygen rich conditions. Zhang et al. utilized GC × GC/(+) EI TOF MS to analyze the 2 $\alpha$ -methylhopane series of biomarkers in order to improve the geochemical characterization of 29 crude oil samples obtained from the Pearl River Mouth Basin of China.<sup>170</sup> Data obtained on the 2 $\alpha$ -methylhopane series enabled the assignment of some of the samples to lake source rock and others to lake-deltaic coal bearing source rock. Gao et al. built a homemade gas purge microsyringe extraction device that allowed them to analyze whole crude oil samples without the loss of the highly volatile biomarkers.<sup>171</sup> A crude oil sample was placed in a heated glass tube and connected to a microsyringe that collected the evaporated compounds. The same crude oil was deasphalted and fractionated into saturated hydrocarbons, aromatic compounds, and resins via column chromatography. The compounds in the saturated hydrocarbon fraction were compared to the evaporated sample obtained using the microsyringe. GC × GC/(+) EI TOF MS results obtained for the evaporated sample revealed many biomarkers containing 8–12 carbons, including light saturated hydrocarbons and diamondoids. Many of these compounds were not detected in the saturated hydrocarbon fraction of the same crude oil, thus suggesting that many of the most volatile biomarkers are lost when crude oil is separated via column chromatography.

The use of biomarkers to build chemometric models that would facilitate correlating a crude oil with its origin is of interest.<sup>172</sup> Recent chemometric studies have built models to enable the differentiation of crude oils and other petroleum



samples from one another as this is the first step toward generating predictive models. For example, Sun et al. performed a principal component analysis (PCA) and linear discriminant analysis (LDA) on GC/(+) EI Q MS data obtained for C2 chrysenes to build a model that can accurately predict whether a petroleum sample is crude oil, heavy fuel oil, or light fuel oil.<sup>173</sup> The GC/(+) EI Q MS data of the C2 chrysenes measured for a total of 172 samples, consisting of crude oil, heavy fuel oil, and light fuel oil samples, were used to build the PCA plus LDA model. Using this model, 128 test samples were correctly assigned to one of the three categories with 99% accuracy. On the other hand, Chang et al. performed PCA on the abundances of four volatile compounds, methylcyclohexane, dimethylcyclopentane, heptane, and toluene, to differentiate crude oils obtained from two locations in Zhu, China.<sup>174</sup> The compounds were identified using GC/(+) EI Q MS. A gas purge microsyringe extraction (GP-MSE) device, described previously,<sup>171</sup> was coupled to the GC/(+) EI Q MS to introduce hydrocarbons into the instrument. The same GP-MSE was attached to the front of a GC-FID to obtain accurate abundances for these four compounds. The PCA model was built based on the abundances measured for these four compounds in 14 crude oil samples obtained from each location. The PCA model was then used to correctly assign four test samples to their proper location, demonstrating the usefulness of light hydrocarbons to develop accurate chemometric models for crude oil.

#### ■ FUTURE DIRECTIONS

It is evident that the proper selection of the ionization method, or preferably several methods, prior to mass spectrometric analysis is a prerequisite for reliable analysis of petroleum samples. Fractionation prior to crude oil analysis has also been demonstrated to be critically important. Numerous independent efforts by various research groups have aimed at improving petroleum fractionation techniques, mass spectrometric ionization and analysis methods, and mass spectrometric instruments. Very high-resolution mass spectrometers can be used to identify differences in elemental compositions of compounds in petroleum samples with different geographical origins. Methods based on CAD can provide detailed information on the structures of the compounds in different petroleum samples. However, fast and automated chemometrics, data predictive, and data visualization tools are also needed to extract meaningful information from MS data regarding the chemical compositions and origins of different petroleum samples. With the wealth of chemical information that can now be obtained for petroleum samples, the mass spectrometry community is primed to solve many current and future challenges that face the petroleum industry.

#### ■ AUTHOR INFORMATION

##### Corresponding Author

\*Phone: +1 (765) 494 0882. Fax: +1 (765) 494 9421. E-mail: [hilkka@purdue.edu](mailto:hilkka@purdue.edu).

##### ORCID

Hilkka I. Kenttämää: 0000-0001-8988-6984

##### Present Address

<sup>‡</sup>R.Y.: Moderna Therapeutics, Cambridge, Massachusetts 02139, United States.

##### Author Contributions

<sup>†</sup>E.N. and J.M.M. contributed equally to this work.

#### Notes

The authors declare no competing financial interest.

#### Biographies

**Edouard Niyonsaba** obtained a B.S. in ACS Biochemistry and a minor in Mathematics from the University of Central Arkansas in 2015. He is currently a Ph.D. candidate in the Analytical Chemistry Division under the direction of Professor Hilkka I. Kenttämää at Purdue University. His research focuses on mass spectrometric analysis of crude oils of different API gravity and different origins and mass spectrometric method development for identification of drug metabolites.

**Jeremy M. Manheim** is a Ph.D. candidate in Professor Hilkka Kenttämää's group at Purdue University. He received his B.S. in Chemistry from the University at Albany, SUNY, in 2015 with an emphasis in forensic sciences. At Purdue, he is pursuing his interests in applied and fundamental aspects of mass spectrometry. His current projects include chemical characterization of crude oils and base oils, exploring the mechanism(s) of APCI of saturated hydrocarbons, and structural analysis of metals dissolved in organic solutions.

**Ravikiran Yerabolu** received his B.S. in Pharmacy from Dr. M.G.R. Medical University and his M.S. in Analytical Chemistry from Governor's State University. He received his Ph.D. in Chemistry from Purdue University in 2018 under the supervision of Professor Hilkka Kenttämää. His graduate research work focused on developing analytical methods for the characterization of complex mixtures, including crude oil, asphaltene, and drug metabolites. Since graduation, he has been working as a scientist at Moderna Therapeutics, Cambridge, MA. His current research focuses on developing mass spectrometry methods for the identification, quantitation, and structural characterization of nucleic acids, proteins, lipids, drug metabolites, and other biomolecules.

**Hilkka I. Kenttämää** received her Ph.D. in Organic Chemistry from Helsinki University, Finland, in 1986. She held postdoctoral and research scientist positions with Professor Graham Cooks at Purdue University from 1986 to 1989. She began her faculty career at Purdue University in 1989 and is currently the Frank Brown Distinguished Professor of Chemistry at Purdue University. Her research focuses on fundamental organic radical chemistry and development of mass spectrometric methods for the characterization of complex mixtures of organic compounds, such as crude oil, crude oil conversion products, biomass degradation products, fuels, and drug metabolites.

#### ■ ACKNOWLEDGMENTS

The authors thank Leah Easterling and Xueming Dong from Purdue University for their contributions towards editing this review.

#### ■ REFERENCES

- (1) Marshall, A. G.; Rodgers, R. P. *Acc. Chem. Res.* **2004**, *37* (1), 53–59.
- (2) Altgelt, K. H.; Boduszynski, M. M. *Composition and Analysis of Heavy Petroleum Fractions*; CRC Press, 1993.
- (3) Miller, R. J. *Petroleum Economics*. In *Standard Handbook of Petroleum and Natural Gas Engineering*; Elsevier, 1996; pp 985–1033, DOI: 10.1016/B978-088415643-7/50011-X.
- (4) Pan, Y.; Liao, Y.; Shi, Q. *Energy Fuels* **2017**, *31* (2), 1126–1135.
- (5) Borton, D.; Pinkston, D. S.; Hurt, M. R.; Tan, X.; Azyat, K.; Scherer, A.; Tykwinski, R.; Gray, M.; Qian, K.; Kenttämää, H. I. *Energy Fuels* **2010**, *24* (10), 5548–5559.
- (6) Hendrickson, C. L.; Quinn, J. P.; Kaiser, N. K.; Smith, D. F.; Blakney, G. T.; Chen, T.; Marshall, A. G.; Weisbrod, C. R.; Beu, S. C. *J. Am. Soc. Mass Spectrom.* **2015**, *26* (9), 1626–1632.

- (7) Shaw, J. B.; Lin, T.-Y.; Leach, F. E.; Tolmachev, A. V.; Tolić, N.; Robinson, E. W.; Koppenaal, D. W.; Paša-Tolić, L. *J. Am. Soc. Mass Spectrom.* **2016**, *27* (12), 1929–1936.
- (8) Rodgers, R. P.; Schaub, T. M.; Marshall, A. G. *Anal. Chem.* **2005**, *77* (1), 20 A–27 A.
- (9) Rodgers, R. P.; McKenna, A. M. *Anal. Chem.* **2011**, *83* (12), 4665–4687.
- (10) Cho, Y.; Ahmed, A.; Islam, A.; Kim, S. *Mass Spectrom. Rev.* **2015**, *34* (2), 248–263.
- (11) Smith, D. F.; Podgorski, D. C.; Rodgers, R. P.; Blakney, G. T.; Hendrickson, C. L. *Anal. Chem.* **2018**, *90* (3), 2041–2047.
- (12) Cho, E.; Witt, M.; Hur, M.; Jung, M.-J.; Kim, S. *Anal. Chem.* **2017**, *89* (22), 12101–12107.
- (13) Rüger, C. P.; Miersch, T.; Schwemer, T.; Sklorz, M.; Zimmermann, R. *Anal. Chem.* **2015**, *87* (13), 6493–6499.
- (14) Rüger, C. P.; Sklorz, M.; Schwemer, T.; Zimmermann, R. *Anal. Chem.* **2015**, *407* (20), 5923–5937.
- (15) Benigni, P.; DeBord, J. D.; Thompson, C. J.; Gardinali, P.; Fernandez-Lima, F. *Energy Fuels* **2016**, *30* (1), 196–203.
- (16) Krajewski, L. C.; Rodgers, R. P.; Marshall, A. G. *Anal. Chem.* **2017**, *89* (21), 11318–11324.
- (17) Gavard, R.; Rossell, D.; Spencer, S. E. F.; Barrow, M. P. *Anal. Chem.* **2017**, *89* (21), 11383–11390.
- (18) Martins, L. L.; Pudenz, M. A.; da Cruz, G. F.; Nascimento, H. D. L.; Eberlin, M. N. *Energy Fuels* **2017**, *31* (7), 6649–6657.
- (19) Vaz, B. G.; Silva, R. C.; Klitzke, C. F.; Simas, R. C.; Lopes Nascimento, H. D.; Pereira, R. C.; Garcia, D. F.; Eberlin, M. N.; Azevedo, D. A. *Energy Fuels* **2013**, *27* (3), 1277–1284.
- (20) Handle, F.; Harir, M.; Füssl, J.; Koyun, A. N.; Grossegger, D.; Hertkorn, N.; Eberhardsteiner, L.; Hofko, B.; Hospodka, M.; Blab, R.; Schmitt-Kopplin, P. *Energy Fuels* **2017**, *31* (5), 4771–4779.
- (21) Rüger, C. P.; Neumann, A.; Sklorz, M.; Schwemer, T.; Zimmermann, R. *Energy Fuels* **2017**, *31* (12), 13144–13158.
- (22) Cho, Y.; Birdwell, J. E.; Hur, M.; Lee, J.; Kim, B.; Kim, S. *Energy Fuels* **2017**, *31* (8), 7874–7883.
- (23) Schmidt, E. M.; Pudenz, M. A.; Santos, J. M.; Angolini, C. F. F.; Pereira, R. C. L.; Rocha, Y. S.; Denisov, E.; Damoc, E.; Makarov, A.; Eberlin, M. N. *RSC Adv.* **2018**, *8* (11), 6183–6191.
- (24) Kostyukevich, Y.; Zhrebek, A.; Vlaskin, M. S.; Borisova, L.; Nikolaev, E. *Anal. Chem.* **2018**, *90* (15), 8756–8763.
- (25) Liu, Z.; Phillips, J. B. *J. Chromatogr. Sci.* **1991**, *29* (6), 227–231.
- (26) Vendeuvre, C.; Ruiz-Guerrero, R.; Bertocini, F.; Duval, L.; Thiébaud, D.; Hennion, M.-C. *J. Chromatogr. A* **2005**, *1086* (1), 21–28.
- (27) van der Westhuizen, R.; Ajam, M.; De Coning, P.; Beens, J.; de Villiers, A.; Sandra, P. *J. Chromatogr. A* **2011**, *1218* (28), 4478–4486.
- (28) Luning Prak, D. J.; Romanczyk, M.; Wehde, K. E.; Ye, S.; McLaughlin, M.; Luning Prak, P. J.; Foley, M. P.; Kenttämää, H. I.; Trulove, P. C.; Kilaz, G.; Lan, X.; Cowart, J. S. *Energy Fuels* **2017**, *31* (12), 13802–13814.
- (29) Vozka, P.; Mo, H.; Šimáček, P.; Kilaz, G. *Talanta* **2018**, *186*, 140–146.
- (30) Alexandrino, G. L.; de Sousa, G. R.; de A. M. Reis, F.; Augusto, F. *J. Chromatogr. A* **2018**, *1536*, 82–87.
- (31) Potgieter, H.; Bekker, R.; Beigley, J.; Rohwer, E. *J. Chromatogr. A* **2017**, *1509*, 123–131.
- (32) Jennerwein, M. K.; Eschner, M. S.; Wilharm, T.; Zimmermann, R.; Gröger, T. M. *Energy Fuels* **2017**, *31* (11), 11651–11659.
- (33) American Society for Testing and Materials (ASTM). *Standard Test Method for Boiling Point Distribution of Samples with Residues Such as Crude Oils and Atmospheric and Vacuum Residues by High Temperature Gas Chromatography*, ASTM D7169-11, 2011.
- (34) Byer, J. D.; Siek, K.; Jobst, K. *Anal. Chem.* **2016**, *88* (12), 6101–6104.
- (35) Cumeras, R.; Figueras, E.; Davis, C. E.; Baumbach, J. I.; Gràcia, I. *Analyst* **2015**, *140* (5), 1376–1390.
- (36) May, J. C.; McLean, J. A. *Anal. Chem.* **2015**, *87* (3), 1422–1436.
- (37) Ridgeway, M. E.; Lubeck, M.; Jordens, J.; Mann, M.; Park, M. *A. Int. J. Mass Spectrom.* **2018**, *425*, 22–35.
- (38) Cumeras, R.; Figueras, E.; Davis, C. E.; Baumbach, J. I.; Gràcia, I. *Analyst* **2015**, *140* (5), 1391–1410.
- (39) Fernandez-Lima, F. A.; Becker, C.; McKenna, A. M.; Rodgers, R. P.; Marshall, A. G.; Russell, D. H. *Anal. Chem.* **2009**, *81* (24), 9941–9947.
- (40) Lalli, P. M.; Jarvis, J. M.; Marshall, A. G.; Rodgers, R. P. *Energy Fuels* **2017**, *31* (1), 311–318.
- (41) Lalli, P. M.; Corilo, Y. E.; Rowland, S. M.; Marshall, A. G.; Rodgers, R. P. *Energy Fuels* **2015**, *29* (6), 3626–3633.
- (42) Santos, J. M.; Galaverna, R.; de, S.; Pudenz, M. A.; Schmidt, E. M.; Sanders, N. L.; Kurulugama, R. T.; Mordehai, A.; Stafford, G. C.; Wisniewski, A.; Eberlin, M. N. *Anal. Methods* **2015**, *7* (11), 4450–4463.
- (43) Farenc, M.; Corilo, Y. E.; Lalli, P. M.; Riches, E.; Rodgers, R. P.; Afonso, C.; Giusti, P. *Energy Fuels* **2016**, *30* (11), 8896–8903.
- (44) Ahmed, A.; Cho, Y.; Giles, K.; Riches, E.; Lee, J. W.; Kim, H. I.; Choi, C. H.; Kim, S. *Anal. Chem.* **2014**, *86* (7), 3300–3307.
- (45) Farenc, M.; Paupy, B.; Marceau, S.; Riches, E.; Afonso, C.; Giusti, P. *J. Am. Soc. Mass Spectrom.* **2017**, *28* (11), 2476–2482.
- (46) Ibrahim, Y. M.; Garimella, S. V. B.; Prost, S. A.; Wojcik, R.; Norheim, R. V.; Baker, E. S.; Rusyn, L.; Smith, R. D. *Anal. Chem.* **2016**, *88* (24), 12152–12160.
- (47) Panda, S. K.; Andersson, J. T.; Schrader, W. *Angew. Chem.* **2009**, *121* (10), 1820–1823.
- (48) Gaspar, A.; Zellermann, E.; Lababidi, S.; Reece, J.; Schrader, W. *Anal. Chem.* **2012**, *84* (12), 5257–5267.
- (49) Ruddy, B. M.; Hendrickson, C. L.; Rodgers, R. P.; Marshall, A. G. *Energy Fuels* **2018**, *32*, 2901–2907.
- (50) Klesper, G.; Röhlgen, F. *J. Mass Spectrom.* **1996**, *31* (4), 383–388.
- (51) Qian, K.; Dechert, G. *J. Anal. Chem.* **2002**, *74* (16), 3977–3983.
- (52) Hourani, N.; Kuhnert, N. *Anal. Methods* **2012**, *4* (3), 730–735.
- (53) Hourani, N.; Muller, H.; Adam, F. M.; Panda, S. K.; Witt, M.; Al-Hajji, A. A.; Sarathy, S. M. *Energy Fuels* **2015**, *29* (5), 2962–2970.
- (54) Yerabolu, R.; Kotha, R. R.; Niyonsaba, E.; Dong, X.; Manheim, J. M.; Kong, J.; Riedeman, J. S.; Romanczyk, M.; Johnston, C. T.; Kilaz, G.; Kenttämää, H. I. *Fuel* **2018**, *234*, 492–501.
- (55) Tose, L. V.; Cardoso, F. M. R.; Fleming, F. P.; Vicente, M. A.; Silva, S. R. C.; Aqueje, G. M. F. V.; Vaz, B. G.; Romão, W. *Fuel* **2015**, *153*, 346–354.
- (56) Jin, C.; Viidanoja, J.; Li, M.; Zhang, Y.; Ikonen, E.; Root, A.; Romanczyk, M.; Manheim, J.; Dziekonski, E.; Kenttämää, H. I. *Anal. Chem.* **2016**, *88* (21), 10592–10598.
- (57) Zhang, T.; Li, Z.-Y.; Zhang, M.-Q.; He, S.-G. *J. Phys. Chem. A* **2016**, *120* (25), 4285–4293.
- (58) Wu, C.; Qian, K.; Walters, C. C.; Mennito, A. *Int. J. Mass Spectrom.* **2015**, *377*, 728–735.
- (59) Ren, L.; Han, Y.; Zhang, Y.; Zhang, Y.; Meng, X.; Shi, Q. *Energy Fuels* **2016**, *30* (6), 4486–4493.
- (60) Kim, D.; Yim, U. H.; Kim, B.; Cha, S.; Kim, S. *Anal. Chem.* **2017**, *89* (17), 9056–9061.
- (61) Tang, W.; Sheng, H.; Jin, C.; Riedeman, J. S.; Kenttämää, H. I. *Rapid Commun. Mass Spectrom.* **2016**, *30* (7), 953–962.
- (62) Valencia-Dávila, J. A.; Blanco-Tirado, C.; Combariza, M. Y. *Fuel* **2017**, *193*, 168–177.
- (63) Tose, L. V.; Murgu, M.; Vaz, B. G.; Romão, W. *J. Am. Soc. Mass Spectrom.* **2017**, *28* (11), 2401–2407.
- (64) Vetere, A.; Schrader, W. *Anal. Chem.* **2015**, *87* (17), 8874–8879.
- (65) Lu, J.; Zhang, Y.; Shi, Q. *Anal. Chem.* **2016**, *88* (7), 3471–3475.
- (66) Basuri, P.; Sarkar, D.; Paramasivam, G.; Pradeep, T. *Anal. Chem.* **2018**, *90* (7), 4663–4668.
- (67) Cha, E.; Jeong, E. S.; Han, S. B.; Cha, S.; Son, J.; Kim, S.; Oh, H. B.; Lee, J. *Anal. Chem.* **2018**, *90* (6), 4203–4211.
- (68) Pomerantz, A. E.; Wu, Q.; Mullins, O. C.; Zare, R. N. *Energy Fuels* **2015**, *29* (5), 2833–2842.

- (69) Acter, T.; Lee, S.; Cho, E.; Jung, M.-J.; Kim, S. *J. Am. Soc. Mass Spectrom.* **2018**, *29* (1), 85–94.
- (70) Cho, Y.; Na, J.-G.; Nho, N.-S.; Kim, S.; Kim, S. *Energy Fuels* **2012**, *26* (5), 2558–2565.
- (71) Bissada, K. K.; Tan, J.; Szymczyk, E.; Darnell, M.; Mei, M. *Org. Geochem.* **2016**, *95*, 21–28.
- (72) Bissada, K. K.; Tan, J.; Szymczyk, E.; Darnell, M.; Mei, M. *Fuel* **2016**, *173*, 217–221.
- (73) Robson, W. J.; Sutton, P. A.; McCormack, P.; Chilcott, N. P.; Rowland, S. J. *Anal. Chem.* **2017**, *89* (5), 2919–2927.
- (74) Putman, J. C.; Rowland, S. M.; Podgorski, D. C.; Robbins, W. K.; Rodgers, R. P. *Energy Fuels* **2017**, *31* (11), 12064–12071.
- (75) Giraldo-Dávila, D.; Chacón-Patiño, M. L.; Orrego-Ruiz, J. A.; Blanco-Tirado, C.; Combariza, M. Y. *Fuel* **2016**, *185*, 45–58.
- (76) Pinkston, D. S.; Duan, P.; Gallardo, V. A.; Habicht, S. C.; Tan, X.; Qian, K.; Gray, M.; Müllen, K.; Kenttämä, H. I. *Energy Fuels* **2009**, *23* (11), 5564–5570.
- (77) Huba, A. K.; Gardinali, P. R. *Sci. Total Environ.* **2016**, *563*–564, 600–610.
- (78) Otto, S.; Streibel, T.; Erdmann, S.; Sklorz, M.; Schulz-Bull, D.; Zimmermann, R. *Anal. Chim. Acta* **2015**, *855*, 60–69.
- (79) Vanini, G.; Pereira, V. B.; Romão, W.; Gomes, A. O.; Oliveira, L. M. S. L.; Dias, J. C. M.; Azevedo, D. A. *Microchem. J.* **2018**, *137*, 111–118.
- (80) Genuit, W.; Chaabani, H. *Int. J. Mass Spectrom.* **2017**, *413*, 27–32.
- (81) Li, S.; Cao, J.; Hu, S. *Fuel* **2015**, *158*, 191–199.
- (82) Li, X.; Yan, X.; Cooks, R. G. *Int. J. Mass Spectrom.* **2017**, *418*, 79–85.
- (83) Li, G.; Li, X.; Ouyang, Z.; Cooks, R. G. *Angew. Chem., Int. Ed.* **2013**, *52* (3), 1040–1043.
- (84) Demirbas, A.; Alidrisi, H.; Balubaid, M. A. *Pet. Sci. Technol.* **2015**, *33* (1), 93–101.
- (85) Han, Y.; Zhang, Y.; Xu, C.; Hsu, C. S. *Fuel* **2018**, *221*, 144–158.
- (86) Corilo, Y. E.; Rowland, S. M.; Rodgers, R. P. *Energy Fuels* **2016**, *30* (5), 3962–3966.
- (87) Purcell, J. M.; Hendrickson, C. L.; Rodgers, R. P.; Marshall, A. G. *J. Am. Soc. Mass Spectrom.* **2007**, *18* (9), 1682–1689.
- (88) Lobodin, V. V.; Juyal, P.; McKenna, A. M.; Rodgers, R. P.; Marshall, A. G. *Energy Fuels* **2014**, *28* (1), 447–452.
- (89) Maleki, H.; Ghassabi Kondalaji, S.; Khakinejad, M.; Valentine, S. J. *Energy Fuels* **2016**, *30* (11), 9150–9161.
- (90) Lobodin, V. V.; Robbins, W. K.; Lu, J.; Rodgers, R. P. *Energy Fuels* **2015**, *29* (10), 6177–6186.
- (91) Laali, K. K.; Hupertz, S.; Temu, A. G.; Galembeck, S. E. *Org. Biomol. Chem.* **2005**, *3* (12), 2319–2326.
- (92) Takino, M.; Daishima, S.; Yamaguchi, K.; Nakahara, T. *J. Chromatogr. A* **2001**, *928* (1), 53–61.
- (93) Acter, T.; Kim, D.; Ahmed, A.; Ha, J.-H.; Kim, S. *J. Am. Soc. Mass Spectrom.* **2017**, *28* (8), 1687–1695.
- (94) Bjerk, T. R.; de Menezes, E. W.; Pereira, M. B.; Caramão, E. B.; Benvenutti, E. V.; Zini, C. A. *J. Chromatogr. A* **2016**, *1470*, 104–110.
- (95) Wang, M.; Zhao, S.; Liu, X.; Shi, Q. *Anal. Chem.* **2016**, *88* (19), 9837–9842.
- (96) Wang, M.; Zhao, S.; Chung, K. H.; Xu, C.; Shi, Q. *Anal. Chem.* **2015**, *87* (2), 1083–1088.
- (97) Wang, M.; Zhu, G.; Ren, L.; Liu, X.; Zhao, S.; Shi, Q. *Energy Fuels* **2015**, *29* (8), 4842–4849.
- (98) Wang, P.; Xu, C.; Zhang, Y.; Wang, M.; Shi, Q. *Energy Fuels* **2018**, *32*, 10571–10579.
- (99) Wang, X.; Schrader, W. *Int. J. Mol. Sci.* **2015**, *16* (12), 30133–30143.
- (100) Zhu, G.; Wang, M.; Zhang, Y.; Zhang, Z. *Energy Fuels* **2018**, *32* (6), 6770–6773.
- (101) Dijkmans, T.; Djokic, M. R.; Van Geem, K. M.; Marin, G. B. *Fuel* **2015**, *140*, 398–406.
- (102) Ha, J.; Cho, E.; Kim, S. *Energy Fuels* **2017**, *31* (7), 6960–6967.
- (103) Kim, D.; Jin, J. M.; Cho, Y.; Kim, E.-H.; Cheong, H.-K.; Kim, Y. H.; Kim, S. *Fuel* **2015**, *157*, 48–55.
- (104) Chen, X.; Liu, Y.; Li, S.; Feng, X.; Shan, H.; Yang, C. *Energy Fuels* **2017**, *31* (4), 3659–3668.
- (105) Celis-Cornejo, C. M.; Pérez-Martínez, D. J.; Orrego-Ruiz, J. A.; Baldovino-Medrano, V. G. *Energy Fuels* **2018**, *32* (8), 8715–8726.
- (106) Cho, Y.; Ahmed, A.; Kim, S. *Anal. Chem.* **2013**, *85* (20), 9758–9763.
- (107) Ahmed, A.; Kim, S. *J. Am. Soc. Mass Spectrom.* **2013**, *24* (12), 1900–1905.
- (108) Acter, T.; Cho, Y.; Kim, S.; Ahmed, A.; Kim, B.; Kim, S. *J. Am. Soc. Mass Spectrom.* **2015**, *26* (9), 1522–1531.
- (109) Kim, E.; Cho, E.; Ahmed, A.; Kim, Y. H.; Kim, S. *Fuel* **2017**, *194*, 503–510.
- (110) Vasconcelos, G. A.; Pereira, R. C.; Santos, C. de F.; Carvalho, V. V.; Tose, L. V.; Romão, W.; Vaz, B. G. *Int. J. Mass Spectrom.* **2017**, *418*, 67–72.
- (111) Rowland, S. M.; Robbins, W. K.; Corilo, Y. E.; Marshall, A. G.; Rodgers, R. P. *Energy Fuels* **2014**, *28* (8), 5043–5048.
- (112) Sheng, Q.; Wang, G.; Liu, Y.; Husein, M. M.; Gao, C.; Shi, Q.; Gao, J. *Energy Fuels* **2018**, *32* (4), 4979–4987.
- (113) Zhang, K.; Yu, J.; Gao, S.; Li, C.; Xu, G. *Energy Fuels* **2017**, *31* (2), 1362–1369.
- (114) Terra, L. A.; Filgueiras, P. R.; Tose, L. V.; Romão, W.; de Castro, E. V. R.; de Oliveira, L. M. S. L.; Dias, J. C. M.; Vaz, B. G.; Poppi, R. J. *Fuel* **2015**, *160*, 274–281.
- (115) Headley, J. V.; Peru, K. M.; Barrow, M. P. *Mass Spectrom. Rev.* **2016**, *35* (2), 311–328.
- (116) Dias, H. P.; Dixini, P. V.; Almeida, L. C. P.; Vanini, G.; Castro, E. V. R.; Aquije, G. M. F. V.; Gomes, A. O.; Moura, R. R.; Lacerda, V.; Vaz, B. G.; Romão, W. *Fuel* **2015**, *139*, 328–336.
- (117) Meriem-Benziane, M.; Bou-Said, B.; Boudouani, N. J. *Pet. Sci. Eng.* **2017**, *158*, 672–679.
- (118) Orrego-Ruiz, J. A.; Gomez-Escudero, A.; Rojas-Ruiz, F. A. *Energy Fuels* **2016**, *30* (10), 8209–8215.
- (119) Rojas-Ruiz, F. A.; Orrego-Ruiz, J. A. *Energy Fuels* **2016**, *30* (10), 8185–8191.
- (120) Barros, E. V.; Dias, H. P.; Gomes, A. O.; Rodrigues, R. R.; Moura, R. R.; Sad, C. M.; Freitas, J. C.; Neto, A. C.; Aquije, G. M.; Romão, W. *J. Pet. Sci. Eng.* **2017**, *154*, 194–203.
- (121) Barros, E. V.; Dias, H. P.; Pinto, F. E.; Gomes, A. O.; Moura, R. R.; Neto, A. C.; Freitas, J. C.; Aquije, G. M. F. V.; Vaz, B. G.; Romão, W. *Energy Fuels* **2018**, *32* (3), 2878–2888.
- (122) Hindle, R.; Noestheden, M.; Peru, K.; Headley, J. J. *Chromatogr. A* **2013**, *1286*, 166–174.
- (123) Colati, K. A. P.; Dalmaschio, G. P.; de Castro, E. V. R.; Gomes, A. O.; Vaz, B. G.; Romão, W. *Fuel* **2013**, *108*, 647–655.
- (124) Valencia-Dávila, J. A.; Witt, M.; Blanco-Tirado, C.; Combariza, M. Y. *Fuel* **2018**, *231*, 126–133.
- (125) Clingenpeel, A. C.; Fredriksen, T. R.; Qian, K.; Harper, M. R. *Energy Fuels* **2018**, *32* (9), 9271–9279.
- (126) Gutierrez-Villagomez, J. M.; Vázquez-Martínez, J.; Ramírez-Chávez, E.; Molina-Torres, J.; Trudeau, V. L. *Talanta* **2017**, *162*, 440–452.
- (127) Davis, B. *Anal. Chem.* **1977**, *49* (6), 832–834.
- (128) Wilde, M. J.; Rowland, S. J. *Anal. Chem.* **2015**, *87* (16), 8457–8465.
- (129) Wilde, M. J.; Rowland, S. J. *Org. Geochem.* **2018**, *115*, 188–196.
- (130) Caumette, G.; Lienemann, C.-P.; Merdrignac, I.; Bouysiere, B.; Lobinski, R. *J. Anal. At. Spectrom.* **2009**, *24* (3), 263–276.
- (131) Akinlua, A.; Torto, N. *Anal. Lett.* **2006**, *39* (9), 1993–2005.
- (132) Sugiyama, I.; Williams-Jones, A. E. *Anal. Chim. Acta* **2018**, *1002*, 18–25.
- (133) Ali, M. F.; Abbas, S. *Fuel Process. Technol.* **2006**, *87* (7), 573–584.
- (134) Beauchemin, D. *Anal. Chem.* **2010**, *82* (12), 4786–4810.
- (135) Sánchez, R.; Todolí, J. L.; Lienemann, C.-P.; Mermet, J.-M. *Spectrochim. Acta, Part B* **2013**, *88*, 104–126.

- (136) Poirier, L.; Nelson, J.; Leong, D.; Berhane, L.; Hajdu, P.; Lopez-Linares, F. *Energy Fuels* **2016**, *30* (5), 3783–3790.
- (137) Walkner, C.; Gratzner, R.; Meisel, T.; Bokhari, S. N. H. *Org. Geochem.* **2017**, *103*, 22–30.
- (138) Balcaen, L.; Bolea-Fernandez, E.; Resano, M.; Vanhaecke, F. *Anal. Chim. Acta* **2015**, *894*, 7–19.
- (139) Czernuszewicz, R. S. *J. Porphyrins Phthalocyanines* **2000**, *4* (4), 426–431.
- (140) Liu, H.; Mu, J.; Wang, Z.; Ji, S.; Shi, Q.; Guo, A.; Chen, K.; Lu, J. *Energy Fuels* **2015**, *29* (8), 4803–4813.
- (141) Liu, T.; Lu, J.; Zhao, X.; Zhou, Y.; Wei, Q.; Xu, C.; Zhang, Y.; Ding, S.; Zhang, T.; Tao, X.; Ju, L.; Shi, Q. *Energy Fuels* **2015**, *29* (4), 2089–2096.
- (142) Gascon, G.; Vargas, V.; Feo, L.; Castellano, O.; Castillo, J.; Giusti, P.; Acavedo, S.; Lienemann, C.-P.; Bouyssiere, B. *Energy Fuels* **2017**, *31* (8), 7783–7788.
- (143) Barbier, J.; Marques, J.; Caumette, G.; Merdrignac, L.; Bouyssiere, B.; Lobinski, R.; Lienemann, C.-P. *Fuel Process. Technol.* **2014**, *119*, 185–189.
- (144) Gutierrez Sama, S.; Desprez, A.; Krier, G.; Lienemann, C.-P.; Barbier, J.; Lobinski, R.; Barrere-Mangote, C.; Giusti, P.; Bouyssiere, B. *Energy Fuels* **2016**, *30* (9), 6907–6912.
- (145) Striegel, A. M. *J. Liq. Chromatogr. Relat. Technol.* **2008**, *31* (20), 3105–3114.
- (146) Nelson, J.; Yamanaka, M.; Lopez-Linares, F.; Poirier, L.; Rogel, E. *Energy Fuels* **2017**, *31* (11), 11971–11976.
- (147) Cunico, R. L.; Sheu, E. Y.; Mullins, O. C. *Pet. Sci. Technol.* **2004**, *22* (7–8), 787–798.
- (148) Pinkston, D. S.; Duan, P.; Gallardo, V. A.; Habicht, S. C.; Tan, X.; Qian, K.; Gray, M.; Müllen, K.; Kenttämää, H. I. *Energy Fuels* **2009**, *23* (11), 5564–5570.
- (149) Pomerantz, A. E.; Hammond, M. R.; Morrow, A. L.; Mullins, O. C.; Zare, R. N. *J. Am. Chem. Soc.* **2008**, *130* (23), 7216–7217.
- (150) Fergoug, T.; Boukratem, C.; Bounaceur, B.; Bouhadda, Y. *Egypt. J. Pet.* **2017**, *26* (3), 803–810.
- (151) Acevedo, S.; Cordero, T. J. M.; Carrier, H.; Bouyssiere, B.; Lobinski, R. *Energy Fuels* **2009**, *23* (2), 842–848.
- (152) Tanaka, R.; Sato, S.; Takanohashi, T.; Hunt, J. E.; Winans, R. E. *Energy Fuels* **2004**, *18* (5), 1405–1413.
- (153) Zheng, C.; Zhu, M.; Zareie, R.; Zhang, D. *J. Pet. Sci. Eng.* **2018**, *168*, 148–155.
- (154) Koolen, H. H.; Gomes, A. F.; de Moura, L. G.; Marcano, F.; Cardoso, F. M.; Klitzke, C. F.; Wojcik, R.; Binkley, J.; Patrick, J. S.; Swarthout, R. F. *Fuel* **2018**, *220*, 717–724.
- (155) Riedeman, J. S.; Kadasala, N. R.; Wei, A.; Kenttämää, H. I. *Energy Fuels* **2016**, *30* (2), 805–809.
- (156) Wittrig, A. M.; Fredriksen, T. R.; Qian, K.; Clingenpeel, A. C.; Harper, M. R. *Energy Fuels* **2017**, *31* (12), 13338–13344.
- (157) Wang, W.; Dong, M.; Song, C.; Cai, X.; Liu, Y.; Liu, Z.; Tian, S. *Fuel* **2018**, *227*, 111–117.
- (158) Tang, W.; Hurt, M. R.; Sheng, H.; Riedeman, J. S.; Borton, D. J.; Slater, P.; Kenttämää, H. I. *Energy Fuels* **2015**, *29* (3), 1309–1314.
- (159) Nyadong, L.; Lai, J.; Thompsen, C.; LaFrancois, C. J.; Cai, X.; Song, C.; Wang, J.; Wang, W. *Energy Fuels* **2018**, *32* (1), 294–305.
- (160) Chacón-Patiño, M. L.; Rowland, S. M.; Rodgers, R. P. *Energy Fuels* **2017**, *31* (12), 13509–13518.
- (161) Chacón-Patiño, M. L.; Rowland, S. M.; Rodgers, R. P. *Energy Fuels* **2018**, *32* (1), 314–328.
- (162) Chacón-Patiño, M. L.; Rowland, S. M.; Rodgers, R. P. *Energy Fuels* **2018**, *32* (9), 9106–9120.
- (163) Podgorski, D. C.; Corilo, Y. E.; Nyadong, L.; Lobodin, V. V.; Bythell, B. J.; Robbins, W. K.; McKenna, A. M.; Marshall, A. G.; Rodgers, R. P. *Energy Fuels* **2013**, *27* (3), 1268–1276.
- (164) Wang, Z.; Stout, S. A.; Fingas, M. *Environ. Forensics* **2006**, *7* (2), 105–146.
- (165) Faraj, M. A. M.; Šolević Knudsen, T.; Nytoft, H. P.; Jovančević, B. *J. Pet. Sci. Eng.* **2016**, *147*, 605–616.
- (166) El-Sabagh, S. M.; El-Naggar, A. Y.; El Nady, M. M.; Ebiad, M. A.; Rashad, A. M.; Abdullah, E. S. *Egypt. J. Pet.* **2018**, DOI: 10.1016/j.ejpe.2018.02.005.
- (167) Hakimi, M. H.; Al-Sufi, S. A. *Egypt. J. Pet.* **2018**, *27* (1), 37–54.
- (168) Yang, C.; Lambert, P.; Zhang, G.; Yang, Z.; Landriault, M.; Hollebone, B.; Fieldhouse, B.; Mirmaghi, F.; Brown, C. E. *Environ. Pollut.* **2017**, *230*, 609–620.
- (169) Mogollón, N. G. S.; Prata, P. S.; dos Reis, J. Z.; Neto, E. V. d. S.; Augusto, F. J. *Sep. Sci.* **2016**, *39* (17), 3384–3391.
- (170) Zhang, W.; Jiang, X.; Pang, L.; Gao, X.; Zhu, S. *Aquat. Geochem.* **2017**, *23* (3), 185–198.
- (171) Gao, X.; Zhu, S.; Zhang, W.; Li, D.; Dai, W.; He, S. *Fuel* **2016**, *182*, 788–797.
- (172) Christensen, J. H.; Tomasi, G. J. *Chromatogr. A* **2007**, *1169* (1–2), 1–22.
- (173) Sun, P.; Bao, K.; Li, H.; Li, F.; Wang, X.; Cao, L.; Li, G.; Zhou, Q.; Tang, H.; Bao, M. *Fuel* **2018**, *222*, 416–423.
- (174) Chang, Z.; Zhang, W.; Ge, X.; Zhu, S. *Fuel* **2018**, *221*, 179–187.

## Differentiating Isomeric Deprotonated Glucuronide Drug Metabolites via Ion/Molecule Reactions in Tandem Mass Spectrometry

John Y. Kong,<sup>†,‡</sup> Zaikuan Yu,<sup>†,‡</sup> McKay W. Easton,<sup>†</sup> Edouard Niyonsaba,<sup>†</sup> Xin Ma,<sup>†,§</sup> Ravikiran Yerabolu,<sup>†</sup> Huaming Sheng,<sup>†</sup> Tiffany M. Jarrell,<sup>§</sup> Zhoupeng Zhang,<sup>||</sup> Arun K. Ghosh,<sup>†,||</sup> and Hilkka I. Kenttämä<sup>\*,†,||</sup>

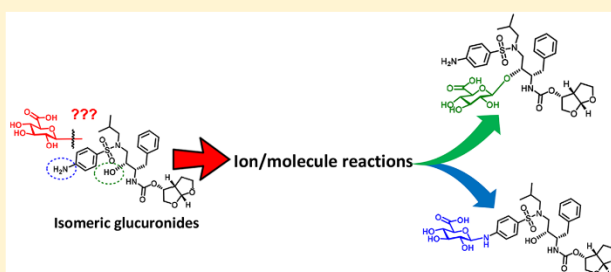
<sup>†</sup>Department of Chemistry, Purdue University, West Lafayette, Indiana 47907, United States

<sup>‡</sup>Department of Analytical Research & Development, Merck & Co., Inc., Rahway, New Jersey 07065, United States

<sup>§</sup>Department of Animal Health, Merck Animal Health, Rahway, New Jersey 07065, United States

<sup>||</sup>Department of Pharmacokinetics, Pharmacodynamics, & Drug Metabolism, Merck & Co., Inc., West Point, Pennsylvania 19486, United States

### Supporting Information



**ABSTRACT:** Isomeric O- and N-glucuronides are common drug metabolites produced in phase II of drug metabolism. Distinguishing these isomers by using common analytical techniques has proven challenging. A tandem mass spectrometric method based on gas-phase ion/molecule reactions of deprotonated glucuronide drug metabolites with trichlorosilane (HSiCl<sub>3</sub>) in a linear quadrupole ion trap mass spectrometer is reported here to readily enable differentiation of the O- and N-isomers. The major product ion observed upon reactions of HSiCl<sub>3</sub> with deprotonated N-glucuronides is a diagnostic HSiCl<sub>3</sub> adduct that has lost two HCl molecules ([M – H + HSiCl<sub>3</sub> – 2HCl]<sup>–</sup>). This product ion was not observed for deprotonated O-glucuronides. Reaction mechanisms were explored with quantum chemical calculations at the M06-2X/6-311++G(d,p) level of theory.

Glucuronidation is a common pathway of drug metabolism for xenobiotic drugs and endobiotic compounds.<sup>1</sup> Glucuronidation is catalyzed by the superfamily of uridine diphosphate glucuronosyl transferase (UGT) enzymes that transfer glucuronic acid from uridine 5'-diphosphoglucuronic acid (UDP-GlcA) to target substrates.<sup>2</sup> Glucuronidation occurs on functional groups that contain a nucleophilic O- or N-atom, such as amino and hydroxyl groups.<sup>3</sup> Even parent drugs that do not possess such groups can have O- and/or N-atoms added through prior oxidative metabolism, making them susceptible to glucuronidation.<sup>4,5</sup> When a parent drug contains both O- and N-heteroatoms, glucuronidation can occur at either site, which can produce isomeric glucuronide metabolites. For instance, carvedilol (1), used for treatment of hypertension, angina, and congestive heart failure, contains three sites susceptible to glucuronidation (2–4) (Scheme 1).<sup>2,5</sup>

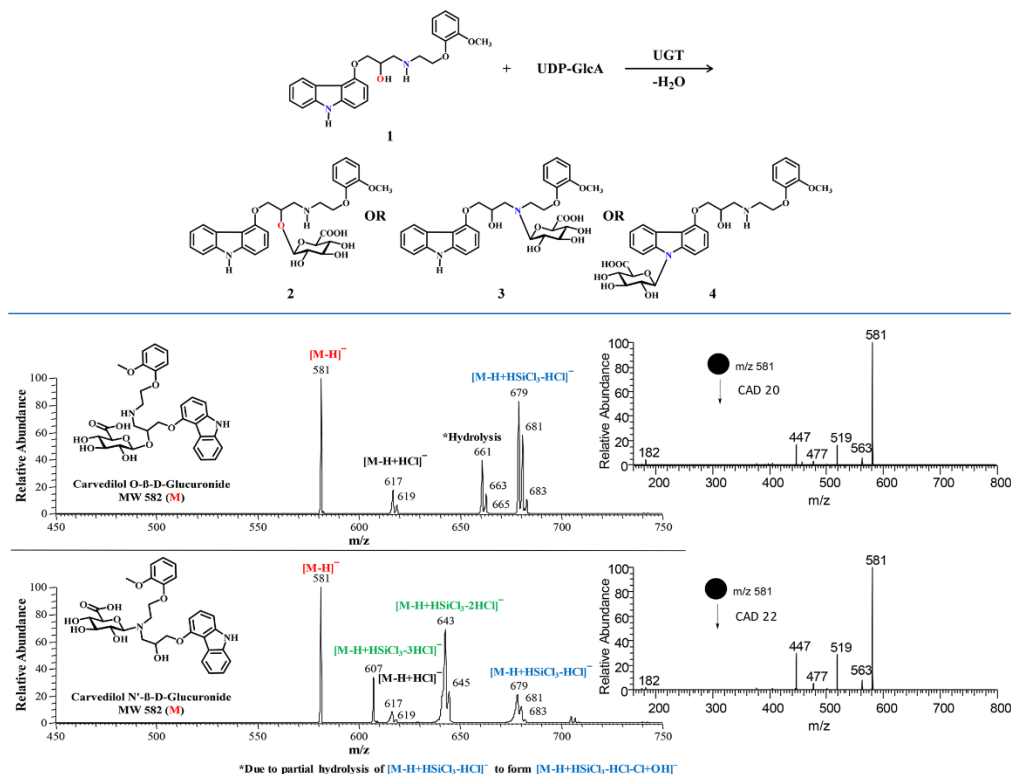
More than 20% of current drugs are glucuronidated by UGTs to produce water-soluble glucuronide metabolites that are more easily excreted in bile or urine.<sup>6</sup> Glucuronidation shortens the half-life of drugs,<sup>7</sup> which is often compensated for by administering a higher dosage of the drug. This, however, can lead to undesirable side effects.<sup>8</sup> Knowing the glucuronidation site allows targeted chemical modifications of the drug to prohibit glucuronidation, thereby improving the efficacy of the drug.<sup>9</sup> The various approaches appearing in the literature for the identification of the glucuronidation sites of drugs are limited in scope and practicality. For example, selective acetylation of the hydroxyl and/or amino groups

Received: May 10, 2018

Accepted: July 9, 2018

Published: July 9, 2018



Scheme 1. Carvedilol (1) and Its Possible *O*-Glucuronide (2) and *N*-Glucuronide (3,4) Metabolites

**Figure 1.** Mass spectra measured after 30 ms reaction of deprotonated carvedilol *O*-β-D-glucuronide (top) and carvedilol *N*'-β-D-glucuronide (bottom) with HSiCl<sub>3</sub>. The chlorine isotopes support the identification of the products. As a result of the existence of trace levels of water in the ion trap, the primary product ion [M - H + HSiCl<sub>3</sub> - HCl]<sup>-</sup> is sometimes partially hydrolyzed to form a secondary product ion [M - H + HSiCl<sub>3</sub> - HCl - Cl + OH]<sup>-</sup> (indicated above as \*Hydrolysis). Also, a simple HCl adduct ([M - H + HCl]<sup>-</sup>) is sometimes formed due to the generation of HCl via decomposition of HSiCl<sub>3</sub> upon reactions with water in the ion trap. Inserts show the CAD mass spectra of isolated deprotonated carvedilol *O*-β-D-glucuronide (top) and *N*'-β-D-glucuronide (bottom).

within a glucuronide has been explored for the identification of the site of glucuronidation based on the number of acetyl groups added.<sup>2</sup> However, this approach, which requires time-consuming isolation and derivatization of the metabolite, has only proven reliable for carvedilol.<sup>5</sup> In another study, the pH stability of <sup>14</sup>C-labeled glucuronides was used to differentiate *O*- and *N*-glucuronides.<sup>4,9</sup> Although this method is simple, the extensive modification of glucuronides by radiolabeling prevents its application to high-throughput analysis. While NMR is the gold standard for elucidating the structures of organic molecules, it requires high quantities of relatively pure compounds and therefore is not suitable for elucidating the structures of trace compounds in complex metabolite mixtures.<sup>10</sup>

Mass spectrometry (MS) combined with chromatography is a powerful approach for identifying minor components of complex mixtures. However, electron ionization mass spectrometry often requires authentic compounds for unambiguous identification and even then sometimes fails to differentiate

isomeric compounds. The same is true for tandem mass spectrometry (MS/MS) based on collision-activated dissociation (CAD). For example, the major fragmentation pathway for many positively and negatively charged glucuronides corresponds to the elimination of the glucuronyl moiety, which hinders the differentiation of isomeric glucuronides.<sup>2,11</sup> In some cases, the CAD mass spectra of ionized isomeric glucuronides are essentially identical, as for example, those of deprotonated carvedilol *N*- and *O*-glucuronides shown in Figure 1. Another example of uninformative CAD mass spectra is shown in Figure S1 for deprotonated carvedilol isomers. On the other hand, gas-phase ion/molecule reactions have been successfully utilized in MS/MS experiments to elucidate the structures of many isomeric compounds that cannot be differentiated by CAD,<sup>12–29</sup> including drug metabolites. We report here the discovery of a diagnostic reaction between trichlorosilane (HSiCl<sub>3</sub>) and deprotonated *N*-glucuronides that can be used for the unambiguous differentiation of *N*- and *O*-glucuronides.

**Table 1. Primary Product Ions and Their Branching Ratios<sup>a</sup> along with Their Observed Secondary Product Ions for Reactions of Deprotonated *O*- and *N*-Glucuronides and Glucuronic Acid with HSiCl<sub>3</sub>**

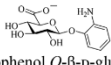
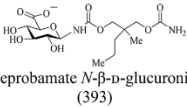
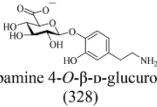
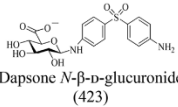
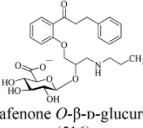
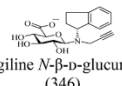
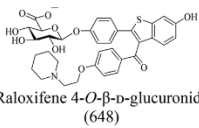
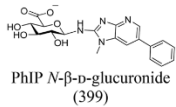
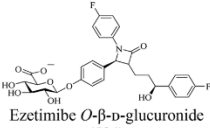
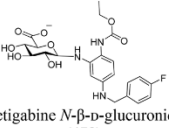
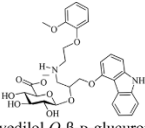
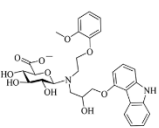
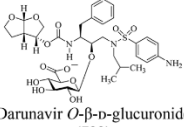
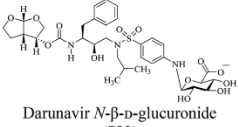
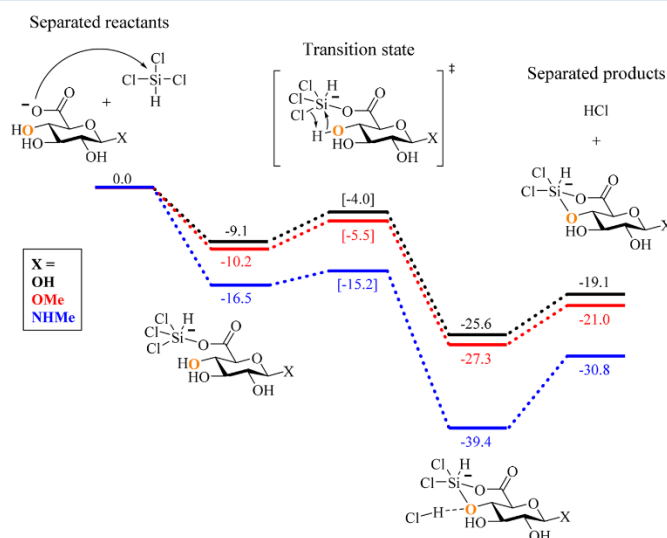
<i>O</i> -Glucuronides ( <i>m/z</i> of deprotonated analyte)	1° ionic reaction products ( <i>m/z</i> ) and their branching ratios  2° ionic reaction products	<i>N</i> -Glucuronides ( <i>m/z</i> of deprotonated analyte)	1° ionic reaction products ( <i>m/z</i> ) and their branching ratios  2° ionic reaction products
 2-Aminophenol <i>O</i> -β-D-glucuronide (284)	$[M-H+HCl]^-$ (320) 29% $[M-H+HSiCl_3-HCl]^-$ (382) 71% Hydrolysis <sup>b</sup> (2°)	 Meprobamate <i>N</i> -β-D-glucuronide (393)	$[M-H+HSiCl_3-2HCl]^-$ (455) 94% $[M-H+HSiCl_3-HCl]^-$ (491) 6%
 Dopamine 4- <i>O</i> -β-D-glucuronide (328)	$[M-H+HCl]^-$ (364) 10% $[M-H+HSiCl_3-HCl]^-$ (426) 90% Hydrolysis <sup>b</sup> (2°)	 Dapsone <i>N</i> -β-D-glucuronide (423)	$[M-H+HCl]^-$ (459) 2% $[M-H+HSiCl_3-2HCl]^-$ (485) 97% $[M-H+HSiCl_3-HCl]^-$ (521) 1%
 Propafenone <i>O</i> -β-D-glucuronide (516)	$[M-H+HCl]^-$ (552) 32% $[M-H+HSiCl_3-HCl]^-$ (614) 68% Hydrolysis <sup>b</sup> (2°)	 Rasagiline <i>N</i> -β-D-glucuronide (346)	$[M-H+HCl]^-$ (382) 25% $[M-H+HSiCl_3-2HCl]^-$ (408) 53% $[M-H+HSiCl_3-HCl]^-$ (444) 22% Hydrolysis <sup>b</sup> (2°)
 Raloxifene 4- <i>O</i> -β-D-glucuronide (648)	$[M-H+HCl]^-$ (683) 22% $[M-H+HSiCl_3-HCl]^-$ (746) 78% Hydrolysis <sup>b</sup> (2°)	 PhIP <i>N</i> -β-D-glucuronide (399)	$[M-H+HCl]^-$ (434) 1% $[M-H+HSiCl_3-2HCl]^-$ (461) 99%
 Ezetimibe <i>O</i> -β-D-glucuronide (584)	$[M-H+HCl]^-$ (619) 13% $[M-H+HSiCl_3-HCl]^-$ (682) 87% Hydrolysis <sup>b</sup> (2°)	 Retigabine <i>N</i> -β-D-glucuronide (478)	$[M-H+HCl]^-$ (513) 1% $[M-H+HSiCl_3-2HCl]^-$ (540) 99%
 Carvedilol <i>O</i> -β-D-glucuronide (581)	$[M-H+HCl]^-$ (617) 22% $[M-H+HSiCl_3-HCl]^-$ (679) 78% Hydrolysis <sup>b</sup> (2°)	 Carvedilol <i>N'</i> -β-D-glucuronide (581)	$[M-H+HCl]^-$ (617) 5% $[M-H+HSiCl_3-2HCl]^-$ (643) 71% $[M-H+HSiCl_3-HCl]^-$ (679) 24% $[M-H+HSiCl_3-3HCl]^-$ (2°)
 Darunavir <i>O</i> -β-D-glucuronide (722)	$[M-H+HCl]^-$ (758) 1% $[M-H+HSiCl_3-HCl]^-$ (820) 99% Hydrolysis <sup>b</sup> (2°)	 Darunavir <i>N</i> -β-D-glucuronide (722)	$[M-H+HSiCl_3-2HCl]^-$ (784) 75% $[M-H+HSiCl_3-HCl]^-$ (820) 25% $[M-H+HSiCl_3-3HCl]^-$ (2°)

Table 1. continued

<i>O</i> -Glucuronides ( <i>m/z</i> of deprotonated analyte)	1° ionic reaction products ( <i>m/z</i> ) and their branching ratios  2° ionic reaction products	<i>N</i> -Glucuronides ( <i>m/z</i> of deprotonated analyte)	1° ionic reaction products ( <i>m/z</i> ) and their branching ratios  2° ionic reaction products
 4-Hydroxytamoxifen <i>O</i> - $\beta$ -D-glucuronide (562)	$[M-H+HCl]^-$ (598) 74% $[M-H+HSiCl_3-HCl]^-$ (660) 26% Hydrolysis <sup>b</sup> (2°)	 4-Hydroxytamoxifen <i>N</i> - $\beta$ -D-glucuronide <sup>c</sup> (562)	$[M-H+HCl]^-$ (598) 59% $[M-H+HSiCl_3-HCl]^-$ (660) 41% Hydrolysis <sup>b</sup> (2°)
 Morphine 6- <i>O</i> - $\beta$ -D-glucuronide (460)	$[M-H+HCl]^-$ (496) 36% $[M-H+HSiCl_3-HCl]^-$ (558) 64% Hydrolysis <sup>b</sup> (2°)	 Glucuronic acid (193)	$[M-H+HSiCl_3-2HCl]^-$ (255) 98% $[M-H+HSiCl_3-HCl]^-$ (291) 2% $[M-H+HSiCl_3-3HCl]^-$ (2°)

<sup>a</sup>Branching ratios were obtained after reaction with  $HSiCl_3$  for 100 ms. <sup>b</sup>Partial hydrolysis of  $[M-H+HSiCl_3-HCl]^-$  forms  $[M-H+HSiCl_3-HCl-Cl+OH]^-$ . <sup>c</sup>Doped with a base to promote deprotonation.



**Figure 2.** Calculated free energy surfaces for the reactions of  $HSiCl_3$  with deprotonated glucuronic acid (black) and *O*- (red) and *N*-glucuronides (blue) via addition followed by elimination of one  $HCl$  molecule containing the hydrogen atom from the O4 position (indicated by O). Calculations were performed at the M06-2X/6-311++G(d,p)//M06-2X/6-311++G(d,p) level of theory; free energies (in kcal/mol) are relative to the deprotonated analyte and  $HSiCl_3$ .

## EXPERIMENTAL SECTION

**Reagents and Materials.** Darunavir *O*- $\beta$ -D-glucuronide was purchased from Sussex Research. 4-Nitrophenol *O*- $\beta$ -D-glucuronide and trichlorosilane were purchased from Sigma-Aldrich. The remaining *O*- and *N*-glucuronides were purchased from Toronto Research Chemicals. All purchased chemicals were used as received.

**Ion/Molecule Reactions.** The experiments were carried out in a Thermo Scientific linear quadrupole ion trap (LQIT)

mass spectrometer modified with an external reagent mixing manifold.<sup>18</sup> The studied glucuronides were ionized by negative mode electrospray ionization (ESI). The deprotonated glucuronides were isolated in the ion trap with an isolation width of 2 mass units and allowed to react with  $HSiCl_3$  for 30–100 ms.  $SiHCl_3$  was introduced into the ion trap via the external reagent mixing manifold at a flow rate 3  $\mu$ L/hour. No harmful effects to the instrumentation have been observed, likely because of the very small amount of the reagent introduced. A detailed description of the instrumentation used



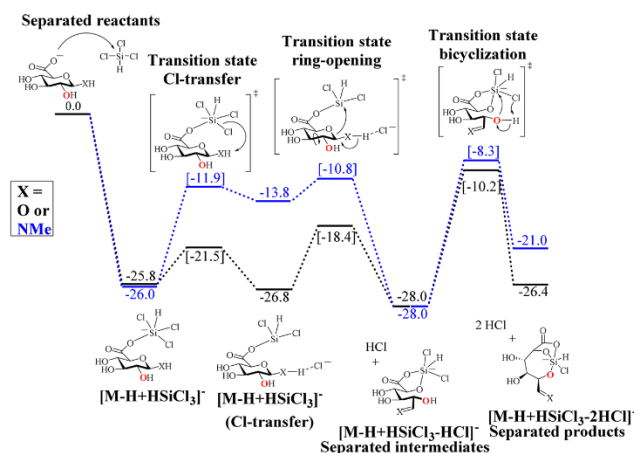


**Figure 3.** Calculated free energy surfaces for the reactions of  $\text{HSiCl}_3$  with deprotonated glucuronic acid (black) and deprotonated methyl *N*-glucuronide (blue) via addition followed by elimination of two  $\text{HCl}$  molecules (note that the product complex is not shown). Calculations were performed at the M06-2X/6-311++G(d,p) level of theory; free energies (in kcal/mol) are relative to the deprotonated analyte and  $\text{HSiCl}_3$ .

here for performing ion/molecule reactions can be found in the literature.<sup>15</sup>

**Quantum Chemical Calculations.** All density functional calculations were performed at the M06-2X/6-311++G(d,p) level of theory by using the Gaussian 09 program.<sup>30,31</sup> All transition state structures were confirmed to possess exactly one negative eigenvalue corresponding to the reaction coordinate. Intrinsic reaction coordinate (IRC) calculations were performed for all transition states. The free energies used to construct the potential energy surfaces were calculated using ideal gas statistical mechanics.

**HPLC/MS/MS.** HPLC/MS/MS experiments were performed on a Thermo Surveyor HPLC coupled to an LQIT. The samples were injected via an autosampler with full-loop injection (25  $\mu\text{L}$ ). The mobile phases used were water (A) and methanol (B), both containing 0.1% formic acid. The column used was an Agilent ZORBAX SB-C18 5  $\mu\text{m}$ , 4.6  $\times$  250 mm column. The eluate was subsequently ionized by ESI in negative ion mode, and the selected ions were isolated and allowed to react with the reagent for 30 ms.

## RESULTS AND DISCUSSION

Reactions of all deprotonated *O*-glucuronides and some *N*-glucuronides generate an  $\text{HSiCl}_3$  adduct that has lost one  $\text{HCl}$  molecule ( $[\text{M} - \text{H} + \text{HSiCl}_3 - \text{HCl}]^-$ ) as a primary product ion (Table 1 and Figures S1–S17). However, only deprotonated *N*-glucuronides yield a diagnostic dominant  $\text{HSiCl}_3$  adduct that has lost two  $\text{HCl}$  molecules ( $[\text{M} - \text{H} + \text{HSiCl}_3 - 2\text{HCl}]^-$ ). This reaction allows the differentiation of *O*- and *N*-glucuronides. For example, deprotonated carvedilol *N'*- $\beta$ -*D*-glucuronide formed the diagnostic product ion  $[\text{M} - \text{H} + \text{HSiCl}_3 - 2\text{HCl}]^-$  while its *O*-glucuronide isomer did not (Figure 1). The *N*-glucuronide also formed a product ion  $[\text{M} - \text{H} + \text{HSiCl}_3 - 3\text{HCl}]^-$ , which is likely to be a dissociation product of the  $[\text{M} - \text{H} + \text{HSiCl}_3 - 2\text{HCl}]^-$  product ion (for reaction kinetics, see Figure S24). Therefore, this product ion may also be diagnostic for *N*-glucuronides.

Quantum chemical calculations were performed on simple model compounds to obtain insights into the mechanisms of the reactions of  $\text{HSiCl}_3$  with deprotonated glucuronides. In these model compounds, the complex drug moiety was replaced by an *O*-methyl (for *O*-glucuronides) or *N*-methyl moiety (for *N*-glucuronides) to obtain representative results within a reasonable amount of computation time. On the basis of the calculations, the reactions are initiated by binding of  $\text{HSiCl}_3$  to the carboxylate group of the deprotonated glucuronic acid, generating a covalently bound pentacoordinated silicon anion that is in close proximity to the 4-OH group (Figure 2). The electron withdrawing nature of the chloro-substituents in  $\text{HSiCl}_3$  enhances the electrophilicity of the silicon atom, which promotes hypervalency and also enhances the reactivity of the Si–Cl bonds.<sup>32–34</sup> In the second step, a chloride anion cleaves off from the silicon atom and forms a hydrogen bond with the 4-OH group (as indicated by O in Figure 2) of the *O*- or *N*-methylglucuronide, concerted with formation of a Si–O bond. Elimination of an  $\text{HCl}$  molecule yields the ionic product  $[\text{M} - \text{H} + \text{HSiCl}_3 - \text{HCl}]^-$  (Figure 2).

Calculations further suggest that the formation of the diagnostic product ion  $[\text{M} - \text{H} + \text{HSiCl}_3 - 2\text{HCl}]^-$  for deprotonated *secondary N*-glucuronides can be explained by an alternative pathway that is in competition with the formation of the primary product ion  $[\text{M} - \text{H} + \text{HSiCl}_3 - \text{HCl}]^-$ . This new pathway begins with adduct formation in a conformation wherein the silicon atom is in close proximity with the ring oxygen (as opposed to the 4-OH), as shown in the blue pathway in Figure 3 (this conformation is more stable than that shown in Figure 2). This is followed by the breaking of a Si–Cl bond followed by bond formation between the chloride anion and the hydrogen atom bound to the anomeric nitrogen of the *N*-glucuronides (Figure 3). This transfer does not occur for *O*-glucuronides, since they do not have a hydrogen attached to the anomeric oxygen, but it may occur for glucuronic acid, because it has a hydrogen at the anomeric oxygen, as shown in Figure 3 (black pathway).

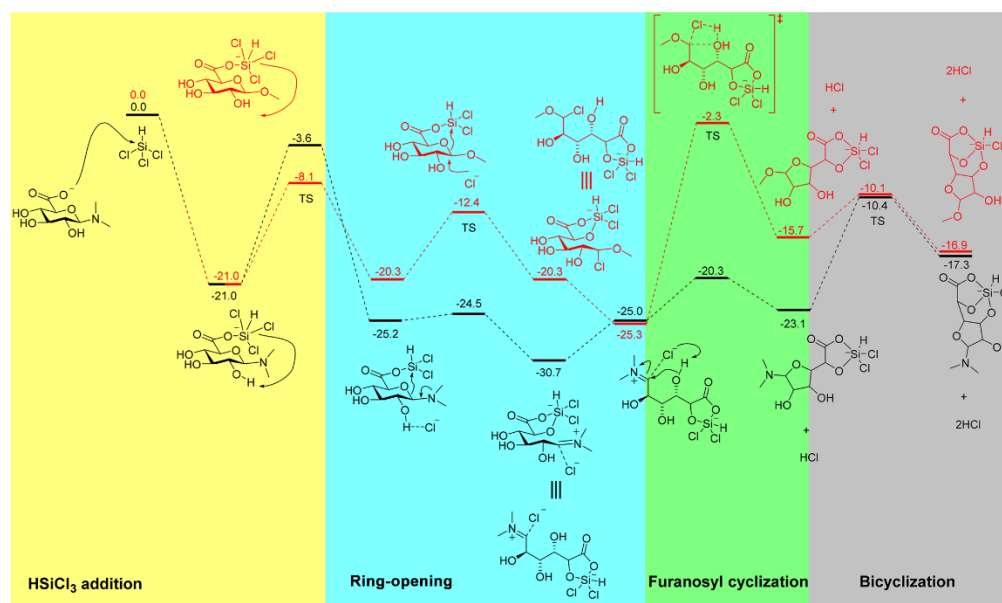


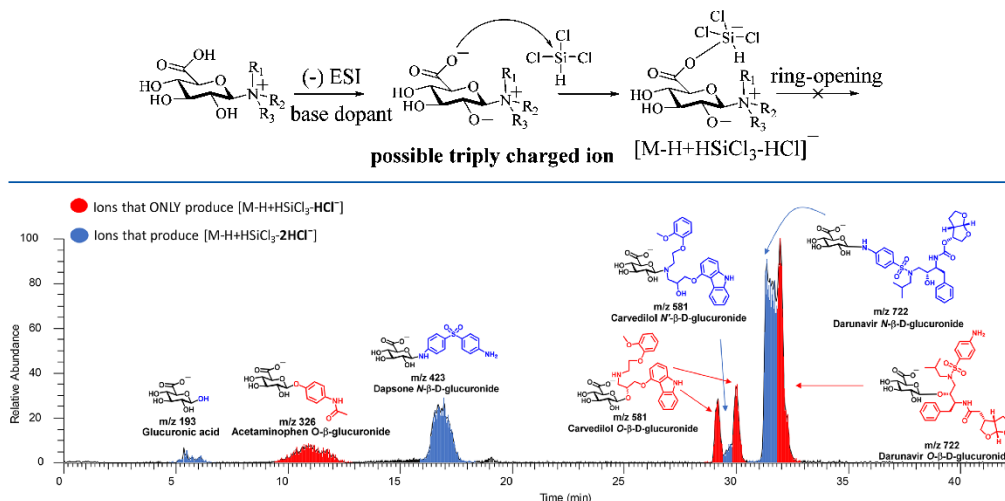
**Figure 4.** Calculated free energy surfaces for the reactions of  $\text{HSiCl}_3$  with deprotonated dimethyl *N*-glucuronide (black) and deprotonated methyl *O*-glucuronide (red) via addition followed by elimination of two  $\text{HCl}$  molecules (note that the product complex is not shown). Calculations were performed at the M06-2X/6-311++G(d,p) level of theory; free energies (in kcal/mol) are relative to the deprotonated analyte and  $\text{HSiCl}_3$ .

Hydrogen chloride is then eliminated in concert with opening of the ring and formation of two bonds, a  $\text{C}=\text{N}$  bond at the anomeric position (or a  $\text{C}=\text{O}$  bond in the case of glucuronic acid) and an  $\text{O}-\text{Si}$  bond with the endocyclic oxygen (Figure 3). The flexibility afforded by the ring-opening enables a hydroxyl group to add to the silicon atom. According to calculations, the kinetically most favorable attack involves the  $\text{O}2$  atom (as indicated by a red  $\text{O}$  in Figure 3). This leads to a concerted breaking of a  $\text{Si}-\text{Cl}$  bond and formation of a  $\text{Si}-\text{O}$  bond, which accounts for the loss of the second  $\text{HCl}$  molecule. The importance of ring-opening in this pathway is substantiated by the fact that underivatized deprotonated glucuronic acid also produces the characteristic  $[\text{M} - \text{H} + \text{HSiCl}_3 - 2\text{HCl}]^-$  product ion upon reactions with  $\text{HSiCl}_3$ , since deprotonated glucuronic acid can undergo ring-opening via the same mechanism as deprotonated *N*-glucuronides (Figure 3). It is important to note here that the mere presence of a second protic nucleophilic group is not enough to cause the second loss of  $\text{HCl}$  in the pathways shown in Figure 3. Even for deprotonated *O*-glucuronides with nearby protic nucleophilic groups (e.g., 2-aminophenol, dopamine, and carvedilol *O*-glucuronides, Table 1), no  $[\text{M} - \text{H} + \text{HSiCl}_3 - 2\text{HCl}]^-$  product ion was observed.

A deviation from the above behavior was observed for deprotonated *tertiary N*-glucuronides. They do not have a hydrogen atom bound to the anomeric nitrogen atom, but they nevertheless form the characteristic  $[\text{M} - \text{H} + \text{HSiCl}_3 - 2\text{HCl}]^-$  product ion. Calculations suggest that *tertiary N*-glucuronides can form this diagnostic product through a four-step reaction pathway (Figure 4, black trace). After the deprotonated carboxylic acid moiety is added to the silicon

atom, a chloride anion migrates and forms a hydrogen bond with the hydrogen atom at the 2-OH group. This transition corresponds to the highest-energy transition state. The positioning of the chloride anion facilitates ring-opening, as it stabilizes the resulting iminium cation via a loose interaction with the partially positively charged carbon. This ring-opening occurs in concert with formation of a  $\text{Si}-\text{O}$  bond between  $\text{Si}$  and the ether oxygen. Rotation of the molecule brings the chloride ion in proximity to the 4-OH group, and the oxygen atom of this group adds to the iminium carbon, which leads to furanosyl cyclization and loss of the first  $\text{HCl}$ . The second  $\text{HCl}$  is lost in the same manner as the second loss of  $\text{HCl}$  in the pathways of Figure 3—nucleophilic attack of a hydroxyl to the silica to form a bicyclic trioxosilane.

To account for the lack of formation of  $[\text{M} - \text{H} + \text{HSiCl}_3 - 2\text{HCl}]^-$  in reactions of deprotonated *O*-glucuronides with  $\text{HSiCl}_3$ , calculations analogous to those discussed above were carried out for deprotonated methyl *O*-glucuronide (Figure 4, red trace). This ion is able to readily proceed through the first two steps of the reaction pathway discussed above. However, the energy of the transition state for the furanosyl cyclization is much higher than for the deprotonated *N*-glucuronide. This is accounted for by the fact that the chloride forms a covalent bond with the anomeric carbon during the ring-opening step. However, the transition state is still below the total energy level of the system. Indeed, when deprotonated methyl-*O*-glucuronide was allowed to react with  $\text{HSiCl}_3$ , it showed the product ion  $[\text{M} - \text{H} + \text{HSiCl}_3 - 2\text{HCl}]^-$  expected to be diagnostic only for *N*-glucuronides. Therefore, a model compound more representative of drug glucuronides, deprotonated phenyl-*O*-glucuronide, was examined. The barrier

Scheme 2. No Electron Lone Pairs on Nitrogen in Cationic Quaternary *N*-Glucuronides To Facilitate Ring-Opening

**Figure 5.** HPLC/MS/MS chromatogram of 10–20  $\mu\text{M}$  mixture of six model compounds, including one racemic mixture. HPLC analysis was performed using an analytical C18 column ( $4.6 \times 250 \text{ mm}$ ) and gradient elution (solution A: 0.1% formic acid in water; solution B: 0.1% formic acid in methanol; flow rate:  $4 \text{ mL min}^{-1}$ ; B%: 5–80% within 40 min). The eluates were ionized by using ESI in negative ion mode and allowed to react with  $\text{HSiCl}_3$  in the ion trap. The formation of the  $[\text{M} - \text{H} + \text{HSiCl}_3 - 2\text{HCl}]^-$  product ions diagnostic for *N*-glucuronides and  $[\text{M} - \text{H} + \text{HSiCl}_3 - \text{HCl}]^-$  product ions formed for both *O*- and *N*-glucuronides were monitored as a function of time. In the chromatogram, the peaks corresponding to analyte compounds that generated the diagnostic product ions are colored blue and those that generated  $[\text{M} - \text{H} + \text{HSiCl}_3 - \text{HCl}]^-$  product ions but not the diagnostic ions are colored red. Glucuronic acid was formed upon hydrolysis of *N*-glucuronides.

calculated for the furanosyl cyclization of this compound was found to be 7.2 kcal/mol above the energy level of the system, which prevents this compound from forming the product ion of interest. Steric hindrance caused by the phenyl group is the likely cause for the high transition state energy. The same situation is expected to apply to real drug glucuronides, as none of them are as simple as methyl *O*-glucuronide. Steric hindrance will have a less profound effect on *N*-glucuronides than on *O*-glucuronides, since the barriers for furanosyl cyclization are much lower (e.g.,  $-20.3 \text{ kcal/mol}$  for dimethyl *N*-glucuronide compared to  $-2.3$  for methyl *O*-glucuronide). Thus, no false positive results are expected due to *O*-glucuronides other than methyl *O*-glucuronide.

Quaternary *N*-glucuronides are special cases that are generally not ionized in negative ion mode because of their cationic nature. However, when doped with ammonium hydroxide, they generate a triply charged ion, overall with one negative charge (Scheme 2). This ion was found to react with  $\text{SiHCl}_3$  to form the  $[\text{M} - \text{H} + \text{HSiCl}_3 - \text{HCl}]^-$  product ion (Scheme 2).

The absence of the  $[\text{M} - \text{H} + \text{HSiCl}_3 - 2\text{HCl}]^-$  product ion diagnostic for *N*-glucuronides supports the proposed mechanism involving ring-opening, as quaternary *N*-glucuronides cannot undergo ring-opening. Fortunately, quaternary *N*-glucuronides can be distinguished from other *O*- and *N*-glucuronides by being easily ionized in positive ion mode but not in negative ion mode without a base dopant.

**High-Throughput HPLC/MS/MS/Ion/Molecule Reactions.** To demonstrate the practicality of above analytical approach, an HPLC/LQIT was equipped with a reagent mixing manifold to carry out HPLC/MS/MS experiments

based on ion/molecule reactions. A mixture of six glucuronidated drug metabolites, consisting of two pairs of isomers, carvedilol and darunavir *O*- and *N*- $\beta$ -*D*-glucuronides as well as acetaminophen *O*- $\beta$ -*D*-glucuronide and dapsone *N*- $\beta$ -*D*-glucuronide, were separated by reversed-phase HPLC (Figure 5). The observation of glucuronic acid (eluted at 5.5 min) is likely a result of hydrolysis of the *N*-glucuronides, which is known to occur under acidic conditions.<sup>4</sup> The eluted compounds were ionized by ESI in negative ion mode in the LQIT, isolated in the ion trap and allowed to react with  $\text{HSiCl}_3$  for 30 ms. The formation or absence of the  $[\text{M} - \text{H} + \text{HSiCl}_3 - 2\text{HCl}]^-$  product ions diagnostic of *N*-glucuronides, as well as the  $[\text{M} - \text{H} + \text{HSiCl}_3 - \text{HCl}]^-$  ions formed for both *O*- and *N*-glucuronides, was monitored. Each analyte reacted as expected on the basis of the pure model compound studies. As carvedilol is a racemic mixture, two peaks eluting at 29.2 and 30.8 min were observed. Notably, carvedilol *N'*- $\beta$ -*D*-glucuronide was found in the valley between these two peaks. More remarkably, peaks corresponding to darunavir *O*- and *N*- $\beta$ -*D*-glucuronides were unambiguously identified even though the HPLC resolution was not high enough to resolve the two peaks.

## CONCLUSIONS

Unambiguous differentiation of *O*- and *N*-glucuronides was achieved by gas-phase ion/molecule reactions of deprotonated glucuronides with  $\text{HSiCl}_3$  in a quadrupole ion trap mass spectrometer. The diagnostic  $[\text{M} - \text{H} + \text{HSiCl}_3 - 2\text{HCl}]^-$  product ion was observed for deprotonated secondary and tertiary *N*-glucuronides. Several mechanistic pathways that

underlie the formation of the diagnostic product ion were identified via quantum chemical calculations. Coupling of this ion/molecule reaction MS/MS experiment with HPLC demonstrates the practicality of this approach in high-throughput analysis of complex metabolite mixtures.

## ■ ASSOCIATED CONTENT

### Supporting Information

The Supporting Information is available free of charge on the ACS Publications website at DOI: 10.1021/acs.analchem.8b02083.

Experimental details; table of studied glucuronides; ion/molecule reaction MS/MS spectra; HPLC/MS/MS ion/molecule reaction chromatograms and MS/MS spectra; computational data (PDF)

## ■ AUTHOR INFORMATION

### Corresponding Author

\*Tel.: +1 (765) 494 0882; Fax: +1 (765) 494 9421; E-mail: hilikka@purdue.edu (H.I.K.)

### ORCID

Xin Ma: 0000-0002-7058-0165

Arun K. Ghosh: 0000-0003-2472-1841

Hilikka I. Kenttämää: 0000-0001-8988-6984

### Author Contributions

\*J.Y.K. and Z.Y. contributed equally.

### Notes

The authors declare no competing financial interest.

## ■ ACKNOWLEDGMENTS

We thank Merck & Co., Inc., Kenilworth, NJ, USA, for financial support. The National Institutes of Health are acknowledged for partial funding to AG (GM 53386).

## ■ REFERENCES

- (1) Tephly, T. R.; Green, M. D.; Coffman, B. L.; King, C.; Cheng, Z.; Rios, G. *Adv. Pharmacol.* **1997**, *42*, 343–346.
- (2) Schaefer, W. H.; Goalwin, A.; Dixon, F.; Hwang, B.; Killmer, L.; Kuo, G. *Biol. Mass Spectrom.* **1992**, *21* (4), 179–188.
- (3) Jancova, P.; Anzenbacher, P.; Anzenbacherova, E. *Biomed. Pap.* **2010**, *154* (2), 103–116.
- (4) Babu, S. R.; Lakshmi, V. M.; Huang, G. P.-W.; Zenser, T. V.; Davis, B. B. *Biochem. Pharmacol.* **1996**, *51* (12), 1679–1685.
- (5) Schaefer, W. H.; Politowski, J.; Hwang, B.; Dixon, F., Jr; Goalwin, A.; Gutzait, L.; Anderson, K.; DeBrosse, C.; Bean, M.; Rhodes, G. R. *Drug Metab. Dispos.* **1998**, *26* (10), 958–969.
- (6) Fujiwara, R.; Yoda, E.; Tukey, R. H. *Drug Metab. Pharmacokinet.* **2018**, *33* (1), 9–16.
- (7) Blum, M. R.; Liao, S. H.; Good, S. S.; de Miranda, P. *Am. J. Med.* **1988**, *85* (2A), 189–194.
- (8) Basu, N. K.; Kole, L.; Basu, M.; McDonagh, A. F.; Owens, I. S. *Biochem. Biophys. Res. Commun.* **2007**, *360* (1), 7–13.
- (9) Ciotti, M.; Lakshmi, V. M.; Basu, N.; Davis, B. B.; Owens, I. S.; Zenser, T. V. *Carcinogenesis* **1999**, *20* (10), 1963–1969.
- (10) Spraul, M.; Freund, A. S.; Nast, R. E.; Withers, R. S.; Maas, W. E.; Corcoran, O. *Anal. Chem.* **2003**, *75* (6), 1536–1541.
- (11) Shimizu, A.; Ohe, T.; Chiba, M. *Drug Metab. Dispos.* **2012**, *40* (8), 1456–1459.
- (12) Watkins, M. A.; Price, J. M.; Winger, B. E.; Kenttämää, H. I. *Anal. Chem.* **2004**, *76* (4), 964–976.
- (13) Campbell, K. M.; Watkins, M. A.; Li, S.; Fiddler, M. N.; Winger, B.; Kenttämää, H. I. *J. Org. Chem.* **2007**, *72* (9), 3159–3165.
- (14) Duan, P.; Gillespie, T. A.; Winger, B. E.; Kenttämää, H. I. *J. Org. Chem.* **2008**, *73* (13), 4888–4894.
- (15) Habicht, S. C.; Vinuesa, N. R.; Archibold, E. F.; Duan, P.; Kenttämää, H. I. *Anal. Chem.* **2008**, *80* (9), 3416–3421.
- (16) Fu, M.; Duan, P.; Li, S.; Eismann, R. J.; Kenttämää, H. I. *J. Am. Soc. Mass Spectrom.* **2009**, *20* (7), 1251–1262.
- (17) Somuramasami, J.; Winger, B. E.; Gillespie, T. A.; Kenttämää, H. I. *J. Am. Soc. Mass Spectrom.* **2010**, *21* (5), 773–784.
- (18) Habicht, S. C.; Vinuesa, N. R.; Amundson, L. M.; Kenttämää, H. I. *J. Am. Soc. Mass Spectrom.* **2011**, *22* (3), 520–530.
- (19) Fu, M.; Duan, P.; Gao, J.; Kenttämää, H. I. *Analyst* **2012**, *137* (24), S720–S722.
- (20) Jarrell, T.; Riedeman, J.; Carlsen, M.; Replogle, R.; Selby, T.; Kenttämää, H. *Anal. Chem.* **2014**, *86* (13), 6533–6539.
- (21) Sheng, H.; Williams, P. E.; Tang, W.; Zhang, M.; Kenttämää, H. I. *Analyst* **2014**, *139* (17), 4296–4302.
- (22) Tang, W.; Sheng, H.; Kong, J. Y.; Yerabolu, R.; Zhu, H.; Max, J.; Zhang, M.; Kenttämää, H. I. *Rapid Commun. Mass Spectrom.* **2016**, *30* (12), 1435–1441.
- (23) Brodbelt, J. S. *Mass Spectrom. Rev.* **1997**, *16* (2), 91–110.
- (24) Gronert, S. *Chem. Rev.* **2001**, *101* (2), 329–360.
- (25) O'Hair, R. A. J.; Freitas, M. A.; Gronert, S.; Schmidt, J. A. R.; Williams, T. D. *J. Org. Chem.* **1995**, *60* (7), 1990–1998.
- (26) Lam, A. K. Y.; Li, C.; Khairallah, G.; Kirk, B. B.; Blanksby, S. J.; Trevitt, A. J.; Wille, U.; O'Hair, R. A. J.; da Silva, G. *Phys. Chem. Chem. Phys.* **2012**, *14* (7), 2417–2426.
- (27) Reid, G. E.; Tichy, S. E.; Pérez, J.; O'Hair, R. A. J.; Simpson, R. J.; Kenttämää, H. I. *J. Am. Chem. Soc.* **2001**, *123* (6), 1184–1192.
- (28) Thomas, M. C.; Mitchell, T. W.; Harman, D. G.; Deeley, J. M.; Murphy, R. C.; Blanksby, S. J. *Anal. Chem.* **2007**, *79* (13), 5013–5022.
- (29) Thomas, M. C.; Mitchell, T. W.; Harman, D. G.; Deeley, J. M.; Nealon, J. R.; Blanksby, S. J. *Anal. Chem.* **2008**, *80* (1), 303–311.
- (30) Frisch, M. J.; Trucks, G. W.; Schlegel, H. B.; Scuseria, G. E.; Robb, M. A.; Cheeseman, J. R.; Scalmani, G.; Barone, V.; Mennucci, B.; Petersson, G. A.; Nakatsuji, H.; Caricato, M.; Li, X.; Hratchian, H. P.; Izmaylov, A. F.; Bloino, J.; Zheng, G.; Sonnenberg, J. L.; Hada, M.; Ehara, M.; Toyota, K.; Fukuda, R.; Hasegawa, J.; Ishida, M.; Nakajima, T.; Honda, Y.; Kitao, O.; Nakai, H.; Vreven, T.; Montgomery, J. A., Jr; Peralta, J. E.; Ogliaro, F.; Bearpark, M.; Heyd, J. J.; Brothers, E.; Kudin, K. N.; Staroverov, V. N.; Kobayashi, R.; Normand, J.; Raghavachari, K.; Rendell, A.; Burant, J. C.; Iyengar, S. S.; Tomasi, J.; Cossi, M.; Rega, N.; Millam, J. M.; Klene, M.; Knox, J. E.; Cross, J. B.; Bakken, V.; Adamo, C.; Jaramillo, J.; Gomperts, R.; Stratmann, R. E.; Yazyev, O.; Austin, A. J.; Cammi, R.; Pomelli, C.; Ochterski, J. W.; Martin, R. L.; Morokuma, K.; Zakrzewski, V. G.; Voth, G. A.; Salvador, P.; Dannenberg, J. J.; Dapprich, S.; Daniels, A. D.; Farkas, O.; Foresman, J. B.; Ortiz, J. V.; Cioslowski, J.; Fox, D. J. *Gaussian 09*, revision A.02; Gaussian, Inc.: Wallingford, CT, 2009.
- (31) Zhao, Y.; Truhlar, D. G. *Theor. Chem. Acc.* **2008**, *120* (1–3), 215–241.
- (32) Wilhite, D. L.; Spalter, L. J. *Am. Chem. Soc.* **1973**, *95* (7), 2100–2104.
- (33) Buckner, S. W.; Gord, J. R.; Freiser, B. S. *J. Am. Chem. Soc.* **1988**, *110* (20), 6606–6612.
- (34) Pestunovich, V. A.; Kirpichenko, S. V.; Lazareva, N. F.; Albanov, A. I.; Voronkov, M. G. *J. Organomet. Chem.* **2007**, *692* (11), 2160–2167.



Contents lists available at ScienceDirect

Fuel

journal homepage: [www.elsevier.com/locate/fuel](http://www.elsevier.com/locate/fuel)

Full Length Article

## Molecular profiling of crude oil by using Distillation Precipitation Fractionation Mass Spectrometry (DPF-MS)



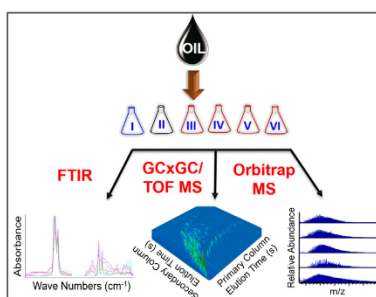
Ravikiran Yerabolu<sup>a</sup>, Raghavendhar R. Kotha<sup>a</sup>, Edouard Niyonsaba<sup>a</sup>, Xueming Dong<sup>a</sup>, Jeremy M. Manheim<sup>a</sup>, John Kong<sup>a</sup>, James S. Riedeman<sup>a</sup>, Mark Romanczyk<sup>a</sup>, Cliff T. Johnston<sup>b</sup>, Gozdem Kilaz<sup>c</sup>, Hilkka I. Kenttämä<sup>a,\*</sup>

<sup>a</sup> Purdue University, Department of Chemistry, West Lafayette, IN 47906, United States

<sup>b</sup> Purdue University, Department of Agronomy, West Lafayette, IN 47906, United States

<sup>c</sup> Purdue University, School of Engineering Technology, IN 47906, United States

### GRAPHICAL ABSTRACT



### ARTICLE INFO

#### Keywords:

Crude oil fractionation  
Molecular weight determination  
High-resolution mass spectrometry  
Molecular level characterization

### ABSTRACT

Molecular profiling of crude oil is a tremendous challenge due to its inherent complexity. An accurate molecular fingerprint of a crude oil may facilitate rational design of crude oil recovery efforts, such as enhanced oil recovery, improve the efficiencies of the refining processes, and enable a better assessment of the value of the crude oil. Herein, a new approach (Distillation Precipitation Fractionation Mass Spectrometry (DPF-MS) method) is introduced for the molecular level characterization of crude oil. This method involves the separation of crude oil into six fractions followed by high-resolution mass spectral analysis optimized for each individual fraction. The separation methods are distillation, precipitation, and fractionation in an auto column followed by solid phase extraction. Initially, the fractions were examined by using Fourier transform infrared spectroscopy to determine the bulk chemical nature of each individual fraction, such as the extent of aromaticity, degree of polarity, etc. Based on this bulk information, model compounds representative of compounds in each fraction were selected and employed to develop the optimal high-resolution mass spectrometric analysis method for each fraction. An especially important aspect of this work was the optimization of the ionization method separately for each fraction by using appropriate model compounds so that most compounds in each fraction are ionized at approximately the same efficiency to generate only one type of stable ions (either molecular ions, protonated molecules or cations formed by hydride abstraction) containing the intact analyte molecule. This allows the DPF-

\* Corresponding author.

E-mail address: [hilkka@purdue.edu](mailto:hilkka@purdue.edu) (H.I. Kenttämä).

<https://doi.org/10.1016/j.fuel.2018.07.028>

Received 18 March 2018; Received in revised form 3 July 2018; Accepted 6 July 2018

Available online 17 July 2018

0016-2361/ © 2018 Elsevier Ltd. All rights reserved.



MS method to produce reasonably accurate relative abundances for compounds present in each fraction, thereby making the method semi-quantitative. The compositional data thus obtained for the individual fractions were utilized to provide meaningful molecular level information for the crude oil. Inclusion of a mass balance for each fraction allows for data consolidation, which provides an accurate overall analysis of the crude oil, including average molecular weight and weight percentages of different compound classes.

## 1. Introduction

The light oil deposits of the world are depleting, which has generated a need to better understand the chemical composition of crude oil of different geographical origins. Specifically, for chemically enhanced oil recovery processes, this information would enable producers to investigate the phase and interfacial interactions between oil, surfactants, and reservoir rock, and thereby help the industry develop smarter, more efficient solutions for the economic recovery of oil [1–3]. Further, the ability to obtain an accurate estimate of the average molecular weight of crude oil would facilitate the optimization of refinery processes [4]. This is especially important for conversion of crude oil via reactions such as alkylation, dimerization, cracking, and hydrotreating, since access to an accurate average molecular weight would enable a better estimation of the amount of reagent required for the conversion [4].

The challenge of analyzing crude oil is that it is a complex mixture, predicted to contain as many or more compounds than the number of genes in the human genome [5]. To study such complex mixtures, powerful high-resolution mass spectrometers, such as Fourier-transform ion cyclotron resonance or orbitrap mass spectrometers, are desirable [6,7]. These high-resolution instruments can be used to determine the elemental compositions of ionized crude oil components, which facilitates categorizing them into different compound classes (such as the hydrocarbon class containing only carbon and hydrogen and heteroatom classes containing oxygen, nitrogen and/or sulfur in addition to carbon and hydrogen) or compound types (e.g., saturated and aromatic compounds). While the information provided by these techniques is invaluable, problems associated with the ionization methods employed include inefficient ionization, competition for ionization, and matrix effects, all of which may reduce sensitivity toward or even entirely prevent the detection of some components of crude oil. Indeed, most of these studies have employed atmospheric pressure chemical ionization (APCI) for nonpolar analytes [8], atmospheric pressure photo ionization (APPI) for aromatic analytes [7,9] and electrospray ionization (ESI) for polar analytes [10,11]. Unfortunately, all these methods selectively ionize only some of the crude oil components.

Above problems of competition for ionization and matrix effects are reduced when the mass analysis is preceded by a chromatographic separation [12–14]. Chromatography reduces the complexity of the mixture by separating it into fractions, but it does not necessarily eliminate issues having to do with mixture components with widely differing ionization efficiencies.

In this paper, a new separation and characterization method for crude oil is introduced, entitled Distillation Precipitation Fractionation Mass Spectrometry (DPF-MS). DPF-MS involves separation of the crude oil into several fractions that contain compounds with similar chemical characteristics, followed by molecular level characterization of each fraction by using an optimized mass spectrometric method. The novelty of this method lies in the optimization of the ionization and mass spectrometry method separately for each fraction by using representative model compounds so that all compounds in each fraction are ionized at approximately the same efficiency to yield stable ionized molecules, which makes the DPF-MS method semi-quantitative. Following the weighing and analysis of each fraction, consideration of mass balance facilitated the molecular profiling of the fractionated crude oil.

## 2. Experimental section

### 2.1. Sample

Freshly collected crude oil from an active oil well in the Illinois oil basin was provided by the Pioneer Oil Company (Illinois). The crude oil was collected and stored in amber colored glass bottles to prevent oxidation and the container was tightly sealed with a screw cap to minimize loss of volatile compounds. The viscosity and density of the crude oil (at 20 °C) were measured to be 12.28 cP and 0.87 g/cm<sup>3</sup>, respectively.

### 2.2. Chemicals and materials

HPLC grade *n*-hexane (C<sub>6</sub>H<sub>14</sub>), dichloromethane (CH<sub>2</sub>Cl<sub>2</sub>) and isopropanol (i-C<sub>3</sub>H<sub>7</sub>OH) were used as eluents in flash chromatography. A normal-phase silica (40 g) auto column was purchased from Teledyne Isco, Inc. A total of 23 model compounds were used in this study. Table S1 in the supporting information gives details of the model compounds used and their purities.

### 2.3. Separation of crude oil into fractions

Crude oil was separated into six fractions by using different techniques. As a first step, the most volatile compounds in the crude oil were separated by vacuum distillation at room temperature to yield fraction I (distillate) to avoid their loss during fractionation. The remaining residue was separated into asphaltenes (fraction II) and maltenes (all remaining fractions) through precipitation of the asphaltenes by using hexane as reported in the literature [15]. Maltenes were further chromatographically separated into three fractions (C<sub>6</sub>H<sub>14</sub>-eluted fractions III and IV combined, CH<sub>2</sub>Cl<sub>2</sub>-eluted fraction V, and i-C<sub>3</sub>H<sub>7</sub>OH-eluted fraction VI) on an auto column (Combi-flash Rf 200 from Teledyne Isco, Inc.) by using hexane (C<sub>6</sub>H<sub>14</sub>), dichloromethane (CH<sub>2</sub>Cl<sub>2</sub>) and isopropanol (i-C<sub>3</sub>H<sub>7</sub>OH) as eluents. The C<sub>6</sub>H<sub>14</sub>-eluted fractions were further separated into fractions III and IV by using a solid phase extraction technique reported in the literature [16,17]. Further details of each separation step are provided in the Supporting information (Table S2). All the fractions were weighted gravimetrically to obtain mass balance and recovery.

### 2.4. Mass spectrometry

#### 2.4.1. GCxGC/TOF mass spectrometry

A LECO Pegasus 4D GCxGC/(EI)TOF instrument equipped with an Agilent 7890B two-dimensional gas chromatograph (Agilent technologies, Santa Clara, CA) and a high-resolution time-of-flight (TOF) mass spectrometer (up to 50,000 resolution) was used for the analysis of the volatile compounds (fraction I) in crude oil. Two columns (Rxi-17sil ms (intermediate polarity), 60 m, and Rxi-1 ms (nonpolar), 4 m) were connected in series by using a modulator that enhances the peak capacity available for the chromatographic system. After separation of the compounds, positive ion mode electron ionization (EI) (70 eV) was used to ionize the compounds upon entrance into the mass spectrometer. The EI mass spectra measured (at high resolution) for unknown compounds were compared to extensive EI mass spectral libraries for identification (NIST libraries). This analysis yielded a list of identified compounds, their gas chromatographic peak areas and two retention times, and

their chemical formulas and chemical classes. Experimental conditions are detailed in the [Supporting information](#) (Table S3). Additionally, GCxGC/(EI)TOF was used to optimize the solid phase extraction parameters for optimal separation of the  $C_6H_{14}$ -eluted fraction III from IV. The efficiency of solid phase extraction was evaluated by monitoring the percentage of coelution or carryover of different chemical classes of compounds into the separated fractions. Experimental conditions are detailed in [Supporting information](#) (Table S4).

#### 2.4.2. LQIT orbitrap XL mass spectrometry

All fractions (excluding the distillates fraction) were characterized using direct infusion positive ion mode atmospheric pressure chemical ionization (APCI) combined with high-resolution mass spectrometry. A linear quadrupole ion trap (LQIT) coupled with a high-resolution orbitrap detector, LTQ Orbitrap XL mass spectrometer (Thermo Fischer Scientific, San Jose, CA), with a maximum resolution of 100,000 (at  $m/z$  400) was used for the analysis. The optimized ionization methods, including the solvents and ionization reagents, tube lens voltages, types of sheath and auxiliary gases, and temperatures, chosen for the analysis of the different fractions are shown in [Table S5](#).

#### 2.4.3. Ionization methods

Positive ion mode atmospheric pressure ionization methods using different nebulizing gases and solvents, such as APPI/ $N_2$ / $CS_2$ , APCI/ $N_2$ / $CS_2$ , APCI/ $O_2$ / $n$ -hexane, APCI/ $N_2$ / $n$ -hexane, APCI/ $N_2$ / $n$ -hexane and methanol, APCI/ $N_2$ /toluene, APCI/ $N_2$ /methanol, and ESI/ $N_2$ /methanol, were tested for specific fractions (II, III, IV, V and VI). Three different APCI techniques were identified to be most effective for these five fractions. APCI/ $N_2$ / $CS_2$  was selected for the analysis of fractions II, IV, and V, APCI/ $O_2$ / $n$ -hexane for fraction III, and APCI/ $N_2$ / $n$ -hexane and methanol for fraction VI. The optimized parameters used for the ionization of compounds in these fractions are summarized in [Table S5](#).

Xcaliber version 2.2 (Thermo Fischer Scientific, Inc, San Jose, CA) was used for data acquisition and analysis. The normalized peak height threshold for peak picking was 5%. After peak picking, elemental formulas were assigned based on accurately measured  $m/z$  values that were within 3 ppm from the theoretical value (accepted mass accuracy with external calibration). Elements used for formula assignments were carbon, hydrogen, nitrogen, oxygen and sulfur. While no limits were placed on the number of carbons and hydrogens used for the elemental composition assignment, limits of 4 nitrogen, 5 oxygen, and 5 sulfur atoms were used. The degree of unsaturation, also known as ring and double bond (RDB) equivalent, represents the number of rings plus the number of double bonds in a molecule. This value was calculated based

on the assigned elemental composition by using [Eq. \(S1\)](#) provided in the [supporting information](#). Data sorting for plotting the graphs and heteroatom classification was performed using Excel. RDB equivalent versus carbon number plots and heteroatom distribution plots were prepared by using OriginPro (version 93E).

#### 2.5. FTIR analysis

FTIR measurements were performed on all the separated crude oil fractions with a Nicolet 6700 FTIR spectrometer (Thermo Scientific). The FTIR spectra were collected using a liquid  $N_2$  cooled MCT (HgCdTe) detector. The scans involved wave numbers from 4000 up to  $650\text{ cm}^{-1}$  with a resolution of  $2\text{ cm}^{-1}$  and 64 scans co-added per sample. The spectrum of each fraction was corrected against the background spectrum obtained by using the clean, dry cell. Attenuated total reflectance (ATR-FTIR) measurements were made using two different methods. For liquid fractions with sufficient volume of 0.5 mL, a 10-bounce horizontal ATR cell (Pike Technologies, Madison, WI) was used. The internal reflection element (IRE) used was a ZnSe crystal with dimensions of 73 mm by 7 mm and an angle of incidence of  $45^\circ$ . The total volume of the cell was 2 mL. For viscous fractions or semi-solid materials (e.g., asphaltenes), a single bounce diamond ATR cell (GladiATR™ Pike Technologies) was used.

### 3. Results and discussion

In order to illustrate some of the problems associated with detection of all compounds in crude oil by mass spectrometry without prior separation, a simple equimolar mixture containing typical crude oil components, i.e., two alkylaromatic compounds ( $n$ -decylbenzene,  $n$ -hexylbenzene), an alkane (pentadecane), two cycloalkanes (cycloheptane, methylcyclopentane), an alkene (1-decene) and an alkyne (1-hexyne), was analyzed by using APCI and APPI. This mixture cannot be ionized using the traditional APCI and APPI solvent systems, water and/or methanol, as the hydrocarbons are not soluble in these solvents. Carbon disulfide ( $CS_2$ ) has been successfully used in the past as a solvent for APCI of hydrocarbon mixtures [8]. Therefore, the model compound mixture was dissolved in  $CS_2$  and analyzed by using both APCI/ $N_2$ / $CS_2$  ( $N_2$  was used as the nebulizing gas) and APPI/ $N_2$ / $CS_2$  ionization methods in a LQIT-orbitrap MS. [Fig. 1](#) shows the APCI/ $N_2$ / $CS_2$  mass spectrum of the model mixture.

Compounds in this mixture were also analyzed individually by using APCI/ $N_2$ / $CS_2$  to identify the ions (fragment ions and intact molecular ions) produced by each individual compound. The linear alkane

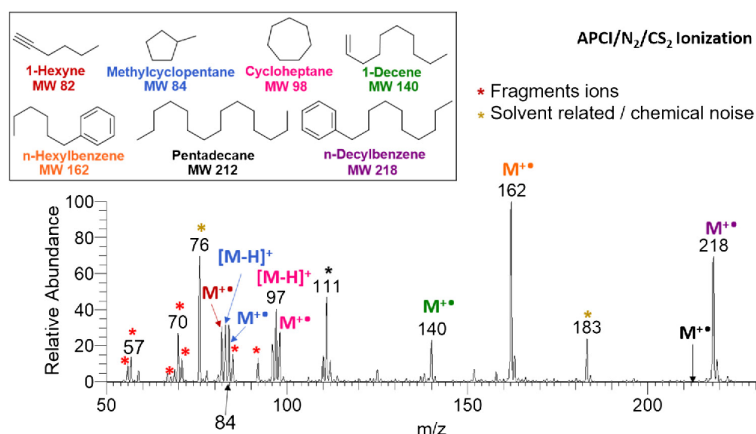


**Fig. 1.** APCI/ $N_2$ / $CS_2$  mass spectrum of an equimolar mixture (1 mM) of seven nonpolar model compounds measured using an injection flow rate of  $5\text{ }\mu\text{L min}^{-1}$ . Linear alkane and alkene yielded several fragment ions, including those of  $m/z$  57, 70, 71 and 85. Cycloalkanes generated molecular ions ( $M^{+\bullet}$ ) as well as  $[M-H]^+$  ions. Alkylaromatic compounds and the alkyne generated predominantly stable molecular ions.

fragmented completely upon ionization, generating fragment ions of  $m/z$  57, 71 and 85 and no visible molecular ions, which makes detection of this alkane challenging. The alkyne generated stable molecular ions as well as minor fragment ions of  $m/z$  67. The alkene also produced both stable molecular ions as well as fragment ions of  $m/z$  57 and 70. However, the fragmentation was extensive, with some fragment ions having an equal abundance as the molecular ions. The alkylaromatic compounds were observed to generate mostly stable molecular ions, with minimal fragmentation to form ions of  $m/z$  92. The cycloalkanes generated stable molecular ions, molecular ions that had lost a hydrogen atom and fragment ions of  $m/z$  56, which complicates data analysis. The APPI/ $N_2$ /CS<sub>2</sub> method produced similar results (Fig. S1 in the supporting information). In conclusion, the mass spectrum shows more fragment ions than molecular ions, and the molecular ions of different compounds have widely differing relative abundances. Some molecular ions fragment only to a small extent while others have extensive fragmentation. Alkane (pentadecane) did not produce stable molecular ions and hence cannot be easily detected in the mixture. Accurate characterization of the mixture based on these data is not possible. However, if this sample was first separated into different chemical classes, then an ideal ionization method could be selected and optimized for the mass spectrometric analysis of each fraction. This is the approach presented here for the analysis of crude oil.

The methods selected here for the separation of crude oil into six fractions are discussed first. Then, the bulk characterization of each fraction by using FTIR spectroscopy is detailed to determine the classes of compounds in each fraction. This information was used to select appropriate model compounds for each fraction that then were used to develop the optimal mass spectrometric analysis method for each fraction.

### 3.1. Separation of crude oil

Distillation, precipitation, autocolumn fractionation and solid phase extraction were used to separate the compounds in the crude oil into six fractions based on their differences in volatility, solubility and polarity. A schematic for the complete separation process is presented in Fig. 2.

As the first step, the most volatile compounds in the crude oil were separated by room-temperature vacuum distillation from the non-volatile portion (residue) to generate fraction 1. During distillation, the receiving flask was kept at a low temperature by using dry ice and acetone ( $< -70$  °C) to collect and condense the volatile components. The remaining residue was separated into asphaltenes (fraction II) and

maltenes (all remaining fractions) through precipitation of the asphaltenes by using *n*-hexane as described in literature [15]. Maltenes were chromatographically separated into three fractions (*n*-hexane-eluted fraction (corresponding to fractions III and IV) and fractions V and VI) based on their differences in polarity. This separation was accomplished by using an auto column coupled with evaporative light scattering (ELSD) and UV detectors and the eluents *n*-hexane (*n*-C<sub>6</sub>H<sub>14</sub>), dichloromethane (CH<sub>2</sub>Cl<sub>2</sub>) and isopropanol (*i*-C<sub>3</sub>H<sub>7</sub>OH), used in this order. Fig. 3 shows a typical auto column chromatogram of maltenes.

The presence of both ELSD and UV signals in the later eluting part of the hexane-eluted fraction (Fig. 3) indicated co-elution of two different analyte classes, aliphatic (no UV absorption) and aromatic hydrocarbons (UV absorption). To test this hypothesis, this fraction was analyzed using GCxGC/(EI)TOF MS. Indeed, based on the total ion current GC/GC chromatogram (Fig. S2A in supporting information), the *n*-C<sub>6</sub>H<sub>14</sub>-eluted fraction is a co-eluted mixture of heavy saturated (cyclic, linear and branched) and light aromatic hydrocarbons. Therefore, an additional separation step was necessary. The saturated and aromatic hydrocarbon classes in the *n*-hexane-eluted fraction were separated via solid phase extraction to produce fractions III (heavy saturated hydrocarbons) and IV (light aromatic hydrocarbons), thus increasing the total number of maltene fractions from three to four (the last two being fractions V and VI eluted by dichloromethane and isopropanol, respectively). The success of the solid phase extraction was evaluated by using GCxGC/(EI)TOF MS to analyze fraction III (Fig. S2B in supporting information). This analysis revealed a small percentage (~9% based on GC peak areas) of aromatic hydrocarbon carryover into the saturated hydrocarbon fraction (III), which could not be avoided.

After the separation of the crude oil into six fractions, each fraction was gravimetrically weighted. The gravimetric weight percentages of the fractions I, II, III, IV, V and VI are 8%, 1%, 44%, 21%, 9% and 8%, respectively (Table S6). The separation method achieved about 92% sample recovery. Before high-resolution mass spectral analysis of the individual fractions, they were studied by using FTIR spectroscopy to determine the bulk chemical nature of each individual fraction, such as polarity and the extent of aromaticity.

It should be noted here that minor amounts of polymers and surfactants eluted from the auto column when a fourth solvent, methanol, was used after isopropanol elution. Analysis of this fraction by using (+)ESI allowed for the ionization and detection of these contaminants (Fig. S3A). ESI mass spectrum of methanol eluted fraction obtained from pristine crude oil did not show these compounds (Fig. S3B).

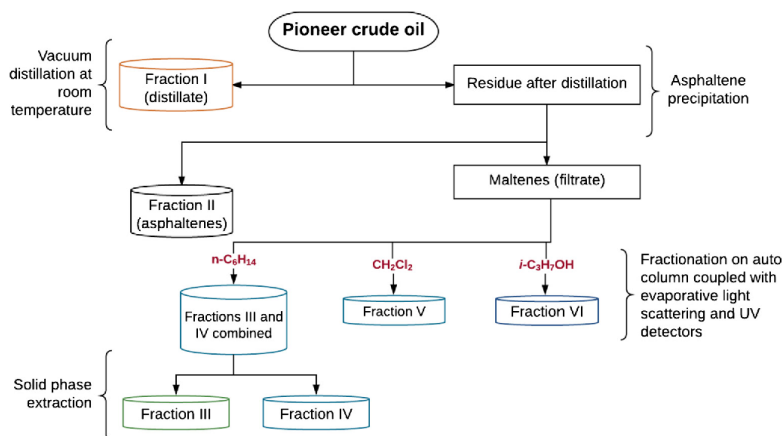


Fig. 2. DPF scheme for separation of crude oil into six fractions (I–VI).



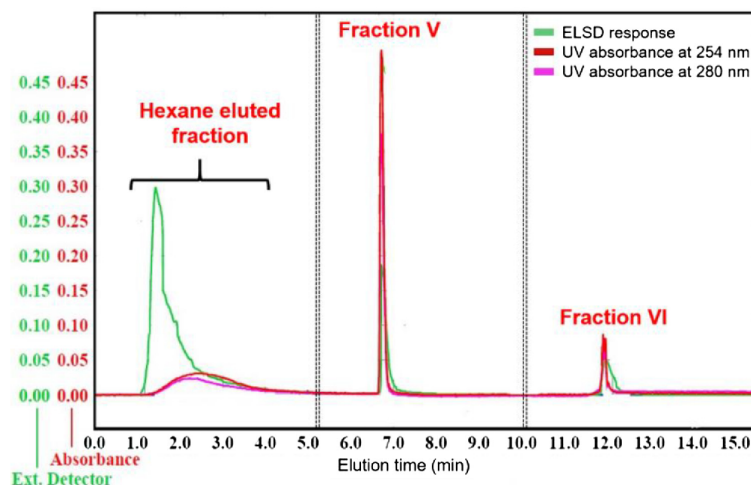


Fig. 3. Auto column-ELSD/UV chromatogram of maltenes, indicating the separation of maltenes into three fractions. The presence of both ELSD and UV signals in the later eluting part of the *n*-hexane-eluted fraction indicates co-elution of aromatic compounds (UV absorption: red and purple traces) along with aliphatic compounds (no UV absorption).

### 3.2. Characterization of individual fractions by FTIR spectroscopy

The FTIR absorption spectra measured for the crude oil fractions, the band assignments, and the functional groups they indicate are provided in Section V of supporting information. To summarize, the spectra measured for the distillate (fraction I) and for the heavy saturated hydrocarbons (fraction III) indicated the predominant presence of saturated hydrocarbons in both fractions. Spectral analysis of the asphaltenes (fraction II) revealed the presence of heteroatoms and significant aromaticity, as expected. The spectrum measured for light aromatic hydrocarbons (fraction IV) indicated the presence of only alkyl aromatic compounds. The spectrum of dichloromethane eluted compounds (fraction V) revealed the presence of heteroatoms and significant aromaticity similar to asphaltenes (fraction II). This fraction is therefore referred to as heteroaromatic compound fraction hence forward. The isopropanol-eluted compounds (fraction VI) were found to contain heteroatoms and have minimal aromaticity. This fraction will be referred to as polar compounds. The bulk information obtained from the FTIR spectral analysis for each fraction was used to select model compounds representative of the compound types present in each fraction. These model compounds were utilized to identify or develop an optimal analysis and mass spectrometric ionization method for each fraction.

### 3.3. Identification of an ionization method for each individual fraction

Based on the FTIR results, the distillate (fraction I) contains saturated hydrocarbons. As this fraction is volatile, the compounds were separated and analyzed using GCxGC/electron ionization (EI) high-resolution time-of-flight (TOF) MS. EI is a universal ionization method (able to ionize all organic compounds) and it provides library-searchable, highly reproducible mass spectra, which allowed for identification of many of the compounds. The suitability of this method for the semi-quantitative analysis of volatile saturated hydrocarbons has been evaluated earlier by using model compound mixtures [18]. The most abundant compounds identified in this fraction are alkanes and cycloalkanes containing 7–10 carbons. The full list of compounds identified is provided in Section VI of supporting information.

The remaining five nonvolatile fractions were analyzed using methods other than GCxGC/MS as this method can be reliably used only for relatively volatile compounds. FTIR spectral analysis of fractions II (asphaltene), IV (light aromatic compounds) and V (heteroaromatic

compounds) revealed the presence of predominantly aromatic compounds. The APCL/N<sub>2</sub>/CS<sub>2</sub> method is well suited for the ionization of these types of compounds as it has been reported [8] to ionize different types of aromatic analytes at nearly equal efficiency by predominant formation of stable molecular ions without substantial fragmentation (see Fig. S4 in supporting information for confirmation of this finding by using a model compound mixture). Therefore, compounds in the fractions II, IV and V were ionized by using this method. Other ionization methods, such as APCL/N<sub>2</sub>/toluene and APCL/N<sub>2</sub>/methanol, were also examined. However, they were found to be less successful than the APCL/N<sub>2</sub>/CS<sub>2</sub> ionization method (see Fig. S5 in supporting information). Though APCL/N<sub>2</sub>/CS<sub>2</sub> method has been demonstrated to be successful in ionizing polyaromatic model compounds with long alkyl chains without substantial fragmentation [8], ionization of monoaromatic model compounds with long alkyl chains (*n*-phenyldecane, *n*-phenyldodecane and *n*-heptadecylbenzene) was observed here to result in the formation of a fragment ion of *m/z* 92 (toluene radical cation) (see Fig. S6 in supporting information). All three compounds studied generate this fragment ion.

The APCL/N<sub>2</sub>/CS<sub>2</sub> ionization method discussed above is inappropriate for the analysis of heavy saturated hydrocarbons (fraction III) based on a study of an equimolar mixture containing cholestane (C<sub>27</sub>H<sub>48</sub>, a fused tetracyclic alkane), squalene (C<sub>30</sub>H<sub>50</sub>, a branched polyalkene), and pentatriacontane (C<sub>35</sub>H<sub>72</sub>, a linear alkane; Fig. 4B). This method generates stable molecular ions for the cyclic alkane but [M–H]<sup>+</sup> ions for the linear and branched alkanes. Also, the cyclic alkane is ionized at a substantially greater efficiency than the linear and branched alkanes. In addition, considerable fragmentation was observed (~22%) especially for linear and branched alkanes. Field ionization is a soft ionization method most commonly employed by the petroleum industry for the ionization of heavy saturated hydrocarbons [19]. However, this ionization method suffers from poor reproducibility [20]. Therefore, the heavy saturated hydrocarbons (fraction III) were instead ionized by using an alternative APCI method. APCI with oxygen as the nebulizing gas and *n*-hexane as the solvent (APCI/O<sub>2</sub>/*n*-hexane) has been reported [20] to produce comparable results to FI in ionizing large saturated hydrocarbons. Fig. 4A shows that the APCI/O<sub>2</sub>/*n*-hexane method generates stable [M–H]<sup>+</sup> ions by hydride abstraction with minimal fragmentation (< 4–6%) and with a similar ionization efficiency for cholestane, squalene and pentatriacontane.

Based on the FTIR results, fraction VI (polar compounds) contains mostly heteroatom-containing nonaromatic compounds. Analysis of an

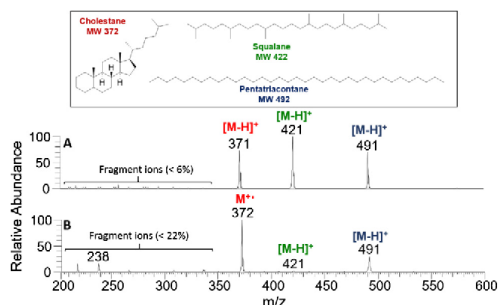


Fig. 4. (A) APCI/ $O_2$ / $n$ -hexane mass spectrum measured at an injection flow rate of  $5 \mu\text{L min}^{-1}$  and tube lens voltage of 20 V and (B) APCI/ $N_2$ / $CS_2$  mass spectrum measured at an injection flow rate of  $5 \mu\text{L min}^{-1}$  and tube lens voltage of 30 V for an equimolar mixture (1 mM) comprised of saturated hydrocarbon model compounds (no ions were observed below  $m/z$  200).

equimolar mixture of nonaromatic compounds with different heteroatoms ( $n$ -butylamine,  $n$ -hexylamine, 5-nonanone and diisopropyl sulfide) by using the APCI/ $N_2$ / $CS_2$  method revealed generation of more than one ion type for each component except for the amines (Fig. S7), which makes this method unsuitable for fraction VI. As these analytes should be easy to protonate, the traditional APCI/ $N_2$ /methanol method was explored. Unfortunately, polar compounds (fraction VI) derived from crude oil are not completely soluble in methanol. Therefore, the fraction was first dissolved in a small amount of  $n$ -hexane (approx. 15–25% of final volume) followed by dissolution in methanol (approx. 75–85% of final volume). Interestingly, while pure hexane and methanol are not miscible with each other, they are completely miscible in the presence of the polar compounds isolated from the crude oil. Fig. 5 shows the mass spectrum obtained for the model compound mixture ( $n$ -butylamine,  $n$ -hexylamine, 5-nonanone and diisopropyl sulfide) by using the (+)APCI/ $N_2$ /hexane, methanol ionization method. Only protonated compounds with reasonably similar relative abundances were observed. At higher injection flow rates ( $> 20 \mu\text{L min}^{-1}$ ) and/or higher concentrations ( $> 5 \text{ mM}$ ), competition for ionization and adduct formation were observed, leading to more than one type of ion for each compound (Fig. S8). The optimized ionization conditions required for ideal analysis of polar compounds (fraction VI) are provided in Table S5.

### 3.4. Characterization of crude oil fractions by using high-resolution mass spectrometry

The high-resolution mass spectrometry instruments and ionization methods that were selected for the analysis of the individual crude oil fractions based on model compound studies are summarized in Fig. 6.

Based on the total ion-chromatogram (Fig. 7A) obtained for the distillate (fraction I) by using a high-resolution GCxGC/((+))EI/TOF mass spectrometer (for the conditions, see Table S3), the majority of its components are cyclic and acyclic saturated hydrocarbons with a small percentage of small aromatic hydrocarbons (see Section VI of supplementary information). An earlier examination of equimolar model compound mixtures containing cyclic and acyclic saturated hydrocarbons and aromatic hydrocarbons (same compound classes as in the distillate) by using the same mass spectrometer revealed similar instrumental average relative response factors for the cyclic and acyclic saturated hydrocarbons [18]. However, aromatic hydrocarbons were observed to show 30–40% higher response than saturated hydrocarbons [18]. Since most compounds in the distillate (fraction I) are saturated hydrocarbons, this method should yield semi-quantitative information for the distillate.

Fig. 7B shows the (+)APCI mass spectra obtained for the five nonvolatile crude oil fractions by using high-resolution LQIT Orbitrap

mass spectrometers (for conditions, see Table S5). The data obtained under these optimized conditions are semi-quantitative and provide the MW values and elemental compositions for most of the compounds in the fractions. Analysis of these data is discussed below.

#### 3.4.1. Average molecular weight (Avg MW) of the crude oil

In order to test the accuracy of the optimized mass spectrometry methods discussed above for the determination of the average molecular weights (Avg MW) of the crude oil fractions and ultimately the crude oil itself, the experimental Avg MW was determined for the four model compound mixtures discussed above by using the optimized methods (Table S7). Further, the experimental Avg MW had been determined previously for an equimolar model compound mixture containing volatile hydrocarbons ( $n$ -decane,  $n$ -dodecane,  $n$ -propylcyclohexane, isopropylbenzene and  $n$ -butylbenzene) that had been analyzed by using the same GCxGC/((+))EI/TOF mass spectrometer (Table S7) used in this study [18]. The molecular weights were determined by considering all the ions observed in the mass spectrum, including the fragment ions, because it is often challenging to differentiate fragment ions from unfragmented ions when analyzing complex unknown mixtures. The experimental Avg MW, theoretical Avg MW and experimental errors for all the model compound mixtures are summarized in the Supporting information (Table S7). From these data, the determination of the average molecular weights for the model compound mixtures was quite accurate (the error for four of the mixtures was  $\leq 3\%$ ; the greatest error, 7%, was observed for the mixture containing alkyl benzenes with long alkyl chains). These findings are summarized in Table S7.

The Avg MW for all crude oil fractions (I, II, III, IV, V and VI) analyzed by using the optimized mass spectrometric methods are summarized in Table 1. The Avg MW for all the fractions excluding the distillate (fraction I) ranged between 496 and 570 Da. Using the Avg MW values and weight percentages of each fraction, the Avg MW for the entire crude oil is estimated to be 473 Da. Although prior evidence indicates (for example, see Fig. 1) that direct analysis of crude oil without prior separation is far from ideal, a mass spectrum was measured for the unfractionated crude oil by using the APCI/ $N_2$ / $CS_2$  ionization method for comparison purposes (Fig. S9 in the supporting information). The Avg MW of the unfractionated crude oil determined based on this mass spectrum was 460 Da (obtained using Eq. (S3)). This value is close to that measured for the fractionated crude oil (473 Da; Table 1) in spite of the fact that the APCI/ $N_2$ / $CS_2$  ionization method completely fragments acyclic saturated hydrocarbons (see Fig. 1). The similarity of these values may be explained based on the similar Avg MW values measured for the individual fractions (with the exception of the distillate (fraction I) but this fraction contributes only  $\sim 8\%$  to the Avg MW). This may not be true for other crude oils. A study comparing the compositions and Avg MWs of crude oils with different geographical origins is ongoing.

It should be noted here that determination of the Avg MW of the crude oil studied here by using other common but indirect techniques,

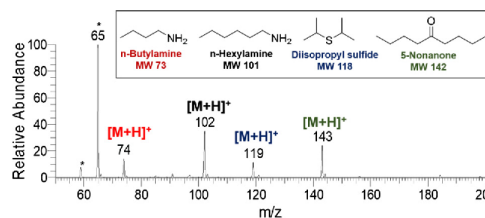


Fig. 5. APCI/ $N_2$ / $n$ -hexane, methanol mass spectrum of an equimolar mixture (1 mM) of nonaromatic polar compounds measured at an injection flow rate of  $1 \mu\text{L min}^{-1}$  and tube lens voltage of 50 V (\* denotes solvent peaks).

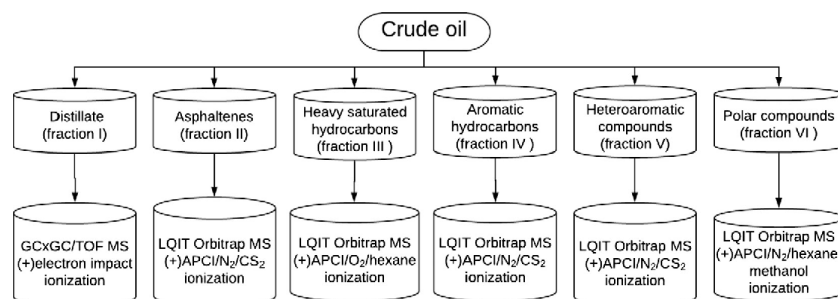


Fig. 6. Instruments and ionization methods used for high-resolution mass spectral analysis of the six fractions of crude oil.

such as freezing point depression and GC simulated distillation techniques, provided much lower estimates (230 Da and 339 Da, respectively) than the direct molecular weight measurement values obtained by using the DPF MS method (473 Da) and the APCI/N<sub>2</sub>/CS<sub>2</sub> mass spectrometry approach without fractionation (460 Da). Therefore, values obtained using these other approaches should be considered erroneous.

### 3.4.2. Molecular profiling of crude oil

High-resolution MS data were employed to assign elemental compositions and ring and double bond (RDB) equivalence values for ionized compounds derived from the different crude oil fractions. RDB equivalence plots provide information on the degree of unsaturation and number of rings in the compounds, specifically, the number of alicyclic and aromatic rings and double and triple bonds.

**3.4.2.1. RDB equivalence plots.** Fig. 8 shows the RDB equivalence versus carbon number (RDB equivalence plots) for ionized compounds derived from the six different fractions of the crude oil. Ions containing the heteroatoms N, O and/or S are color coded in the figure for visual differentiation.

Based on these data, most of the hydrocarbons in the distillate (fraction I) are saturated and some contain ring structures (see Section VI of supporting information). Further, a small number of aromatic

Table 1

Avg MW of crude oil determined from the Avg MW of individual fractions (determined using Eqs. (S2)–(S6) provided in supporting information) and their percent gravimetric weight percentages. It should be noted that 11% of the crude oil was not recovered, which explains the deviation of the sum of the weight% values from 100%.

Fractions of crude oil	Avg MW (Da)	Weight (%)
Fraction I (distillate)	141	8
Fraction II (asphaltenes)	570	1
Fraction III (heavy saturated hydrocarbons)	496	45
Fraction IV (aromatic hydrocarbons)	504	20
Fraction V (heteroaromatic compounds)	527	9
Fraction VI (polar compounds)	532	6
Avg MW of fractionated crude oil	473	100

compounds (with RDB  $\geq 4$ ) was detected, in agreement with the mass spectrometry data discussed above (Fig. 7A). Most of the compounds in this fraction contain 7–10 carbons and have RDB values of either one or two (minimal degree of unsaturation).

The RDB equivalence plot for heavy saturated hydrocarbons (fraction III) surprisingly indicated the presence of compounds with large RDB values (upto 8; Fig. 8). This could be due to the presence of aliphatic or aromatic rings, or double or triple bonds. However, since the FTIR data for fraction III revealed no aromatic, alkene or alkyne

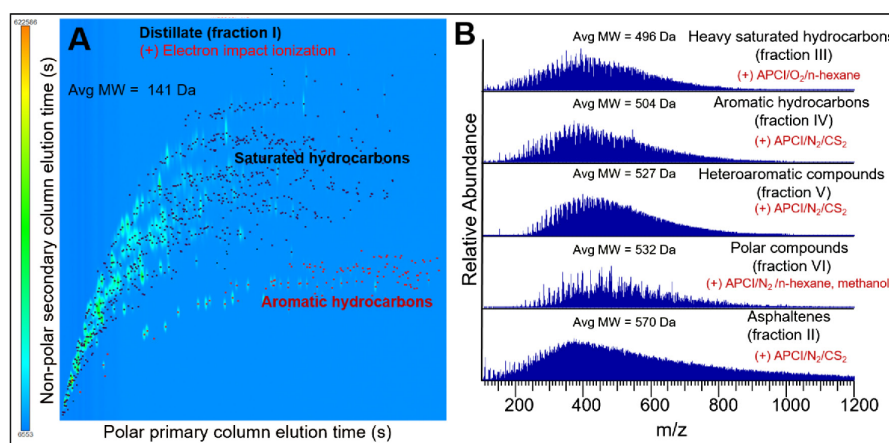
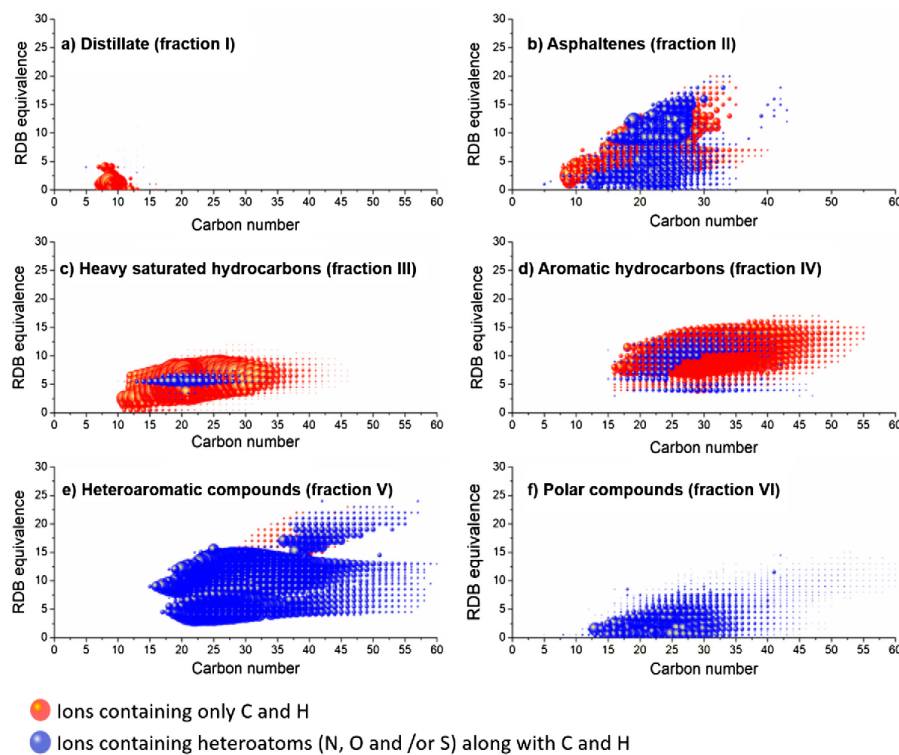


Fig. 7. A) GCxGC/((+)EI)TOF total ion chromatogram for the distillate (fraction I) of the crude oil. The aromatic hydrocarbons are color coded in red and saturated hydrocarbons in black. B) Positive ion mode APCI mass spectra obtained for the five nonvolatile crude oil fractions (fractions II–VI). Avg MW denotes the weighted average molecular weight (discussed below). (For interpretation of the references to color in this figure legend, the reader is referred to the web version of this article.)



**Fig. 8.** Color-mapped bubble plots of ring and double bond (RDB) equivalence versus carbon number for ionized compounds derived from the six crude oil fractions that were separated and characterized by using the DPF-MS method. Bubble size indicates the relative abundance of the ions. (For interpretation of the references to colour in this figure legend, the reader is referred to the web version of this article.)

signatures (see [Section V of supporting information](#)), the large RDB values can be attributed to the presence of compounds containing 1–8 saturated rings. Most of the compounds in this fraction contain 10–35 carbons. Finally, some compounds in fraction III contain a heteroatom, specifically, sulfur (see discussion on compound class distributions below).

Most compounds in the aromatic hydrocarbon group (fraction IV) contain 15–45 carbons. No aliphatic compounds were detected as all the RDB values are greater or equal to four as expected based on FTIR analysis. However, some heteroatom containing compounds were observed and are discussed in the next section.

Most compounds in the heteroaromatic and polar compound groups (fractions V and VI) contain heteroatoms but these two fractions differ drastically from each other in their carbon number and extent of aromaticity ([Fig. 8](#)). The majority of the compounds in fraction V contain 15–50 carbons while the compounds in fraction VI only contain 12–35 carbons. While the heteroaromatic compound group contains both aromatic compounds ( $\text{RDB} \geq 4$ ) and nonaromatic compounds ( $\text{RDB} < 4$ ), the majority of the compounds in the polar compound class are nonaromatic ( $\text{RDB} < 4$ ). These observations are in agreement with the FTIR results obtained for these fractions.

Asphaltenes (fraction II) contain not only aromatic and heteroaromatic compounds but also compounds that are not aromatic ( $\text{DBE} < 4$ ). The compounds in asphaltenes contain 8–35 carbons.

**3.4.2.2. Compound class distributions.** Assigning accurate elemental compositions for ionized compounds is critical for the accurate

estimation of compound class distributions. However, when analyzing mixtures as complex as crude oil, this requires much greater resolution and mass accuracy than available on the orbitrap (100,000 resolution) and TOF instruments (50,000 resolution) used in this research [21–24]. However, after DPF separation of the crude oil into six fractions based on the volatility, solubility and polarity of the compounds, much simpler mixtures are generated and the compounds in each mixture have similar properties. This makes assigning elemental compositions much easier when using lower resolution instruments.

Elemental composition data thus obtained for ionized compounds derived from the different crude oil fractions can be utilized to further classify the compounds into different compound classes. [Fig. 9 \(Table S8\)](#) shows compound class distributions and their relative abundances for the six fractions.

The percentage relative abundance of the hydrocarbon (HC) class was found to be different for each fraction, being the greatest for the distillate (fraction I) and the smallest for the polar compounds (fraction VI). The asphaltenes (fraction II) contain a relatively large number of compounds with a variety of different heteroatoms. While N atoms and  $\text{SO}_3$  groups were most abundant in heteroaromatic compounds (fraction V), SO, O and  $\text{SO}_4$  atoms/groups are most abundant in polar compounds (fraction VI). Interestingly, some compounds in the aromatic hydrocarbon fraction were found to contain not only S but also  $\text{NS}_2$ . To summarize, all the fractions are drastically different in their compound class distributions and their relative abundances.

From the gravimetric weight percentage of individual fractions and their compound class distributions, the weight percentage distribution



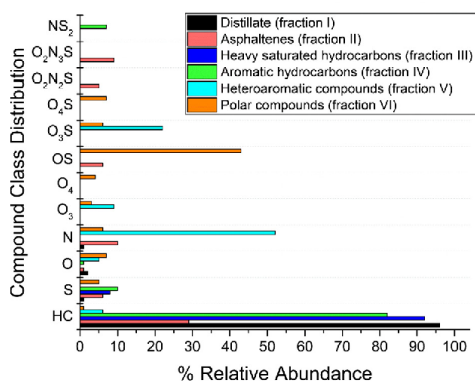


Fig. 9. Compound class distributions and their percentage relative abundances for crude oil fractions separated and analyzed by using the DPF-MS method. The y-axis indicates the assigned elemental compositions by using abbreviations such as  $\text{NS}_2$ , which implies compounds containing one nitrogen and two sulfur atoms, in addition to hydrogen and carbon atoms.

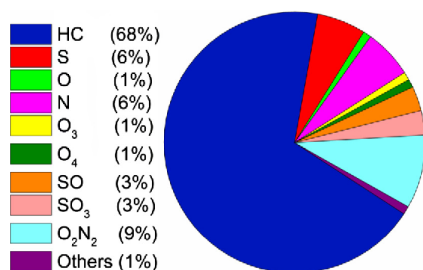


Fig. 10. Weight percentages of compound classes in the crude oil, consolidated from the data obtained for individual fractions.

of individual compound classes in the whole crude oil can be obtained by using Eq. (S7). Fig. 10 (Table S8) shows the summarized weight percentage distributions for the different compound classes consolidated from the data obtained for the individual fractions. These data

provide a simplified picture on the presence of different compound classes and their abundances in the whole crude oil. Based on these consolidated results, this crude oil consists of about 12% sulfur containing compounds (S, OS and  $\text{O}_3\text{S}$ ). It can also be deduced that this crude oil is very low (3%) in oxygen content (O,  $\text{O}_3$  and  $\text{O}_4$ ).

Further information on individual fractions can be obtained by exploiting the tandem MS capabilities of the LQIT/orbitrap mass spectrometer. This mass spectrometer allows the isolation of a group of isomeric and isobaric ions of a given  $m/z$ -value followed by collision-activated dissociation (CAD) in the ion trap. The resulting MS/MS CAD spectra can provide structural information on crude oil components, such as the number of carbons in alkyl groups and the size of the aromatic cores in asphaltenes [25,26].

Fig. 11 shows the CAD mass spectra obtained by using the same “normalized” CAD energy (25 arbitrary units) for molecular ions of  $m/z$  400 (generated upon (+) APCI/ $\text{N}_2/\text{CS}_2$  ionization) derived from three different fractions (fractions II, IV and V). The fragmentation patterns (indicated by red dotted lines) observed for these ions indicate that they are very different from each other. The decay patterns observed for the ions derived from the asphaltenes are consistent with the fragmentation patterns previously reported for asphaltenes [8], indicating large aromatic cores and short alkyl chains (fastest fragmentations involving elimination of methyl and ethyl radicals). On the other hand, the ions derived from the aromatic hydrocarbon fraction contain small aromatic cores and long alkyl chains. Fragmentation of the ions derived from the heteroaromatic fraction indicates the presence of fairly long alkyl chains in these compounds, information that was not obtained from any of the experiments discussed above.

Fig. S10 in the supporting information shows more examples of the fragmentation patterns observed for ionized heteroaromatic compounds and asphaltenes (fractions II and V). Fig. S11 in the supporting information shows representative CAD mass spectra of protonated compounds derived from the polar compounds fraction. These protonated compounds fragment via unique losses of polar molecules, such as water and formaldehyde, thus confirming the presence of polar functional groups.

#### 4. Conclusions

A separation and characterization method entitled Distillation Precipitation Fractionation Mass Spectrometry (DPF-MS) is introduced here for the analysis of crude oil at the molecular level. This method involves separation of the crude oil into six fractions. These fractions are the distillate (fraction I) mostly containing volatile saturated

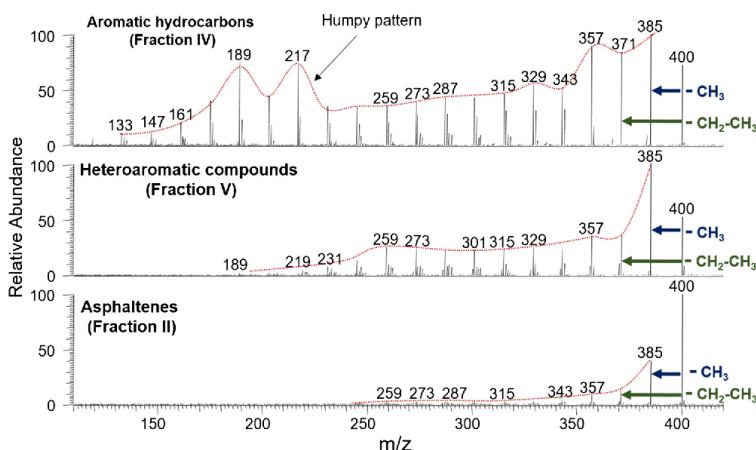


Fig. 11. CAD mass spectra obtained by using the same “normalized” CAD energy (25 arbitrary units) for the radical cation of  $m/z$  400 derived from three different fractions of the crude oil. The different fragmentation patterns are highlighted using a red dotted line. (For interpretation of the references to color in this figure legend, the reader is referred to the web version of this article.)

hydrocarbons but also light aromatic hydrocarbons, asphaltenes (fraction II) containing predominantly aromatic and heteroaromatic compounds, heavy saturated hydrocarbons (fraction III) containing cyclic, branched and linear hydrocarbons, aromatic hydrocarbons (fraction III) containing predominantly alkylaromatic compounds, heteroaromatic compounds (fraction V) containing mostly aromatic compounds, and polar compounds (fraction VI) containing nonaromatic polar compounds. High-resolution mass spectrometry instruments, specifically, GCxGC/TOF and LQIT/orbitrap mass spectrometers, were used for the molecular level characterization of each individual fraction. An optimized ionization method was developed for each fraction to ionize all of its components with similar efficiency and to generate only one type of ions, either molecular ions, protonated molecules or cations formed upon hydride abstraction. While (+) EI ionization method coupled with GCxGC/TOF was utilized for the characterization of the volatile distillate (fraction D), (+) APCI approaches with different nebulization gases and solvent systems were used for each nonvolatile fraction (fractions II, III, IV, V, VI).

DPF-MS provides semi-quantitative molecular level information (elemental compositions and molecular weights) that can be further processed to obtain accurate average molecular weight, ring and double bond equivalence values and percentage abundances of different compound classes in the different crude oil fractions. This method excels over previous methods by including the mass balance for each fraction, thus allowing for data consolidation (data obtained from different fractions consolidated into one data set), which provides an accurate overall analysis of the crude oil, including average molecular weight, heteroatom content, and weight percentage of different compound classes.

#### Acknowledgements

The authors thank Pioneer Oil Company for their generous financial support. We thank Dr. Rituraj Borgohain, Jeremy Holyslaw and Jacob Milton for their valuable comments and Gnanasiri S. Premachandra for help with the FTIR data.

#### Appendix A. Supplementary data

Supplementary data associated with this article can be found, in the online version, at <https://doi.org/10.1016/j.fuel.2018.07.028>.

#### References

- [1] Denekas MO, Mattax CC, Davis GT. Effects of crude oil components on rock wettability. Kansas City: Society of Petroleum Engineers; 1959. p. 330–3.
- [2] Tang G-Q, Morrow NR. Influence of brine composition and fines migration on crude oil/brine/rock interactions and oil recovery. J Pet Sci Eng 1999;24:99–111. [https://doi.org/10.1016/S0920-4105\(99\)00034-0](https://doi.org/10.1016/S0920-4105(99)00034-0).
- [3] Walters CC. Oil–oil and oil–source rock correlation. Geochemistry. Dordrecht: Springer Netherlands; 1998. p. 442–4. [https://doi.org/10.1007/1-4020-4496-8\\_222](https://doi.org/10.1007/1-4020-4496-8_222).
- [4] Schneider DF. Select the right hydrocarbon molecular weight correlation. Chem Eng Prog 1998;94:40.
- [5] Marshall AG, Rodgers RP. Petroleomics: the next grand challenge for chemical analysis. Acc Chem Res 2004;37:53–9. <https://doi.org/10.1021/ar020177t>.
- [6] Bae E, Na J-G, Chung SH, Kim HS, Kim S. Identification of about 30 000 chemical components in shale oils by electrospray ionization (ESI) and atmospheric pressure photoionization (APPI) coupled with 15 T Fourier transform ion cyclotron resonance mass spectrometry (FT-ICR MS) and a comparison to conventional oil. Energy Fuels 2010;24:2563–9. <https://doi.org/10.1021/ef100060b>.
- [7] Purcell JM, Hendrickson CL, Rodgers RP, Marshall AG. Atmospheric pressure photoionization Fourier transform ion cyclotron resonance mass spectrometry for complex mixture analysis. Anal Chem 2006;78:5906–12. <https://doi.org/10.1021/ac060754h>.
- [8] Owen BC, Gao J, Borton DJ, Amundson LM, Gray M, Kenttämäa HI, et al. Carbon disulfide reagent allows the characterization of nonpolar analytes by atmospheric pressure chemical ionization mass spectrometry. Rapid Commun Mass Spectrom 2011;25:1924–8. <https://doi.org/10.1002/rcm.5063>.
- [9] Chiaberge S, Fiorani T, Savoini A, Bionda A, Ramello S, Pastori M, et al. Classification of crude oil samples through statistical analysis of APPI FTICR mass spectra. Fuel Process Technol 2013;106:181–5. <https://doi.org/10.1016/j.fuproc.2012.07.023>.
- [10] Rodgers RP, Marshall AG. Petroleomics: advanced characterization of petroleum-derived materials by Fourier transform ion cyclotron resonance mass spectrometry (FT-ICR MS). In: Mullins OC, Sheu EY, Hammami A, Marshall AG, editors. Asph. Heavy Oils Pet. New York: Springer; 2007. p. 63–93. [https://doi.org/10.1007/0-387-68903-6\\_3](https://doi.org/10.1007/0-387-68903-6_3).
- [11] Pakarinen JMH, Teräsväinen MJ, Pirkkanen A, Wickström K, Vainiotalo P. A positive-ion electrospray ionization Fourier transform ion cyclotron resonance mass spectrometry study of Russian and North Sea crude oils and their six distillation fractions. Energy Fuels 2007;21:3369–74. <https://doi.org/10.1021/ef700347d>.
- [12] Zhu X, Shi Q, Zhang Y, Pan N, Xu C, Chung KH, et al. Characterization of nitrogen compounds in Coker heavy gas oil and its subfractions by liquid chromatographic separation followed by Fourier transform ion cyclotron resonance mass spectrometry. Energy Fuels 2011;25:281–7. <https://doi.org/10.1021/ef101328n>.
- [13] Klein GC, Angström A, Rodgers RP, Marshall AG. Use of saturates/aromatics/resins/asphaltenes (SARA) fractionation to determine matrix effects in crude oil analysis by electrospray ionization Fourier transform ion cyclotron resonance mass spectrometry. Energy Fuels 2006;20:668–72. <https://doi.org/10.1021/ef050353p>.
- [14] Liu P, Shi Q, Chung KH, Zhang Y, Pan N, Zhao S, et al. Molecular characterization of sulfur compounds in Venezuela crude oil and its SARA fractions by electrospray ionization Fourier transform ion cyclotron resonance mass spectrometry. Energy Fuels 2010;24:5089–96. <https://doi.org/10.1021/ef100904k>.
- [15] Buenostro-Gonzalez E, Lira-Galeana C, Gil-Villegas A, Wu J. Asphaltene precipitation in crude oils: theory and experiments. AIChE J 2004;50:2552–70. <https://doi.org/10.1002/aic.10243>.
- [16] Yang Z, Yang C, Wang Z, Hollebone B, Landriault M, Brown CE. Oil fingerprinting analysis using commercial solid phase extraction (SPE) cartridge and gas chromatography-mass spectrometry (GC-MS). Anal Methods 2011;3:628–35. <https://doi.org/10.1039/C0AY00715C>.
- [17] Alzaga R, Montuori P, Ortiz L, Bayona JM, Albaiges J. Fast solid-phase extraction-gas chromatography-mass spectrometry procedure for oil fingerprinting: application to the prestige oil spill. J Chromatogr A 2004;1025:133–8. <https://doi.org/10.1016/j.chroma.2003.10.080>.
- [18] Luning Prak DJ, Romanczyk M, Wehde KE, Ye S, McLaughlin M, Luning Prak PJ, et al. Analysis of catalytic hydrothermal conversion jet fuel and surrogate mixture formulation: components, properties, and combustion. Energy Fuels 2017. <https://doi.org/10.1021/acs.energyfuels.7b02960>.
- [19] Liang Z, Hsu CS. Molecular speciation of saturates by on-line liquid chromatography – field ionization mass spectrometry. Energy Fuels 1998;12:637–43. <https://doi.org/10.1021/ef970216v>.
- [20] Jin C, Viidanoja J, Li M, Zhang Y, Ikonen E, Kenttämäa HI, et al. Comparison of atmospheric pressure chemical ionization and field ionization mass spectrometry for the analysis of large saturated hydrocarbons. Anal Chem 2016;88:10592–8. <https://doi.org/10.1021/acs.analchem.6b02789>.
- [21] Wang Y, Gu M. The concept of spectral accuracy for MS. Anal Chem 2010;82:7055–62. <https://doi.org/10.1021/ac100888b>.
- [22] Kind T, Fiehn O. Metabolomic database annotations via query of elemental compositions: mass accuracy is insufficient even at less than 1 ppm. BMC Bioinf 2006;7:234. <https://doi.org/10.1186/1471-2105-7-234>.
- [23] Khodjanlyazova S, Nazari M, Garrard KP, Matos MPV, Jackson GP, Muddiman DC. Characterization of the spectral accuracy of an orbitrap mass analyzer using isotope ratio mass spectrometry. Anal Chem 2017. <https://doi.org/10.1021/acs.analchem.7b03983>.
- [24] Marshall AG, Blakney GT, Chen T, Kaiser NK, McKenna AM, Rodgers RP, et al. Mass resolution and mass accuracy: how much is enough? Mass Spectrom 2013;2. <https://doi.org/10.5702/massspectrometry.S0009>.
- [25] Jarrell TM, Jin C, Riedeman JS, Owen BC, Tan X, Scherer A, et al. Elucidation of structural information achievable for asphaltenes via collision-activated dissociation of their molecular ions in MSn experiments: a model compound study. Fuel 2014;133:106–14. <https://doi.org/10.1016/j.fuel.2014.04.040>.
- [26] Borton D, Pinkston DS, Hurt MR, Tan X, Azyat K, Scherer A, et al. Molecular structures of asphaltenes based on the dissociation reactions of their ions in mass spectrometry. Energy Fuels 2010;24:5548–59. <https://doi.org/10.1021/ef1007819>.